

HYDROTHERMAL LIQUEFACTION OF MICROALGAE AND SUBSEQUENT BIO-CRUDE CATALYTIC UPGRADING

CHRISTOPHER MICHAEL THOMAS

Doctor of Philosophy

ASTON UNIVERSITY

March 2022

© Christopher Michael Thomas, 2022

Christopher Michael Thomas asserts their moral right to be identified
as the author of this thesis.

This copy of the thesis has been supplied on condition that anyone who consults it
is understood to recognise that its copyright belongs to its author and that no quotation
from the thesis and no information derived from it may be published without permission
or acknowledgment.

Aston University

Hydrothermal liquefaction of microalgae and subsequent bio-crude catalytic upgrading

Christopher Michael THOMAS

Doctor of Philosophy, March 2022

Thesis Abstract

This PhD research project aimed to study the hydrothermal liquefaction of microalgae with subsequent catalytic upgrading of HTL-derived bio-crudes. Five macroalgae (*Ascophyllum nodosum*, *Fucus serratus*, *Fucus vesiculosus*, *Himantalia elongate* and *Ulva lactuca*) and three microalgae (*Arthrospira platensis*, *Isochrysis galbana* and *Nannochloropsis sp.*) were characterised as a potential feedstock for hydrothermal processing. The results from the characterisation work are utilised for feedstock screening and as starting points for reaction pathways and bio-crude formation.

Preliminary HTL experiments for macro and microalgae species included the utilisation of a 25 ml batch reactor followed by larger-scale processing of model components and microalgae in a 300 ml batch reactor over a temperature range of 200-350 °C. Microalgae were found to produce higher bio-crude yields compared to macroalgae species. HTL processing at higher temperatures resulted in higher bio-crude yields with the highest bio-crude yield of 51.6 wt.% achieved at a liquefaction temperature of 300 °C for the microalgae species *Nannochloropsis sp.*. The bio-crudes were found to have high levels of nitrogen and oxygen which negatively affects the bio-crudes utility as a transportation fuel.

Model components (glucose, xylose, oleic acid, stearic acid, L-glutamine, L-leucine and soy protein isolate) chosen to represent the main macromolecular compounds in microalgae were introduced to thermal degradation studies both by the analytical pyrolysis (Py-GC-MS) and HTL processing in a 300 ml batch reactor in order to gain insight into macromolecular reaction pathways.

Bio-crude from the HTL treatment of microalgae, model compounds and catalytically upgraded algal oils were analysed using a novel combination of advanced NMR techniques for the chemical characterisation. These included two-dimensional techniques of Heteronuclear Single Quantum Coherence (HSQC), Heteronuclear Multiple Bond Correlation (HMBC) and the spectral edited ¹³C pulse sequence known as PENDANT (Polarisation Enhancement During Attached Nucleus Testing). The utilisation of these advanced techniques allowed for the characterisation of the whole bio-crude and upgraded liquids samples, not just the fraction that are able to elute from a gas chromatography (GC) column prior to the mass spectrometry (MS) detection.

Upgrading of the HTL algal bio-crude was investigated, applying catalysts (Pd/C, Pt/C, Ru/C, HZSM-5 and NiMo) was investigated via supercritical water upgrading at 450 °C. Upgrading resulted in improvements in atomic ratios and HHV. The nitrogen content of the upgraded oils were reduced to levels of 1.9-2.6 wt. %. Oxygen content was dramatically reduced, from 19.9 wt. % to values ranging between 1.3-4.8 wt. %. Analysis of the upgraded oil revealed the content was predominantly composed of C6-C16 alkanes and substituted aromatic compounds.

The techno-economic assessment (TEA) proposed using microalgae as the feed to a commercial-scale HTL processing plant designed for a throughput of 2,000 kg/h dry ash-free algae, producing primarily diesel fraction and naphtha co-product liquid fuels. Sensitivity analysis shows the process to be sensitive to feedstock cost, capital expenditure, bio-crude yield and incoming algal slurry concentration. Although technically feasible, the economic results from the TEA propose an MFSP of £2.64/litre, identifying that algae derived biofuels are far from competitive in this scenario.

I'd like to dedicate this thesis to my partner Stef who has been a constant source of support, my two daughters Penny and Juniper who light up my life and to my parents for their continued support, love and understanding.

Acknowledgements

Firstly, I would like to acknowledge Dr Daniel Nowakowski for the guidance and support and for going above and beyond his role as my Main PhD Supervisor; I couldn't have done it without him.

I would also like to thank to Dr Gareth Griffiths for his guidance during the PhD as Associated Supervisor.

Dr Jinesh Cherukkattu Manayil who has always been there to help me in the laboratory and Dr Khalid Doudin for helping me with NMR analysis and unravelling the data.

I would also like to thank the staff in the postgraduate research office for their support during the COVID-19 pandemic.

Thanks go out to all MEng students I worked with for their engagement and efforts in the labs and interesting conversations, particularly Regina Siu, who went on to start her PhD.

Finally, thanks to all the staff and students at EBRI for making me feel very welcome and at home.

List of Contents

Chapter 1 - Introduction	16
1.1. Background	16
1.2. Aim and objectives	20
1.3. PhD thesis structure	20
1.4. Dissemination of research outputs	22
1.4.1. Up-to-date disseminated items	22
1.4.2. Planned dissemination including peer-reviewed publications	22
Chapter 2 - Literature review	24
2.1. Introduction	24
2.2. Algae Cultivation	24
2.2.1. Nutritional Requirements	25
2.2.2. Photoautotrophic production of algae	25
2.2.3. Microalgal harvesting technologies	29
2.3. Biochemical composition of algae	30
2.3.1. Chemical composition	30
2.3.2. Protein and Amino acids	31
2.3.3. Lipids	31
2.3.4. Carbohydrates	32
2.3.5. Pigments in algae	33
2.4. Algae species	34
2.4.1. Microalgae	34
2.4.2. Macroalgae	35
2.5. Previous Work on Biomass Conversion	36
2.5.1. Algae to bio-fuels conversion techniques	36
2.6. Overview of hydrothermal liquefaction of algae	44
2.6.1. Hydrothermal liquefaction theoretical background	44
2.6.2. HTL processing modes	45
2.7. HTL bio-crude upgrading	60
2.7.1. Physical upgrading of HTL bio-crude	60
2.7.3. Chemical upgrading routes	62

Chapter 3 - Methodology	75
3.1. Materials.....	75
3.1.1. Model compounds	75
3.1.2. Macroalgae species.....	75
3.1.3. Microalgae species	76
3.1.4. Solvents and reference materials.....	76
3.1.5. Catalysts	76
3.2. Analytical protocols.....	77
3.2.1. Elemental analysis.....	77
3.2.1 Heating values	77
3.2.2 Ash content analysis.....	77
3.2.4 Thermogravimetric analysis (TGA).....	78
3.2.5 Analytical pyrolysis (Py-GC-MS)	78
3.2.6. GC-MS analysis of liquid samples.....	78
3.2.7. One- and two-dimensional NMR spectroscopy.....	79
3.3. Hydrothermal processing.....	81
3.3.1 Testing of New Liquefaction Equipment.....	81
3.3.2 Batch Processing.....	82
3.4. Heterogeneous catalytic upgrading.....	83
3.4.1 Catalyst preparation.....	83
3.4.2 Catalyst characterisation	84
3.4.3 Catalytic supercritical water upgrading	84
3.5. Product Handling	85
3.5.1 Product separation.....	85
Chapter 4 - Feedstock characterisation and selection.....	86
4.1. Introduction	86
4.2. Characterisation of algal feedstock	87
4.2.1. Proximate and ultimate analysis of algae	87
4.3. Thermal Analysis TGA.....	89
4.4. Py-GC-MS analysis	91

4.4.1. Py-GC-MS of macroalgae species	91
4.4.2. Py-GC-MS of microalgae species	93
4.5. Model compounds characterisation.....	95
4.5.1. Proximate and ultimate analysis of model compounds.....	96
4.5.2. Thermogravimetric analysis.....	97
4.5.3. Py-GC-MS of model compounds.....	98
Chapter 5 - Hydrothermal processing of algal and model compound feedstocks	109
5.1. Introduction	109
5.2. Results and discussion	110
5.2.1. Preliminary HTL processing in 25 ml batch reactor	110
5.2.2. HTL processing of microalgae in 300 ml batch reactor	115
5.2.3. Model Compound Liquefaction.....	117
5.3. Conclusions	145
Chapter 6 Catalytic upgrading	147
6.1. Introduction	147
6.2 Materials and Methods	147
6.2.1 Catalysts	147
6.2.2 HTL bio-crude feed	147
6.3. Results and discussion	148
6.3.1 Catalyst screening results	148
6.3.2 SCW upgrading product yields	153
6.3.3 Characterisation of upgraded bio-crude	156
6.4. Conclusions	166
Chapter 7 - Techno-economic assessment	167
7.1. Introduction	167
7.2. HTL Model Development.....	168
7.2.1. Hydrothermal liquefaction.....	169
7.2.2. Catalytic hydrothermal gasification of aqueous phase	170
7.2.3. Bio-crude hydrotreating	171
7.2.4. Steam methane reforming	173
7.3. Techno-economic analysis	174

7.3.1. Introduction	174
7.3.2. Total capital investment (TCI)	175
7.3.3. Operating costs.....	179
7.3.4. Discounted cash flow.....	181
7.3.5. Sensitivity analysis.....	182
7.4. Process economics results and discussion.....	183
7.4.1. Economic assessment.....	183
7.4.2 Sensitivity analysis.....	185
7.5. Conclusions	188
Chapter 8 - Conclusions and recommendations	189
8.1. Conclusions	189
8.2. Recommendations.....	191
References	193
Appendices	207

List of abbreviations and acronyms

BPRV	Back -pressure regulating valves
barg	Bar gauge pressure
C	Carbon
°C	Celsius (degree)
CoNiMoW/ γ Al ₂ O ₃	Cobalt-Nickel-Molybdenum-Tungsten on γ -alumina
CoMo/Al ₂ O ₃	Cobalt-Molybdenum on γ -alumina
CSTR	Continuous stirred tank reactor
DCM	Dichloromethane
DHA	Docosahexaenoic acid
d.b.	Dry basis
DEPT	Distortionless Enhancement by Polarisation Transfer
DMSO-d ₆	Deuterated dimethyl sulfoxide-d ₆
FAME	Fatty Acid Methyl Ester
GC	Gas Chromatography
H	Hydrogen
HDO	Hydrodeoxygenation
HHV	Higher Heating Value
HZSM-5	Zeolite
HMBC	Heteronuclear Multiple-Bond Coherence
HPLC	High Pressure Liquid Chromatography
HSQC	Heteronuclear Single Quantum Coherence
HTL	Hydrothermal Liquefaction
K	Kelvin (degree)
LHSV	Liquid Hourly Space Velocity
ml	Millilitres
MJ	Mega Joules
MPa	Mega Pascals
N	Nitrogen
NaOH	Sodium hydroxide
NOE	Nuclear Overhauser Effect
NO _x	Nitrogen oxides
NiMo/Al ₂ O ₃	Nickel-Molybdenum on γ -alumina
NMR	Nuclear Magnetic Resonance
O	Oxygen
OLS	Ordinary Least Squares regression
Pd/C	Palladium on carbon
PENDANT	Polarisation Enhancement Nurtured During Attached Nucleus Testing
PFR	Plug Flow Reactor
PLS	Partial Least Squares regression
PNNL	Pacific Northwest National Laboratory
Pt	Platinum
Pt/C	Platinum on carbon
Pt/Al ₂ O ₃	Platinum on γ -alumina
PUFAs	Polyunsaturated fatty acids
Py-GC-MS	Pyrolysis – gas chromatography – mass spectrometry
Ru/C	Ruthenium on carbon
Ru/Al ₂ O ₃	Ruthenium on γ -alumina
S	Sulphur
SCWG	Supercritical Water Gasification
SO _x	Sulfur Oxides
TAG	Triacylglycerols
TAN	Total Acid Number
TGA	Thermogravimetric Analysis

wt.%
ZSM-5

Weight Percent
Zeolite catalyst

List of Tables

Table 2.1. Comparison of photobioreactor and raceway pond production methods	29
Table 2.2. Summary of selected batch HTL literature studies.....	46
Table 2.3. Composition of commonly studied microalgae	51
Table 2.4. Summary of continuous hydrothermal liquefaction of algae feedstocks.....	56
Table 2.5. Hydrogen consumption for HDO reactions presented alongside activation energy (E_A) and iso-reactive temperature (T_{iso}) for various functional groups in the presence of a $CoMoS_2/Al_2O_3$ catalyst.....	65
Table 2.6. Summary of bio-crude upgrading pathways and their technical feasibility	71
Table 3.1. Catalyst surface area measured by BET	84
Table 4.1. Proximate analysis of the micro and macroalgae feedstocks	87
Table 4.2. Ultimate analysis and calculated HHVs of the micro and macroalgae feedstocks	89
Table 4.3. Major compounds identified from the pyrolysis of all macroalgae samples at 500 °C using Py-GC/MS.	92
Table 4.4. Major compounds identified from the pyrolysis of the microalgae samples at 500 °C using Py-GC/MS.	94
Table 4.5. Proximate and ultimate analysis, HHV, atomic ratios of model compounds and microalgae	97
Table 5.1. Products Obtained from Liquefaction Experimental Runs all treated at 300 °C, residence time of 10 minutes.....	111
Table 5.2. Yields (wt.% daf basis) of the HTL products at 300 °C and 10 min residence time with elemental composition (wt.% daf basis) and HHV (MJ/kg) of the bio-crude.....	111
Table 5.3. Effect of final reaction temperature on elemental composition, HHV, atomic ratios and energy recovery	115
Table 5.4. Outline of model compound liquefaction runs	117
Table 5.5. Elemental Composition and Bio-Crude properties	121
Table 5.6. The integrated regions specified for functional groups from the ^{13}C NMR spectra of all the bio-crudes shown in Figure 5.10.	128
Table 6.1. Product yields for the upgrading experiments of bio-crude oils from the HTL treatment of <i>Nannochloropsis sp.</i>	153
Table 6.2. Elemental composition (wt.% daf) of the algae feedstock, HTL bio-crude and upgraded oils produced with different catalysts.	156

Table 6.3. Composition of the bio-crude and catalytically upgraded oils (% of total peak area from GC-MS).....	159
Table 7.1. Aspen model assumptions.....	169
Table 7.2. Hydrotreating Aspen plus model assumptions.....	171
Table 7.3. Assumptions for the Nth plant model.....	174
Table 7.4. Costs for Determining Total Capital Investment.....	176
Table 7.5. Scaling exponents for equipment costs based on [93].....	177
Table 7.6. Installation factors.....	178
Table 7.7. Biorefinery plant fixed operating costs.....	179
Table 7.8. Variable operating costs and supporting assumptions.....	180
Table 7.9. Catalytic hydrothermal gasification ruthenium catalyst manufacture and renewal cost assumptions taken from [93].....	181
Table 7.10. MFSP cost breakdown.....	185
Table 7.11. Variables represented in the sensitivity analysis.....	185

List of Figures

Figure 1.1. Schematic PFD of the HTL Process for Microalgae	19
Figure 2.1. Plan view of a raceway pond.....	26
Figure 2.2. Medium scale tubular photobioreactor at Varicon Aqua (USA site)	27
Figure 2.3. Indoor horizontal tubular photobioreactor at GICON®	28
Figure 2.4. Algal species used in this study	35
Figure 2.5. Potential algae conversion processes.	36
Figure 2.6. Transesterification of oil to biodiesel, R ₁₋₃ are hydrocarbon groups.....	43
Figure 2.7. Phase diagram of water	44
Figure 2.8. Process flow diagram for the HTL series arrangement of a CSTR followed by a plug flow reactor used by Elliott et al	57
Figure 2.9. Reactions associated with catalytic bio-crude upgrading.....	64
Figure 2.10. Cracking reaction example.	70
Figure 3.1. Autoclave Testing Runs Pressure Profiles.....	81
Figure 3.2. Cross-section of the Parr 500 series stirred reactor.	83
Figure 3.3. Separation of HTL and catalytic upgrading liquids.	85
Figure 4.1. DTG profiles of all algae species in nitrogen at 25 °C min ⁻¹ solid lines for macroalgae species and dashed lines for microalgal species.	90
Figure 4.2. Py-GC-MS profile at 500 °C for the macroalgae species <i>Himantalia elongata</i>	91
Figure 4.3. Py-GC-MS profile at 500 °C for <i>Nannochloropsis</i> sp.	93
Figure 4.4. DTG profiles of selected model compounds (oleic acid, soy protein and glucose) in nitrogen at 25 °C min ⁻¹	98
Figure 4.5. GC-MS chromatogram for glucose pyrolysed at 500 °C.	99
Figure 4.6. GC-MS chromatogram for xylose pyrolysed at 500 °C	99
Figure 4.7. Primary structure of a hypothetical protein in algae [Adapted from [55]].....	101
Figure 4.8. GC-MS chromatogram for soy protein pyrolysed at 500 °C.	101
Figure 4.9. GC-MS chromatogram for L-Glutamine pyrolysed at 500 °C.....	103
Figure 4.10. GC-MS chromatogram for L- Leucine pyrolysed at 500 °C	104
Figure 4.11. Oleic Acid Py-GC-MS Chromatogram	105
Figure 4.12. Stearic Acid Py-GC-MS Chromatogram.....	106
Figure 4.13. GC-MS chromatogram for <i>Nannochloropsis</i> sp.pyrolysed at 500 °C.....	107
Figure 5.1. Van Krevelen diagram for micro and macroalgae feedstock and HTL derived algal bio-crudes	113

Figure 5.2. Run 5 GC/MS profile at 300 °C for the liquefaction treatment of <i>Arthrospira platensis</i> with hydrogen atmosphere	114
Figure 5.3. Bio-crude yields with varying HTL final reaction temperature.	116
Figure 5.4. Fatty Acids (a) Oleic acid and (b) Stearic Acid	118
Figure 5.5. Protein Fractions, (a) Soybean protein isolate and amino acids (b) L-Leucine and (c) L-Glutamine	119
Figure 5.6. Carbohydrate Fractions, (a) Glucose, (b) starch from corn and (c) cellulose.....	119
Figure 5.7. Product yields from the HTL treatment of algae and model compounds.....	120
Figure 5.8. Van Krevelen plot H/C vs O/C for algae and model compound feedstock and HTL bio-crudes.	122
Figure 5.9. GC-MS chromatograms for the bio-crudes formed from the HTL treatment of <i>Nannochloropsis</i> sp. (A), the model compounds: soy protein (B), oleic acid (C) and glucose (D) alongside a softwood fast pyrolysis oil (E) for comparison.	125
Figure 5.10. ¹³ C NMR spectra of bio-crudes from (A) Glucose, (B) Microalgae - <i>Nannochloropsis</i> sp., (C) Soy Protein, (D) Pyrolysis Oil, (E) Oleic acid.....	129
Figure 5.11. PENDANT ¹³ C NMR spectra of the HTL bio-crudes from the model microalgae and model compound treatment with a fast pyrolysis oil for comparison, (A) Glucose, (B) <i>Nannochloropsis</i> sp., (C) Soy Protein, (D) Pyrolysis oil and (E) Oleic acid.....	135
Figure 5.12. 2D HSQC NMR spectra for the HTL bio-crudes produced from <i>Nannochloropsis</i> sp. (green), Glucose (blue), Soy protein (pink) and oleic acid (red).	140
Figure 5.13. Highlighted Area 1 (Aliphatic region) from Figure 5.13, for the HTL bio-crudes produced from <i>Nannochloropsis</i> sp. (green), Glucose (blue), Soy protein (pink) and oleic acid (red).	141
Figure 5.14. Highlighted Area 2 (Aromatic region) from Figure 5.13, for the HTL bio-crudes produced from <i>Nannochloropsis</i> sp. (green), Glucose (blue), Soy protein (pink) and oleic acid (red).	142
Figure 5.15. Full 2D HSQC NMR spectra comparison of <i>Nannochloropsis</i> sp. biocrude (green) and fast pyrolysis oil (orange).....	143
Figure 5.16. HSQC NMR spectra of soft wood fast pyrolysis oil with assignments of each carbon in levoglucosan.	144
Figure 6.1. GC-MC pyrolysis chromatograms of <i>Nannochloropsis</i> sp. pyrolysed with Pd/C (A), Pt/C (B) and Ru/C (C).....	149
Figure 6.2. Pyrogram of glucose pyrolysed with Ru/C catalysts at 500 °C.....	150
Figure 6.3. Pyrogram of soy protein pyrolysed with Ru/C catalysts at 500 °C.....	151
Figure 6.4. Pyrogram of oleic acid pyrolysed with Ru/C catalysts at 500 °C.....	152

Figure 6.5. Van Krevelen diagrams of raw algal feedstock, HTL bio-crude and upgraded oil products. (a) H/C vs O/C (b) H/C vs N/C.....	158
Figure 6.6. Total ion chromatogram from bio-crude (a) and selected upgraded bio-oils from the supercritical water upgrading with Pt/C catalyst (b), NiMo/Al ₂ O ₃ (c) and Pd/C catalyst (d).	161
Figure 6.7. PENDANT ¹³ C NMR spectra of the HTL bio-crude (d) with the SCW treated oils by HZSM5 (a), Pd/C (b) and Pt/C (c).	163
Figure 6.8. Superposition of the total 2D HSQC NMR spectra for the HTL bio-crude (green) and SCW upgraded oils with the catalysts Pd/C (blue), Pt/C (orange) and HZSM5 (red).	164
Figure 6.9. Superposition of the 2D HSQC NMR spectra for the HTL bio-crude (green) and SCW upgraded oils with the catalysts Pd/C (blue), Pt/C (orange) and HZSM5 (red).	165
Figure 7.1. Block diagram for the overall microalgae HTL conversion process to transportation fuels.	168
Figure 7.2. Aspen process flow diagram for the hydrothermal liquefaction process.....	170
Figure 7.3. Aspen plus process flow diagram for the bio-crude hydrotreating block.....	172
Figure 7.4. Installed plant equipment cost from the major processing zones.	183
Figure 7.5. Breakdown of total operating costs (OPEX).	184
Figure 7.6. Tornado plot showing the effects of selected sensitivities with respect to the £/l of the MFSP.....	186
Figure 7.7. Effect of the plant capacity on the minimum fuel selling price (MFSP).	187

Chapter 1 - Introduction

1.1. Background

Today, fossil-derived fuels and energy are a constant source of discussion, with many forecasting that natural reserves will 'run out' towards the end of the century. It is widely accepted that we are now at a tipping point, the beginning of the end of cheap fossil fuels. Many factors affect the price of carbon fossil resources (oil, gas and coal), including the reduced productivity of previously high yielding oil fields, increased demand and geopolitical issues. Oil companies now have to employ more complex and, therefore, more expensive extraction techniques/technology in order to keep up with demand and an ever-increasing, more affluent global population.

There is also now a greater emphasis and somewhat global desire to control and, if possible, reduce emissions to tackle issues surrounding global warming and climate change. Presently, issues surrounding climate change are daily, whether in the news, in the products we consume and, for some, in our everyday choices. Our very presence and activities contribute to climate change, and, for many, a moral obligation is felt, compelling them to reduce their effect on the Earth's atmosphere and ecosystems. Human influences on climate change are often referred to as global warming.

Global warming is a very real threat; it is estimated that human influence is extremely likely (90-100% certainty) to have been the dominant cause of the observed warming of the atmosphere and oceans since the mid-20th century [1]. Greenhouse gases contributed to a global mean surface warming, likely (66-100% certainty) to be in the range of 0.5 °C to 1.3 °C over the period of 1951 to 2010 [1]. Greenhouse gases include: CO₂ (carbon dioxide), CH₄ (methane), N₂O (dinitrogen monoxide), and fluorinated gases.

The adoption of the 2015 Paris Agreement was a landmark moment. The international accord, which was signed by almost every nation on Earth, aims to address climate change and its negative impacts. The agreement provides a framework for global climate action which includes climate change mitigation, adaptation and finance. In 2008 the UK introduced a domestic climate change act which legislated that "the net UK carbon account for the year 2050 is at least 80% lower than the 1990 baseline" [2]. Following the Paris Agreement in 2019 the UK Government increased their target to 100% (net-zero emissions) by 2050 [3].

The impacts of global warming are numerous and the potential future effects from an increase in global temperature are hard to predict due to the complex relationships between all aspects of the Earth's environmental mechanisms and ecological systems. Some common climate change risks as global temperatures rise are: an increasing risk of extinction of many species; lower crop yields and, finally, increased sea levels, meaning millions more people potentially exposed to flooding [4].

There are two major solutions to combat global warming. Firstly, reduction in the emissions that contribute to the warming of the planet and secondly, stopping deforestation. Reducing emissions represents the most significant pathway in the fight against global warming. Reducing greenhouse gas emissions can be at a personal level but equally from a wider business and governmental position.

Over a quarter of the total energy demand worldwide is from the transportation sector where liquid fuels are ubiquitous and represent the predominant form. There already exist many renewable technologies that can produce clean energy but there are still issues surrounding the production of sustainable and renewable liquid fuels and chemicals from biomass. Figures from 2012 show that the transportation of people and freight accounts for approximately 25% of total global energy demand, passenger transportation from light-duty vehicles accounts for the largest proportion of this figure (45%), consuming more than all freight movement combined [5]. The rise of electric vehicles is likely to play a significant role in the reduction of emissions from the transportation sector but are currently unable to match liquid hydrocarbon energy density. For example hydrocarbon fuels such as diesel, gasoline and kerosene have typical energy densities of ≥ 33 MJ/l (volumetric) and ≥ 44 MJ/kg (gravimetric) whereas current best technology in lithium ion energy densities for electric vehicles are 500-700 Wh/l (≈ 1.8 -2.5 MJ/l) [6].

It is clear that there is still a requirement for liquid fuels especially in larger-scale transportation sectors such as freight and air travel. Biofuels represent a potential solution but there are a number of factors to be considered in order to produce marketable and sustainable liquid bio-based fuels. They need to be sustainably produced, be based on an abundant and non-food source feedstock, ability for incorporation into the existing multi trillion dollar hydrocarbon infrastructure and be able to conform to all current regulations on fuel specifications and standards.

Biofuels can in essence be divided into three major categories: solid, liquid and gas much like their fossil derived counterparts. It is liquid bio-fuels that are currently attracting a lot of attention from industry and academia as these, after some refining can be used in existing transportation platforms as fuels with little modification to existing technology and infrastructure [7].

For many years first-generation biofuels have been successfully produced from feedstocks that are mainly derived from crops grown for human consumption such as sugar cane, maize and rapeseed among others. This is now seen as unworkable as competing with food stocks will inevitably lead to food shortages, competition for water supplies and contribute to deforestation [8].

Second-generation biofuels attempted to address some of these issues, they are derived from lignocellulosic (plant dry matter) and are obtained from the by-products of food crops and forestry waste (waste biomass) as well as crops specifically grown for conversion (energy biomass). Similarly to first-generation bio-fuels these second-generation bio-fuel feedstocks whilst using waste products and non-food feedstocks also require large amounts of arable land, water and fertilisers for the cultivation of crops specifically grown for energy biomass. These second-generation biofuels can therefore not be considered as the solution to a sustainable and renewable source of liquid biofuels, they can at best support other processes through the utilisation of waste products.

It is clear that for truly sustainable production of biofuels an alternative feedstock is needed that does not compete with the cultivation of food crops. It is now thought that third-generation biofuels, derived from micro and macroalgae could represent a potential solution.

Microalgae are very primitive plants, lacking roots, leaves and stems, the majority are unicellular organisms measuring less than half a millimetre. A microalgae's function is energy conversion, they absorb sunlight, assimilate carbon dioxide from the air and nutrients from their surroundings. Microalgae produce large amounts of lipids when compared to macroalgae. Microalgae grow very rapidly and can be harvested almost daily; with exponential growth rates, some species can double their biomass in as little as 3.5 hours [9]. They can be grown in facilities sited on waste or marginal land and therefore are not in competition with food production as they do not require agricultural land.

They can also be used in the treatment of wastewater, environmental remediation and carbon sequestration from heavy industry - 1kg of algae can fix 1.8kg of CO₂ [10]. They are also commonly grown for extraction of high-value products such as dietary supplements and pigments. As microalgae can be grown continuously their oil productivity greatly surpasses that of traditional terrestrial oilseed crops such as rapeseed, with proposed bio-diesel yields of 12,000 l/ha compared to 1190 l/ha respectively [11].

Microalgae based biofuels have before now been commercialised, these are based on microalgae grown for lipid content, subsequent extraction and transesterification to biodiesel. This process is an expensive pathway due to the high costs associated with highly controlled algae cultivation,

harvesting and dewatering processes, added to this is the accompanying slow growth rates caused by nitrogen starvation necessary to produce lipid contents high enough for extraction and transesterification. Average lipid contents of microalgae are in the region of 1-40% [12], levels higher than 40% are normally achieved under nutrient limitation, in such cases the lipid content can reach values of up to 85% of the dry weight [13].

A potential solution to reduce the cost of producing biofuels from algae is in the application of thermochemical treatment of the whole algae cells, enabling the utilisation of fast-growing algae which are able to produce the most biomass in the shortest time. Once harvested both micro and macroalgae have high water contents, in order to use conventional and well-developed methods of thermochemical treatments such as pyrolysis and gasification the algae would first need to be dried, introducing large energy requirements for the drying process [7]. An alternative option is a process known as hydrothermal liquefaction (HTL) which is able to process wet biomass slurries directly with no need for a drying stage. A biorefinery process centred on HTL processing is presented in **Figure 1.1**.

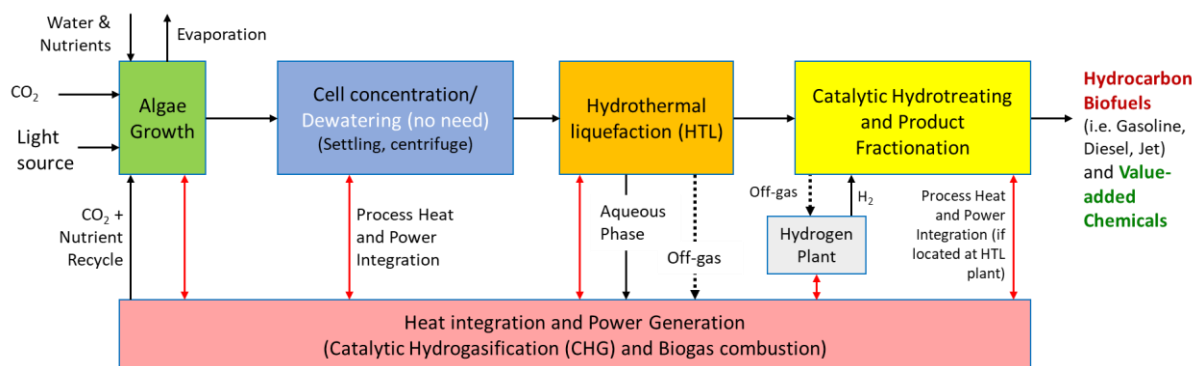


Figure 1.1. Schematic PFD of the HTL Process for Microalgae

HTL has a number of advantages, processing the whole algae leads to bio-crude yields above the initial lipid content, recovery of essential nutrient for algal growth to the aqueous phase, single-step process with no drying of feedstock, water which acts as the solvent and reactant is abundant and non-toxic. The resultant bio-crude product from the HTL treatment of algae is a very complex liquid, with relatively high amounts of heteroatom content in particular nitrogen from the conversion of algal proteins. As a result, a significant amount of refining and upgrading of the bio-crude is required to transform it into a useable transportation fuel that will meet current and future fuel specifications and standards. An investigation of catalytic upgrading of raw HTL bio-crude from microalgae is presented in **Chapter 6**, the techno-economic considerations for bio-crude upgrading are discussed in **Chapter 7**.

1.2. Aim and objectives

The aim of this PhD research project was to study the hydrothermal liquefaction of microalgae with subsequent catalytic upgrading of HTL-derived bio-crudes.

The measurable objectives for the carried out research included:

- In-depth, comprehensive literature review to identify gaps in knowledge that the PhD research project could address.
- Characterisation of macro- and microalgae feedstock using a wide range of analytical methods, including elemental analysis, thermogravimetric analysis and analytical pyrolysis.
- Selection of the most promising algal feedstock for hydrothermal processing based on outputs from applied characterisation methods.
- Setting up and testing high-pressure, high-temperature batch reactors for HTL processing and catalytic upgrading work, meeting all Health and Safety requirements.
- Hydrothermal liquefaction trials with selected algal feedstock with different process parameters to optimise the yields of bio-crudes produced for the subsequent catalytic upgrading.
- Screening commercially available catalysts (using the analytical pyrolysis methods) to establish potential thermal degradation products forming bio-crudes.
- Catalytic upgrading of HTL algal bio-crude in order to produce bioliquids with improved fuel characteristics.
- Application of advanced NMR spectrometry methods for in-depth characterisation of generated bio-liquids
- Technoeconomic assessment of proposed algal biorefinery process with the utilisation of research outputs from the experimental laboratory work and available literature data.

1.3. PhD thesis structure

Chapter 1 gives the general introduction to the PhD research project subject highlighting the importance of biofuels production from algae-derived bio-liquids through the hydrothermal liquefaction route. The PhD research project aim and objectives are presented in this chapter, along with listed research outputs up-to-date disseminated from the project.

Chapter 2, after the presentation of algae cultivation and their biochemical composition, presents biomass conversion technologies, followed by the current literature review related to the production

of liquid fuels from algal biomass, specifically via hydrothermal liquefaction and chemical upgrading routes towards bio-liquids or value-added chemicals.

Chapter 3 gives a detailed description of analytical protocols used for the characterisation of feedstock (model compounds, micro- and macroalgae) and catalysts, bio-crudes produced from hydrothermal liquefaction experiments and bio-liquids from catalytic upgrading studies. This chapter also gives a methodology for the application of high-pressure, high-temperature stirred batch reactors used for liquefaction and catalytic upgrading studies.

Feedstock characterisation with the application of different analytical methods, including elemental and thermogravimetric analyses along with analytical pyrolysis, is presented in **Chapter 4**. Revised and discussed results from the feedstock characterisation studies were used for the selection of the algal sample for further hydrothermal liquefaction studies.

Chapter 5 presents and discusses results from the preliminary HTL experiments with a 25 ml batch reactor and larger-scale processing of model components and microalgae in a 300 ml batch reactor. This chapter also reports the in-depth characterisation of produced bio-crudes with the utilisation of gas chromatography-mass spectrometry and one- and two-dimensional NMR spectroscopy methods.

Firstly, **Chapter 6** reports the screening of commercially available catalysts for potential application in upgrading studies of HTL-derived bio-cruds. The second part of this chapter focuses on reporting catalytic upgrading experiments with the application of a 50 ml high-pressure, high-temperature batch autoclave. This chapter is concluded with the presentation and discussion of product yields and full characterisation of upgraded bio-crude.

A techno-economic assessment of a microalgae biorefinery concept is presented in **Chapter 7**. This concept, utilising HTL as the thermochemical conversion route, was assessed by applying process modelling software (Aspen plus) to generate mass and energy balances. The results from the modelling were used to conduct the techno-economic assessment of the proposed process, with targeted calculations to determine the minimum fuel selling price.

Chapter 8 discusses the met research objectives and summarises the contribution to the subject research's knowledge. Presented in this chapter conclusions were withdrawn from the reported and discussed research work in chapters 4-7. This chapter also reflects on the limitations of the research carried out during the PhD project and explores implications for future research.

1.4. Dissemination of research outputs

Research findings from this PhD were presented throughout the duration of the project and are listed in section 1.4.1. Planned dissemination, including two peer-reviewed research papers, are listed in section 1.4.2.

1.4.1. Up-to-date disseminated items

C.M. Thomas, D.J. Nowakowski, G. Griffiths and A.V. Bridgwater; *Hydrothermal liquefaction of algal feedstocks*; 2nd International Conference on Marine Biomass as Renewable Energy; Glasgow, 5-6 March 2018. [conference oral presentation]

C.M. Thomas, D.J. Nowakowski, G. Griffiths and A.V. Bridgwater, *Hydrothermal Liquefaction of Algae*; 26th European Biomass Conference and Exhibition - EUBCE 2018, Copenhagen (Denmark), 14-17.05.2018. [conference poster]

C.M. Thomas, D.J. Nowakowski, G. Griffiths and A.V. Bridgwater, *Assessment of algal feedstock for production of fuels and value-added chemicals by Py-GC-MS*; 22nd International Symposium on Analytical and Applied Pyrolysis, Kyoto (Japan), 3-8.06.2018. [conference poster]

C.M. Thomas and D.J. Nowakowski, *Application of Py-GC-MS for analysis of thermal decomposition products from algae*; 41st International Symposium on Chromatographic Methods for Investigating the Organic Compounds, Szczyrk (Poland), 19-22.06.2018. [conference oral presentation]

C.M. Thomas and D.J. Nowakowski, *Application of Py-GC-MS for analysis of thermal decomposition products from algae*; Analytix Seminar, Boldon (UK), 28.06.2018. [oral presentation and RSC poster competition]

C.M. Thomas and D.J. Nowakowski; *An investigation into macromolecular reaction pathways in the hydrothermal treatment of microalgal model compounds*; 27th European Biomass Conference and Exhibition - EUBCE 2019, Lisbon (Portugal), 27-30.05.2019. [conference poster]

C.M. Thomas and D.J. Nowakowski; *Characterisation of algal feedstock including catalytic pyrolysis*; International eConference on Analytical and Applied Pyrolysis (ePYRO2021), Ghent (Belgium), on-line conference 12-13.04.2021. [e-conference presentation]

1.4.2. Planned dissemination including peer-reviewed publications

C.M. Thomas, K. Doudin and D.J. Nowakowski, *Characterisation of microalgal HTL bio-crudes and fast pyrolysis liquids by NMR spectroscopy*; 23rd International Conference on Analytical and Applied Pyrolysis, Ghent (Belgium), 15-20.05.2022. [accepted; conference oral presentation]

C.M. Thomas, D.J. Nowakowski, G. Griffiths and A.V. Bridgwater, *Advanced characterisation of upgraded HTL bio-crudes for drop-in transportation fuels*; 23rd International Conference on Analytical and Applied Pyrolysis, Ghent (Belgium), 15-20.05.2022. [accepted; conference poster]

C.M. Thomas, , D.J. Nowakowski and G. Griffiths ; Hydrothermal liquefaction of *Nannochloropsis* sp. with subsequent catalytic upgrading of HTL-derived bio-crudes [drafted; planned submission to the "Bioresource Technology"]

C.M. Thomas, K. Doudin, D.J. Nowakowski – *Investigation macromolecular reaction pathways in the hydrothermal processing of microalgae* [drafted; planned submission to the RSC "Green Chemistry"]

Chapter 2 - Literature review

2.1. Introduction

This chapter provides a review of the current literature related to the production of liquid fuels from algal biomass, specifically via the process of hydrothermal liquefaction (HTL). Firstly algal cultivation and harvesting are discussed, secondly the possible conversion pathways for producing fuels from biomass are outlined. Following this a review of HTL is conducted firstly on a batch scale basis covering the effects of retention time, solvents, reaction conditions, algal species and reactor loading and the application of in-situ catalysts. Next the HTL treatment of microalgae on a continuous basis is reviewed, this is followed by a final review section exploring the options and previous studies centred around the upgrading of HTL bio-crudes.

The starting point for this chapter was the utilisation of some research findings and literature review carried out for the Meng project [14, 15] which this PhD is a continuation of at the same research institution. This literature review also tries to understand the current application of hydrothermal processing methods for algal derived bio-crude production with subsequent catalytic upgrading as well as to identify gaps in the research.

2.2. Algae Cultivation

Micro and macroalgae are two very different types of aquatic plants, macroalgae (seaweeds) are multi-cellular plant-like aquatic organisms, they have much higher photosynthetic activities when compared to terrestrial biomass sources, 6-8% and 1.8-2.2% respectively [6]. They are easier to harvest (every 3-6 months) than microalgae and contain higher amounts of carbohydrates. Whereas microalgae are very primitive plants, lacking roots, leaves and stems, the majority are unicellular organisms measuring 0.4 mm in diameter or less. A microalgae's function is energy conversion, they absorb sunlight, assimilate carbon dioxide from the air and nutrients from their surroundings. Microalgae produce large amounts of lipids when compared to macroalgae. Microalgae grow very rapidly and can be harvested almost daily; with exponential growth rates, some species can double their biomass in as little as 3.5 hours [9].

This section will focus on the cultivation of microalgae as this is where the majority of the current research regarding the feedstock used for thermochemical liquefaction of algae resides.

2.2.1. Nutritional Requirements

In order to successfully grow algae on an industrial scale the growth environment needs to be tightly controlled in order to meet as many of the particular requirements of the algae strain to be cultivated as possible. These parameters may include temperature, light and culture media make-up. There are two major types of algae nutritional pathways, autotrophy and heterotrophy. Autotrophy is where the algae obtain all the growth materials they need from inorganic compounds whereas conversely heterotrophs are algae which need organic compounds in order to grow, these organic compounds are synthesised by other organisms such as bacteria. The group of autotrophs can be further be classified into two groups, photoautotrophs – using light as their source of energy for metabolism and chemoautotrophs – who use electron donors (oxidation of inorganic compounds/ions) as a source of energy. Most algae fall into the photoautotroph category, utilising light in order to reduce CO₂ by the oxidation of inorganic compounds normally water which produces oxygen [12].

2.2.2. Photoautotrophic production of algae

At this time photoautotrophic production is the method most frequently used to cultivate algae as it is easy to scale up to large industrial applications, it is also able to utilise the CO₂ contained within waste flue gas as a source of inorganic carbon [16]. There are two main systems that are used in the large scale photoautotrophic production of microalgae, they are open air (raceway ponds) and closed systems (tubular photobioreactors) [9].

2.2.2.1. Open-air systems

Most of the very large commercial systems are based upon open-air systems, also known as open pond systems; they can be split into four major types, large shallow ponds, tanks, circular ponds and raceway ponds. The choice of which type of open pond system to utilise is down to a number of factors, including; land cost, climatic conditions, intrinsic properties of the target algae and cost of water [11]. Raceway ponds are a mature technology and consequently the most common system; they have been used for the mass culture of microalgae since the 1950s [9].

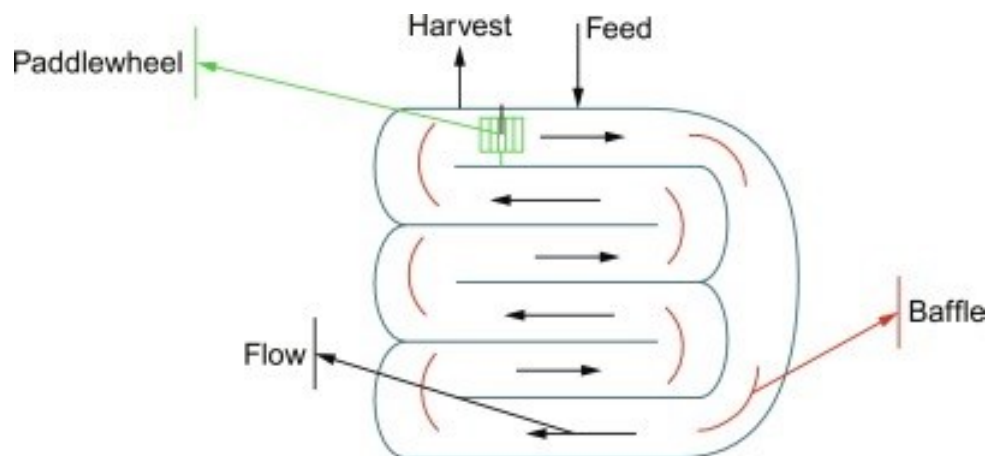


Figure 2.1. Plan view of a raceway pond
Adapted from [9]
 [Public Resource – Image Licence CC BY 4.0]

Raceway ponds are commonly channels of between 0.2 m to 0.5 m in depth, arranged in a loop, shown in **Figure 2.1** [9]. A paddlewheel circulates and mixes the algae and culture medium around the channels, raceway ponds are commonly constructed from concrete and lined with plastic [12]. The algal concentration is inherently low when compared to closed photobioreactors due to a number of factors; the raceways are poorly mixed, temperature fluctuations, evaporative losses and low CO₂ levels among others.

Raceway ponds require very selective environments due to their open to the environment nature in order to protect from contamination from other algae species, bacteria and other protozoa. Therefore only certain algal species are suitable, these include *Arthrospira p. (Spirulina)* which is able to adapt to highly alkaline conditions, *Chlorella* as they are adaptable to nutrient rich culture conditions and finally *D.salina* as they are able to grow in highly saline environments [11].

2.2.2.2. Closed systems

Due to the disadvantages of open systems discussed in the previous section a lot of research effort has been focused on the development of closed tubular photobioreactors [11]. They have been used for a number of years but due to a higher capital cost when compared to open raceways they have not been used for the commercial production of algae until recently [17]. Photobioreactors allow for the production of a monoculture for prolonged durations. They are able therefore to produce algae free from pollution and contamination, particularly important if the algae species is sensitive to contamination from other species or if the algae also contain valuable co-products such as PUFAs and pigments.



Figure 2.2. Medium scale tubular photobioreactor at Varicon Aqua (USA site)
[Public Resource – Image Licence CC BY 4.0]



Figure 2.3. Indoor horizontal tubular photobioreactor at GICON®
[Public Resource – Image Licence CC BY 4.0]

Photobioreactors consist of a number of transparent tubes typically <10 cm in diameter that act as a solar array as shown in **Figure 2.2** and **2.3**. Photobioreactors are able to produce much higher concentrations of algae (4 kg/m^3 vs. 0.14 kg/m^3) when compared to raceways, therefore the tubes need to be kept small in order for sunlight to penetrate through the whole culture [9]. The ideal growth temperature for many algal species is between 20 and 30°C, temperatures exceeding the upper range may damage or kill the cells. As the tubes are exposed directly to sunlight the culture needs to be cooled, this can be provided by simple heat exchangers or by spraying water onto the tubes to facilitate evaporative cooling [18].

Table 2.1. compares a photobioreactor set-up to a raceway pond production method, in both cases to produce 100,000 kg of biomass per year.

Table 2.1. Comparison of photobioreactor and raceway pond production methods
Adapted from [9]

Variable	Photobioreactor facility	Raceway ponds
Annual biomass production (kg)	100,000	100,000
Volumetric productivity ($\text{kg m}^{-3} \text{d}^{-1}$)	1.535	0.117
Areal productivity ($\text{kg m}^{-2} \text{d}^{-1}$)	0.048 ^a 0.072 ^c	0.035 ^b
Biomass concentration in broth (kg m^{-3})	4.00	0.14
Dilution rate (d^{-1})	0.384	0.250
Area needed (m ²)	5681	7828
Oil yield ($\text{m}^3 \text{ha}^{-1}$)	136.9 ^d 58.7 ^e	99.4 ^d 42.6 ^e
Annual CO ₂ consumption (kg)	183,333	183,333
System geometry	132 parallel tubes/unit; 80 m long tubes; 0.06 m tube diameter	978 m ² /pond; 12 m wide, 82 m long, 0.30 m deep
Number of units	6	8

^a based on facility area, ^b based on actual pond area, ^c based on projected area of photobioreactor tubes, ^d Based on 70% by weight oil in biomass, ^e based on 30% by weight oil in biomass.

During photosynthesis oxygen is produced, within a photobioreactor this can be as much as $10 \text{ g O}_2 \text{ m}^{-3} \text{ min}^{-1}$, this increases the levels of dissolved oxygen within the algal culture, high levels of oxygen can lead to photooxidative damage to the algal cells. The oxygen must be removed in a degassing zone, where air is bubbled through the liquid in order to strip out the dissolved oxygen. Carbon dioxide is used as the inorganic source of carbon for autotrophic algae, this can be provided in the degassing section and at injection points along the tubes in order to prevent growth limitations from low levels of available carbon [9].

2.2.3. Microalgal harvesting technologies

It is widely accepted that the economic feasibility of microalgae production lies in the harvesting and dewatering of the algal suspension into concentrated slurries that are suitable to be processed further[12, 16].

The process starts with the harvest of the microalgae culture from the bioreactors, the harvested algae (0.1 g to 2 g of dried microalgae per litre of culture) (0.02-0.06% dry solids [12]) is then concentrated via dewatering techniques. Dewatering can be achieved using a single technique of a combination of

a number of techniques which include: filtration, flocculation, centrifugation, gravity sedimentation, flotation and electrophoresis techniques in order to achieve a final cell concentration of >200 g dry algae per litre of culture (~20 wt.%). At this cell concentration the mixture becomes a thick sludge [16, 19].

Flocculation is an attractive bulk harvesting/dewatering technique due to its low energy requirements. Flocculation only requires the addition of a flocculant (cationic, anionic and non-ionic polyelectrolytes) to the algal culture which causes the algal cells to stick together forming larger agglomerated particles which settle faster and are easier to remove [19].

Following flocculation centrifugation and filtration can be used to further thicken the slurry and decrease the water content; these are usually more energy intensive steps [11]. In all cases the final product from dewatering usually achieves a dry solids concentration of ~20 wt. %, many processes used to convert algae into biofuels need a dry algae feedstock of less than 30 % moisture [20]. To further reduce the moisture content the algae would need to be dried. Drying the algae can account for up to 30% of the total production costs [12]. It would therefore be advantageous if the process used to convert algal biomass into fuels was able to handle algal feedstocks with high moisture content. This would decrease the overall energy demand of the process and could reduce the final cost of the fuels produced.

2.3. Biochemical composition of algae

2.3.1. Chemical composition

When compared to traditional sources of biomass such as terrestrial plant species algae have a very different chemical composition, the main constituents of plants are cellulose, hemicellulose and lignin which in some cases can total in excess of 95% [21]. In contrast, the main constituents of algae are proteins, lipids, waxes and carbohydrates alongside other valuable compounds found in much smaller quantities such as vitamins [22, 23] and pigments [24].

Chemical composition can vary greatly from species to species; some algae can be high in proteins whereas others will have high content of lipids. These intrinsic variations in composition mean that certain species are better suited to certain applications, such as the conversion to biofuels from algae containing a high proportion of lipids to applications such as food supplements and animal feeds from algae containing high amounts of protein and vitamins.

The chemical composition of algae isn't fixed, a number of environmental factors can greatly influence the final composition of the algal biomass. These factors have been widely researched and several key parameters have been identified as key to obtaining an algae product with the desired composition. Large variations in algae composition have been reported by varying; nitrogen and CO₂ levels, pH of the growth medium, temperature, illumination regime and intensity, nutrients and population density [13].

2.3.2. Protein and Amino acids

The high protein content of many microalgae species has attracted a lot of attention in recent decades as an unconventional source of protein for human consumption.

The nutritional quality of protein is determined by its amino acid spectrum, plants are capable of producing all amino acids whereas animals and humans can only synthesise certain amino acids, known as the non-essential amino acids. Therefore, the amino acids that we cannot create ourselves (essential amino acids) must be sourced from food. The essential amino acids are isoleucine, methionine, phenylalanine, leucine, lysine, methionine along with phenylalanine, threonine, tryptophan and valine [12]. *Spirulina* was found to be partly deficient in methionine, cysteine and lysine [22], a characteristic of many plant-based proteins due to these amino acids containing sulphur [12].

2.3.3. Lipids

Algal lipids in recent years have proven to be of considerable commercial value, with the development of modern analytical methods facilitating significant progress in the identification of new classes and lipids and fatty acid constituents in algae [25]. Lipids and fatty acids are present in all types of plant cells their roles are mainly in providing energy reserves and in the structural components of the semi-permeable barriers that encapsulate the assorted cellular organelles (cell membranes). It is also understood that as well as their general compositional role within cell membranes each lipid type has its own unique role and specific biochemical function in regulating the economy of the cell [26].

Algae and higher-plant oil seeds share the same basic pathways for lipid synthesis, where algae differ is their ability to; produce unique long-chain or highly unsaturated fatty acids [12] such as polyunsaturated fatty acids (PUFAs) [25], their fatty-acid composition in response to fluctuations in growth conditions and applied stresses and finally, the oil producing cells within the algae are directly

performing photosynthesis meaning a complete pathway from CO₂ fixation to fatty acid production can be adjusted directly by the cell.

With regards to the production of biodiesel from algae it is the lipids within the algae that are the main contributor to the production of biodiesel. Average lipid contents of microalgae are in the region of 1-40% [12] levels higher than 40% are normally achieved under nutrient limitation, in such cases the lipid content can reach values of up to 85% of the dry weight [13]. Of all the types of lipids produced within the algae it is the non-polar triacylglycerols (TAGs) that are the most suitable substrate for producing biodiesel [13].

Polyunsaturated fatty acids (PUFAs) are high-value molecules, higher-plants and animals aren't able to synthesise PUFAs of more than 18 carbon atoms in length, therefore they must be sourced from their diet. Traditional sources of PUFAs are from fish and their oils, which have come under scrutiny due to the possible accumulation of toxins, their unpleasant smell and taste and unsuitability for those whom exclude animal products from their diets. One PUFA, docosahexaenoic acid (DHA) is the only type of algal derived PUFA; DHA is important for brain and eye development in infants and has been added to infant formula milk. It has also been shown to support cardiovascular health in adults [27].

2.3.4. Carbohydrates

Algae also contain varying amounts of carbohydrates, macroalgae typically have much higher amounts of carbohydrates when compared to microalgae where carbohydrate content can vary greatly from species to species. Certain microalgae strains can accumulate over 50% carbohydrates intracellularly when certain cultivation conditions are met [28].

Like higher plant species carbohydrates are the major products from carbon fixation during the process of photosynthesis. Carbohydrates can be accumulated inside the cells as energy reserves in the form of starch; they are also a main constituent of cell walls in the form of cellulose, pectin and sulphated polysaccharides. As macroalgae have high amounts of carbohydrates there has been a lot of interest in using them as a feedstock in the production of bioethanol. The main sugars (carbohydrates) within brown macroalgae are glucan, mannitol and alginate, glucan and mannitol are easily converted to bioethanol using microbes whereas alginate – a polysaccharide - is not easily metabolised by microbial means and presents a major barrier in the economic conversion of macroalgal biomass to bioethanol [28].

As the carbohydrates present in microalgae are mainly in the form of starch and cellulose, they are much easier to convert to monosaccharides when compared to traditional bioethanol feedstocks containing lignin [29].

2.3.5. Pigments in algae

2.3.5.1. Chlorophyll

There are a great range of very different pigments that can be produced by algae, some are unique to them, and others are shared with plants, bacteria and yeasts. Some of the pigments produced by algae are considered to be commercially important and highly valuable. The pigment chlorophyll is present in all species of algae; five different types of chlorophyll have been found in total through the nine phyla of algae. Chlorophyll-*a* is found in all algae and is the only type of chlorophyll present in cyanobacteria such as *Spirulina* (*Arthrospira*), which contains approximately 0.8-1.5% of the dry weight in both *A. maxima* and *A. platensis*. [22] other species have a mixture of chlorophyll-*a* and chlorophyll-*b* (chlorophyta and euglenophyta), other species of algae can contain the remaining types of chlorophylls: -*c*, -*d* and -*e* [12].

2.3.5.2. Carotenoids

Another group of pigment present in all species of algae are the carotenoids [12], these are responsible for the yellow, orange and red colours seen in some algae species. Carotenoids can only be synthesised by plants, algae and some bacteria and fungi, there are over 700 types of pigments within the carotenoid group. Carotenoids are used as food colourants and as a feed additive in aquaculture (primarily salmon farms) and poultry [30]. There are two main carotenoids that are used commercially today, β -carotene and astaxanthin [27], the latter astaxanthin is responsible for producing the pink/red colouring in the flesh of salmonids as well as crustaceans such as lobsters, shrimps and crayfish [30].

In the year 2000 astaxanthin sold for \sim US\$2500 kg⁻¹ with a worldwide market estimated to be \sim US\$200 million, over 95% of the market uses synthetically derived astaxanthin [30], it was hoped that naturally sourced astaxanthin as a feed for aquaculture would become more popular due to an assumed consumer preference for naturally pigmented salmon. This doesn't appear to be true and demand for natural astaxanthin is not as high as expected. This has been attributed to consumer awareness, many are unaware that the majority of salmon are farmed and fed synthetic pigments. It is hoped that increased consumer awareness or regulations that preclude the use of synthetic pigments/favour the

use of natural products will increase the demand for natural astaxanthin produced from algae as has already happened for the carotenoid β -carotene [31].

The carotenoid β -carotene has a wide range of applications from food colouring agents to additives in cosmetics and in a nutraceutical capacity as a source of pro-vitamin A in food and animal feeds and for its antioxidative properties [32]. The algae *Dunaliella salina* is recognised as one of the best natural sources of β -carotene, the amount of β -carotene accumulated can be as much as 10-14% dry weight when under such stress conditions such as high salinity in the growth medium and high light intensity [12, 32].

2.3.5.3. Phycobiliproteins

Alongside carotenoids many algae species produce phycobiliproteins, accounting for approximately 1% dry weight [12]. Phycobiliproteins are deep-coloured water-soluble proteinaceous accessory pigments which allow the algae to utilise solar radiation more efficiently by almost closing the light-energy gap left by chlorophyll-*a* and the carotenoids [12]. The primary utilisation of these accessory pigments is in natural dyes used in the food, pharmaceutical and cosmetics industries [27].

2.4. Algae species

2.4.1. Microalgae

Microalgae are primitive plants, lacking roots, leaves and stems, the majority are unicellular organisms measuring 0.4 mm in diameter or less. A microalgae's function is energy conversion, they absorb sunlight, assimilate carbon dioxide from the air and nutrients from their surroundings. Microalgae produce large amounts of lipids compared to macroalgae, lipids are favourable for the production of bio-diesel. Microalgae grow very rapidly and can be harvested almost daily; with exponential growth rates they can double their biomass in as little as 3.5 hours. Microalgae species typically have an oil content of around 20-50% (dry weight); 1kg of algae can fix 1.83kg of CO₂, especially pertinent for the improvement of air quality from heavy industries. As microalgae can be grown continuously their oil productivity greatly surpasses that of traditional oilseed crops such as rapeseed, with proposed biodiesel yields of 12,000 l/ha compared to 1190 l/ha [11].

It has been reported that none of the current strains of algae appear to be suitable as a raw material in an economically viable production of biofuels, further work is needed towards both technological advances alongside work towards genetic improvements of algae strains [33]. One species of *Nannochloropsis* (*Nannochloropsis* sp.) has shown to be a haploid alga, amenable to targeted gene

manipulation through the use of homologous recombination [34]. These genetic engineering approaches could be used to further improve the productivity of alga species with the view to making them more economically competitive.

Three species of microalgae are considered in detail within this report, they are *Arthrospira platensis* (commonly known as *Spirulina*), *Nannochloropsis sp.* and *Isochrysis galbana* species used for the purpose of this research project can be observed in **Figure 2.4**.

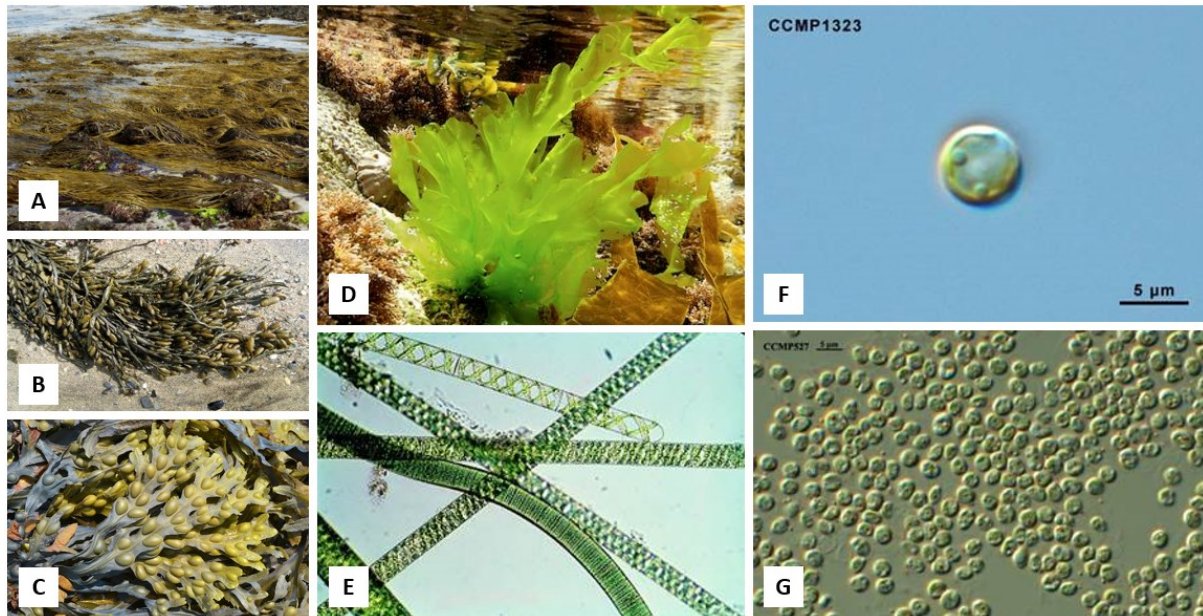


Figure 2.4. Algal species used in this study

A - *Himantalia elongate*; B - *Ascophyllum nodosum*; C - *Fucus vesiculosus*; D - *Ulva lactuca*;
E - *Arthrospira platensis*; F - *Isochrysis galbana*; G - *Nannochloropsis sp.*

[Public Resource – Image Licence CC BY 4.0]

2.4.2. Macroalgae

Macroalgae (seaweeds) are multicellular plant-like aquatic organisms, they have much higher photosynthetic activities when compared to terrestrial biomass sources, 6-8% and 1.8-2.2% respectively [8]. They are easier to harvest (every 3-6 months) than microalgae and contain higher amounts of carbohydrates, ideal for the production of bioethanol. The species of macroalgae considered in this report are; *Himantalia elongata*, *Ulva lactuca*, *Ascophyllum nodosum*, *Fucus vesiculosus* and *Fucus serratus*.

2.5. Previous Work on Biomass Conversion

2.5.1. Algae to bio-fuels conversion techniques

This section outlines the potential routes available for the conversion of algal biomass to various forms of biofuels; many of the conversion processes presented are also used for the conversion of conventional terrestrial biomass. The conversion technologies for algae to biofuels can be separated into two distinct categories, namely; thermochemical and biochemical conversion pathways.

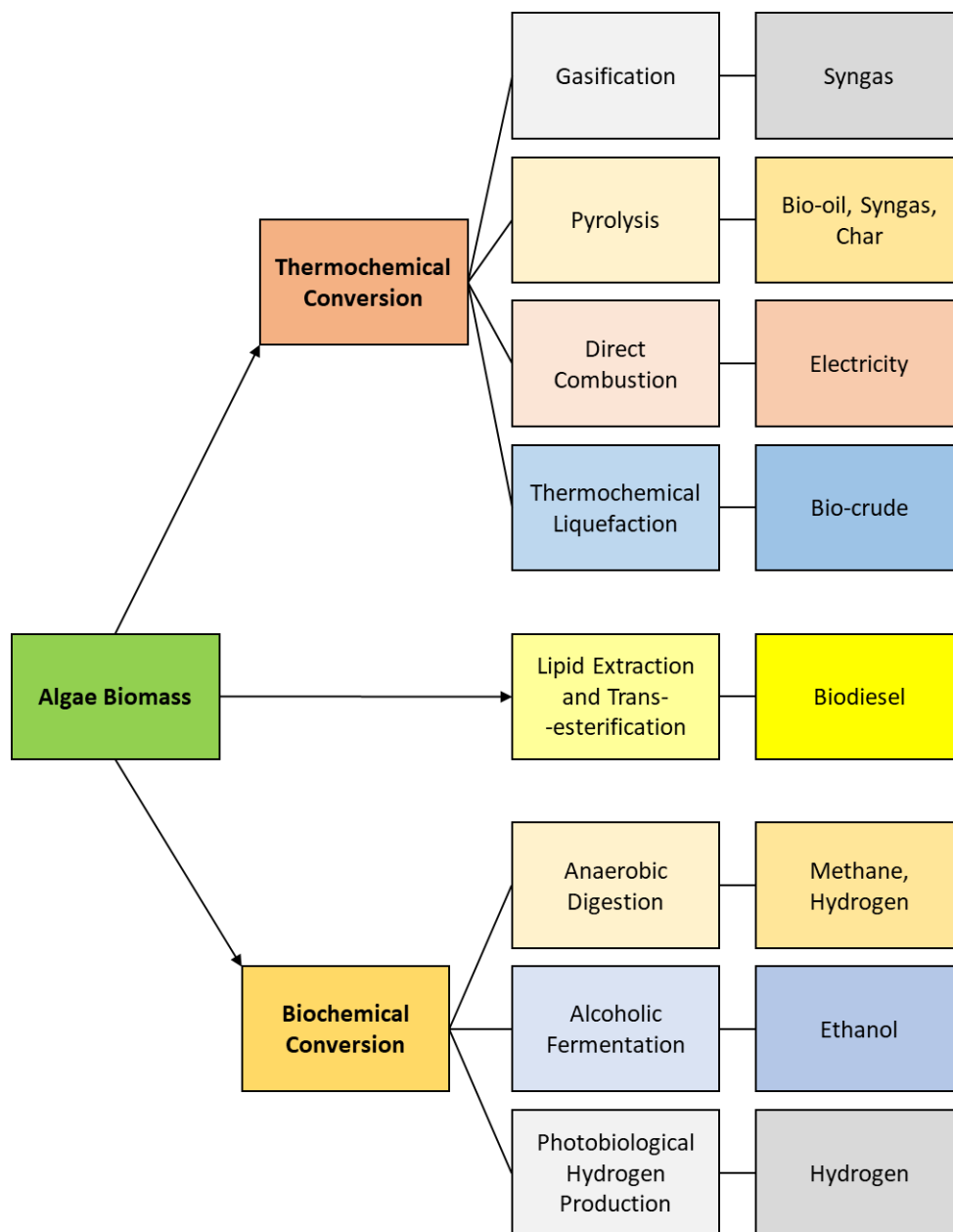


Figure 2.5. Potential algae conversion processes.

2.5.1.1. Thermochemical conversion

2.5.1.1a Introduction

Thermochemical conversion can be subdivided into a number of different techniques, namely liquefaction, pyrolysis, gasification and direct combustion. As demonstrated in **Figure 2.5** each technique produces a certain product. Liquefaction mainly produces liquid products (bio-oil and a nutrient rich aqueous phase); it also produces some gaseous products. Pyrolysis produces solid liquid and gaseous products, the proportion of which depending upon the intensity of the process. Fast-pyrolysis produces more oils whereas slow pyrolysis produces larger amounts of solid residues. As the name suggests, gasification primarily produces a gaseous product, the composition of which depends upon the type of atmosphere the biomass is reacted in. Finally direct combustion is where the biomass is burnt directly and the chemical energy within the biomass converted to electricity through the use of steam turbines.

2.5.1.1b. Liquefaction

Thermochemical liquefaction is carried out in autoclave type reactors on a batch (laboratory scale) or continuous basis, liquefaction is usually carried out at temperatures between 250-350 °C and pressures of 10-20 MPa, in some cases a catalyst and/or a reducing atmosphere can be used to increase bio-oil yields [7]. The reactor feed consists of an algal slurry containing the solid algae and a solvent normally <40 wt.% water. At these elevated temperatures the combined high pressure ensures that the water within the wet biomass substrate remains in the liquid state where it acts as a solvent, although other organic solvents can also be used to increase bio-oil yields [35]. HTL utilises the high water activity present at sub-critical conditions in order to breakdown and reform the biomass into bio-oil. The macromolecules within the biomass are first hydrolysed and/or degraded into smaller more reactive/unstable molecules that can in some cases recombine into new molecules [36].

The resulting bio-crude product has a much higher energy density; this bio-oil can be directly burnt as a raw fuel or further refined into fuel for transportation [11]. The bio-oil is formed alongside a char (solid) fraction, an aqueous fraction and a gaseous fraction. The overall yield of bio-crude from the hydrothermal liquefaction treatment of biomass is greatly dependent on the starting composition of the algae with reaction conditions affecting both oil yields and bio-oil composition and quality. The process of hydrothermal liquefaction is discussed in more detail in Section 2.6.

2.5.1.1c. Pyrolysis

The technique of pyrolysis can be split into two distinct types based upon residence time, fast pyrolysis and slow pyrolysis. Slow pyrolysis produces high amounts of solid residues (coke/charcoal) which in some cases can be used as a solid fuel whereas fast pyrolysis produces a larger quantity of bio-oils, up to 80 wt.% dry feed. Pyrolysis involves converting biomass into a gaseous product which then condenses into three distinct fractions, bio-oil, syngas and charcoal at temperatures ranging from 350-700 °C in the absence of air under much lower pressures (1 to 5 atm) [37] when compared to liquefaction [11]. Pyrolysis of terrestrial biomass has been extensively studied for a number of years and it has been concluded to be a viable pathway for industrial scale production of bio-fuels.

There are a number of essential parameters needed in the fast pyrolysis of biomass, these include: a very high heat transfer rate meaning a dry and fine biomass feedstock is needed, careful reactor temperature control to maintain temperatures between 450-550 °C and finally the pyrolysis vapours must be cooled rapidly to avoid the liquid portion reacting and cracking [37].

Typically, pyrolysis produces two organic liquid fractions following condensation of the vapours, one which is water soluble and one which is not, they also contain far more oxygen than oils obtained through liquefaction. There are also other compositional issues surrounding pyrolysis oils, including: oil acidity (pH ~2.5) [37], stability issues, solid content and chemically dissolved water [11]. Pyrolysis has a lower capital cost than liquefaction and is currently being used commercially whereas liquefaction is not [37].

2.5.1.1c. Gasification

Gasification is a form of pyrolysis [38], where biomass reacts (partial oxidation) with air, oxygen or steam in order to produce a combustible gas mixture, known as syngas or producer gas. Both gas types contain varying amounts of CO, H₂, CO₂, CH₄, and N₂. Producer gas is when the biomass feedstock is reacted with air; it produces a gas with a higher nitrogen content and lower concentrations of the other listed components when compared to syngas [37]. Gasification is performed at very high temperatures, in the region of 800 to 900 °C in order to optimise gas production. Producer gas is of low calorific value, approximately 4-6 MJ/N m³ and is therefore only suitable for combustion to produce electricity or heat [37, 39]. Syngas on the other hand is a more valuable product, used in the production of fuels and chemicals [39], examples of syngas utilisation are in the production of hydrogen by the water gas-shift reaction, methanol via methanol synthesis and alkanes by Fischer-Tropsch Synthesis (FTS) [37].

In order for the gasification process to perform well there are a number of characteristics that the biomass feedstock must have, firstly a low moisture content is vital. Biomass feedstocks having moisture content of 30% or greater are very undesirable, high moisture contents in the feed makes the ignition of the biomass difficult and reduces the calorific value of the product gas. For feedstocks with high moisture contents which needs to be evaporated inside the gasifier before gasification can occur therefore reducing the temperature of the process leading to incomplete cracking and poor product quality (low calorific value). Waste heat from the gasification process (gas turbine) has been successfully used to reduce a willow feedstock from 35% moisture to 15% [20].

The biomass should also have low ash content, high inorganic content (mineral) within the gasifier biomass feed render gasification impossible as it can cause blockages within equipment due to the temperatures present within the gasifier being above the melting point of the ash compounds, producing a solid slag/clinker. Clinker and slag production is particularly problematic when ash content is above 5% in the feed, even more so when the ash has a high salt or alkali oxide content, leading to the production of eutectic mixtures that have low melting points, making them more likely to occur in all gasification regions [20].

The gasification of macroalgae has been studied by Ross et al [40], it was found that typical ash contents of ~10-18 wt.% for 5 macroalgae samples from the British Isles. This value is very high when compared to the ash content values from typical terrestrial energy crops such as Oat straw, *Miscanthus* and willow coppice (6.7, 2.1 and 3.0 wt.% respectively). It was concluded that the dominance of potassium and sodium within the ash content makes macroalgae unsuitable for gasification.

2.5.1.1d. Direct combustion

Direct combustion of fuels is the most widely used conversion process in the world for converting fuels into energy, most commonly through the burning of gas and coal to produce electricity and heat. This can be on a large industrial scale >2000 MW or on a domestic scale with home boilers etc. With respect to biomass feedstocks it is possible to burn any type of biomass providing it has a low moisture content <50%, which for some sources of biomass such as algae would require a pre-treatment process. The biomass would first need to be dried, which adds to the energy demand of the process and increases the overall cost of energy production, because of this biomass with high moisture contents is more suited to liquefaction or biological conversion processes [39].

Direct combustion of an algae feedstock is where the algae is burnt directly with air in order to produce hot gases in the region of 800 to 1000 °C, the hot gases are then used to raise steam to drive steam turbines for electricity production [39]. The electrical production efficiency for a power plant running solely on biomass are in the region of 20 to 40%, higher efficiencies are possible when the biomass is co-combusted in existing large scale coal fired power stations [38].

There is sparse research concerning the viability of direct combustion of algae species, similarly to the technique of gasification the direct combustion of macroalgae are deemed unsuitable due to their ash content, which if used could lead to equipment failure [40].

In the case of microalgae the co-firing of *Spirulina platensis* in a pulverised coal fired power station has been investigated. *Spirulina platensis* was cultivated using the flue gas emitted from the coal fired power plant, the microalgae was harvested and then underwent a thermal pre-treatment technique called torrefaction (mild form of pyrolysis), a process where the algae is heated to between 200 to 300 °C at atmospheric pressure in order to improve the quality of the fuel. After torrefaction the agglomerated algae has a fuel quality close to coal, the torrefied algae can then be blended with coal and pulverised in existing size reduction machinery [41]. It has been summarised that the utilisation of microalgae in the co-firing of coal fired power plants has the potential to reduce greenhouse gas emissions and air pollution through CO₂ sequestration and reduced coal usage [42].

2.5.1.2. Biochemical conversion

Biochemical conversion processes include anaerobic digestion (AD), alcoholic fermentation and lipid extraction.

2.5.1.2a. Anaerobic Digestion

Anaerobic digestion is carried out in large digesters in the absence of oxygen, it is used to produce a gas which is mainly a mixture of methane and carbon dioxide [38]. The gas is produced through the utilisation of bacteria that act to breakdown the raw biomass and directly produce a gas known as biogas; the biogas produced has an energy content of approximately 20 to 40% of the initial feedstock's lower heating value.

In contrast to thermochemical conversion techniques excluding liquefaction, anaerobic digestion can be used for biomass feedstocks that have very high moisture contents, circa 80 to 90% which is particularly applicable to algal biomass even before mechanical drying techniques [39]. Anaerobic digestion is a commercially mature and proven technology, traditionally it has been used to convert

farm and domestic wastes such as animal manure and sewage [38, 43], however, recently interest in the anaerobic digestion of algae has increased. In general microalgae have low carbon to nitrogen ratios (C/N) 4 to 8, it is reported that there is an imbalance between the carbon and nitrogen when the C/N ratio is below 20, the methanogenic bacteria used in the digesters become less efficient due to the release of nitrogen in the form of ammonia, a known inhibitor of bacterial function [43]. One way to overcome this problem is to introduce to the algal feedstock another form of biomass, potential sources include; pig manure[44, 45], cow manure [46, 47] and waste paper[48]. Co-digestion with these sources of biomass all increased the amount of methane produced. In the scenario of adding waste paper to a mixed microalgae feedstock comprising of *Scenedesmus sp.* and *Chlorella sp.*, an optimum algae to paper mass ratio of 1:1 was found to double the amount of biogas produced [48]. Ward 2014 [43]states that anaerobic digestion is a key process in tying together the production of bio-fuels from algae and the treatment of wastewater. Through the use of algae residues from lipid extraction and recycling of the digestate (material remaining after anaerobic digestion) as a nutrient rich growing supplement.

2.5.1.2b. Alcoholic Fermentation

Alcoholic fermentation is the production of ethanol by the fermentation of carbohydrates (sugars, starch and cellulose), the most common feedstock in the production of ethanol from biomass is sugar cane [38]. Fermentation is currently the most used technology in producing bio-fuels. In 2001 the USA produced over 6.6 billion litres of ethanol Brazil's production was almost double at over 11 billion litres [37].

Fermentation is a relatively simple process where the biomass is first ground down/crushed; the starch is then converted to sugars by enzymes. This is then mixed with water (typically 20 wt.% sugar) and yeast and heated to 105-110 °C to reduce microbial contamination it is then kept at 30-38 °C for 28 to 48 hours at pH values of 4-5, typical ethanol yields for sugar cane are 160-190 litres per ton of raw sugar cane [37].

2.5.1.2c. Lipid Extraction

As mentioned previously lipid content within the algae is the major contributor to the yield and quality of the products obtained from the thermochemical conversion processes mentioned. The process of lipid extraction is focused on microalgae; this method is used in the direct production of microalgae biodiesel. Biodiesel is currently produced from oil seed crops, it involves the transesterification of an oil or fat to mono-alkyl esters in order to achieve a viscosity similar to that of diesel derived from fossil

sources [49]. The technology used for producing and using biodiesel from traditional plant and animal oils has been developed and used for over 50 years. The future production of biodiesel from microalgae feedstocks is expected to use the same techniques [9].

The process of lipid extraction and transesterification of microalgae firstly starts with the harvest of the microalgae culture from the bioreactors, the harvested algae (0.1 g to 2 g of dried microalgae per litre of culture) is then concentrated via dewatering techniques. Dewatering can be achieved using a combination of a number of techniques including filtration, flocculation and centrifugation in order to achieve a final cell concentration of >200 g dry algae per litre of culture (~20 wt.%). At this cell concentration the mixture becomes a thick sludge, flocculation is the most attractive dewatering technique due to its low energy requirements. Flocculation only requires the addition of a flocculant (cationic, anionic and non-ionic polyelectrolytes) to the algal culture which causes the algal cells to stick together forming larger agglomerated particles which settle faster and are easier to remove [19].

The concentrated algal sludge is in most cases then pre-treated, pre-treatment is performed in order to increase the effectiveness of downstream processes such as lipid extraction. Cell disruption is one form of pre-treatment, this is where the cellular structures of the algae are ruptured which forces the release of lipids contained within the cells into the bulk of the mixture, the resultant product is known as disrupted concentrate. This can be further pre-treated through drying and milling to fine powders in order to improve the amount of lipid able to be extracted [19].

There are a number of different methods used in the extraction of lipids from algae, pressing, solvent extraction and supercritical fluid extraction [49]. The most common method is where an organic solvent (typically hexane) is added to the pre-treated algae where it extracts the lipids from within the cells [19]. Pressing the algae to extract the oil can yield approximately 70-75% of the oils in the algae whereas supercritical fluid extraction using supercritical carbon dioxide which acts as a solvent can achieve almost 100% oil extraction [49].

Post lipid extraction the resultant stream is a mixture of extraction solvent, water (in the case where the algae feedstock is a slurry/undried), extracted lipids (oils) and cell debris alongside untreated algae. The solid fraction (cell debris etc.) within the mixture is separated (filtered/centrifuged); this can be sent to anaerobic digestion units. The solvent and any water is then stripped from the mixture using liquid-liquid extraction techniques such as distillation or vacuum evaporation, thus leaving behind the lipid fraction [19].

The lipids are then subject to transesterification shown in **Figure 2.6**, this is the reaction of the esters (lipids) present such as triglycerides with an alcohol, normally methanol due to its low cost in the

presence of an acid (H₂SO₄) or base catalyst (normally KOH) at a concentration of about 1% by weight of oil [9]. Other alcohols can also be used, with ethanol and 2-propanol producing biodiesels with better fuel characteristics [37]. Alkali catalysed transesterification is carried out on a batch basis at approximately 60 °C (boiling point of methanol is 65 °C) and at atmospheric pressure, the reaction takes approximately 90 minutes [9].

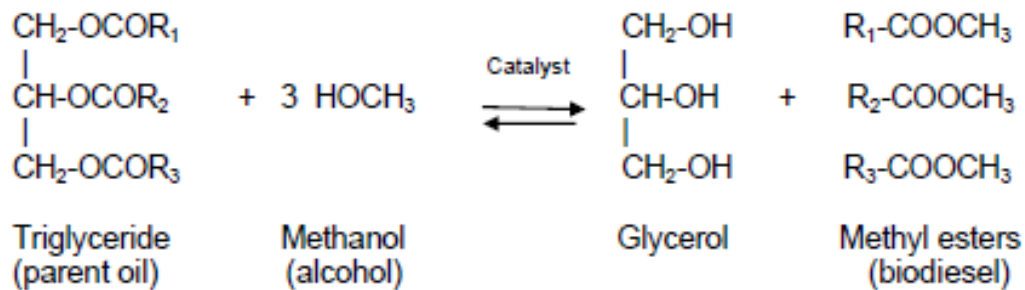


Figure 2.6. Transesterification of oil to biodiesel, R₁₋₃ are hydrocarbon groups
Adapted from [9].

Transesterification produces fatty acid methyl esters (FAME) known as biodiesel alongside glycerol. The resulting mixture after transesterification contains a number of contaminants that need to be separated from the biodiesel, these include; glycerol, excess solvent, catalyst and any un-esterified lipid molecules [19].

There are a number of reported advantages of biodiesel over traditional fossil derived diesel fuels, these include: derived from a renewable resource, reduction in harmful exhaust emissions except for nitrogen oxides, biodiesels also have higher flash points which make them safer to handle and transport. When biodiesels are blended with petroleum derived diesels they act to reduce amount of CO, particulates and hydrocarbon emissions [37].

2.6. Overview of hydrothermal liquefaction of algae

2.6.1. Hydrothermal liquefaction theoretical background

Hydrothermal Liquefaction (HTL) is a thermochemical conversion process commonly used in the treatment of intrinsically wet organic feedstocks. The process utilises an aqueous material such as water as both the transport medium and the reaction solvent, acting to bring about chemical changes in the biomass structures. The use of water has a number of key advantages, it is ubiquitous in all but the harshest environments and therefore inexpensive, it is also environmentally benign. During HTL there are hundreds of simultaneous and competing reactions, in order to cause chemical disintegration of the biomass' macromolecular structures the activation energies of a range of chemical bonds needs to be overcome. To provide the energy required, HTL processing is conducted at elevated temperatures. To deliver the most energy possible to the reaction whilst also maintaining the reaction in the liquid phase processing is conducted at raised pressures to suppress vaporisation of the water and thus prevent the energy losses associated with the latent heat of vaporisation. Typically, HTL processing is carried out at temperatures and pressures approaching the critical point of water. At these extreme conditions the properties of water change dramatically.

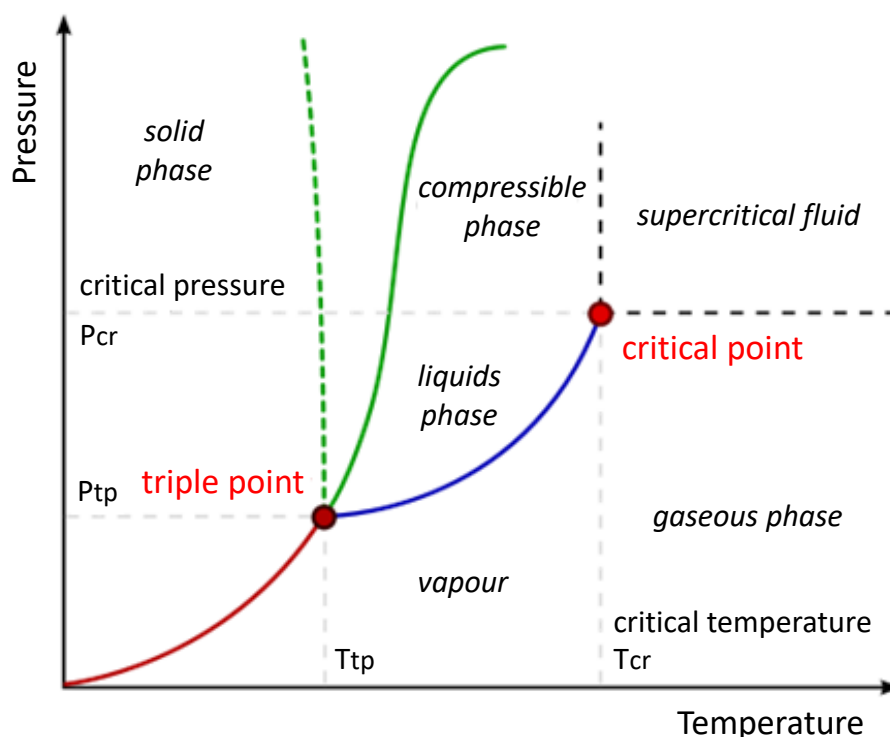


Figure 2.7. Phase diagram of water T_{cr} = critical temperature (374 °C), P_{cr} = critical pressure (221 bar)
Reproduced from [50]

As shown in **Figure 2.7**, below the critical point water can exist as vapour and liquid, above the critical point (374 °C and 221 bar) water exists as one phase known as supercritical water. With respect to HTL, treatment of biomass in hot compressed water at subcritical conditions approaching its critical point imparts useful characteristics related to its role as both a solvent and a reactant. At these conditions the dielectric constant is dramatically reduced from a value of 78.5 at ambient conditions to a value of approximately 9 [51] at the 370 °C phase boundary, this is comparable to dichloromethane at ambient conditions. This is due to the weakening of the hydrogen bonding network between water molecules, decreasing the polarity of water. This decreasing polarity allows for the dissolution of an increasing number of non-polar molecules as temperatures rise during processing. When the desired residence time has been reached the temperature and pressure of the reaction medium can be lowered to allow for the polarity of water to increase which allows for the spontaneous separation of the non-polar compounds from the reaction mixture.

2.6.2. HTL processing modes

2.6.2.1. Batch processing

Usually in laboratory settings studies, hydrothermal liquefaction is carried out in autoclave type reactors on a batch (laboratory scale) or continuous basis at temperatures between 250-350 °C and pressures of 10-20 MPa. In some cases a catalyst and/or a hydrogen atmosphere can be used to increase bio-crude yields and improve physiochemical properties [7]. Typically the HTL reactor feed consists of an algal slurry containing the solid algae and a solvent (normally >40 wt. % water). At the elevated temperatures and the combined high pressure ensures that the water within the wet biomass substrate remains in the liquid state where it acts as a solvent, although other organic solvents can also be used to increase bio-crude yields [35]. HTL utilises the high water activity present at sub-critical conditions in order to breakdown and reform the algal biomass into bio-crude. The macromolecules within the biomass are first hydrolysed and/or degraded into smaller more reactive and unstable molecules that can in some cases recombine into new molecules [36].

The resulting bio-crude has a much higher energy density than the raw feedstock; this bio-crude can be directly burnt as a raw fuel or further refined into fuel for transportation [11]. The bio-crude is formed alongside a char (solid) fraction, an aqueous fraction and a gaseous fraction. The overall yield of bio-crude from the hydrothermal liquefaction treatment of biomass is greatly dependent on the starting composition of the algae feedstock with reaction conditions affecting both yields and composition and quality of the resultant bio-crude.

Table 2.2. Summary of selected batch HTL literature studies

Feedstock	Reactor Volume	Temperature (°C)	Pressure (bar)	Residence Time (min.)	Co-Solvent	Catalyst	Biocrude HHV (MJ/kg)	Biocrude Yield (%)	Reference
<i>Nannochloropsis sp.</i>	1800 ml	300	60-80	30	Water	Ni/TiO ₂	35	48.23	[52]
<i>Nannochloropsis sp.</i>	100 ml	260-320	40	30	Deionised Water	-	35.92-37.88	39.05-54.11	[53]
<i>Sargassum</i>	100 ml	260-320	40	30	Deionised Water	-	33.63-35.23	3.11-9.49	[53]
<i>Chlorella pyrenoidosa</i>	100 ml	280	6.9	120	Ethanol-Water	-	31.4-32.2	57.3	[54]
<i>Scenedesmus</i>	1.8 L	350	2	60	Dichloromethane	-	29.8	33.6	[55]
<i>Scenedesmus</i>	1.8 L	350	2	60	n-hexane	-	-	31.2	[55]
<i>Nannochloropsis salina</i>	1.8 L	350	1.4	60	Water	-	39.1	44-59	[56]
<i>Galdieria sulphuraria</i>	1.8 L	350	1.4	60	Water	-	36.6-39.9	23-31	[56]
<i>Scenedesmus</i>	500 ml	300	100-120	30	Dichloromethane	-	35.3	45	[57]
<i>Spirulina</i>	500 ml	300	100-120	30	Dichloromethane	-	35.8	31	[57]
<i>Spirulina plantensis</i>	1.8 L	350	20	60	Deionised Water	-	35.27	39.9	[58]
<i>Spirulina plantensis</i>	1.8 L	350	20	60	Deionised Water	Na ₂ CO ₃	36.29	51.6	[58]
<i>Spirulina plantensis</i>	1.8 L	350	20	60	Deionised Water	NiO	38.41	30.2	[58]
<i>Spirulina plantensis</i>	1.8 L	350	20	60	Deionised Water	Ca ₃ (PO ₄) ₂	35.07	34.5	[58]
<i>Nannochloropsis gaditana</i>	10 mL	350	20	15	Dichloromethane	-	37.1	60.0	[59]

<i>Scenedesmus almeriensis</i>	10 mL	350	20	15	Dichloromethane	-	34.4	57.7	[59]
<i>Nannochloropsis sp.</i>	31 mL	350	0.7	60	Deionised Water	-	38.46	35	[60]
<i>Nannochloropsis sp.</i>	31 mL	350	0.7	60	Deionised Water	Pd/C	38.67 ¹	57	[60]
<i>Nannochloropsis sp.</i>	31 mL	350	0.7	60	Deionised Water	Pt/C	39.63 ¹	47	[60]
<i>Nannochloropsis sp.</i>	31 mL	350	0.7	60	Deionised Water	Ru/C	37.61 ¹	50	[60]
<i>Nannochloropsis sp.</i>	31 mL	350	0.7	60	Deionised Water	Ni/SiO ₂ -Al ₂ O ₃	38.38 ¹	50	[60]
<i>Nannochloropsis sp.</i>	31 mL	350	0.7	60	Deionised Water	CoMo/Al ₂ O ₃	38.83 ¹	54	[60]
<i>Nannochloropsis sp.</i>	31 mL	350	0.7	60	Deionised Water	Zeolite	35.38 ¹	45	[60]
<i>Spirulina</i>	1 L	270	250	30	Ethanol-Water	Ni/SAPO-34	31.04	59.85	[61]
<i>Spirulina</i>	1 L	270	250	30	Ethanol-Water	Ni/USY	34.58	59.12	[61]
<i>Tetraselmis sp.</i>	1.2 L	350	-	30	Deionised Water	-	33.3	31.0	[62]
<i>Tetraselmis sp.</i>	1.2 L	350	-	30	Deionised Water - 10% IPA	-	32.9	35.4	[62]
<i>Tetraselmis sp.</i>	1.2 L	350	-	30	Deionised Water- 10% Ethylene Glycol	-	34.4	30.4	[62]
<i>Tetraselmis sp.</i>	1.2 L	350	-	30	Deionised Water - 10% Ethanol	-	34.2	30.7	[62]
<i>Tetraselmis sp.</i>	1.2 L	350	-	30	Deionised Water - 10% Glycol	-	35.3	39.0	[62]
<i>Sargassum Tenerrimum</i>	100 ml	260	40-90	15	Water	-	-	11.5	[63]

<i>Sargassum Tenerrimum</i>	100 ml	280	40-90	15	Water	-	-	16.33	[63]
<i>Sargassum Tenerrimum</i>	100 ml	300	40-90	15	Water	-	-	14.67	[63]
<i>Sargassum Tenerrimum</i>	100 ml	280	40-90	15	Ethanol	-	-	23.8	[63]
<i>Sargassum Tenerrimum</i>	100 ml	280	40-90	15	Methanol	-	-	23.8	[63]

¹HHV values were calculated using The Dulong Formula ($HHV \text{ (MJ/kg)} = 0.338C + 1.428(H - O/8) + 0.095S$) as per data provided by referenced source

Table 2.2 presents a selection of batch studies utilising different process parameters alongside bio-crude yields and calculated HHVs. The up-to-date literature information on the HTL processing highlights a number of key operating parameters that affect the physiochemical properties and overall yield of the bio-crude product. These include reaction time (reactor residence time), final reaction temperature, final pressure, biochemical composition of algae species and slurry loading concentrations, catalysts and finally the reaction atmosphere. These are described in further detail in the sections below.

2.6.2.1a. Reaction temperature

Temperature is widely considered to be the most important influence on the yield and quality of bio-crude, correct temperature selection is essential to ensure that the process is as economic as it can be whilst producing a high yield of quality bio-crude under safe conditions. The effect of altering reaction temperature and found a maximum bio-oil yield of 36.9% at a reaction temperature of 360 °C of microalgae *Dunaliella tertiolecta*, with a reaction time of 30 minutes [64]. For the HTL treatment of a marine microalgae *Nannochloropsis sp* it was shown that a temperature of 350°C produced the highest bio-oil yield of 43%, reaction time 60 minutes [65]. The optimum thermochemical liquefaction conditions for converting *Spirulina platensis* was investigated, it was found that the highest yield of bio-oil (39.9%) was achieved at a reaction temperature of 350 °C, 60 minutes holding time, solids concentration of 20% [66]. Similarly at a reaction temperature of 350 °C it was found that the highest yield of bio-crude (19.3 wt.%) was achieved for the macroalgae *Laminaria saccharina*, reaction time of 15 minutes and a biomass to water ratio of 1:10 [67]. It was also shown that when HTL was performed on *Nannochloropsis sp*. the highest bio-crude yield was ~50% at a temperature of 300°C, reaction time of 20 minutes [68].

The literature review clearly indicates that the maximum bio-crude yield occurs within the temperature range 250-360 °C with a desirable temperature in the region of 300-350 °C for many algae species.

2.6.2.1b. Reaction time

The reaction time is an additional crucial parameter to consider during the hydrothermal liquefaction process. For batch processing this is defined as the length of time that the algae slurry spends in the reactor once the reactor contents have reached the desired temperature. The reaction time has a great effect on the economics of the industrial application, too long spent in the reactor wastes energy, reduces potential production throughput and can affect the quality/composition of the bio-crude

product. A reaction time of 30-60 minutes in the HTL treatment of *Spirulina* is most desirable as it was found that as reaction time increased so did the bio-crude yield up to a maximum time of 60 minutes where the yield of bio-crude started to reduce as the lighter hydrocarbons present in the bio-crude are converted to gaseous products [66]. Lowering the reaction time could dramatically enhance the economical attractiveness of HTL, a reduction in the reaction time would mean that smaller equipment could be utilised, reducing operational costs. It has been shown through previous research that reaction times as low as 5-15 minutes can achieve acceptable yields of bio-crude [66, 67], whilst these short reaction times don't fully realise the bio-crude yield potential of the algae biomass, they may represent a more economically viable production pathway. It was demonstrated that a yield of 40.5% of bio-oil from the HTL treatment of the microalgae *Nannochloropsis sp.* at 300 °C is achieved at a short reaction time of 5 minutes, this increased to 41.9%, 43.8% and 46.6% at reaction times of 15, 30 and 60 minutes respectively [69].

2.6.2.1c. Pressure

The control of pressure in the hydrothermal reaction systems is vital for maintaining a single-phase media i.e. subcritical phase; thereby avoiding large energy inputs needed for phase changes [70]. The reaction pressure is directly related to the solvent density, a solvent with a higher density could be more effective at penetrating biomass and also at accelerating the release of H⁺, both increasing the decomposition/extraction and increasing the stabilisation effect on the liquefaction intermediates, leading to increased bio-crude yields [35, 70]. It was also found that HTL treatment of *Nannochloropsis sp.* under different water densities (pressures) (0.3-0.5 g/mL) at a constant temperature had very little (within experimental error) to no effect on product yields [68].

2.6.2.1d. Algae species and loading concentration

The loading concentration of algae in the form of slurry has an influence on both the yield and the quality of bio-crudes produced; it also needs to be carefully considered as it greatly affects the economics of commercial production. A rule of thumb is to ensure a solids loading be in excess of 15-20 wt.% in order to achieve practical economies. At low concentrations <15 wt% the increased equipment size leading to increased capital costs and the higher water content that needs pumping and treating make the process economically unattractive [71]. The effect of solids concentration (10-50%) was examined on bio-crude yield and established that in the case of HTL treatment of *Spirulina platensis*. the highest biocrude yield was achieved at a solids concentration of 20% [66], agreeing with the recommendation by Peterson et al [71]. It has been shown in the case of the HTL treatment of *Nannochloropsis sp.* the bio-crude yield increased (36 - 46 wt. %) from a solids

concentration of 5 to 35 wt.% respectively. It is likely to be the case that each algae species have individual optimum loading concentrations [68].

Table 2.3 summarises typical composition of common microalgal species studied. It is the lipid content of the algal biomass that produces the bulk of the bio-crude yield. Also proteins and carbohydrates within the algae can be converted and contribute to bio-liquids with bio-crude yields typically 10-15% higher than the lipid content of the algae [72]. This is in contrast to conventional bio-diesel production via lipid extraction and their subsequent transesterification to FAMES.

Table 2.3. Composition of commonly studied microalgae

Microalgae Strain	Protein	Carbohydrate	Lipid
	wt.% (daf)		
<i>Chlorella vulgaris</i> [72]	55	9	25
<i>Nannochloropsis oculata</i> [72]	57	8	32
<i>Porphyridium cruentum</i> [72]	43	40	8
<i>Spirulina</i> [72]	65	20	5
<i>Nannochloropsis sp.</i>	59 [68]	20 [68]	14 [68]
	52.4 [73]	21.9 [73]	14.1 [73]
<i>Chlorella sp.</i> [73]	9.3	13.2	59.9

Spirulina and *Chlorella vulgaris* have very high protein contents and are widely used as food additives and in some cases for their medicinal value [11]. Li, H et al studied the HTL treatment of two microalgae; a high-lipid low-protein species (*Chlorella sp.*) and a low-lipid high-protein species (*Nannochloropsis sp.*). The highest bio-crude yield for *Chlorella sp.* (high-lipid) was 82.9% whereas the highest bio-crude yield achieved from *Nannochloropsis sp.* (low-lipid) was 55%. Not only did the bio-crudes differ in terms of yield achieved but it was also the case that the composition and therefore the quality of the bio-oil differed between the two products. The bio-crude derived from *Nannochloropsis sp.* contained a higher proportion of hydrocarbons, important in high-grade fuels [73]. The composition of the bio-crude can be further tuned through the manipulation of the raw algae's composition which depends greatly on growing condition. High nitrogen and oxygen content in the bio-crude is considered to negatively affect quality, the bio-crude would need to be upgraded in order to render it usable [11].

2.6.2.1e. Catalysts

Duan et al [60] studied the effects of six different heterogeneous catalysts under an inert gas atmosphere (helium) were compared to see the effect on product yield and final composition of bio-crudes during the HTL treatment of *Nannochloropsis sp.* It was found that in the absence of added hydrogen all of the catalysts increased the yield of bio-crude but when hydrogen was present the bio-crude yield showed little sensitivity to the presence of a catalyst. It was proposed that the reason for the catalysts' ineffectiveness in a reducing environment is that the HTL derived bio-crudes produced already had 80% of the C and H atoms from the algae feedstock, therefore giving little scope for the catalyst to increase the oil yields any further. The catalysts did however drastically improve the quality of the bio-crude, reducing nitrogen and sulphur content.

Homogeneous catalysts have also been investigated by Jena et al [66], and these include alkali hydroxides, carbonates, bicarbonates and alkali formates. It was found that Na_2CO_3 increased bio-crude yields by 29.2 wt. % to 51.6 wt. % in the thermochemical liquefaction of *Arthrospira platensis*.

2.6.2.1f. Reaction atmosphere/hydrogen donors

The HTL process can be carried out using a reducing atmosphere or hydrogen donors in order to promote the production of bio-crude. The reducing species act to inhibit the condensation, cyclisation and re-polymerisation of the free-radical (intermediate products) which lead to the formation of char [70]. Hydrogen gas has been shown to be a very effective reducing species, aiding in the stabilisation of aromatic radicals, other effective species include steam, nitrogen, argon and synthesis gas (CO or H_2). The effect of different process gases in the subcritical hydrothermal liquefaction of cattle manure has been studied in detail. It was found that CO was the most effective process gas at increasing bio-crude yields, followed closely by hydrogen, 48.76 wt. % and 44.72 wt. % respectively. It was apparent that reactive gases were more effective than inert gases; N_2 achieved a bio-crude yield of 38.49 wt. % under the same reaction conditions (310 °C, reaction time 15 minutes, manure/water mass ratio of 0.25 and 0.5 mol of NaOH) [74].

It was found that the bio-crude yield increased by >20% during a hydrogenated HTL process (hydrogen atmosphere) from 55.6 wt.% (no catalyst, nitrogen atmosphere) to 78.5 wt.% ($\text{Ni-Mo/Al}_2\text{O}_3$ catalyst and hydrogen atmosphere) in the HTL treatment of *Nannochloropsis salina*. [73]. It is therefore unclear as to how much of an effect H_2 has when used without a catalyst. It has also been reported that the yield of bio-crude from the HTL treatment of *Nannochloropsis sp.* (350 °C, 3500 kPa H_2) is increased in

the presence of a hydrogen (reducing) atmosphere for an uncatalysed system, from 35 wt. % to ~45 wt. % [60].

Hydrogen donor solvents are considered to be a more favourable option for providing a reducing atmosphere [70][43]. It has been shown that bio-crude yields could be significantly increased when organic solvents are used instead of water at 300 °C, reaction time 15 minutes in the HTL treatment of a macro algae *Ulva fasciata*. The use of supercritical (due to lower boiling point) methanol and ethanol as opposed to subcritical water increased the bio-crude yield from 11% (water) to 44 wt. % and 40 wt.% for methanol and ethanol respectively [35].

2.6.2.2. Continuous processing

This section summarises the recent technological underpinning and techniques that have enabled for the recently observed transition from batch to continuous liquefaction processing of algal biomass in order to produce bio-crudes that can undergo further upgrading.

The vast majority of research in the area of hydrothermal liquefaction centres on processing using small batch reactors. In order move our reliance away from fossil derived fuels it is essential to commercialise the production of algae derived biofuels utilising liquefaction, therefore a move to continuous algal processing is essential. Continuous HTL experiments will supply a design basis for techno-economic assessments and life cycle analysis required in order to move technological readiness levels (TRL) further to enable process commercialisation.

A number of researchers have reported on the continuous HTL of algae species [75-81]. There have also been a number of other studies that have reported the continuous processing of other biomass feedstocks, including wood [82-84], corn stover [82], rice bran and sunflower oil [85], distillers grains [86-88], a macroalgae *Saccharina spp.* [89], food waste streams [90] and fungi [91]. The most recent scientific literature presents data from a limited number of continuous liquefaction set-ups. In truth there are only approximately five different designs worldwide reported in the literature that have been used in the conversion of algal biomass. One of the main reasons for so few continuously fed liquefaction studies is in part due to the capital cost of the equipment, due to the high reaction pressures needed necessitating the use of modified HPLC pumps or piston pumps and expensive processing equipment able to handle high pressures at raised temperatures.

Table 2.4 shows that the majority of trials have been undertaken using low algal loadings of below 10 wt.%, this has mainly been due to problems with pumping the algal mixture [77] at such small scales and also due to the formation of blockages downstream of the reactor, specifically around

the pressure reducing apparatus [78]. Some researchers have been able to process algae at loadings of 18-20 wt.% [49, 54], but by far the best processing has been achieved by Elliott et al [76] based at the Pacific Northwest National Laboratory (PNNL) in the United States who successfully process a 34 wt.% algal slurry of the microalgae *Nannochloropsis sp.*

It is apparent that to date only one HTL reactor configuration is reliably able to process algal loadings of above 20 wt. %, that used at PNNL [76], the study by Albrecht et al [80] who processes chlorella at 20.3 wt. % uses HTL reactor configuration located at PNNL. Whilst it has been proved that algal concentration has little impact on the yield the main driver for increasing the concentration of algae in the feed is down to economics of the process as a whole due to the fact that the bio-crude is a low value product, therefore efficiencies need to be made wherever they can be. One such efficiency consideration is in the feedstock delivery, pumping a greater algal concentration will mean that less energy is required per unit volume to heat the slurry, therefore smaller pieces of equipment can be used - reducing the capital costs of the processing equipment.

A number of authors have reported that the minimum fuel selling price of algal derived biofuels is considerably more than fossil derived fuels, in the region of \$2.07/gallon to \$7.11/gallon [92] and \$4.77/gallon [93] and as high as \$10.7/gallon to \$14.1/gallon when seasonal variations in algal growth are taken into consideration [94]. Together these studies draw attention to the fact that the feedstock is the major cost driver when running a liquefaction plant, the cost of the feedstock can account for up to 74 % of the fuel production cost [93]. Collectively these studies outline a critical point; that the cultivation of algae for the sole purpose of producing biofuels via hydrothermal liquefaction is unlikely to be economically viable in the near future. In view of this, other characteristics of algae should be exploited before transforming them into fuels. A number of options exist; HTL could be undertaken on the residues left behind in the production of high value products such as PUFAs [95], pigments [24] and proteins or other products [30, 32, 96] which have all been proven to be economically viable in their own right. Another option would be to use the algae in activities such as carbon sequestration from heavy industry, remediation of heavy metals in waste streams or in the treatment of wastewater, both municipal and industrial.

Using wastewater to grow algae has another advantage in that the algae will be freshwater species, the processing of marine species with their inherently high chloride content due to their growth media can cause chloride stress corrosion on the stainless steels commonly used in the fabrication of reactor vessels and processing equipment [78].

The laboratory-scale continuous hydrothermal liquefaction has a number of key operational units and their individual design challenges. The sections below outline the key unit operations of many of the common features that present the most influence on the success and ease of operation in continuous liquefaction experimental equipment found in the literature.

2.6.2.2a. Pumping

The continuous liquefaction studies used a number of different methods for feeding the biomass slurries through the reactor, they can be split into two distinct categories.

The first category includes the usage of pumps that act directly on the biomass slurries such as; syringe pumps [76, 77, 80, 83], hydraulic metering pump [81, 97], double screw press [75], screw and piston pump combination [78]. These are the type of pump configuration that would be used in a scale-up of the process to a commercial size, a summary report by *Berglin et al* [98] discusses the different options available for industrial scale pumping of biomass slurries, primarily aimed at lignocellulosic feedstocks which are known to be much more difficult to process when compared to microalgal slurries. Berglin et al [98] report that pump manufacturers are very confident that the slurries required for HTL could be pumped at high solids loading and to the required pressures of over 200 barg. With many vendors already having experience at pumping industrial sludges, fibrous materials and pastes to high pressures. As microalgae slurry concentrations of 34 wt. % have already been successfully processed on a small laboratory scale then slurry concentrations of >40 wt. % for an industrial scenario is therefore reasonable [77].

The second category of pumping method for lab scale applications is where a secondary fluid/gas is pressurised, this then acts to pressurise the primary biomass slurry, this has the advantage of keeping the solid particulates away from the moving parts of traditional pumps, this interaction can be problematic due to the very small tolerances found in laboratory scale models. Examples of these used in the literature are the single injector [90] and dual injector systems [87, 97] where High Pressure Liquid Chromatography (HPLC) pumps use water as the service fluid in order to pressurise the injectors, the injectors themselves contain a movable piston that separates the two fluids. A more recent adaptation of this solution is through the use of bottles of highly pressurised nitrogen used as the driving force behind the pistons instead of water pressurised by pumps employed previously, this design means that no expensive pumping equipment is needed and is ideal for laboratory-based trials [79].

Table 2.4. Summary of continuous hydrothermal liquefaction of algae feedstocks

Reactor Set-up	Algae Strain	Reaction Conditions	Algal Loading	Pressure Regulation	Yield	HHV [MJ kg ⁻¹]	Researched by
PNNL Setup 415 ml CSTR flowed by a 270 ml PFR	<i>Chlorella</i>	350 °C, 3000 Psig (207 barg)/LHSV 2.2	14.7 – 20.3 wt. %	Back pressure regulator valve of the gas byproduct	35-71 % normalised	Not stated	Albrecht et al 2016 [80]
190 ml CSTR	<i>Nannochloropsis gaditana</i> <i>S almeriensis</i>	350 °C, 20 MPa, 15 minutes	9.1 and 18.2 wt. % for both species	BPRV with PID controller	NG 50.8 – 54.8 Sa 42.6 – 51.0	36.2-37.3 35.8-36.3	Barreiro et al 2015 [75]
PFR 98 ml, Downsized Facsimile of the one used by Jazrawi [78]	<i>Chlorella</i>	350 °C, 185 barg, 5.8 & 1.4 minutes	10 wt. %	Swagelok KPB backpressure regulator	39.7 @ 1.4 min. 36.8 @ 5.8 min.	32.9 @1.4 min 36.1 @5.8 min	Biller et al 2015 [81]
PNNL Setup 415 ml CSTR flowed by a 270 ml PFR	All are <i>Nannochloropsis sp</i> - Lipid Extracted (Solix LEA) - NB238 - Low Lipid (Cellana LL) - High lipid (Cellana HL)	344-362 °C, 2966 – 3020 psig, LHSV 1.5-2.2	17.00 – 34.42 wt. %	Back pressure regulator valve of the gas byproduct	- 53.2 wt. % DAF - 38 wt. % DAF - 60.8 wt. % DAF - 63.6 wt. % DAF	Not stated	Elliott et al 2013 [76]
2 litre small bore PFR	<i>Chlorella</i> <i>Spirulina</i>	250-350 °C, 150-200 barg, 3-5 minutes	1-10 wt.%	~10 bar downstream pressure control valve PCV (Type 1711 needle valve, Badger Meter Inc., Germany)	Max of 41.7 wt.%	<i>Chlorella</i> 27.9-33.8 <i>Spirulina</i> 28.0-32.0	Jazrawi et al 2013 [78]
Micro scale quartz lined 2 ml PFR	<i>Nannochloropsis sp</i>	300-380 °C, 180 barg, 0.5-4 minutes	1.5 wt. % With 10 wt. % cyclohexane	Back pressure regulating valve	23.12-38.0	36.6-39.3	Patel et al 2015 [77]
Double tube PFR arrangement	Mixture of <i>Chlorella</i> and <i>Scenedesmus</i> grown on municipal wastewater.	300-340 °C, 160-165 barg, 3-7 ml min ⁻¹	5 wt. %	BPRV on the outlet gas	Max 21.9 wt. %	Not stated	Wagner et al 2017 [79]

2.6.2.2b. Reactor design

The continuous liquefaction processing of biomass has used a number of different types of reactors, mainly in the categories of a Continuous Stirred Tank Reactor (CSTR) [75], Plug Flow Reactors (PFR) [78, 79, 81, 83-88, 90, 91, 97, 99], miniature PFRs [77] and a combination of the two reactor types in series [76, 80, 89]. Drawing on the extensive range of sources it is clear that PFRs are the preferred reactor type for laboratory-based trials and are anticipated to be the design chosen for commercial operations.

The reactor design used at PNNL [76] (**Figure 2.8**) uses a 415 ml continuous stirred tank reactor (CSTR) to preheat the algal slurry, once heated to the reaction temperature the slurry then passes through a 270 ml plug flow reactor (PFR). This combination of reactors is very expensive due to the provision of two large reactors and is therefore unexpected to be used widely in the research environment and in industry.

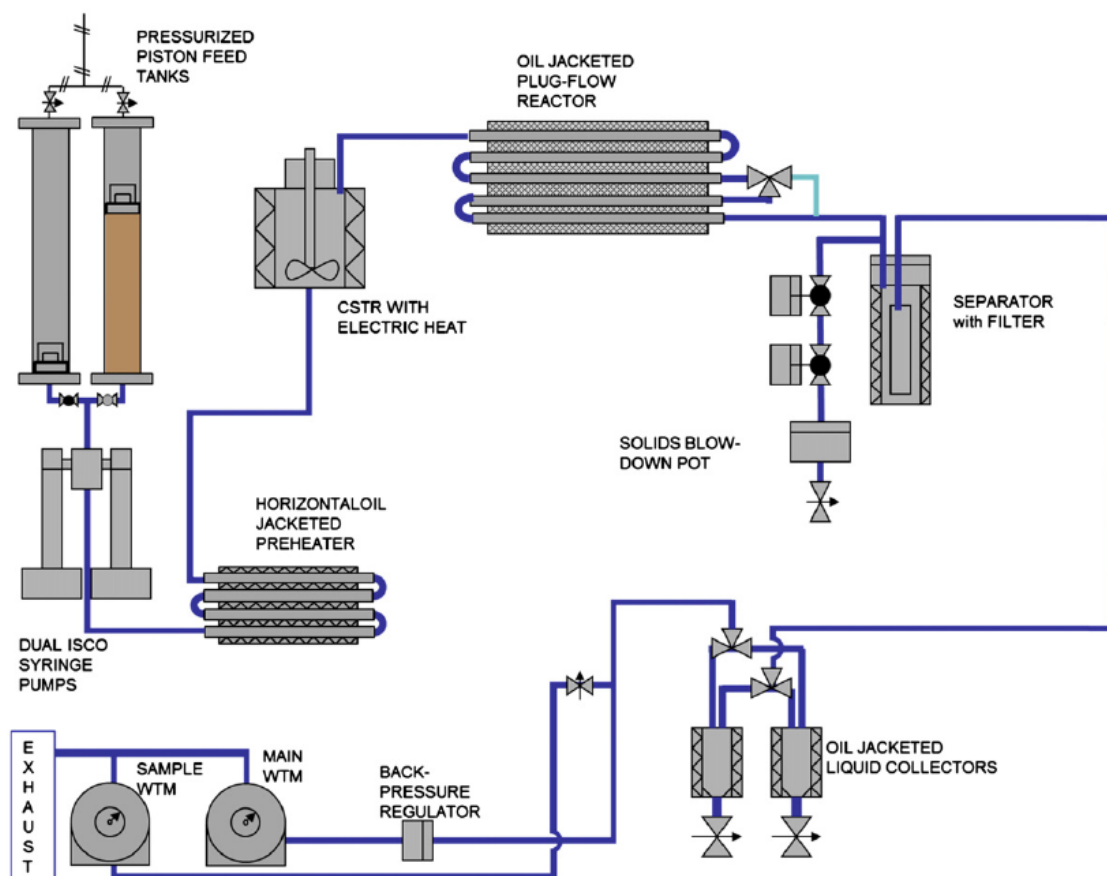


Figure 2.8. Process flow diagram for the HTL series arrangement of a CSTR followed by a plug flow reactor used by Elliott et al

Adapted from [76].

Patel et al [77] provided a novel study where the continuous liquefaction of the microalgae *Nannochloropsis sp.* was studied in a miniature quartz lined PFR of just 2 ml in volume was investigated. A major criticism of this work is the use of very low solids loading of 1.5 wt. % solvent (cyclohexane) at 10 wt.% within the biomass feed, this is in an effort to reduce the amount of char formation.

2.6.2.2c. Reactor downstream pressure regulation

Back pressure regulating valves (BPRV) are commonly used in order to keep the pressure within the reactor constant whilst allowing the products to leave the reactor, they do this by maintaining pressure upstream of themselves. The subject literature [75, 77, 78, 81] indicates that the back pressure regulating valves have been fitted directly to the exit stream of the reactor, the disadvantage of this set-up is that the valve needs to be able to simultaneously deal with multiple fluids and solid particulates. The solid particulates formed in the reactor can easily block the small orifice sizes (region of 20-90 μm [78]) required for laboratory-scale pressure regulating valves. The advantage of this arrangement is that the bio-crude can be collected continuously in a single vessel.

Another possible arrangement is where the reactor products are sent to two separate collection vessels [76, 79] where the bio-crude is collected at near reaction pressures, this necessitates the batch-wise removal of the liquid products from the collection vessels which act to separate the liquid products from the gaseous fraction. With this arrangement it has been possible to position the BPRV on the off-gas system, reducing the likelihood of the valve blocking. One disadvantage is that the bio-crude product can't be continuously removed from the system, it has to be removed on a batch basis into separate collection vessels that have to be switched when full, drained and then re-pressurised to the system pressure. This method is acceptable for laboratory-scale processing but is unlikely to be used in commercial applications.

A novel method of achieving depressurisation found in the literature as an alternative to the conventional BPRV is in the use of capillary tubes employed on the rig detailed in two studies by Sintamarean et al [83] and Pedersen et al [84]. They used a collection of differing lengths and diameters of coiled tubes in series which act to dissipate the kinetic energy within the product stream. This is possible because the pressure drop in coiled pipes is greater than that of a straight pipe of the same length due to the secondary flow caused by the centrifugal forces within the tube [100]. There are many advantages of this arrangement, the spreading of mechanical stress over a length of pipe rather than at a single point (valve internals), cheap, ease of manufacture and less likely to become blocked [100]. The main drawbacks with this type of pressure reducing mechanism are that these sections of capillary tubes have to be a number of metres long even in the smallest set-ups; this

introduces a lot of excess volume meaning that the whole process will take a lot longer to reach steady state.

The continuous hydrothermal liquefaction of microalgae demonstrates that there is a great deal of future potential in the commercialisation of this hydrothermal liquefaction approach to create biologically based liquid fuels. A number of varied and complex biomass feedstocks have been successfully treated at high feed concentrations resulting in bio-crudes with much improved fuel characteristics. All reported trials to date have been conducted on small laboratory-based experimental rig settings, larger demonstration sized processing units are required in order to fully understand the process. There still remain a number of obstacles to overcome, mainly in the pumping of highly viscous biomass slurries, reliable reactor pressure control and the general optimisation of a continuous process. One area that is key is in coupling the use of algae to remediate waste streams which can feed a continuous liquefaction unit to process the algae to liquid fuels.

2.6.2.3 Commercial-scale HTL

There are a number of companies who are in the process of commercialising HTL technology for processing various biomass feedstocks, one of the most advanced operations is the Danish-Canadian company Steeper Energy. They have worked with the University of Aalborg (Denmark) at a pilot scale. They are developing HTL technology known as Hydrofaction™, in November 2021 they completed the commissioning a commercial scale demonstration plant, with a nominal production capacity of 30 barrels per day situated in Tofte, Norway. Steeper's Hydrofaction™ technology feature two key attributes that separate it from other approaches, these are operating at supercritical conditions and secondly in the recirculation of the aqueous phase to the slurry feed preparation [101]. Steeper energy claim to be able to produce bio-crude yields of 45% with oxygen content <10% and 85% energy recovery [102].

There are other companies with pilot/demonstration facilities under development, these include Licella (NSW, Australia) who have developed a catalytic HTL technology branded Cat-HTR™, they have a pilot facility capable of processing 7500 tonnes of slurry [103]. Muradel Pty Ltd with their process known as Green2Black™ and Genifuel with the CatLiq process, a development of PNNLs continuous process mentioned previously.

2.7. HTL bio-crude upgrading

Processing biomass via hydrothermal liquefaction results in an energy dense bio-crude, microalgae are a well-suited feedstock due to their inherently high moisture content. The moisture content does not need to be reduced prior to processing via the application of thermal energy to vaporisation some of the moisture content. HTLs ability to accept high moisture content feedstock results in substantial energy savings when compared to conversion technologies that require a feedstock with very low moisture content. When compared to pyrolysis derived bio-oils HTL produces bio-crudes with greatly reduced oxygen content resulting in far higher HHVs ranging between 28 and 34 MJ/kg vs <20 MJ/kg [104], lower resultant bio-crude water content and high yields of typically between 35 and 50% [72] with respect to the dry microalgal biomass. The physiochemical properties as well as the chemical and elemental composition are mainly dependant on the raw biomass composition and the applied conversion conditions such as temperature and residence time or WHSV for continuous experiments.

Bio-crudes from the non-catalytic hydrothermal liquefaction of microalgae have not yet been produced that are directly suitable for use in transportation, they are very viscous in nature and contain significant amounts of heteroatoms. HTL bio-crudes are high in nitrogen and oxygen with slightly raised sulphur content when compared to typical sweet fossil crude oils, typically <0.5 wt.% S [105].

It is accepted that the raw bio-crude needs to be upgraded before it is useful as a transportation fuel. The chemical content of microalgal bio-crude from the HTL of microalgae is very complex, in general it is composed of a small amount of water and ash with the remainder organic compounds. The organic components consist mainly of linear and branched hydrocarbons, heterocyclic compounds, phenolic derivatives and other oxygenates, fatty acids and esters.

There are a number of upgrading techniques available to improve the physical and chemical characteristics of the bio-crude, the following section briefly discusses the most commonly used methods and presents a summary of the major advantages and disadvantages in **Table 2.6**.

2.7.1. Physical upgrading of HTL bio-crude

2.7.1.1. Solvent addition

Solvent addition is one of the simplest ways of improving the characteristics of bio-oils, when applied to pyrolysis oils it involves the introduction of selected polar solvents such as acetone, methanol, ethanol or ethyl acetate, its effect is to markedly lower viscosity and raise the oils HHV due to the inherently high heating value of the solvent. Addition of acetone to a softwood fast pyrolysis oil at

various concentrations (3 to 15 wt.%) was shown to initially dramatically decrease viscosity but did not stop the increase in viscosity and acidity during aging studies [106].

2.7.1.2. Emulsification

Similar to solvent addition emulsification involves the combination of the raw bio-crude with other fuels such as diesel. It is a very simple method owing to the simple processing steps required and the absence of chemical reactions where a surfactant/emulsifier is added to a bio-crude and diluent mix.

An equal ratio of the surfactant Atlox 4914 to bio-crude was found to produce a stable and effective emulsion over a 30-day period. Using such high proportions of surfactants will result in a more costly product [107].

An emulsification of bio-crude from the liquefaction of the microalgae *Chlorella pyrenoidosa* with diesel and the surfactant Span-80 was shown to produce a fuel with better combustion characteristics, through the lowering of the ignition temperature to below that of pure diesel [108]. An emulsion of bio-crude (10 wt.%) from the liquefaction of agricultural wastes, light cycle oil (85 wt.%) and the inexpensive emulsifier octanol (5 wt.%) was shown to improve values for acid number, density, viscosity, HHV, pour point and elemental composition when compared to the raw bio-crude. Even so the resultant emulsion still fell short of fuel specifications set for viscosity and acid number [109].

2.7.1.3. Bio-crude separation

In an attempt to improve fuel characteristics prior to any further upgrading steps the mature and very well understood process of fractional distillation can be employed to provide a final or pre-treatment step depending on product cut composition. If used as a pre-treatment step fractional distillation can reduce the burden on downstream processes for heteroatom removal and physicochemical improvements. There are only a handful of studies of this nature within the literature relating to the distillation of HTL derived bio-crude. One of the earliest studies showed that a very simplistic vacuum distillation setup with a single distilled product collected achieved a dramatic increase of HHV from ~32-36 MJ/kg to ~40MJ/kg alongside a notably dramatic reduction of O in some instances by >90% to values below 1.5 wt.%. Nitrogen content was also decreased to a lesser extent ~15 to 45% but still remained too high for direct use in transportation, sulphur content was also decreased by 30 to 60% [110]. Elemental analysis of the cuts from fractional distillation of both algal [111] and food waste [112] HTL bio-crude reveals that the majority of the oxygen content is contained within the light distillate region.

When used prior to more traditional hydrotreating methods the reduction in heteroatom content achieved from distillation is advantageous due to the decrease in downstream hydrogen consumption, reduced catalyst coking potential [113] and greater miscibility in traditional fossil refinery feeds.

Only one study could be found for the further upgrading of an algal HTL bio-crude distillate fraction, Xie et al [113] studied the upgrading of two algae species (*Auxenochlorella pyrenoidosa* and *Arthrospira platensis*) HTL bio-crude distillate fractions blended with a waste product, namely used engine oil and the precious metal catalyst Pt/C. Both the hydrotreated blends and raw bio-crude showed dramatically reduced O and N content as low as 0.23 wt.% and 0.63 wt.% respectively. C and H content was increased to average values of 85.5 and 13.7 wt.% respectively, this resulted in very high HHVs of ~48MJ/kg. The hydrotreating of the blended feedstock is shown to reduce S content considerably but the blending of the very low sulphur content used engine oil (0.01 wt.%) is likely to contribute greatly to this and it is not thought that there are any synergetic effects.

2.7.3. Chemical upgrading routes

2.7.3.1. Esterification

Previously, algal based biofuels focused on the extraction and transesterification of the triacylglyceride lipid fraction to FAME, this was seen to be the desirable pathway to produce third generation biofuels. This however was shown to be an expensive route due to dry extraction techniques, low productivity during the lipid accumulation phase and solvent recovery [114]. A direct comparison of FAME yields from the bio-crude obtained from the HTL conversion of the diatom *Fistulifera solaris* demonstrate that yields of FAME are considerably increased when compared to those from traditional solvent extraction methods [115].

As the HTL bio-crude is known to contain high amounts of fatty acids it is also a potential candidate for esterification. The subcritical catalytic esterification of algal bio-crudes has not been widely researched with only a small number of reports found studying the esterification of *Spirulina* HTL bio-crude in ethanol [116] and methanol [117]. Yang et al [118] studied the near-supercritical and supercritical fluid esterification of *Chlorella* derived HTL bio-crude in ethanol, it was found that under full supercritical conditions the yield was >90 wt.% and resultant bio-oil displayed desirable changes in viscosity and a greatly increased ester content. Similarly the treatment of HTL bio-crude from the microalgae *Nannochloropsis* was subject to upgrading experiments with the solvents methanol, ethanol, acetone, water and water with a Ru/C catalyst. Elemental analysis showed that C and H content increased a small amount and N content was in some cases reduced by ~50%, O content was also reduced in most cases but not to the same degree. Heteroatom content was still higher than

required for direct use in transportation applications with nitrogen content >5 wt.%, oxygen >6 wt.% and typical sulphur content of 0.6-0.8 wt.% [119].

2.7.3.2. Hydroprocessing

Hydrotreating represents one of the most mature and widely used techniques for fuel upgrading, the use of selected catalysts and hydrogen donors facilitates the upgrading of the fuel. Hydrotreating aims to achieve the following objectives: removal of impurities such as heteroatoms O, N and S, a requirement for environmental reasons with the aim of reducing NO_x and SO_x emissions during combustion. Removal of metals which is usually carried out in a separate guard reactor where the metal is deposited in the pores of the catalyst and finally in the saturation of olefins and other unstable compounds [120]. Another problem with bio-crudes is their storage stability, due to the presence of highly reactive organic compounds such as olefins which can repolymerise into larger molecules. The presence of ketones, aldehydes and organic acids can also react to form other larger reactive molecules, this leads to the increase in the average molecular mass of the oil and contributes to the increased viscosity and water content which has a negative effect on the HHV [121].

Removal of heteroatoms N, O and S results in the formation of ammonia gas, water and H₂S respectively, as a result the proportion of carbon in the fuel increases and the fuel is also enriched with hydrogen. It is stated that the physical and chemical properties of hydrocarbon fuels are related to their H/C values, H/C values can also reflect the degree of saturation in the average molecule [122].

The reactions are carried out in fixed bed reactors in the presence of a hydrogen donor most frequently in the form of high pressure H₂ gas, the reactors are operated at typical pressures of 5-160 barg and temperatures 260 – 380 °C [123] depending on the feedstock being processed. Temperatures within the hydrotreating reactor should remain low in order to reduce thermal cracking. The higher the feeds boiling point range to be hydrotreated the more severe the reaction conditions are required and the lower the value for the liquid hourly space velocity (LHSV) which are typically in the range of 10 hr⁻¹ and 0.15 h⁻¹ for lower molecular to higher boiling range feedstock respectively.

When hydrotreating is applied to bio-crudes it results in the combination of a complex reaction network due to the vast number of compounds present in the untreated bio-crude. The choice of hydrotreating catalyst is determined by the initial feedstock characteristics and the final desired product specification. As bio-crudes possess greater complexity and variability than traditional fossil-based feeds the selection of a catalyst and moreover the selection of optimal reaction conditions are very challenging. There are many catalysts that are used in hydrotreating, most commonly for fossil

fuels which are based on a porous alumina matrix impregnated with combinations of cobalt, nickel, molybdenum and tungsten.

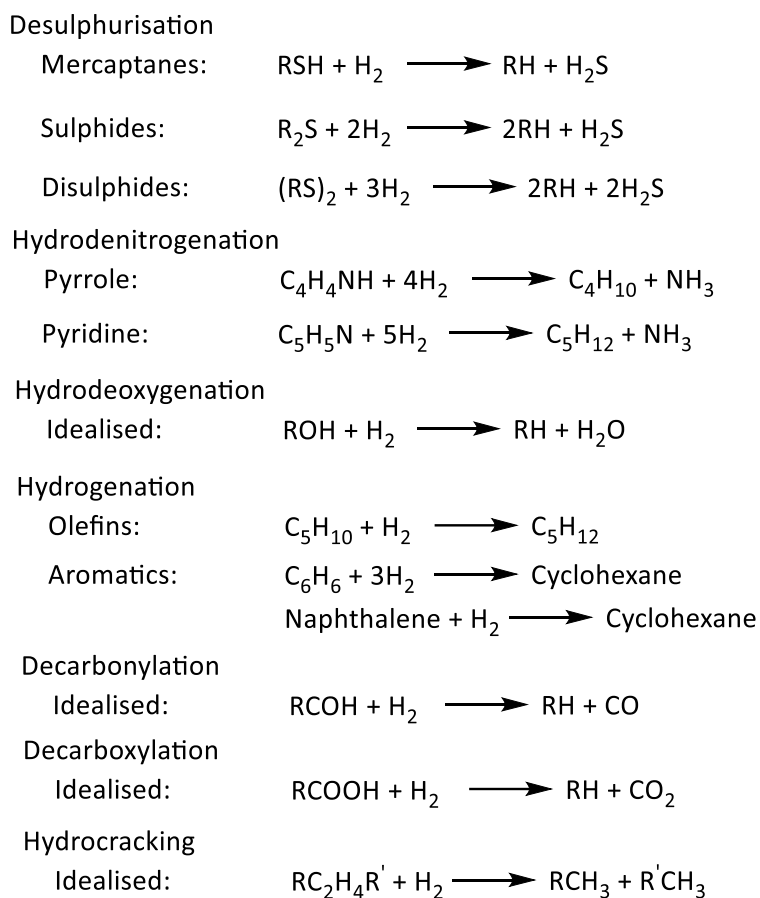


Figure 2.9. Reactions associated with catalytic bio-crude upgrading
Combined from [121, 124]

When compared to fossil crude oils with typical elemental distribution of C 83-87%, H 10-14%, N 0.1-2%, S 0.05-6% and O 0.05-1.5% [125] liquefaction bio-crudes have much higher nitrogen and oxygen content. Bio-crude has approximately equal or lower amounts of sulphur present in most microalgal HTL bio-crudes, therefore the focus of the upgrading routes are through hydrodeoxygenation (HDO) and hydrodenitrogenation (HDN).

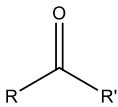
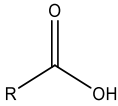
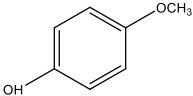
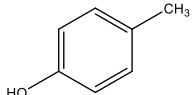
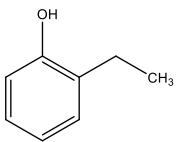
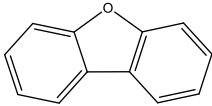
2.7.3.2a. Hydrodexoygenation (HDO)

Algal liquefaction bio-crudes have very high levels of oxygen c.3 to 8 wt.% therefore HDO reactions are of very high importance during the hydrotreatment of pure bio-crude or fossil blends. In more detail, deoxygenation can occur through reactions such as hydrodeoxygenation, decarboxylation, decarbonylation and dehydration forming H_2O , CO_2 and CO respectively all presented in **Figure 2.9**.

Complete deoxygenation of the bio-crude is unlikely as removal of oxygen takes place together with other potentially conflicting reactions therefore a product with residual oxygen is likely to be produced.

Table 2.5. Hydrogen consumption for HDO reactions presented alongside activation energy (E_A) and iso-reactive temperature (T_{iso}) for various functional groups in the presence of a $\text{CoMoS}_2/\text{Al}_2\text{O}_3$ catalyst.

Data from [126, 127].

Molecule/group	Structure	E_A [kJ/mol]	T_{iso} [°C]	Hydrogen consumption
Ketone		50	203	2H ₂ /group
Carboxylic acid		109	283	3H ₂ /group
Methoxyphenol		113	301	≈6H ₂ /molecule
4-Methylphenol		141	340	≈4H ₂ /molecule
2-Ethylphenol		150	367	≈4H ₂ /molecule
Dibenzofuran		143	417	≈8H ₂ /molecule

A very important aspect in hydrodeoxygenation is hydrogen consumption, both the oxygen content in the feed and the type of oxygenated compounds affects the amount of hydrogen required to remove oxygen, **Table 2.5** presents hydrogen consumption of various functional groups relevant to algal bio-crude. Functionality of a molecule has a direct relationship with their reactivity, higher reactivity molecules such as alcohols, ketones, ethers and carboxylic acids consume less hydrogen when compared to more stable molecules with lower reactivities such as cyclic compounds like phenols, furans and their derivatives [128]. Typically for these more stable molecules they require

saturation/hydrogenation prior to deoxygenation, this leads to higher H₂ requirements than those based on stoichiometric predictions in order to achieve high degrees of deoxygenation.

2.7.3.2b. Hydrodenitrogenation

As previously stated, bio-crudes are typically high in N, nitrogen containing compounds are produced by Maillard reactions between sugars and amino acids [129]. Nitrogen containing compounds within bio-crudes are typically in the form of noncyclic compounds such as aliphatic amines, nitriles and aromatic amines alongside the more common heterocyclic compounds such as pyridines, pyrroles and indole among others. The denitrogenation of N containing ring structures is more challenging, requiring the ring saturation prior to cleavage of the C-N bond. Similarly, to the HDO of oxygen containing aromatic compounds the hydrogen demand for HDN is increased with greater molecular complexity for instance degree of saturation.

2.7.3.3. Catalytic hydrotreating

As stated in the previous section, the catalysts used in industry for the hydrotreating of petroleum fractions are based on combinations of nickel, molybdenum, cobalt and tungsten on alumina. Catalysts based on these metals have been tested in the hydrotreating of algal bio-crudes, NiMo/Al₂O₃[81, 130, 131], CoMo/ Al₂O₃[76, 81, 132], NiW/Al₂O₃[130], CoNiMoW/Al₂O₃[133], Ni/C [134], Co/S [134] Ni-Ru/CeO₂[135] and Ni/CeO₂[135]. Mo₂C[132], MoS₂[132], NiSiO₂/Al₂O₃[132], Raney-Ni [132]. With respect to the NiMo or CoMo catalysts they are usually sulphided prior to use, the Co or Ni act as promoters, donating electrons to the Mo atoms, thereby weakening the bond between the Mo and sulphur atoms which generates a sulphur vacancy site where HDS, HDN and HDO reactions can take place [121].

A range of studies has also investigated the application of various noble metal catalysts Pt/C [131-134, 136], Pt/Al₂O₃[131, 137], Pd/C [131-133, 138], Pd/Al₂O₃[131], Ru/C[119, 131-134], Ru/Al₂O₃[131].

Bai et al [132] investigated the application of a wide range of catalysts (Pt, Pd, Ru all on carbon alongside various Co, Mo, Ni and zeolite) on a pre-treated HTL bio-crude from the microalgae *Chlorella pyrenoidosa*. Pre-treatment involved the hydrotreatment of the DCM soluble fraction was with no catalyst for 4 hours at 350 °C, this pre-treated bio-crude was then used in the catalytic upgrading studies. Catalytic upgrading experiments were conducted at 400 °C for 4 hours under an initial 6 MPa H₂. With respect to heteroatom removal Raney Nickel was the most effective at N reduction 4.1 wt. % to 1.6 wt. %, Ru/C achieved the greatest reduction in O, 3.6 wt. % to 1.1 wt. %, a combination of the two catalysts was also investigated, this led to the highest achieved oil yield, low TAN values, second lowest combine N and O proportion (2 wt.% each) and highest HHV of 45.3 MJ/kg.

Billier et al [81] studied two traditional hydrotreating catalysts NiMo/Al₂O₃ and CoMo/Al₂O₃ which were sulphided prior to use, hydrotreatment was conducted at two temperatures of 350 °C and 405 °C, 2 hour residence time and an initial hydrogen pressure of 60 or 66 barg, using bio-crude produced from the continuous liquefaction of *Chlorella*. When compared to the non-catalytic hydrotreating there was little difference between heteroatom content when compared to catalytic hydrotreating at the lower 350 °C. Experiments at the higher 405°C temperature resulted in a more dramatic decrease in heteroatom content, NiMo was shown to be slightly more effective at nitrogen removal 6 wt. % to 2.4 wt. % vs 2.7 wt. % for CoMo. Even so, CoMo was shown to be slightly more effective at deoxygenation, 11.1 wt. % to 1.0 wt. % vs 1.5 wt. % for NiMo achieving a maximum HHV of 45.4 MJ/kg. The higher temperatures led to a better-quality bio-oil but increased the yield of gaseous and char products, hence yields of upgraded bio-oil were significantly lowered by 22% to 56%. The fractionation of the upgraded bio-oils showed it contained approximately 25 % gasoline, 50% diesel with the remaining 25% attributed to heavy fuel fractions, these higher molecular weight compounds were also shown to contain the majority of the oxygen content of the upgraded bio-oil. Successful reduction of the oxygen content was achieved using solvent extraction with pentane, whilst the content of N remained unchanged following solvent extraction.

Patel et al [131] investigated the catalytic upgrading of *Nannochloropsis sp* bio-crude produced from a micro-scale continuous HTL rig with a reactor volume of 2 cm³ processed at a temperature of 380 °C for a very short residence time of 0.5 minutes [77]. Upgrading experiments were conducted at 400 °C under an initial hydrogen pressure of 50 barg, for a residence time of 1 hour. The effect of catalyst support was investigated, the noble metals Pt, Pd and Ru were used on both alumina and carbon supports alongside a traditional NiMo on alumina. The catalytically upgraded bio-crudes possessed a much lower viscosity and had an odour more akin to hydrocarbon fuels when compared to the raw bio-crude and the uncatalysed control experiment. Bio-crude yields were highest for the NiMo/Al₂O₃ catalyst at 96.6 wt. %, yields for the alumina supported noble metal catalyst being much lower at 63.5 to 67 wt. %, the same noble metals on carbon supports achieved slightly higher yields (67 to 72 wt. %) when compared to the alumina support. Heteroatom removal efficacy was varied, deoxygenation was very successful for the noble metal catalysts, reducing O content by a maximum of 87.5 % to a value of 1.6 wt. % for the Pt/Al₂O₃ catalyst because of this also achieving the highest HHV of 45.4 MJ/kg. The remaining noble metals achieving between 71 to 84 % reduction excluding a slight outlier of Pd/C only achieving an O reduction of 53 %. Nitrogen reduction was less effective, the noble metal catalyst achieving a range of 3.1 to 19.8% reduction, with remaining levels in the noble metal upgraded bio-crudes remaining high (2.87 to 3.47 wt.%). Whilst NiMo/Al₂O₃ achieved the greatest reduction (42.7%)

in N to a final value of 2.05 wt.% alongside the highest upgraded bio-crude yield it had no effect at reducing O content which resulted in a fuel with a low HHV of 38.4 MJ/kg.

Barreiro et al [137] investigated a zeolite (HZSM-5) and noble metal catalyst (Pt/Al₂O₃) during the upgrading of two bio-crudes obtained from the continuous liquefaction of the microalgae *Nannochloropsis gaditana* and *Scenedesmus almeriensis*, at a temperature of 350 °C and a retention time 15 minutes. Upgrading reactions were carried out on a batch basis at a final reaction temperature of 400 °C, under initial 4 or 8 MPa hydrogen with respect to experiments carried out with and without added H₂O. Overall deoxygenation was successful, results show that experiments conducted with added H₂O in potentially a supercritical state resulted in higher oxygen content with an achieved average reduction of 60.8%, lower carbon content and therefore lower HHV. When compared to experiments without added H₂O, deoxygenation was improved by an average of 76.7%. Interestingly the degree of denitrogenation was markedly different between the two species with the same catalysts, leading to a reduction of N content by an average of 16.7% and 49.7% for *S almeriensis* and *N gaditana* respectively. This is despite *N gaditana*'s higher N content (6.9 vs 5.5 wt.%) in the raw algal feedstock and their similar elemental N content of 5.7 wt.% and 4.8 wt.% in the HTL bio-crude combined with their similarity in the types of N containing compounds detected through GC-MS analysis. This leads to a possible explanation that it could be due to differences in the structures of the high molecular weight N containing compounds that are not detectable with GC-MS analysis, highlighting the importance of tailoring/trialling the upgrading catalyst to the individual bio-crude feedstock.

A study from Elliott et al [76] represents one of the most commercially relevant studies on the subject of hydrothermal liquefaction of microalgae feedstocks. Bio-crude was first obtained through the continuous liquefaction of 4 different *Nannochloropsis sp.* feedstocks at a temperature of 350 °C and a pressure of 20MPa. The bio-crude was separated gravimetrically without the use of solvents. Hydrotreatment of the bio-crudes was conducted on a continuous basis with biocrude and hydrogen passing through a fixed catalyst bed reactor. One microalgae was processed in two stages, firstly a lower temperature stage at the entrance to the reactor at 125-170 °C followed by the high temperature stage set at 405 °C with the remaining three algae feedstock processed solely at the higher temperature. The catalyst selected was a molybdenum (15% Mo) sulphide with cobalt (4%) promotion supported on a fluorinated alumina support. The HTL processing of a low lipid high growth (highest nitrogen content) *Nannochloropsis sp.* achieved a high bio-crude yield of 60.8 wt. % with a combined heteroatom content of 12.5 wt. % comprised of O 8.0 wt. %, N 4.2 wt.% and S 0.3 wt. %, following upgrading the resultant bio-oil had acceptably low oxygen content (1.8 wt.%) and remarkably low nitrogen content of 0.25 wt. % representing a reduction of 94 %. This is in stark

contrast to the previous studies discussed where typical nitrogen levels after upgrading were 1.6 to 6 wt.%. The degree of heteroatom removal was similar across all processed bio-crudes achieving a range of O (0.8 to 1.8 wt.%), N (0.05 to 0.25 wt.%) and S at <50ppm.

Most recently Chen et al [136] reported a new procedure, during the bio-crude upgrading the investigators periodically replaced the reaction atmosphere with fresh hydrogen in an effort to reduce heteroatom content. During batch upgrading experiments the hydrogen donor solvent tetralin was added to the reactor on a 1:1 basis with respect to the bio-crude, alongside this the catalyst Pt/C was added, the reactor was charged with H₂ to an initial pressure of 8 MPa. Upgrading was investigated over a range of temperatures (300 – 480 °C), residence times of 1 to 8 hours and H₂ replacement frequency. Higher temperatures were shown to decrease upgraded bio-oil yield and increase the formation of gaseous and char products. Increased residence time was shown to slightly decrease the yield of upgraded bio-oil, beyond 4 hours the yield of char increased by ~50% for every additional 2 hours residence time. The combined bio-crude and tetralin had a O content of 4.52 wt.%, N 26,271 ppm and S 2590 ppm. The reaction temperature of 400 °C was found to be a good balance point with regards to upgraded bio-crude yield and product composition. Following upgrading for 4 hours at 400 °C oxygen and nitrogen content was reduced by 81.6% to a value of 0.83 wt.% and by 73.9% to a value of 0.68 wt.% respectively, resulting in a HHV of 44.3 MJ/kg. Finally, a set of experiments were undertaken where the frequency of H₂ replacement was increased during upgrading runs, reaction parameters were set to 6 h RT, 400 °C, 8MPa H₂ and added Pt/C catalyst, number of reaction atmosphere replacement events range from 1 to 5 over the total experiment run time. Increasing the frequency of reaction gas removal and replacement with fresh H₂ correlates with a steady increase in upgraded bio-crude yield (87.3 to 91.0%) and a decrease in heteroatom content with reduction of O achieved of 81.2 to 85.6%, N reduction of 73.9 to 91.5% and S reduction of 98 to 99%. Where the reaction atmosphere was replaced every hour during a 6 h residence time (5 changes) caused a final reduction in heteroatom content of 85.6% O, 91.5 % N and 99.0% S to final values of 0.65 wt.%, 2230 ppm and 25 ppm respectively. Whilst this is a lengthy and labour-intensive method therefore its applicability in a commercial sense is impractical, it does however add support to the findings from Elliot et al [76] and others that heteroatom removal during batch experiments are likely to be equilibrium limited.

2.7.3.4. Cracking

There are a number of disadvantages to hydrotreating, catalyst lifetimes are not very high before they need to be regenerated or replaced, typical lifetimes of HDO/HDN catalysts are less than 200 h due to carbon deposition [121]. There is also a requirement for high pressure hydrogen and reactions

performed at high pressures. An alternative route for bio-crude upgrading is zeolite cracking, zeolites are three-dimensional microporous aluminosilicate materials with very large surface areas and adsorption capacities. Zeolite catalysed cracking reactions are carbocation based reactions [139], these being an ion with a positively charged carbon atoms such as methenium CH_3^+ and methanium C_2H_5^+ and are therefore dependent of the surface structure and acidity of a catalyst. Cracking of heavier molecules is dependent on the strength of the acid sites, acid site density and high external surface area increases the probability of cracking occurring and the accessibility for large hydrocarbon molecules to the acid sites [140].

Similarly to hydrotreating, zeolite cracking involves all the reactions presented in **Figure 2.9** but only to a minor degree with the main reaction occurring as cracking as shown below in **Figure 2.10**.

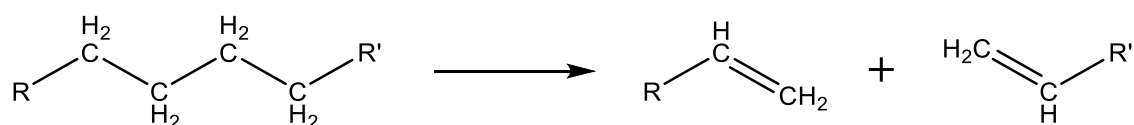


Figure 2.10. Cracking reaction example.

Zeolite cracking does not require the co-feeding of high-pressure hydrogen and can therefore be conducted at atmospheric pressures [121]. Typically zeolite cracking is operated at temperatures of between 500 to 600 °C [141].

There have been a number of studies investigating the use of zeolite-based catalyst on the upgrading of HTL bio-crude derived from microalgae such as the medium pore sized HZSM-5 [132, 137, 142]. Duan et al [143] studied a wide range of nine zeolite based catalysts, upgrading was conducted at 400 °C in supercritical water and is discussed further in Section 2.7.3.5.

Cui et al [144] investigated the upgrading of a glycerol and microalgae mixture under mild conditions, a low reaction temperature of 300 °C for 1 hour under a N_2 atmosphere, the use of 3 bio-crude extraction solvents and 3 catalysts, the zeolite H-beta, Raney Ni and Pt/C. When compared to HZSM-5, H-beta has much larger pore size and medium acidity. Upgraded bio-crude yields were the highest for H-beta when a solvent was used for extraction but the lowest for experiments where the bio-crude was gravimetrically separated. Elemental composition of the upgraded bio-crudes showed that H-beta was not effective at substantially reducing heteroatom content.

Table 2.6. Summary of bio-crude upgrading pathways and their technical feasibility

Adapted from [145, 146]

Upgrading Process	Conditions	Reaction mechanism/process description	Technical feasibility		References
			Advantages	Disadvantages	
Solvent addition	Mild conditions, polar solvents needed such as water, methanol, ethanol and furfural.	Increases HHV and reduces bio-crude viscosity through physical dilution.	Simple process, cheap.	Doesn't convert/remove undesirable components of the bio-crude.	[106]
Emulsification	Mild conditions, needs a surfactant	Can be combined with diesel or biodiesel fuel with the use of surfactants	Simple, less corrosive product	High energy consumption and doesn't convert/remove undesirable components of the bio-crude.	[107-109]
Separation	Mild conditions, potential need for a solvent in certain applications	Solvent extraction, distillation or chemical modification.	Extracts valuable chemicals from the bio-crude, improve fuel quality through heteroatom removal	Separation equipment needed, potential organic solvents.	[110-113]
Esterification	Mild conditions, alcohol needed	A chemical reaction of esterification to convert organic acids to neutral esters.	Relatively simple process, mild conditions low cost of alcohol if methanol is used. Improvement in TAN, storage properties and HHV.	Not effective at removing nitrogen containing compounds.	[115-119]
Hydroprocessing	Mild to severe conditions, ~400-500 °C, high pressure hydrogen. Catalysts needed such as NiMo, CoMo, noble metals or zeolites.	Hydrogenation without simultaneous cracking (eliminating N, O and S as NH ₃ , H ₂ O and H ₂ S)	Removes/reduces heteroatom content, increases HHV, cheap route which is already commercialised for fossil fuels and well understood	Requirement for high pressure equipment, high pressure hydrogen gas supply potential for high coking of catalyst leading to catalyst deactivation.	[76, 81, 119, 130-138]
Hydrocracking	Relatively high pressure and temperature, high pressure hydrogen and catalysts needed e.g. Ni based.	Hydrogenation with simultaneous cracking	Produces large quantities of higher value light products.	Requirement for high pressure equipment, hydrogen gas supply, coking leading to catalyst deactivation and reactor clogging.	[121]
Zeolite cracking (FCC)	Severe temperature conditions needed (500-600 °C), atmospheric pressure, zeolite catalysts.	Cracking heavy molecules to lighter components	Produces large quantities of higher value light products. Reactions at atmospheric pressure.	Very fast catalyst deactivation because of carbon deposition, potentially requiring fluidised catalytic cracking (FCC) unit. Lower fuel quality, lower HHV and low H/C ratio.	[132, 137, 143, 144]
Supercritical fluids (SCFs)	Pressures needed above solvents critical pressure, e.g. >22MPa for water, potentially high temperatures needed (over solvent critical temperature), >375 °C for water.	Promotes the reaction with the unique properties of SCFs, liquid like density and gas like diffusivity and viscosity.	Effective at reducing viscosity and heteroatom content, increases HHV.	Requires high pressure equipment, technology is not advanced and not widely used in large scale fuel applications.	[119, 143, 147-149]

2.7.3.5. Supercritical fluids

The use of supercritical fluids has already been touched upon in **Section 2.7.3.1** with respect to esterification in supercritical ethanol. A supercritical fluid is a state of matter when the interface between liquid and gas is indistinguishable, this is achieved when the fluid's pressure and temperature are raised beyond its critical point. Utilisation of supercritical fluids as solvents have many advantages due to possessing properties of both gases at high pressures (low viscosity and high diffusion coefficients) and liquids (high solubility), these properties facilitate easier penetration into porous media and lead to very high mass transfer rates. Their solvency is also highly tuneable via changes in temperature and pressure, where solvents are selected that are gases under STP then separation of the solvent from the dissolved substances is easily achieved through pressure reduction [150].

Previously the use of supercritical fluids for upgrading has been applied to complex fossil resources such as heavy oils and coal tars [151-155].

There are a small number of studies investigating the catalytic upgrading of microalgal HTL biocrudes in supercritical fluids [119, 133, 143, 147-149] and the previously discussed study from Bai et al [132].

Duan et al [156] studied the supercritical water upgrading of *Nannochloropsis sp.* HTL bio-crude with a Pt/C catalyst, catalyst loading was set to 25 wt.% with respect to the bio-crude, upgrading was performed in a hydrogen atmosphere at 400 °C for 4h. Results showed HHVs achieved in the region of 42-43 MJ/kg from 40 MJ/kg for the raw bio-crude, reduction in both oxygen ~30% and nitrogen ~50% content is achieved, TAN is reduced from 256 to 25 and viscosity is greatly reduced. Similarly to the previous study Duan et al [147] focused on the supercritical upgrading of a HTL bio-crude derived from *Chlorella pyrenoidosa* with a platinum gamma alumina catalyst, similar results were observed where HHV was slightly improved due to reductions in heteroatom content. The rationale for the substitution of the carbon support from the previous study to the gamma alumina support material was due to the ability to calcine the spent catalyst for easy regeneration as well as the gamma alumina having acid sites that would promote acid catalysed reactions. In a later study Duan et al [143] studied the upgrading potential of a number of zeolite catalysts on a pre-treated HTL algal bio-crude produced from *Chlorella pyrenoidosa*. The combination of the bio-crude pre-treating step and subsequent upgrading with the zeolite catalysts showed very good denitrogenation and deoxygenation activity. Firstly in the pre-treatment step (autoclave H₂ atmosphere, 4 hours at 350 °C) achieving a reduction of 23%, 32% and 69% for N, O and S content respectively and an increase of HHV to 40.5 MJ/kg from 38.4 MJ/kg and improved viscosity. The catalytic upgrading of the pre-treated bio-crude resulted in a

further reduction of heteroatom content, all by ~50% to levels of 1.6 to 2.1 wt. % N, 1.5 to 2.5 wt. % O and ~0.1 wt. % S, leading to a further improved HHVs of 44-45 MJ/kg.

Xu et al [149] investigated the supercritical water upgrading of the HTL bio-crude from the microalgae *Nannochloropsis sp*, comparisons were made between the supercritical bio-crude upgrading in fresh water or the separated aqueous fraction and 3 catalysts, two precious metals on carbon, platinum and ruthenium both 5 wt.% catalyst loading and a molybdenum on carbon. Platinum on carbon was found to be the most effective catalyst in terms of heteroatom reduction and increased carbon and hydrogen content. The utilisation of the process water from HTL as the solvent for the subsequent supercritical upgrading experiments resulted in a near comparable quality of upgraded bio-crude when compared to bio-crude treated with Pt/C catalyst in deionised water. This is significant as it may present a cost-effective and viable pre-treatment step prior to catalytic upgrading within existing infrastructure.

Building on the work in the previously discussed study, Xu et al [119] investigated the addition of different solvents (methanol, ethanol, acetone and water) and a Ru/C catalyst with water during subcritical and supercritical upgrading over a temperature range of 240-400 °C. The selected solvents were shown to consistently increase yields; ethanol was shown to result in the highest upgraded bio-crude yield reaching a maximum of 82.8 wt.% at 360 °C. Whilst yields were higher for ethanol and methanol their calculated HHVs were typically lower by 1-1.5 MJ/kg, the presence of organic solvents leads to the esterification of the bio-crude and an increase in O content when compared to reactions with water and the raw HTL bio-crude. Upgrading processes in supercritical solvents involves a wide range of mechanisms, including but not limited to dehydration, hydrogenation, hydrodeoxygenation, and decarboxylation. It has been shown through isotope labelling that supercritical water acts not only as the solvent but is also able to act as a hydrogen donor to stabilise free radicals produced from cracking of higher molecular weight compounds helping to reduce char formation [157].

The majority of studies investigating HTL of algae utilise a solvent to aid in the recovery of part of the organic content within the reactor, common solvents include DCM due to its immiscibility in water and others such as acetone. This solvent fraction is what most researchers class as the bio-crude product. Commercial scale bio-crude production is unlikely to utilise solvents as a means for recovering bio-crude, instead gravity separation is one viable option. He et al [133] investigated the supercritical upgrading of the water-soluble bio-crude included in the removed aqueous phase, 3 different types of noble metals (Pt, Pd and Ru) on carbon were investigated alongside a novel CoNiMoW/ γ -Al₂O₃. The raw water-soluble fraction was shown to have much higher heteroatom content when compared to the water insoluble bio-crude, total Heteroatom content of 32.4 wt.% vs 22.4 wt.% respectively. After upgrading the resultant bio-oils were somewhat improved, HHVs were

increased to 29.5 to 34.2 MJ/kg versus 27 MJ/kg for the feed bio-crude. Pd/C was found to be produce the best quality in terms of elemental composition but the lowest yield at just 37.3 wt.%. Across the board heteroatom removal was poor, nitrogen content was reduced by a maximum of 24% for Pd/C, the degree of deoxygenation was a little better achieving a maximum reduction of 49% again for the Pd/C catalyst. Even after these reductions in heteroatom content, nitrogen and oxygen levels still remain prohibitively high for use as transportation fuels with the amount of N and O at 8.2 wt.% and 10.7 wt.% respectively for the best bio-oil produced using the Pd/C catalyst. This study has shown that it may be sensible for the organic fraction left after the physical separation of the water insoluble bio-crude be upgraded/utilised in a different process, one that is not as sensitive to processing feeds with high heteroatom content. Anaerobic digestion is one option, typical acceptable C:N molar ratios for the feedstock are in the region of 27-32:1, aqueous phase C:N ratios from the HTL of microalgae are in the region of 2.6-5.2:1 [93], this abundance of nitrogen can cause a build-up of ammonia which is harmful to the bacteria involved in anaerobic digestion [158]. Catalytic hydrothermal gasification (CHG) is potentially another process for the recovery of the carbon and nitrogen content in the combined aqueous and water-soluble biocrude phase, CHG is able to process feeds with high nitrogen content producing a fuel gas [159].

The use of alumina supported NiMo catalyst in the presence of water vapour has been shown to reduce the activity of the catalyst to one third of its original value, Laurent et al showed that alumina partly crystallised to a hydrated alumina phase called boehmite [160]. Furthermore typical oxide catalysts and catalyst supports previously mentioned including alumina, silica and zeolites undergo phase transitions and partial dissolution under hydrothermal conditions, this leads to a dramatic loss of surface area and therefore catalytic activity [161].

Supercritical water gasification (SCWG) has been applied to the HTL bio-crude produced from lipid extracted algal residue, resultant gas yields were low, between 2-8 wt.% with the main component as CO₂ (43-46 wt.%) followed by H₂ (32-40 wt.%) using K₂CO₃, NaOH and Ru/C catalysts [162]. Cattle manure derived HTL biocrude has also been subject to SCWG using novel bimetallic catalyst based on Ni and Ru for improved H₂ generation, hydrogen yield was 1.01 mol/mol of carbon in the biocrude feed [163].

Chapter 3 - Methodology

3.1. Materials

3.1.1. Model compounds

The following model compounds representing different chemical groups were used in this PhD study for thermal degradation experiments via analytic pyrolysis (Py-GC-MS) and hydrothermal liquefaction (HTL):

- Carbohydrates
 - D-(+)-Glucose (CAS: 50-90-7, Sigma Aldrich)
 - D-(+)-Xylose (CAS: 58-86-6, Sigma Aldrich)
- Lipids
 - oleic acid (CAS: 112-80-1, Sigma Aldrich)
 - stearic acid (CAS: 57-11-4, Sigma Aldrich)
- Proteins
 - L-glutamine (CAS: 56-58-9, Sigma Aldrich)
 - L-leucine (CAS: 61-90-5, Sigma Aldrich)
 - soy protein isolate (commercially available soy protein isolate)

3.1.2. Macroalgae species

Five macroalgae species used in this study were obtained from Plymouth Marine Laboratory (Plymouth, UK).

1. *Ascophyllum nodosum*
2. *Fucus serratus*
3. *Fucus vesiculosus*
4. *Himanthalia elongate*
5. *Ulva lactuca*

All macroalgae species were received wet as harvested, then dried at 105 °C. Dried macroalgae samples were crushed using a ceramic mortar and pestle to obtain particles in size of approximately 1-2 cm. Samples for analytical characterisation (analytical fraction below 0.25 mm / 60 mesh) was prepared using an IKA A11 analytical mill.

3.1.3. Microalgae species

Three microalgae species, obtained from various sources, were used in this study:

6. *Isochrysis galbana* (T-ISO) obtained from (Alga Energy, Spain)
7. *Arthrospira platensis* obtained from (Alga Energy, Spain)
8. *Nannochloropsis sp.* (Nanno 3600, batch #19337) was provided by Varicon Aqua Solutions Ltd (Hallow, Worcester, UK) and originated from Reed Mariculture (San Diego CA, USA) as wet concentrated slurry. The following characterisation of the *Nannochloropsis sp.* was provided by the supplier (Reed Mariculture, San Diego CA, USA):
 - Biochemical composition: lipids (28 wt.%), proteins (52 wt.%) and carbohydrates (12 wt.%)
 - Cell size: 1-2 microns
 - Cell count: 68 billion per pack (1 litre)
 - Dry weight: 18 wt.%

Note: *Nannochloropsis sp.* after characterisation of all available microalgae samples was selected as the feedstock for all HTL experiments.

3.1.4. Solvents and reference materials

The following solvents were used at different stages of the reported in this thesis experimental work:

- Dichloromethane (DCM) from Fisher Scientific - used for extraction of biocrude from HTL and upgrading experiments.
- Deuterated dimethyl sulfoxide- d_6 (DMSO- d_6) solvent from Goss Scientific - used for preparation of NMR samples.
- Acetone from Sigma Aldrich (GC grade, 99.95% dried over molecular sieve) for prparation of all samples for GC-MS analysis.
- Kerosene from Alfa Aesar used for NiMo/Al₂O₃ sulphiding.
- Dimethyl disulfide from Sigma Aldrich $\geq 99.0\%$ used for NiMo/Al₂O₃ sulphiding.

Pine wood fast pyrolysis oil (bio-oil) from BTG (Netherlands) was used as a reference pyrolysis oil for comparison during the GC-MS and NMR characterisation of algae-derived bio-crudes and upgraded bio-liquids.

3.1.5. Catalysts

The following catalysts were used during the catalytic upgrading of HTL-derived bio-liquids (bio-crudes):

- Palladium on activated carbon (Pd/C; 5 wt.% loading, Sigma Aldrich)
- Platinum on activated charcoal (Pt/C; 5 wt.% loading, Sigma Aldrich)
- Ruthenium on activated charcoal (Ru/C; 5 wt.% loading, Sigma Aldrich)
- Zeolite (ZSM-5; Acros Organics) 30:1 mole ratio of SiO₂:Al₂O₃
- NiMo/Al₂O₃ (commercial hydrotreating catalyst; Alfa Aesar)

3.2. Analytical protocols

3.2.1. Elemental analysis

Elemental analysis was performed to determine the carbon (C), hydrogen (H), nitrogen (N) and sulphur (S) content using a ThermoFisher Scientific Flash 2000 Organic Elemental Analyser. A small amount (~5 mg) of solid samples (algae sample, model compounds solid residues; dried, particle size <60 μm) were placed inside small tin capsules alongside a similar amount of vanadium pentoxide (V₂O₅) as a combustion booster during the analysis. All measurements were repeated in triplicate and the average values were reported. Oxygen (O) was calculated by difference.

Elemental analysis of liquids samples (HTL-derived bio-liquids of liquids from the catalytic upgrading runs) was carried out in the same way described above. The only difference was the application of a liquid absorbent pad (quartz wool) to maintain the liquid samples in the tin crucible.

3.2.1 Heating values

The higher heating value (HHV) of the algae samples was calculated from the results of the elemental analysis using the Dulong formula [164] shown in Equation 3.1.

$$HHV \left(\frac{MJ}{kg} \right) = 0.3383 \times C + 1.443 \times \left(H - \frac{O}{8} \right) + 0.0942 \times S \quad (\text{Eq. 3.1})$$

3.2.2 Ash content analysis

Before each ash content measurements, all samples were dried at 60 °C for the constant weight using a Sartorius MA 38 infrared moisture analyser. Where applicable and reported, the ash content analysis was carried out according to the ASTM E1755-01 standard [165]. Approximately 2 g of dried sample was placed in a ceramic crucible (20 ml volume) and ashed using a Carbolite AAF1100 furnace with the application of the following temperature program: heat to 250 °C at 10 °C min.⁻¹, hold for 30 min., and then increase to 575 °C and hold for 6 h. Samples were then removed from the furnace to be cooled and weighed. Samples were then returned for further ashing at 575 °C for one-hour periods until the sample weight was constant. Each sample was analysed for its ash content in triplicate.

3.2.4 Thermogravimetric analysis (TGA)

The thermogravimetric analysis (TGA) was carried out using a Mettler Toledo TGA/DSC 2. Approximately 5 mg of sample (model components and algal feedstock) was pyrolysed in an alumina crucible using the following temperature program: initial temperature of 50 °C was held for 5 minutes, then increased to 105 °C at 5 °C min⁻¹ and held for 5 minutes, then heated at 25 °C min⁻¹ to the final temperature of 500 °C, where the samples were held for 15 minutes for full char devolatilisation. TGA analysis were carried out under nitrogen at a flowrate of 30 mL min⁻¹.

The resultant char residue from each TGA experiment was then used to determine the ash content of the samples. The sample was held at an initial temperature of 50 °C for 5 minutes, then increased to 105 °C at 5 °C min⁻¹ and held for 5 minutes, then heated at 10 °C min⁻¹ to 575 °C and held for 15 minutes. TGA ash content analysis were carried out under air at a flowrate of 30 mL min⁻¹.

3.2.5 Analytical pyrolysis (Py-GC-MS)

Pyrolysis – gas chromatography – mass spectrometry (Py-GC-MS) analysis of model compounds and algal samples was performed using a CDS 5200 HPR system - CDS Analytics 5200 Pyroprobe (Chemical Data Systems, Oxford, PA) close-coupled with a PerkinElmer Clarus 680 series gas chromatograph and a Clarus 600S series mass spectrometer. The samples (5 mg each in a quartz sample tube) were pyrolysed to a temperature of 500 °C (held for 30 seconds). The pyrolysis products were transferred using helium as the carrier gas at a flow rate of 25 mL/min to the PerkinElmer Elite-1701 GC column (cross-bond: 14% cyanopropylphenyl and 85% dimethyl polysiloxane; length 30 m with an internal diameter of 0.25 mm, film thickness 2.5 µm). The GC oven was held at 45 °C for 2.5 minutes then heated at 2.5 °C min⁻¹ to 250 °C and held for 30 seconds. Proposed assignments ($m/z = 45-300$) of the main peaks were made from mass spectra detection using the NIST 2005 MS library and from assignments seen in the literature [40, 166-168].

In-situ pyrolysis studies with available catalysts were carried out using the same Py-GC-MS laboratory setting, pyrolysis temperature and GC-MS parameters as described above. Feedstock samples (0.2 mg each) were “sandwiched” with the appropriate catalyst at a total catalyst amount of 1.0 mg in a quartz sample tube.

3.2.6. GC-MS analysis of liquid samples

The chemical composition of HTL-derived bio-crudes and upgraded bio-liquids was carried out using a Shimadzu GC-MS-QP2010 SE system. A representative liquid sample was dissolved in GC-grade

acetone (1:5 vol./vol.) and injected (1 μ l) using an AOC-20i Autoinjector onto GC column via the injector port maintained at 300 °C¹ with a split ratio of 25:1. Helium was used as a GC carrier gas at a flow rate of 25 ml min⁻¹. All devolatilised components were separated using a DB-5 silica capillary column (30 m length, 0.25 mm internal diameter, and 0.25 μ m film thickness). The GC oven was programmed as follows: 5 °C min⁻¹ from 45 °C up to 280 °C, which was held for 2.25 min at the final temperature of 280 °C. The MS detector, with ionisation electron energy set up at 70 eV was used for detection of the separated compounds in the molecular mass spectra detection range of m/z = 45-300. The GC injector was maintained at 300 °C, and a split ratio of 25:1. The MS detector was operated. Peak assignments for individual components were done with the National Institute of Standards and Technology (NIST) MS library (2010).

3.2.7. One- and two-dimensional NMR spectroscopy

The structure of the HTL-derived bioliquids and upgraded liquids were determined by NMR analysis using different NMR techniques with specific measurement methods recommended by Doudin et al. [169, 170] after consultation related to this PhD research. NMR analysis was performed on a Bruker Avance-300 spectrometer at ambient temperature and utilising the residual solvent signals as a reference. The NMR samples were prepared in 5 mm NMR tubes by dissolving 300 mg of the bio-crude sample in 0.7 ml of the deuterated dimethyl sulfoxide-d₆ solvent (DMSO-d₆) (Goss Scientific).

3.2.7.1. Quantitative ¹³C NMR

Quantitative ¹³C NMR spectra were recorded at 75 MHz with referenced to the residual DMSO solvent peak at 39.52ppm. In order to achieve accurate ¹³C spectra, inverse gated decoupling was utilised in order to minimise NOE enhancements. The samples of biocrude contain hundreds of complex compounds hence the relative concentration of each of these compounds will be very low, combine this with the very low sensitivity of the ¹³C nuclei meant that the use of >10,000 scans was required to achieve spectra with acceptable signal to noise ratios. In order to achieve accurate measurement of signal intensities a pulse delay time of five times the relaxation time was used.

3.2.7.2. PENDANT ¹³C NMR

The PENDANT (Polarization Enhancement During Attached Nucleus Testing) method is the method for distinguishing CH, CH₂, CH₃, and quaternary carbons. ¹³C NMR spectral edited PENDANT spectra were also obtained at 75MHz for carbon using the PENDANT pulse program with waltz16 decoupling during acquisition, the variable cnst2 contains at the value of 145 Hz, a relaxation delay, d1, of 4 s. The spectra were recorded over a spectral width of 238 ppm, 12 K scans, and referenced to the solvent DMSO peak at 39.52 ppm.

3.2.7.3. Two-dimensional NMR

2D ^1H - ^{13}C Heteronuclear Single Quantum Coherence (HSQC) spectra which correlate ^1H and ^{13}C chemical shifts through a one-bond heteronuclear scalar coupling ($^1J_{\text{CH}}$) were recorded. The cross peaks in the ^1H - ^{13}C HSQC spectra showed chemical shifts of ^1H on one axis (horizontal) that are correlated to ^{13}C (on the other, vertical, axis) belonging to the H-C atoms directly bonded to each other. The pulse sequence utilized several polarisation transfer steps that increased the overall sensitivity of the experiment; the sequence included inverse detection, i.e. ^1H detection rather than ^{13}C detection. The HSQC spectra (64 scans, with the FID time domain F2 having a digital acquisition of 2048 data points and the time domain F1 having 256 data points) were acquired using a relaxation delay of 1.5 s with phase-sensitive states-time proportional phase incrementation (TPPI). Approximately 12 h of spectrometer time was usually necessary to acquire the data for each sample.

Furthermore, 2D ^1H - ^{13}C Heteronuclear Multiple-Bond Coherence (HMBC) spectra, which correlate ^1H and ^{13}C chemical shifts through multiple-bond heteronuclear scalar coupling ($^nJ_{\text{CH}}$, $n = 2$ or 3) were also recorded. The cross peaks in the ^1H - ^{13}C HMBC spectra showed the chemical shifts of ^1H on one axis (horizontal) which correlated to ^{13}C (on the vertical axis) that belong to H and C atoms which are separated by two or three chemical bonds. Just like the HSQC, the HMBC pulse sequence utilized ^1H to ^{13}C polarisation transfer and inverse (^1H) detection for optimum sensitivity.

3.3. Hydrothermal processing

3.3.1 Testing of New Liquefaction Equipment

The reactor to be used in all liquefaction runs is a new piece of equipment, therefore it was decided that the new autoclave needed to be tested to ascertain its limits and therefore decide on a sensible operating region in order to be confident that the reaction conditions were subcritical. **Figure 3.1** above shows the pressure temperature trends during all of the testing runs. A testing regime was created where all tests would be pre-pressurised to 50 barg prior to heating, this is needed to ensure that the contents of the reactor remain subcritical throughout the experiment; any deviation into the supercritical region would mean that the process had transitioned from hydrothermal liquefaction to hydrothermal gasification.

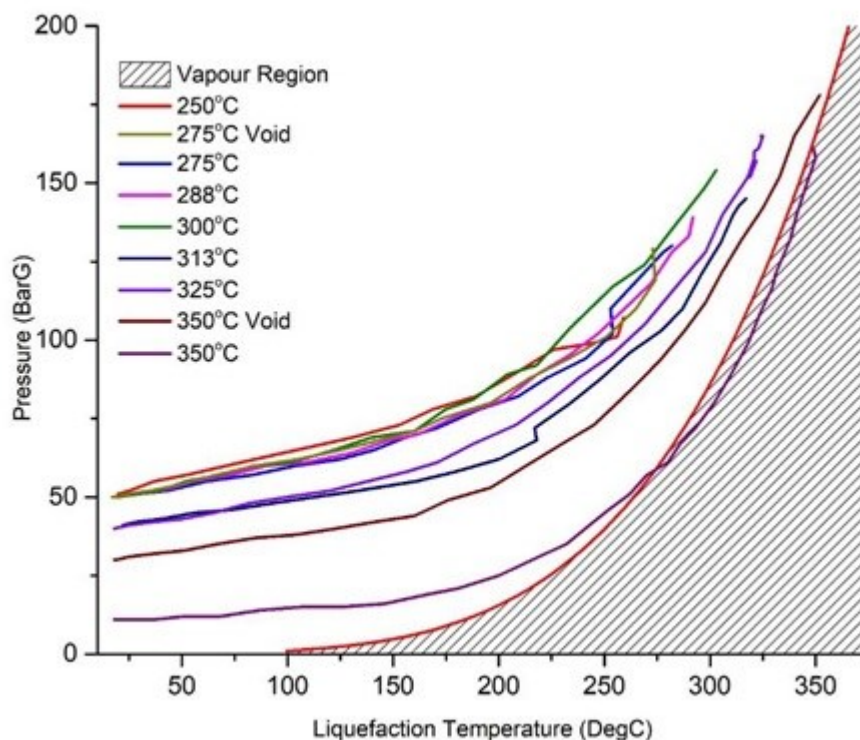


Figure 3.1. Autoclave Testing Runs Pressure Profiles

The tests were started from a low temperature of 250 °C to a maximum temperature of 350 °C. The first run to a final temperature of 250 °C initial pressure of 50 barg ran without any issues. During the second run (275 °C, 50 barg) the rupture disc failed, on inspection it was found that the specification of the fitted rupture disc was rated to ~140 barg at 25 °C, the final pressure achieved at failure was ~129 barg at a temperature of 273 °C. Following on from this and for the remainder of the trials a new

rupture disc was fitted, rated to ~207 barg at 25°C. Runs at final reaction temperatures of 275 °C (repeat), 288 °C and 300 °C were all successful after dropping the initial pressurisation setpoint, it was noted that the final pressure at 300 °C was 154 barg.

For the runs following this it was decided to reduce the initial pressurisation of the reactor to 40 barg, this was in an effort to reduce the final pressure compared to if it was run with a starting pressure of 50 barg. The next two runs at 313 °C and 325 °C were ran successfully using an initial reactor pressurisation of 40 barg, reaching final pressures of 145 and 165 barg respectively.

The next temperature in the set of experiments was 350 °C, another decision was made to lower the initial pressurisation of the reactor, this time to 30 barg, again, in an effort to keep the final reaction pressure within the operating limits of the rupture disc. During the run the temperature did reach 350 °C but during the hold for three minutes the rupture disc failed at ~178 barg. This figure represents a reduction of 29 barg (-14%) to the rupture disc pressure rating at an elevated temperature of 350 °C.

In order to try and achieve a repeatable reaction temperature of 350 °C the initial pressurisation of the reactor was further reduced to 10 barg. The final reaction temperature was able to reach 350 °C but when plotting the temperature/pressure profile as seen in **Figure 3.1** it can be seen that the data points cross over into the vapour phase region at approximately 275 °C, therefore confidence in the future reactions at these operating parameters being in subcritical conditions was low.

Findings from the investigation of the reactor performance it was decided that all future runs will be undertaken at a reaction temperature of 300 °C with an initial reactor pressurisation of 50 barg as these are figures where there is confidence that the reaction stays in the liquefaction (subcritical) region.

3.3.2 Batch Processing

Hydrothermal liquefaction experiments were performed using a batch autoclave reactor, (Parr Instrument Company, 300 ml). The heating rate was approximately 7.5°C min⁻¹ provided by an aluminium block heater. For each experiment the reactor was charged using a glass liner with ~70 g of algal slurry or model compound (dried at 60°C for >1 hour or until no mass change seen) with deionised water, constituting a feedstock dry solids loading concentration of ~20 wt.% in each case. Liquefaction experiments were performed under an inert nitrogen (research grade 5.5) atmosphere. In all experimental runs the reactor was sealed and purged with nitrogen five times prior to final gas charging to an initial pressure of 40 barg in all cases. The reactor was then heated to 300 °C with the pressure inside the reactor increasing autogenously to a region of 130-150 barg during the

experimental run. The reactor contents were continuously stirred at ~500 rpm by an overhead magnetic stirrer in all cases to ensure a homogeneous reaction. The time required to reach 300°C was approximately 40 minutes; once the desired temperature was reached the reaction temperature was maintained for 10 minutes \pm 1 °C. At the end of the run the reactor was left to cool naturally back to room temperature before the reactor was opened and the reaction products removed.

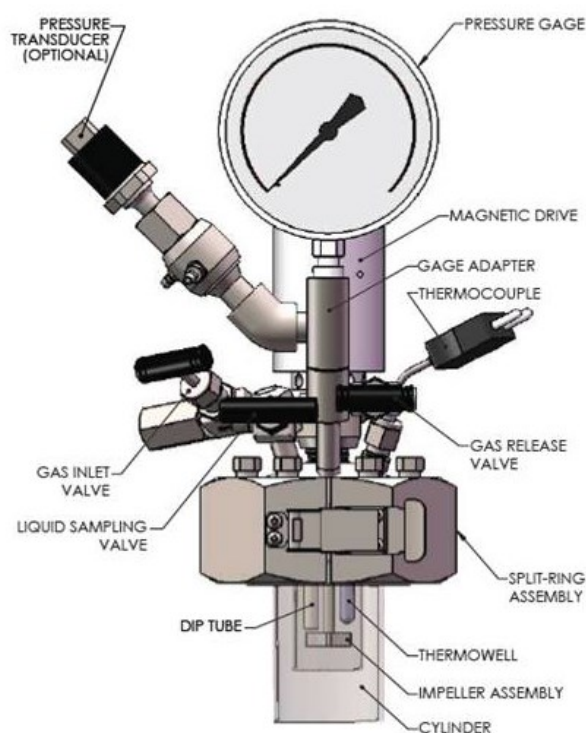


Figure 3.2. Cross-section of the Parr 5000 series stirred reactor.

[Public resource – Image licence CC BY 4.0]

3.4. Heterogeneous catalytic upgrading

3.4.1 Catalyst preparation

The noble metal catalysts were used as received. The ZSM-5 catalyst was calcined in air for 5h at 550 °C to obtain the HZSM-5 form following the procedure set out by Zambare et al [171]

The NiMo/Al₂O₃ was sulphidied prior to use following a similar method to the one outlined by Biller et al [81]. 20 g of NiMo/Al₂O₃ catalyst was heated in a 300 ml Parr stirred reactor under a hydrogen atmosphere in 70 ml of 2 wt.% dimethylsulphide in kerosene solution. Firstly, the reactor was purged with nitrogen five times following which the reactor was flushed with hydrogen five times to an initial

H₂ pressure of 40 barg. The reactor was continuously stirred throughout the heating program, the reactor was first held at 40 °C for 2 hours then ramped to 150 °C and held for 8 hours. The temperature was increased to 270 °C held for 8 hours and ultimately ramped to a final temperature of 300 °C held for 8 hours after which the reactor was left to cool to ambient temperature. The sulphided NiMo/Al₂O₃ was separated from the kerosene solution, washed with DCM and dried under flowing N₂.

3.4.2 Catalyst characterisation

3.4.2.1 Porosimetry

Nitrogen porosimetry was undertaken on a Quantachrome Nova 4000 porosimeter (Hook, UK) on samples degassed at 120 °C for 3 h before analysis at -196 °C. Surface areas (presented in **Table 3.1**) were calculated by the Brunauer–Emmett–Teller (BET) method from the desorption isotherm for $P/P_0 < 0.2$.

Table 3.1. Catalyst surface area measured by BET

Catalyst	Surface area (m ² /g)
Pd/C	1496
Pt/C	1484
Ru/C	1472
HZSM-5	384
NiMo/Al ₂ O ₃	157

3.4.3 Catalytic supercritical water upgrading

Algal bio-crude catalytic upgrading was carried out in water at supercritical state, the experiments were performed using a high pressure high temperature batch autoclave reactor, (Parr Instrument Company model number 4597, 50 ml volume rated to 345 barg at 500 °C. The heating rate was approximately 7.5°C min⁻¹ provided by a ceramic heater. For each experiment the reactor was charged using a glass liner with ~3.5 g of biocrude with 10 ml of deionised water, ~0.88 g of catalyst was added constituting a loading of ~25 wt.% in each case. Upgrading experiments were performed under a hydrogen atmosphere. In all experimental runs the reactor was sealed and purged with hydrogen 5 times prior to final gas charging to an initial pressure of 110 barg. The reactor was then heated to 450 °C with the pressure inside the reactor increasing autogenously during the experimental run. The

reactor contents were continuously stirred at ~500 rpm by an overhead magnetic stirrer in all cases to ensure a homogeneous reaction. The time required to reach 450°C was approximately 1 hour; once the desired temperature was reached the reaction temperature was maintained for 4 hours $\pm 1^\circ\text{C}$. At the end of the run the reactor was left to cool naturally back to room temperature before the reactor was opened and the reaction products removed.

3.5. Product Handling

3.5.1 Product separation

Following both the liquefaction and upgrading runs the products were subject to a number of separation procedures as can be seen in **Figure 3.3**. Firstly 50 ml (30 ml for upgrading experiments) of dichloromethane was added to the reaction mixture in the reactor and used to rinse the reactor furniture. This mixture was then filtered through a Büchner funnel and filter paper (Whatman 1, Qualitative), the resultant two phases were separated in a separatory funnel. The solvent was then separated from the DCM phase to determine the mass of bio-crude performed in a two necked round bottom flask using flowing nitrogen and a magnetic stirrer at room temperature.

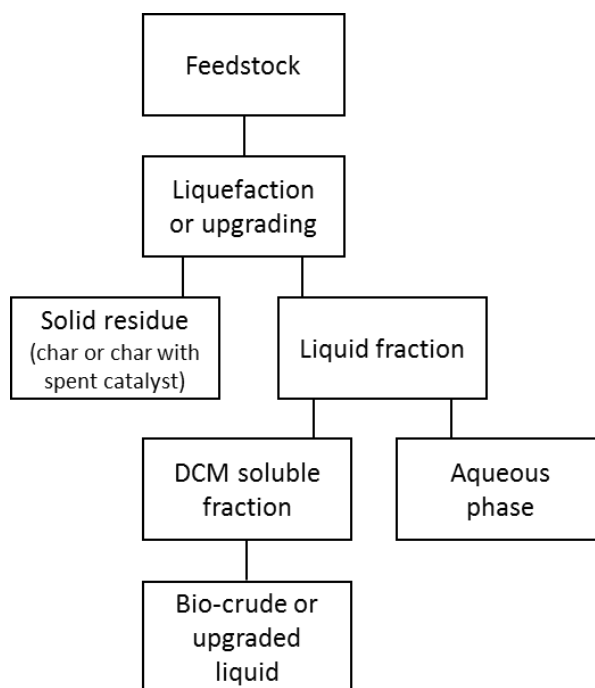


Figure 3.3. Separation of HTL and catalytic upgrading liquids.

Chapter 4 - Feedstock characterisation and selection

4.1. Introduction

This chapter will investigate the biomass and model compound characterisation to inform subsequent HTL feedstock selection based on findings required for additional processing in future research chapters in this thesis. When considering the conversion of any material to a desired product an in-depth understanding of the starting materials is required in order to make informed and appropriate decisions on processing pathways. As discussed in the previous chapter, algae have many potential and real-world applications, their biomolecular variety, tunability and rapid growth rates make them ideal candidates as sources of valuable products and feedstocks for various large-scale applications. There are a number of large-scale applications which favour specific macromolecular constituents of the algae, such as growth for increased lipid content for lipid extraction and transesterification to biodiesel. High protein content is desirable for nutraceutical and fertiliser applications and finally, carbohydrate content is suited to conversion to bioethanol through fermentation. All of these aforementioned applications require a thorough understanding of the feedstock to ensure economic conversion. As previously stated HTL processing is able to convert feedstocks with a wide variance in composition, even so, understanding the feedstock is still vital as it aids in more efficient and well-understood conversion characteristics required for commercial-scale design.

At the first stage of this PhD project five macroalgae from the British Isles (*Fucus serratus*, *Fucus vesiculosus*, *Himantahlia elongata*, *Ulva lactuca* and *Ascophyllum nodosum*) and three microalgae samples (*Nannochloropsis sp.*, *Arthrospira platensis* and *Isochrysis galbana*) were studied as a potential feedstock for hydrothermal processing. Proximate and ultimate analysis was conducted, higher heating values (HHV) were calculated, thermal analysis using TGA and analytical pyrolysis was also undertaken.

The most desirable algal feedstock was selected for further processing based on the following selection descriptors-

- High volatile matter (potentially giving high yields of HTL bio-crude)
- Low ash content (to avoid cracking reactions due to the catalytic impact of inorganics present in the feedstock).
- Low nitrogen (to reduce the degree of denitrogenation in subsequent catalytic upgrading of HTL derived bio-crudes).
- High HHV.

- Moderate to high lipid content (key precursor to bio-crude formation)

The characterisation of nine model compounds were also subjected to the same analysis methods previously described for the algal feedstocks. Compounds were selected to represent the major macromolecular compounds present in microalgae (Lipids – stearic acid and oleic acid, Proteins – Soy protein, l-leucine and l-glutamine and carbohydrates xylose and glucose).

4.2. Characterisation of algal feedstock

4.2.1. Proximate and ultimate analysis of algae

4.2.1.1. Proximate analysis

The species of macro and microalgae used in this study are listed in **Table 4.1** below, alongside the results from the proximate and ultimate analysis of each of the species their respective calculated higher heating values (HHV) are also presented, calculated using the Dulong equation described in Section 3.2.1. Using the data from the TGA the relative proportions of moisture, volatiles and char comprising of ash and fixed carbon all wt.% on a dry basis are presented.

Table 4.1. Proximate analysis of the micro and macroalgae feedstocks.

	Macroalgae					Microalgae		
	AN	FS	FV	HE	UL	SP	NSp	IG
Proximate analysis (wt.%)^(d,b)								
Volatile matter	58.58	54.66	56.56	54.41	45.24	67.44	57.21	51.82
Char	41.42	45.34	43.44	45.59	54.76	32.56	42.79	48.18
Fixed carbon	21.92	19.53	21.57	19.28	29.07	24.92	24.69	21.20
Ash	19.50	25.81	21.87	26.31	25.69	7.64	18.10	26.98

The results from the proximate and ultimate analysis show that the volatile matter yield is in the range of 45-59 wt.% for the macroalgae species, whereas the volatile yield for microalgae is on average a little higher, in the region of 52-67 wt.%. An increased amount of volatile matter contained within the feedstock gives an indication of potentially higher bio-crude yields achievable from thermal processing [172].

There is also a slight contrast in the results for ash content, macroalgae ~19.5-26 wt. % dry basis compared to 7.6-27 wt. % dry basis for the species of microalgae. The ash contents for the microalgae species *Nannochloropsis sp.* and *Isochrysis galbana* are slightly higher than expected, with reported ash content for NSp of 11.8-12.4 wt. % dry basis [59, 173]. The ash contents for the macroalgae species are within an acceptable range based on previous findings of UL of 29.1 wt.% [174] and FV 24 wt.% [166].

It is true that the characterisation of the ash content is recognised as being problematic as the ash can contain significant amounts of volatile inorganic materials and different measurement methods produce varying results [40].

Both macro and to a certain extent microalgae are known to contain higher amounts of alkali earth metals than terrestrial biomass, they are also known to accumulate heavy metals [166]. Both of these contribute to the formation of ash. Therefore it is clear that the ash content for both micro and macroalgae are much higher than terrestrial biomass sources ca 2-7% (wheat straw 4.89 wt.%, switch grass 5.73 wt. %, rape straw 6.58 wt.%) [175] (Miscanthus 2.1 wt.% and willow coppice 3.0 wt.%) [40]. With respect to macroalgae their particularly high ash content could represent a problem in their conversion to fuels due to the potential for equipment fouling, corrosion and slag formation [166, 168].

The ash content of the feedstock being considered for the liquefaction treatment is an important factor, as they will ultimately contribute to the overall efficiency of the treatment process and in the composition of the bio-crude produced.

4.2.1.2. Ultimate analysis

The microalgae species show the highest carbon and lowest oxygen content when compared against the macroalgae (carbon 37-48 wt.% vs. 29-34 wt.% and 22.5-25 wt.% vs. 42-46 wt. % respectively), this results in a lower O/C ratio of the microalgae (0.39-0.46) when compared to the macroalgae (0.82-0.87). Low O/C ratios are known to positively influence the HHV of the biomass [174]. This is supported by the HHV values calculated for the species investigated within this report. The HHV values for the macroalgae species fall in the range of 11.2-12.6 MJ/kg and as expected the HHV for the microalgae species are higher, in the range of 17-23.3 MJ/kg.

The nitrogen content of the microalgae species are noticeably higher than macroalgae ~6-11 wt.% compared to ~1.5-3.7 wt.% respectively. When both micro and macroalgae are compared to traditional terrestrial biomass feedstocks wheat straw 0.66 wt.%, switch grass 0.42 wt.%, rape straw 1.15 wt.% [175] it can be seen that their values are considerably higher. This higher nitrogen content

is associated with the higher amounts of proteins present within the algae. Especially visible for the microalgae *Arthrospira platensis* (Spirulina) (Nitrogen content of 10.9 wt.%) which is known for its very high protein content (60-70 %) as discussed previously. It is therefore expected that the bio-crudes produced from algae feedstocks will contain more nitrogenous species than bio-oil obtained from terrestrial biomass sources.

Table 4.2. Ultimate analysis and calculated HHVs of the micro and macroalgae feedstocks

	Macroalgae					Microalgae		
	AN	FS	FV	HE	UL	SP	NSp	IG
Ultimate analysis (wt.%)^(d,b)								
C	33.81	31.34	32.74	30.28	29.28	48.30	44.16	37.05
H	5.36	4.91	5.18	4.94	5.17	7.85	5.96	5.83
N	1.49	2.24	1.82	1.97	3.71	10.94	6.284	6.89
S	2.36	1.52	2.48	1.45	3.48	0.52	0.47	0.70
O*	37.48	34.18	35.91	35.04	32.67	24.75	25.01	22.54
Atomic ratios								
H/C	1.89	1.87	1.88	1.94	2.10	1.94	1.61	1.88
O/C	0.83	0.82	0.82	0.87	0.84	0.39	0.43	0.46
N/C	0.037	0.061	0.047	0.056	0.109	0.194	0.122	0.159
Higher Heating Values								
HHV (MJ/kg)	12.6	11.7	12.3	11.2	11.8	23.3	19.1	17.0

4.3. Thermal Analysis TGA

Figure 4.1 shows the differential thermogravimetric (DTG) profiles for all of the algal feedstock samples tested. The DTG profile shows the percentage mass loss per minute, the shape of which is related to the composition of the biomass. A clear distinction can be seen between the macro and microalgae samples. The macroalgae species experience a major initial mass loss between 230-300 °C with peak DTG temperatures for each individual species at; AN 270 °C, FS 270 °C, FV 275 °C, HE 265 °C and UL 250 °C. Whereas the microalgae samples experience a major initial mass loss over a broader temperature range from 230-430 °C. They also have higher peak DTG temperatures of; SP 330 °C, NSp 335 °C and IG 325 °C.

It is reported that the peak mass loss during the pyrolysis of cellulose and hemicelluloses are in the temperature range of 180-320 °C and the peaks of protein, starch and lignin probably overlap one-another within the temperature range of 250-460 °C [174]. Pyrolytic decomposition of macroalgae occurs at a much lower temperature compared to terrestrial biomass sources. The main weight loss of the macroalgae species as mentioned previously is in the temperature range of 250-275 °C; this represents the decomposition of carbohydrates, a main constituent of macroalgae. It is also thought that there may be a catalytic influence from the metal content of the macroalgae, particularly potassium [60, 69] as a result of their marine growth environment. There is also a small shoulder feature where there is a temporary constant/small increase in mass loss observed for some of the macroalgae species, occurring at the same temperature as the major mass loss temperature for the microalgae species.

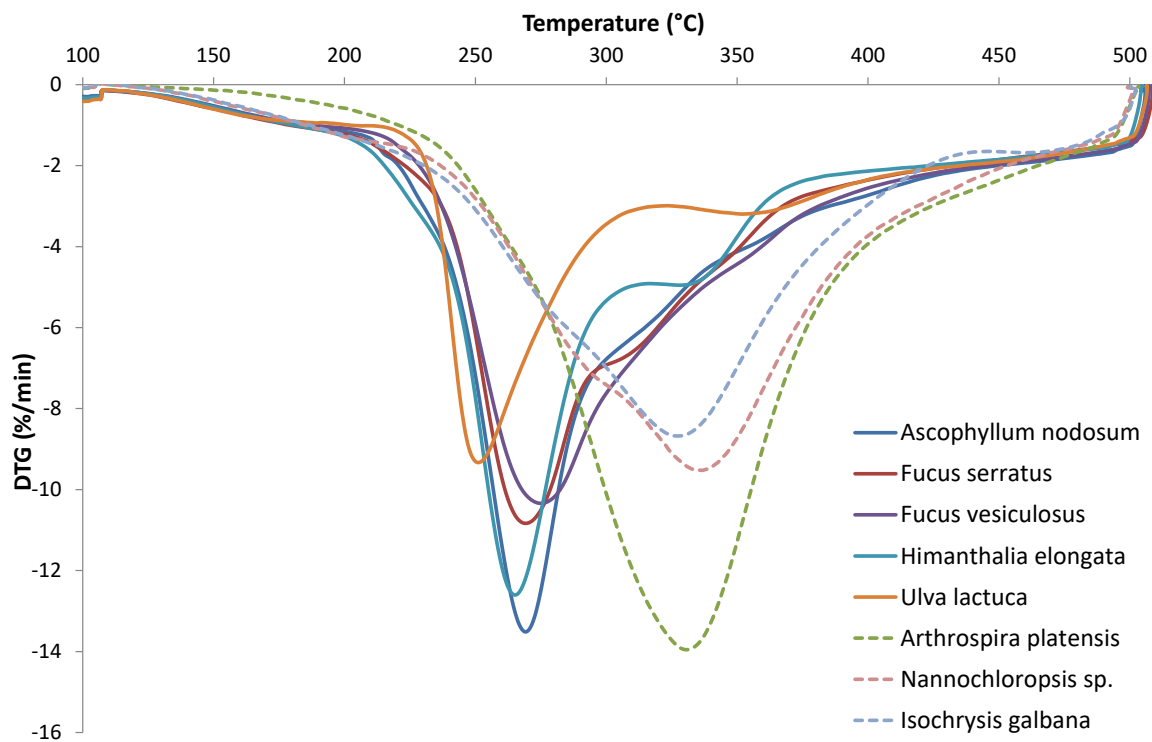


Figure 4.1. DTG profiles of all algae species in nitrogen at 25 °C min⁻¹ solid lines for macroalgae species and dashed lines for microalgal species.

Keblermann et al [168] found that the DTG curve of the total proteins extracted from the microalgae species *Chlamydomonas reinhardtii* displayed a maximum mass loss within the temperature region of 200-500 °C peaking at ca.350-360 °C, accounting for the shift of the maximum mass loss seen for the microalgae samples in **Figure 4.1** due to their much higher protein content when compared to macroalgae [73].

4.4. Py-GC-MS analysis

4.4.1. Py-GC-MS of macroalgae species

Figure 4.2 shows the example Py-GC-MS chromatograms for the macroalgae species *Himanthalia elongata*, **Table 4.3** lists the major compounds and gives details on their structure. All compounds have been identified and assigned using the 2005 NIST mass spectral database. The results from the analytical pyrolysis of the macroalgae species - supported well by previous research [71], indicates the presence of a range of different chemicals, including; phenols, ketones (1-(furan-2-yl)ethan-1-one, 2-hydroxy-3-methylcyclopent-2-en-1-one (MCP)) and aldehydes (5-methylfuran-2-carbaldehyde, furfural), phytol, fatty acids (tetradecanoic acid, hexadecanoic acid and oleic acid) and nitrogen containing compounds in smaller amounts, mainly pyrrole and indole derivatives.

It was observed that the chromatograms of four of the macroalgae species investigated are very similar to one another, that of *Ascophyllum nodosum*, *Fucus serratus*, *Fucus vesiculosus* and *Himanthalia elongata*. All of these algae species are classified as brown seaweeds whereas the remaining macroalgae *Ulva lactuca* (Sea lettuce) is a green seaweed species and the chromatograph from analytical pyrolysis differs from the other four, mainly in the fact that it is missing a key peak at a retention time of around 31 minutes, attributed to dianhydromannitol. Dianhydromannitol is formed from the dehydration of mannitol which is one of the two main types of carbohydrates present in brown seaweeds in the form of sugars [71].

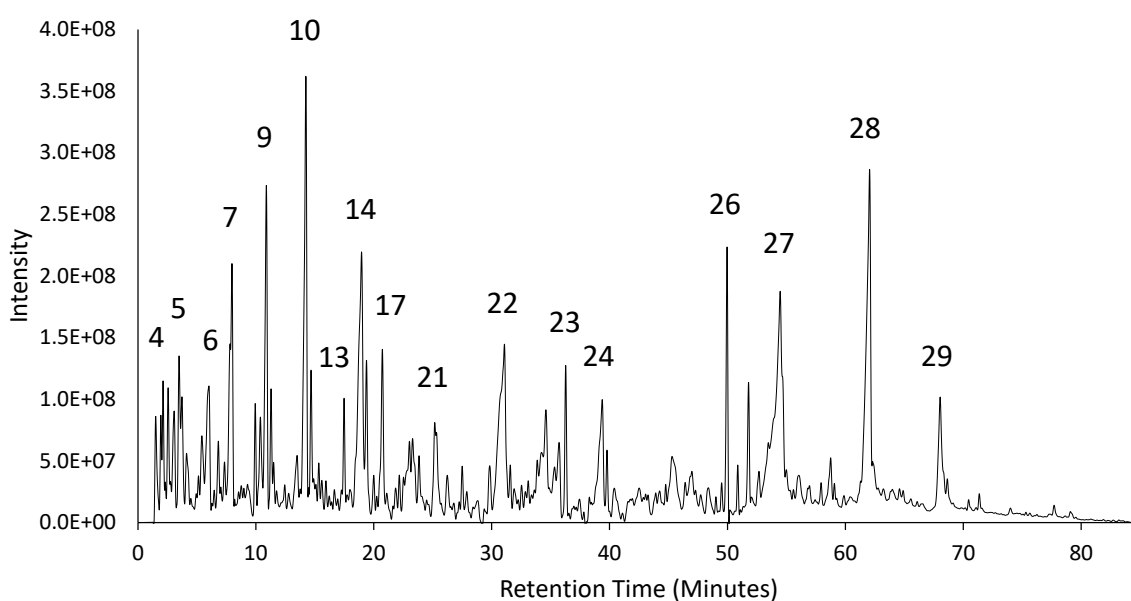


Figure 4.2. Py-GC-MS profile at 500 °C for the macroalgae species *Himanthalia elongata*.

Table 4.3. Major compounds identified from the pyrolysis of all macroalgae samples at 500 °C using Py-GC/MS.

Peak Number	Retention Time (Min)	Compound	Formula	Molecular Weight	Species
1	~1.46	Sulphur dioxide	O ₂ S	64	AN, FS & FV
2	~1.63	<i>N,N</i> -dimethylmethanamine	C ₃ H ₉ N	59	FS & FV
3	1.93	2-methylfuran	C ₅ H ₆ O	82	All Species
4	2.56-2.59	2, 5-dimethylfuran	C ₆ H ₈ O	96	All Species
5	3.45-3.49	Toluene	C ₇ H ₈	92	All Species
6	~5.95	3-methylpyridine	C ₆ H ₇ N	93	AN, FS, FV & HE
7	8.01-8.24	Furfural	C ₅ H ₄ O ₂	96	All Species
8	~10.00	2-methylcyclopent-2-en-1-one	C ₆ H ₈ O	96	AN, FS, FV & HE
9	~11.01	1-(furan-2-yl)ethan-1-one	C ₆ H ₆ O ₂	110	AN, FS, FV & HE
10	~11.58 & 14.22	5-methylfuran-2-carbaldehyde	C ₆ H ₆ O ₂	110	All Species
11	14.74	3-methylcyclopent-2-en-1-one	C ₆ H ₈ O	96	FS
12	14.78 & 14.85	2-hepten-1-ol	C ₇ H ₁₄ O	114	AN & FV
13	~17.56	2,3-dimethylcyclopent-2-en-1-one	C ₇ H ₁₀ O	110	AN, FS & HE
14	~19.08	2-hydroxy-3-methylcyclopent-2-en-1-one	C ₆ H ₈ O ₂	112	AN, FS & HE
15	19.16	3-(hydroxymethyl)-1-methylpyrrolidin-2-one	C ₆ H ₁₁ NO ₂	129	FV
16	19.40	3-ethyl-2-hydroxycyclopent-2-en-1-one	C ₇ H ₁₀ O ₂	126	HE
17	20.75-20.98	Phenol	C ₆ H ₆ O	94	All Species
18	23.44	3-methylphenol	C ₇ H ₈ O	108	AN
19	23.45	Benzene-1,2,3-triol	C ₆ H ₆ O ₃	126	FS
20	23.47	Maltol	C ₆ H ₆ O ₃	126	FV
21	25.16-25.41	4-methylphenol	C ₇ H ₈ O	108	All Species
22	31.70 & 31.84	Dianhydromannitol	C ₆ H ₁₀ O ₄	146	AN, FS, FV & HE
23	36.35-36.48	Indole	C ₈ H ₇ N	117	All Species
24	~39.71	Isosorbide	C ₆ H ₁₀ O ₄	146	AN, FS, FV & HE
25	42.76	8-Heptadecane	C ₁₇ H ₃₄	238	UL
26	~50-52	Phytol	C ₂₀ H ₄₀ O	296	AN, FS, FV & UL
27	~55.12	Tetradecanoic acid	C ₁₄ H ₂₈ O ₂	228	AN, FS, FV & HE
28	62.08 - 62.60	Hexadecanoic acid	C ₁₆ H ₃₂ O ₂	256	All Species
29	68.06 – 68.88	Oleic acid	C ₁₈ H ₃₄ O ₂	282	All Species

4.4.2. Py-GC-MS of microalgae species

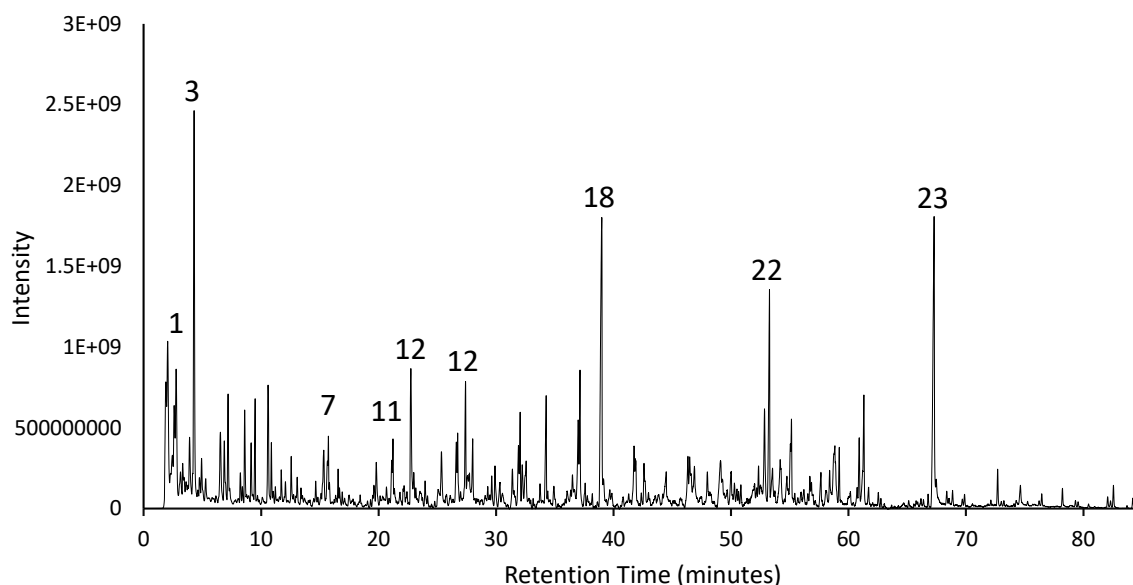


Figure 4.3. Py-GC-MS profile at 500 °C for *Nannochloropsis sp.*

The analytical pyrolysis of the microalgae species produces a large amount of oxygenated compounds, the majority of which occur at a retention time >35 minutes. These oxygenates include alcohols, ketones, long chain alkanes (desirable for transportation fuels) [74], carboxylic acids and aldehydes. These are the pyrolysis degradation products of fatty acids and triglycerides within the algae.

There are a number of key components that are present in all of the microalgae samples, these are; phenol and methyl substituted phenol (~20.5 and 25 minutes), indole (~36 minutes), Phytol (~50-52 minutes) and hexadecanoic acid (~62.5 minutes). Phytol is believed to be derived from the pyrolysis of chlorophyll [65] hence its presence in each chromatograph (all green microalgae species).

Both *I galbana.* and *A platensis.* typically contain higher protein contents than *Nannochloropsis sp.* this was observed in the results due to a greater abundance of protein derived compounds seen in the Py-GC-MS chromatograms at retention times <40 minutes for *I galbana.* and *A platensis.* These protein derived compounds include toluene (~3.5 minutes), phenols (20.5 and 25 minutes), and nitrogen containing compounds such as indole and methyl indole (32.6 and 39.8 minutes), pyrroles (~9 and 12 minutes) and pyridine (~4 minutes).

Table 4.4. Major compounds identified from the pyrolysis of the microalgae samples at 500 °C using Py-GC/MS.

Peak Number	Retention Time (Min)	Compound	Formula	Molecular Weight	Species
1	2.32 & 2.33	Benzene	C ₆ H ₆	78	NSp & IG
2	2.55	2-methylbutanal	C ₅ H ₁₀ O	86	SP
3	3.47 - 3.49	Toluene	C ₇ H ₈	92	All Species
4	3.91 – 3.99	Pyridine	C ₅ H ₅ N	79	All Species
5	5.78 – 5.80	p-Xylene	C ₈ H ₁₀	106	All Species
6	7.81 - 7.89	4-methylpentanenitrile	C ₆ H ₁₁ N	97	All Species
7	8.9 & 9.2	2-methyl-1H-pyrrole	C ₅ H ₇ N	81	All Species
8	10.05 – 10.19	2-Furanmethanol	C ₅ H ₆ O ₂	98	All Species
9	13.21	2,3-dimethyl-1H-pyrrole	C ₆ H ₉ N	95	SP
	12.59 & 13.12				NSp
10	19.48	6,7-dihydro-5H-cyclopenta[<i>b</i>]pyridine	C ₈ H ₉ N	119	SP
11	20.48-20.98	Phenol	C ₆ H ₆ O	94	All Species
12	25.02 – 25.27	methylphenol	C ₇ H ₈ O	108	All Species
13	30.66 & 30.05	Dianhydromannitol	C ₆ H ₁₀ O ₄	146	NSp & IG
14	31.46 - 31.56	3-phenylpropanenitrile	C ₉ H ₉ N	131	All Species
15	32.68	4-(2-methylprop-2-en-1-yl)oxan-2-one	C ₉ H ₁₄ O ₂	154	SP
16	33.30	Hexadec-2-en-1-ol	C ₁₆ H ₃₂ O	240	NSp
17	33.89 & 33.94	Pentadecane	C ₁₅ H ₃₂	212	NSp & SP
18	36.20-36.38	Indole	C ₈ H ₇ N	117	All Species
19	38.53	Isosorbide	C ₆ H ₁₀ O ₄	146	NSp
20	39.71 – 39.86	Methyl-indole	C ₉ H ₉ N	131	All Species
21	43.45 & 43.09	Heptadecane	C ₁₇ H ₃₆	240	SP & NSp
22	49.08 & 49.59	3,7,11-trimethyldodecan-1-ol	C ₁₅ H ₃₂ O	228	SP
	49.05				NSp
23	~50.20 & 51.90	Phytol	C ₂₀ H ₄₀ O	296	All Species
24	54.85 & 55.14	Tetradecanoic acid	C ₁₄ H ₂₈ O ₂	228	NSp & IG
25	56.32	2-[2-methyl-5-(prop-1-en-2-yl)cyclopentyl]acetamide	C ₁₁ H ₁₉ NO	181	SP
26	57.58	Oleanitrile	C ₁₈ H ₃₃ N	263	NSp
27	58.10 & 57.96	Hexadecanenitrile	C ₁₆ H ₃₁ N	237	SP & NSp
28	62.40 – 62.91	Hexadecanoic acid	C ₁₆ H ₃₂ O ₂	256	All Species
29	67.67 & 68.5	Oleic acid	C ₁₈ H ₃₄ O ₂	282	NSp & IG
	68.41				
30	68.89 & 69.18	9,12,15-octadecatrienoic acid	C ₁₈ H ₃₀ O ₂	278	SP & IG
31	71.27	9-Octadecanamide	C ₁₈ H ₃₅ NO	281	NSp
32	71.86 & 71.57	Hexadecanamide	C ₁₆ H ₃₃ NO	255	SP & NG

4.5. Model compounds characterisation

The main biochemical components present in the cells of microalgae are carbohydrates, lipids and proteins, these account for the greatest proportion of the biological content of the cell. There are a number of other components which form a very small fraction of the algal cell matrix such as nucleic acids, chlorophyll, sterols and carotenoids. Together these biological components account for the vast majority of the algal mass on an ash free and dry basis. There are also small quantities of inorganic material such as heavy metals and salts that contribute to the ash fraction. The relative concentrations of each of these components, both organic and inorganic, depends on a great number of factors related to algal species, growth phase when harvested, growth media and other cultivation conditions.

Typically, across the commonly studied microalgae it is protein fraction that is more abundant than both carbohydrates and lipids which typically share the remainder of the mass on a dry ash free basis. Protein contents can range from 10 wt.% to as high as 70 wt.% [12]. Most commonly the crude protein content is in the region of 45-60 wt.%, the most common amino acids present are alanine, arginine, aspartic acid, glutamic acid, glycine, leucine, lysine, phenylamine, proline, serine and threonine [176, 177].

Typical lipid content for microalgae is in the range of 4-20 wt.%, this value can be raised dramatically when grown under stressed conditions through limiting certain nutrients to achieve levels as high as 80 wt.% for certain species [178]. Microalgae can produce varying and different types of lipids, one such type is triacylglycerols, these are neutral lipids which are stored in lipid bodies inside the cell as energy stores, typically only found in meaningful levels when exposed to stressed cultivation conditions. Another category of lipids are polar lipids such as phospholipids found in the extrachloroplast membranes and glycolipids found in the cell membranes. All the aforementioned lipids contain fatty acids in the range of C12 to C24, most commonly with monounsaturated and polyunsaturated fatty acids in the range of C16 to C18. The lipid composition of *Nannochloropsis sp.* used in this study is shown in **Appendix A - Table A.1**, in summary the most abundant fatty acids present as a percentage of the total lipid content are palmitic acid C16 (21.5%), oleic acid C18 (18%) and eicosapentaenoic acid (EPA) C20 (30.3%).

The carbohydrate fraction of microalgae is often overlooked as the main commercial interest in microalgae has centred around the protein fraction for animal and human nutrition and the lipid fraction for its utilisation in third generation biofuels and in a smaller capacity as human nutraceuticals. The carbohydrates within the microalgae are the main product from photosynthesis. They are mainly in the form of polysaccharides and can accumulate in large amounts in the plastids as reserve

materials in the form of starch. Polysaccharides can also be a main component of the cell walls where the inner layer mainly in the form of cellulose and in the outer layer containing pectin, agar or alginate [28]. A study of 46 different microalgae [179] revealed that glucose was present in every species with concentrations across all species of between 5.6% and 66.8% (d.b), other monosaccharides detected in high amounts were mannose, galactose, rhamnose and xylose with maximum concentrations across all species up to 15%, 7%, 3% and 17% (db) respectively.

Isolates/analogues of the major components of the algal feedstock were selected. These include protein fraction related compounds; full protein isolate from soy beans and two pure amino acids; L-Leucine and L-Glutamine. Carbohydrate related compounds; cellulose, starch from corn and glucose. Finally the lipid/fatty acid related compounds; stearic acid (Octadecanoic acid) and oleic acid (Octadecenoic acid) both C:18 molecules were selected. Whilst it is recognised that these model compounds are not perfect comparators to represent the complex mixture of macromolecules present in different microalgal species. It is believed that they provide a good approximation and represent either key linkages to microalgae compounds, or represent an important intermediate product, this is in order to further understand their general behaviour in hydrothermal conditions.

4.5.1. Proximate and ultimate analysis of model compounds

Table 4.5 presents the proximate and ultimate composition of the model compounds. The only model compound with a distinct ash content is soy protein at 5.0 wt.%. Higher ash content negatively affects the HHV as a greater proportion of the biomass sample is non-combustible inorganic matter. The moisture content of all the model compounds varies from between 0 to 12.8 wt.% with the majority of compounds with very low moisture content of 0 to 0.3 wt.% with only 3 model compounds having higher values of 3.6 wt.%, 12.8 wt.% and 8.7 wt.% for cellulose, corn starch and soy protein respectively.

The two lipid model compounds have the highest carbon content of 74.9 wt.% (daf) for both samples and a hydrogen content of 13.0 and 13.3 wt.% (daf) for oleic and stearic acid respectively resulting in very high heating values of 41.9 and 42.5 MJ/kg respectively. The four studied carbohydrate model compounds are very high in oxygen with a range of 52.0 to 54.9 wt.% (daf). Their carbon content is also the lowest of the model compounds 38.3 to 41.6 wt.% (daf). High oxygen and low carbon content results in reduced heating values of 12.4 to 13.8 MJ/kg. The amino acids L-Glutamine and L-Leucine have the highest nitrogen content of 20.2 and 11 wt.% respectively, followed by the soy protein isolate at 15.4 wt.%.

Table 4.5. Proximate and ultimate analysis, HHV, atomic ratios of model compounds and microalgae

Compound	Ash	Moisture	C	H	N	S	O*	HHV (MJ/kg)	H/C	O/C	N/C
Model Compounds											
Glucose	0.0	0.2	39.7	6.8	Nd	Nd	53.5	13.6	2.04	1.01	0.001
Xylose	0.0	0.1	39.6	6.8	Nd	Nd	53.5	13.6	2.04	1.01	0.001
Cellulose	0.0	3.6	41.6	6.3	0.1	Nd	52.0	13.8	1.80	0.94	0.002
Cornstarch	0.1	12.8	38.3	6.5	0.2	Nd	54.9	12.4	2.01	1.07	0.004
Oleic Acid	0.0	0.1	74.9	13.0	Nd	Nd	12.1	41.9	2.06	0.12	0.000
Stearic acid	0.0	0.3	74.9	8.9	0.1	Nd	15.9	35.3	1.42	0.16	0.001
Soy protein	5.0	8.7	44.7	7.3	15.4	0.5	27.1	20.8	1.94	0.45	0.296
L-glutamine	0.0	0.1	40.7	7.0	20.2	Nd	32.1	18.0	2.04	0.59	0.426
L-leucine	0.0	0.1	54.0	10.1	11.0	Nd	24.9	28.3	2.23	0.35	0.175
Microalgae											
Nannochloropsis sp.	18.1	8.7	44.2	6.0	6.3	0.5	25.0	19.1	1.61	0.43	0.122

Variation in the elemental composition of the algal species and characterised model compounds will result in unique chemical composition of HTL derived bio-crudes. Therefore, a set of HTL experiments with selected model components was carried out in order to investigate the reaction pathways for distinct groups of macromolecules with results presented in **Chapter 5 Section 5.2.3**.

4.5.2. Thermogravimetric analysis

Figure 4.4 presents the differential thermogravimetric (DTG) profiles for three of the model compounds representing each of the key algal macromolecules. Oleic acid shows only one main devolatilization peak, a rapid mass loss first occurring at ~200 °C reaching a maximum at 315 °C. The DTG curves for the glucose and soy protein samples display a mass loss over a much broader temperature range. It is observed that the main devolatilization peak occurs at 330 °C with a smaller additional peak seen at 245 °C. TGA of soy protein reveals one broad mass loss event with a maximum mass loss occurring at 320 °C. Similarly, to the macro and microalgae samples from **Section 4.3** and the model compounds herein show full decomposition up to the final temperature of 500 °C, therefore 500 °C was used in the analytical pyrolysis experiments.

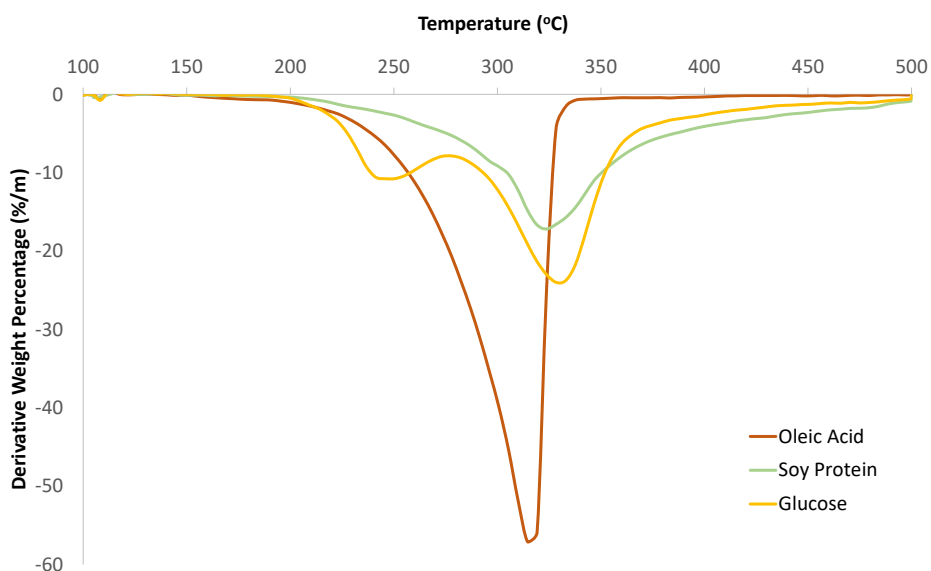


Figure 4.4. DTG profiles of selected model compounds (oleic acid, soy protein and glucose) in nitrogen at 25 °C min⁻¹.

4.5.3. Py-GC-MS of model compounds

Analytical pyrolysis was carried out to understand the thermal degradation routes both for model components and chosen for the HTL processing *Nannochloropsis sp.* sample. Model components were chosen to represent key building blocks of algae species, including carbohydrates, lipids and proteins. The Py-GC-MS analysis, reported in this chapter, was applied to indicate potential end-products from the HTL treatment experiments.

Chromatograms of glucose and xylose samples pyrolysed at 500 °C are given in **Figure 4.5** and **Figure 4.6**, respectively.

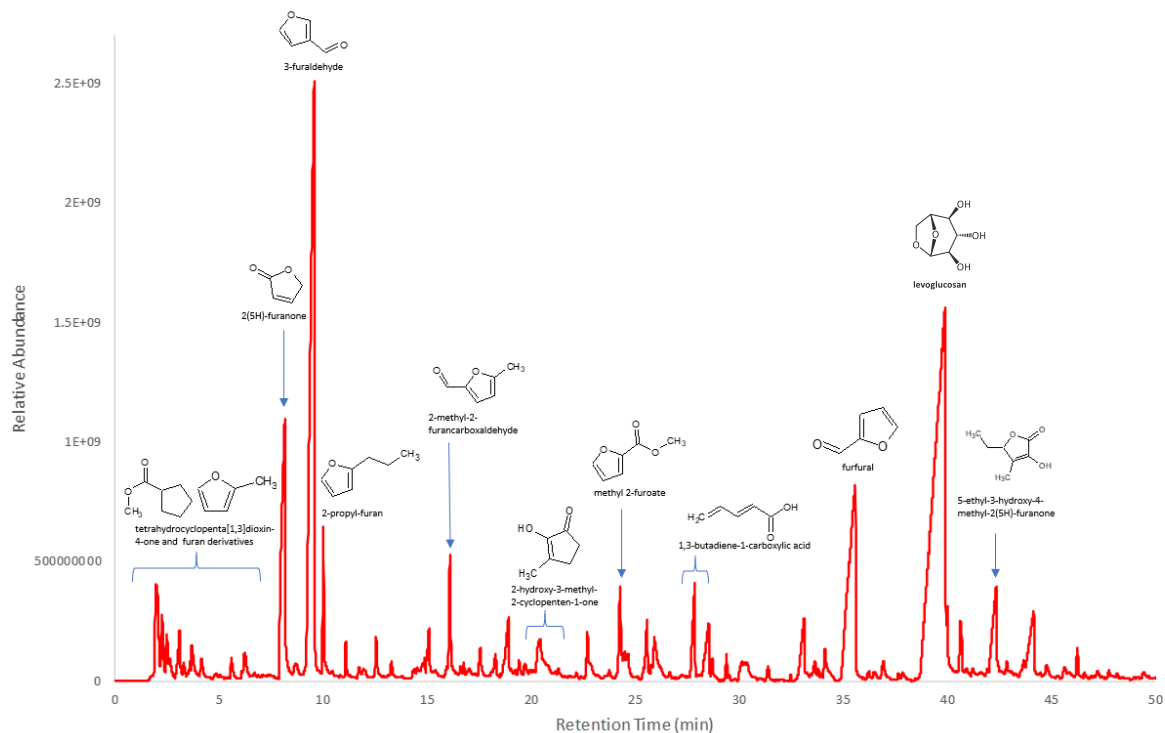


Figure 4.5. GC-MS chromatogram for glucose pyrolysed at 500 °C.

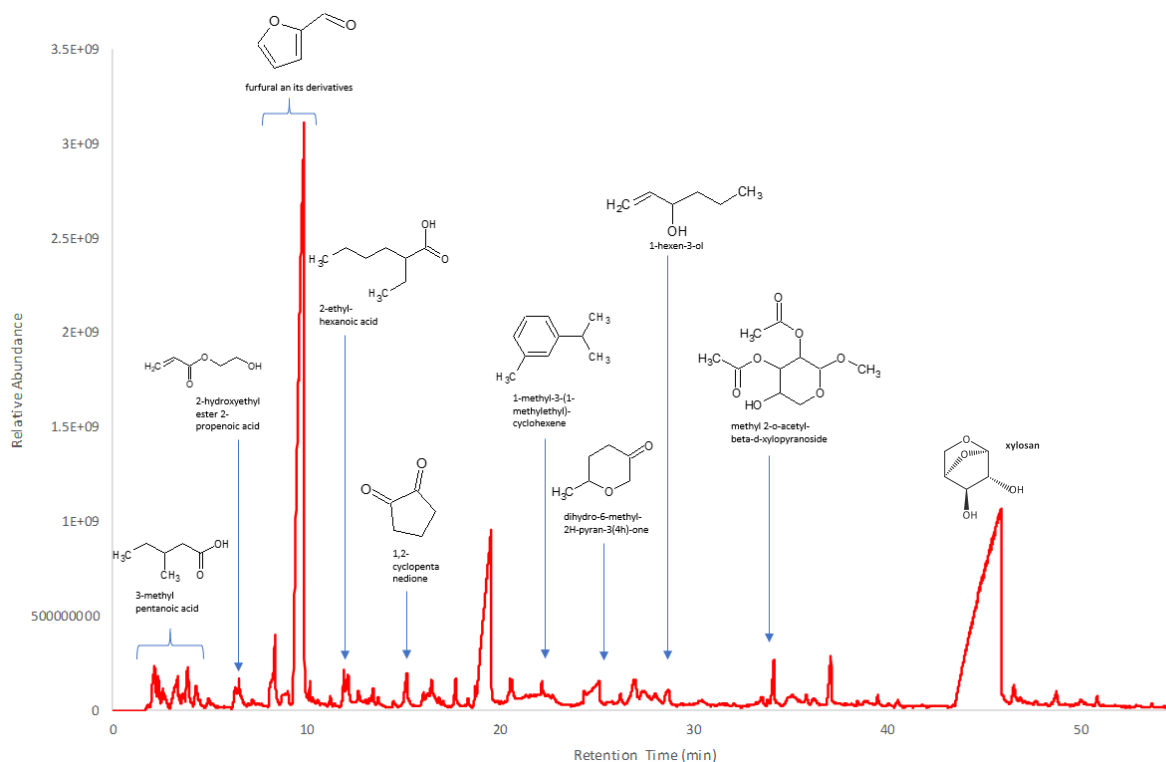


Figure 4.6. GC-MS chromatogram for xylose pyrolysed at 500 °C

The highest yielding components observed from the Py-GC-MS analysis of glucose are tetrahydrocyclopenta[1,3]-dioxin-4-one (2.01 min.) at 7.3 wt.%; 2(5H)-furanone (8.1 min.) at 5.12 wt.%;

3-furaldehyde (9.6 min.) at 14.54 wt.%; 2-hydroxy-3-methyl-2-cyclopenten-1-one (20.4 min.) at 2.85 wt.%; furfural (33.2 min.) at 6.53 wt.% and 1,6-anhydro-D-glucopyranose (39.9 min.) at 21.94 wt.%.

Intermediates resulting from dehydration of both carbohydrates, such as furan and its derivatives, are abundant in the Py-GC-MS chromatogram. Examples of those include 3-furaldehyde (9.8 min.), 2-propyl-furan (10.1 min.), 2-methyl-2-furancarboxaldehyde (16.1 min.) and methyl 2-furoate (24.3 min.). These particular compounds undergo further transformation via dehydration reactions into furanone and cyclopentane derivatives, which can be observed in the Py-GC-MS chromatograms. The following furanone and cyclopentane derivatives were detected: tetrahydrocypenta[1,3]dioxin-4-one (2.1 min.), 2(5H)-furanone (8.2 min.), 2-hydroxy-3-methyl-2-cyclopenten-1-one (20.4 min.), and 5-ethyl-hydroxy-4-methyl-2(5H)-furanone (44.1 min.).

One of the most abundant compounds present at a relatively high yield of 21.94 wt.%, is 1,2,4-benzenetriol. The aldol splitting and cyclisation of furan and furfural derivatives is accounted for the formation of this particular component.

Glucose treated under pyrolytic conditions has produced many more furfurans and furan derivatives compared to xylose. Xylose pyrolysis resulted in many cyclic C5 and aromatic products. The most abundant compounds observed from the xylose Py-GC-MS chromatogram (from left to right) are 3-methyl-pentanoic acid (3.3 min.) at 10.7 wt.%; furfural (9.9 min.) at 22.7 wt.%, 1-methyl-3-(1-methylethyl)-cyclohexene (22.2 min.) at 7.23 wt.% and methyl alpha-d-glucopyranoside (45.9 min.) at 16.4 wt.%.

Carboxylic acids and alcohols were observed with lower retention times, including 3-methyl-pentanoic acid, resulting from carbohydrates undergoing thermal degradation at high temperatures.

Xylose Py-GC-MS chromatogram has shown a lot of cyclic C5 hydrocarbons and aromatics such as 1-methyl-3-(1-methylethyl)-cyclohexene (22.2 min.), dihydro-6-methyl-2H-pyran-3(4H)-one (25.1 min.), methyl 2-O-acetyl-beta-d-xylopyranoside (35.1 min.) and xylosan (45.9 min.). This is resultant of aldol splitting and cyclisation of, furan and furfural derivatives and is representative of the reaction occurring during HTL observed by Lopez Barreiro *et al* [21]. The formation of cyclic C5 hydrocarbons and aromatics was favoured during the thermal degradation of xylose.

Proteins are the key building blocks of microalgae. A primary structure of a hypothetical protein along with some amino acids that can be potentially found in algae is given in **Figure 4.7**.

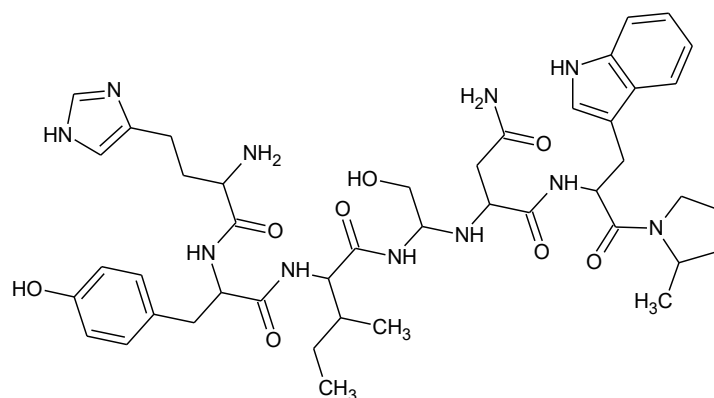


Figure 4.7. Primary structure of a hypothetical protein in algae [Adapted from [55]]

Soy protein, L-glutamine and L-leucine have been examined in this study with a Py-GC-MS to assess potential end-products during thermal degradation at high temperatures. Soy protein (naturally occurring polymer) is often found in chains, while L-glutamine and L-leucine are simple amino acids.

The Py-GC-MS chromatograms for soy protein pyrolysed at 500 °C are given in **Figure 4.8**.

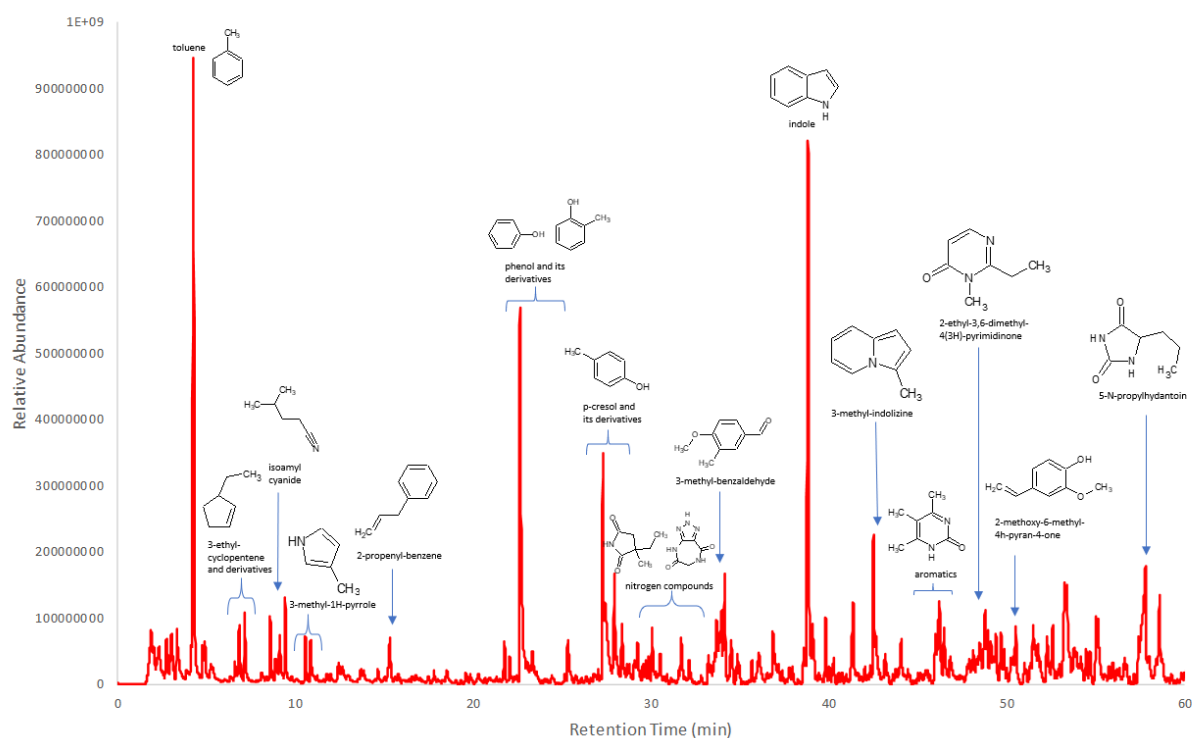


Figure 4.8. GC-MS chromatogram for soy protein pyrolysed at 500 °C.

The most abundant compounds identified after the thermal degradation under pyrolytic conditions were 2-methyl-furan (2.3 min.) at 3.37 wt.%, toluene (4.3 min.) at 6.67 wt.%, phenol (22.6 min.) 5.43 wt.%, p-cresol (27.4 min.) at 3.28 wt.% and indole (38.8 min.) at 4.51 wt.%.

Except for 2-methyl-furan, all major identified compounds from thermal degradation of the soy protein sample are aromatics. Due to the chemical structure of a protein, such high concentrations of aromatic compounds can be associated with the rearrangement of benzene rings in the naturally occurring polymer during thermal degradation.

During hydrothermal liquefaction, it is also essential to consider that amino acids (originated from the hydrolysis of proteins) often undergo two consecutive reactions, such as decarboxylation and deamination.

The decarboxylation reactions are favoured at higher temperatures, whereas deamination reactions are favoured at lower temperatures [34].

The higher concentrations of aromatic compounds can be explained as analytical pyrolysis has occurred at a relatively high temperature of 500 °C. This is due to the decarboxylation of amino acids to form amines, which undergo further deamination and rearrangement reactions to form aromatic compounds. As the hydrothermal liquefaction processes operate at lower temperatures (250-370 °C), this may result in higher deamination rates of amino acids higher concentrations in carboxylic acids (as deamination end-products).

A significant number of nitrogen-containing compounds were identified in soy protein pyrolysis products, such as isoamyl cyanide (9.2 min.), 3-methyl-1H-pyrrole(10.9 min.), indole (38.8 min.), 3-methyl-indolizine (42.6 min.), 2-ethyl-3,6-dimethyl-4(3H)-pyrimidinone (48.8 min.) and 5-N-propylhydantoin (57.8 min.). These heterocyclic N-containing compounds originate from amino acids that undergo Maillard and aldol splitting reactions under pyrolytic conditions.

The most abundant components identified in the pyrolysis products of L-Glutamine (presented in **Figure 4.9**) are 2,3,4-trimethyl-cyclopent-2-ene-1-one (23.9 min.) at 3.87 wt.%, 4-hydroxy-3,5-dimethoxy-benzaldehyde (55.8 min.) at 25.27 wt.%, 1-(4-hydroxy-3,5-dimethoxyphenyl)-ethanone (59.7 min.) at 11.28 wt.%, 2,5-dimethoxy-benzenemethanol acetate (61.5 min.) at 12.86 wt.%, 1,2-dihydro-2-phenyl-3h-indazol-3-one (62.8 min.) at 8.10 wt.%, 4,4,5,6,7,8-hexamethyl-1,2,3,4,5,6,7,8-octahydrophthalen-2-one (67.6 min.) at 1.90 wt.%.

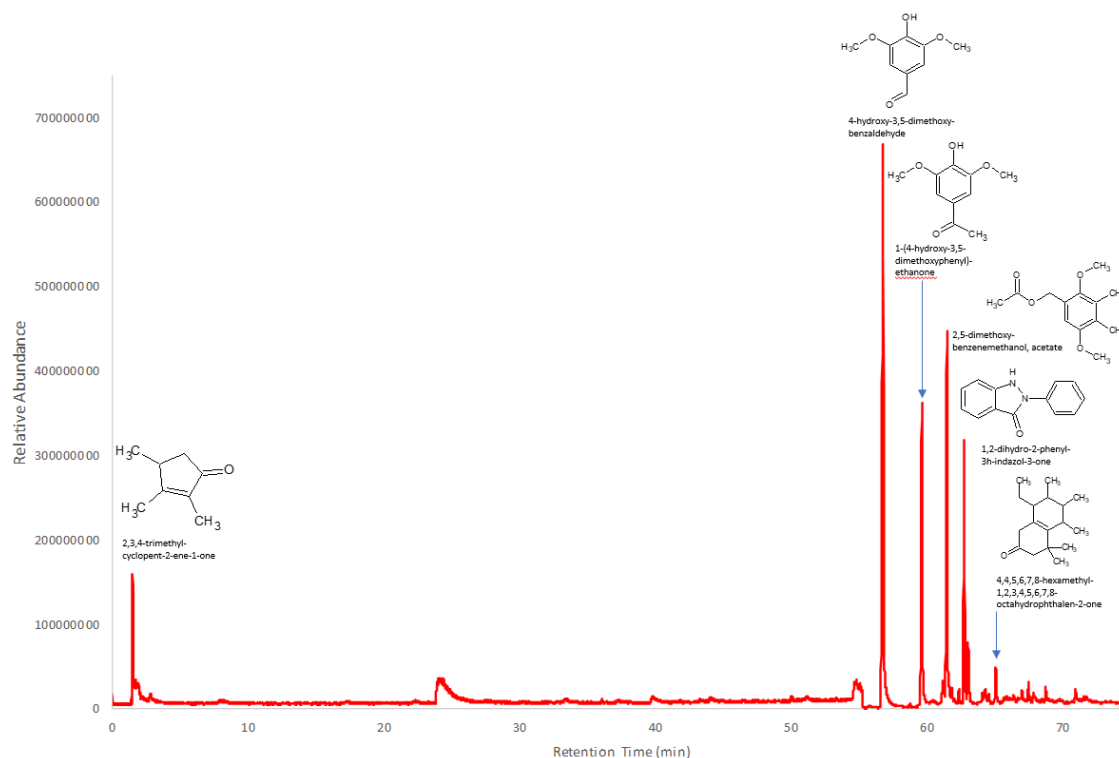


Figure 4.9. GC-MS chromatogram for L-Glutamine pyrolysed at 500 °C

The distribution of pyrolysis products from L-glutamine has displayed the occurrence of aromatisation reaction by closing its simple structure and formation of C6 rings, including benzene-aldehydes. 2,5-dimethoxy-benzene methanol acetate was detected and observed to be an intermediate compound, which undergoes further cracking to produce 4-hydroxy-3,5-dimethoxy-benzaldehyde and 1-(4-hydroxy-3,5-dimethoxyphenyl)-ethanone.

The pyrogram for the amino acid L-Leucine is presented in **Figure 4.10**.

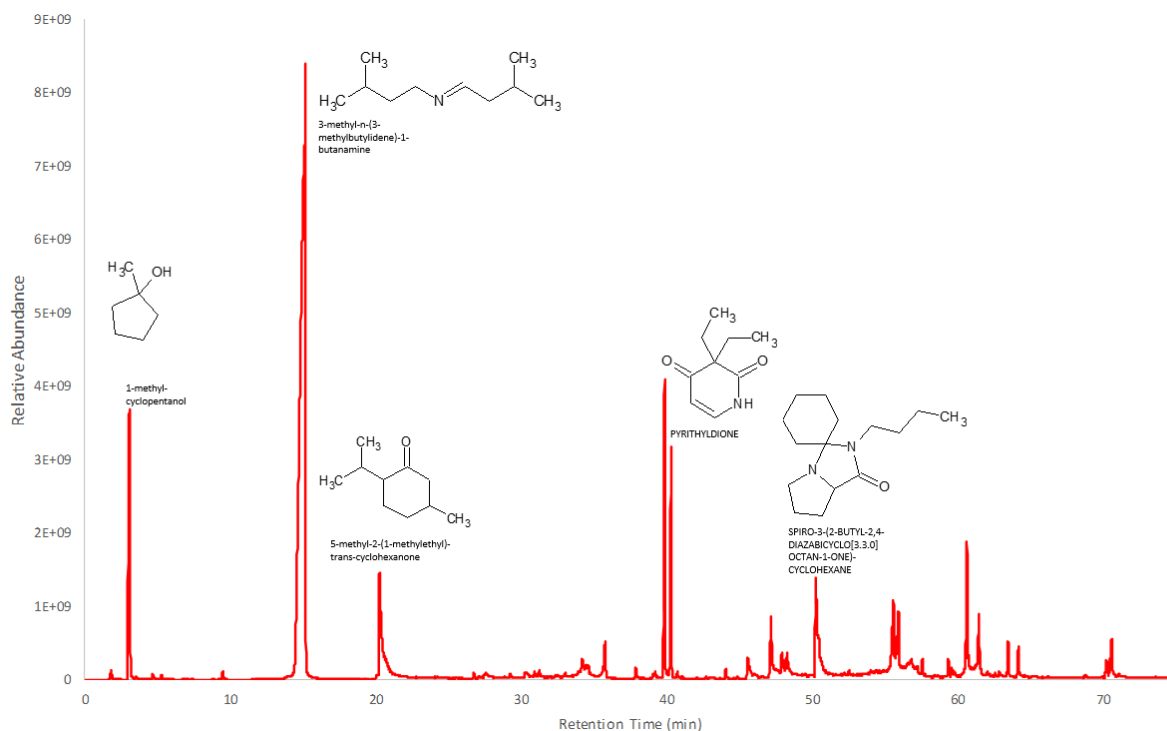


Figure 4.10. GC-MS chromatogram for L- Leucine pyrolysed at 500 °C

The most abundant compounds observed in pyrolysis products are 1-methyl-cyclopentanol (3.1 min.) at 34.13 wt.%, 3-methyl-N-(3-methylbutylidene)-1-butanamine (15.2 min.) at 57.93 wt.%, 5-methyl-2-(1-methylethyl)-trans-cyclohexanone (20.3 min.) at 1.36 wt.%, pyrithyldione (40.3 min.) at 0.57 wt.%, spiro-3-(2-butyl-2,4-diazabicyclo[3.3.0]octan-1-one)-cyclohexane (50.2 min.) at 0.77 wt.%.

The pyrolysed L-Leucine sample has created cyclic compounds through ring-closing rearrangement under pyrolytic conditions. This resulted in the formation of compounds such as pyrithyldione. The most abundant compound observed is 3-methyl-N-(3-methylbutylidene)-1-butanamine and is an example of two butyl-amines undergoing scission under pyrolytic conditions.

Pyrolytic behaviours of lipid during pyrolysis was studied by thermal degradation of two model components - stearic and oleic acids. During pyrolysis, triacylglycerols (TAG) molecules, which are major components of lipids, undergo hydrolysis to form fatty acids and glycerol. During HTL, these fatty acids undergo further reactions to form constituents of bio-crude.

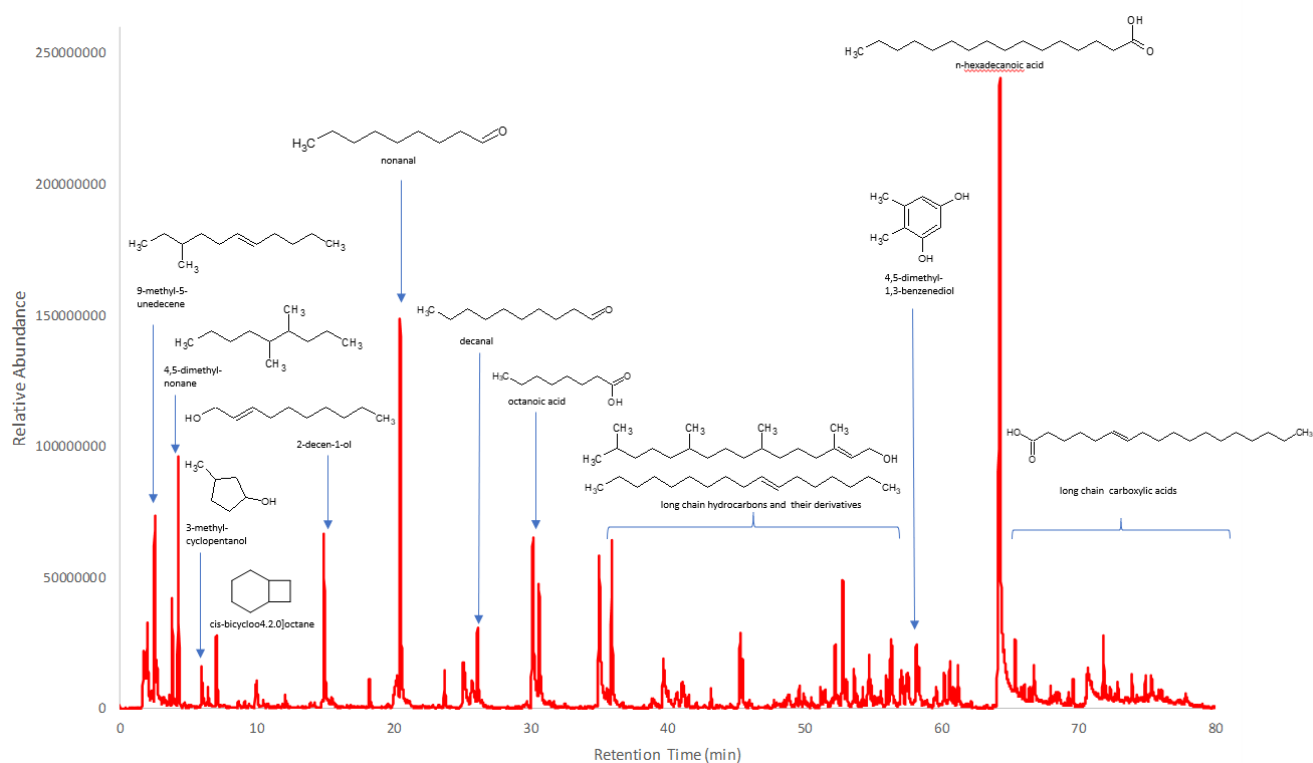


Figure 4.11. Oleic Acid Py-GC-MS Chromatogram

From the oleic acid pyrogram presented in **Figure 4.11** the most abundant component among all pyrolysis compounds is n-hexadecanoic acid (palmitic acid). Many observed long-chain carboxylic acids result from partial cracking of oleic acid under pyrolytic conditions. The presence of 9-methyl-5-undecene, 4,5-dimethyl-nonane and other alkanes or alkenes are due to decarboxylation of the original oleic acid. Other fatty acids resulting from the cracking of oleic acid include decanal (26.1 min.) and 2-methyl-1-pentadecene (30.6 min.). Slight traces of short-chain carboxylic acids were also identified, such as octanoic acid (30.2 min.). These can be related to the formation of cyclic compounds such as 3-methyl-cyclopentanol (3.8 min.), cis-bicyclo[4.2.0]octane (7.1 min.) and 4,5-dimethyl-1,3-benzenediol (52.2 min.).

The pyrogram for the stearic acid (C18 saturated long-chain fatty acid) is presented in **Figure 4.12**.

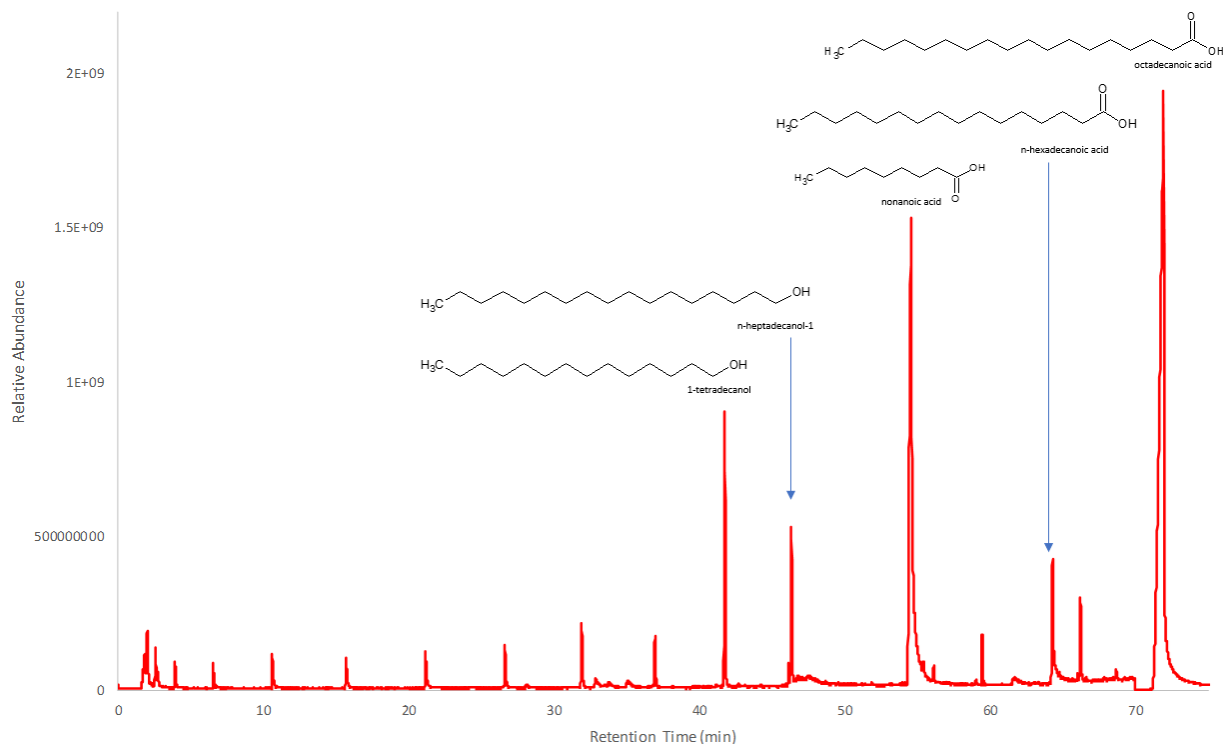


Figure 4.12. Stearic Acid Py-GC-MS Chromatogram

Stearic acid has been proven to be stable under high-temperature pyrolytic conditions, with a noticeable chromatogram peak at 72.3 min. As the most abundant components were identified: 1-tetradecanol (41.6 min.) at 1.10 wt.%, n-heptadecanol-1 (46.3 min.) at 0.66 wt.%, nonanoic acid (54.6 min.) at 4.02 wt.%, n-hexadecanoic (64.3 min.) at 1.92 wt.% and octadecanoic acid also known as stearic acid (71.9 min.) at 87.38 wt.%.

Studied model components described and characterised by Py-GC-MS have been chosen to reflect the real microalgae sample undergoing HTL processing. This develops an understanding of possible thermal degradation products from microalgae that could be obtained through thermal processing, Py-GC-MS chromatogram for *Nannochloropsis sp.* is presented in **Figure 4.13**.

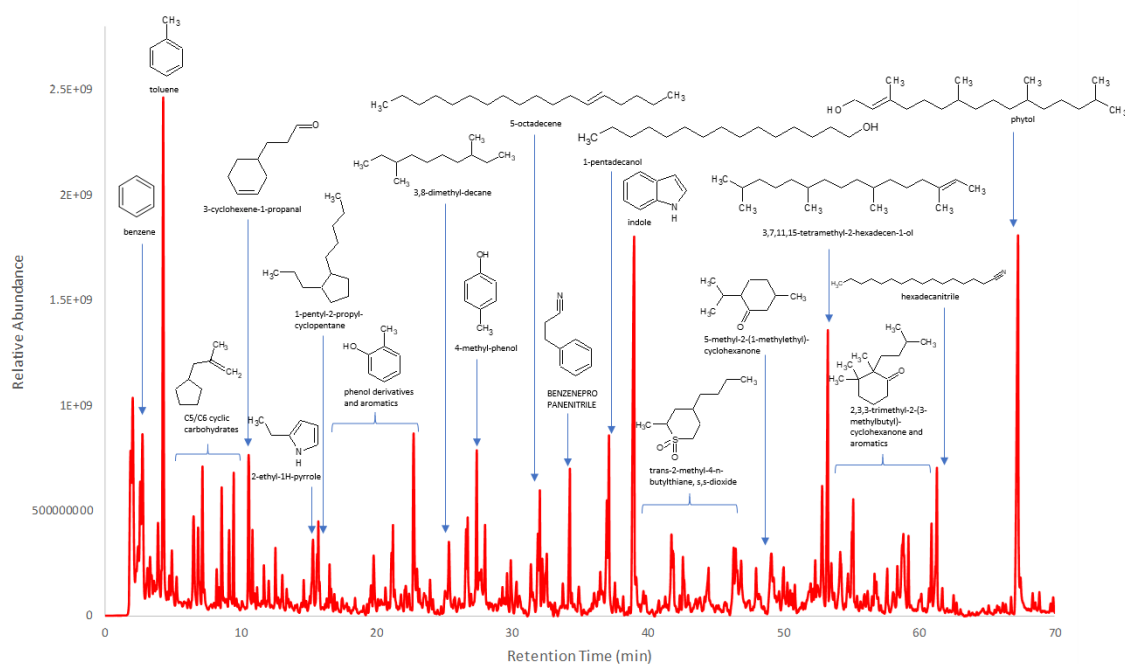


Figure 4.13. GC-MS chromatogram for *Nannochloropsis sp.* pyrolysed at 500 °C

The most abundant compounds found during the analytical pyrolysis of *Nannochloropsis sp.* were: 3-penten-1-ol (1.7 min.) at 4.73 wt.%, benzene (2.8 min.) at 3.06 wt.%, toluene (4.3 min.) at 4.68 wt.%, phenol (22.7 min.) at 2.10 wt.%, indole (39.0 min.) at 3.52 wt.% and phytol (67.3 min.) at 2.68 wt.%. Over 21 wt.% of *Nannochloropsis sp.* pyrolysis products have been identified as aromatic and nitrogen-containing heterocyclic compounds. This coincides with high protein content (52 wt.%) in the chosen *Nannochloropsis sp.* sample. Similar thermal degradation products were observed during the pyrolysis of protein model components. Indole (a soy protein pyrolysis marker) is one of the most abundant compounds noted in **Figure 4.13**. It is an example of products from Maillard and aldol splitting reactions occurring under pyrolytic conditions. 2-ethyl-1-H-pyrrole can be linked to further thermal decomposition of indole. The occurrence of ring formation can explain the formation of other N-aromatic compounds and the aromatisation of short-chain amino acids present within the more complex protein structures following initial hydrolysis and cracking at high temperatures.

Some intermediate compounds such as 1-pentyl-2-propyl-cyclopentane (15.7 min.) can be linked to the presence of carbohydrates. Furan and furfural derivatives (formed during the pyrolytic dehydration of carbohydrates) are further cracked to cyclopentane derivatives such as: 1,3-dimethyl cyclopentane (2.6 min.), 1,2,3-trimethyl-cyclopentane(3.9 min.), methylcyclopentane (5.3 min.)

and 2,3,4-trimethyl-cyclopent-2-ene-1-one (19.8 min.). However, detected C5 cyclic compounds are relatively low in concentration, representing the species' carbohydrate content of 12 wt.%.

Approximately 15 wt.% of *Nannochloropsis sp.* pyrolysis products contain long-chain alkanes and alkenes. This is due to the decarboxylation of long-chain fatty acids present in the biochemical matrix of this algal species following the hydrolysis of TGAs. Short-chain alcohol such as 3-pentene-1-ol (1.7 min.) can be related to the cracking of glycerol, which is formed via the hydrolysis reaction of lipids.

The results from the in-depth characterisation of macro and microalgal samples revealed that the most promising feedstocks for further HTL studies were *Ulva lactuca*, *Himantalia elongata*, *Nannochloropsis sp* and *Arthrospira platensis*. The selection was based on relatively high volatile content, low ash content in the case of the microalgae and potential end products to be generated during HTL treatment based on the Py-GC-MS studies.

Chapter 5 - Hydrothermal processing of algal and model compound feedstocks

5.1. Introduction

This chapter investigates the thermochemical treatment of a number of algal species and model compounds in two distinct parts. The first part of this chapter is focused on the treatment of one microalgae (*Nannochloropsis sp.*), one cyanobacteria (*Arthrospira platensis*) and two macroalgae - one brown (*Himantalia elongata*) and one green species (*Ulva lactuca*). Experiments were carried out on a small batch scale basis, and this work was in order to compare micro and macroalgae HTL yields and product fractions. Experiments were carried out in a 25 ml batch reactor at a constant residence time of 10 minutes and a final reaction temperature of 300 °C. In this HTL processing the influence of reaction atmosphere was also investigated, reactions were performed under nitrogen and hydrogen with final reaction pressures of between 130-150 barg dependant on reaction gas, algal species and loading.

The second part of this chapter focuses on a larger scale batch treatment of *Nannochloropsis sp.* in a 300 ml batch reactor. These experiments were carried out in order to establish the influence of final reaction temperature to maximise bio-crude yields and quality for further liquefaction experiments. Alongside these experiments a number of selected key model compounds were chosen to represent the three main macromolecular bio-constituents of microalga (such as lipids, proteins and carbohydrates) were subjected to liquefaction. All these feedstocks were processed on a batch basis under standard hydrothermal conditions used in the preliminary experiments. The model compounds hydrothermal processing work supports the understanding of the influence of macromolecular compounds on the yields and chemical composition of the resultant products. Experiments were carried out using a 300 ml batch reactor at a constant residence time of 10 minutes and a final reaction temperature of 300 °C. These conditions were chosen as a result of the initial reactor testing in **section 3.3.1** and based on the results from the separate study investigating the effect of reaction temperature, where the temperature was increased in 50 °C steps between 200 and 350 °C.

For the protein fraction a commercially available soy protein isolate and the amino acids L-Leucine and L-Glutamine were treated. The lipid fraction was represented with oleic and stearic acid and finally, the carbohydrate fraction was represented by glucose, cornstarch and cellulose. It is widely reported that bio-crude yields are typically much higher than the lipid content of the alga, this suggests that the

other fractions contribute to the bio-crude fraction. All model compounds were liquified under hydrothermal conditions at 300 °C without a catalyst and in an inert (nitrogen) atmosphere, and more details on experimental work are given in the methodology section (**Chapter 3, Section 3.3.2**). The results have been compared to the bio-products produced from the liquefaction of the microalgae *Nannochloropsis sp.*. The characterisation of the bio-crudes formed from the selected model compounds included elemental analysis, GC-MS and an in-depth NMR spectroscopy study to further understand their chemical composition.

5.2. Results and discussion

Initial hydrothermal experiments using micro and macro algae were undertaken in a small scale 25 ml Parr reactor, this was in order to quickly investigate bio-crude yields and product composition with small amounts of the feedstock. Following on from this a 300 ml Parr high-pressure reactor was used in further larger scale hydrothermal liquefaction experiments to generate increased amounts of bio-crude from the selected microalgae *Nannochloropsis sp* for analysis and for future bio-crude upgrading work covered in **Chapter 6**. The 300 ml reactor was also used in the investigation of model compound hydrothermal liquefaction experiment. More detailed descriptions of reactor setup, conditions and product collection procedure alongside reactor schematics are outlined in **Chapter 3**.

All macroalgae, microalgae and model compounds underwent hydrothermal liquefaction using the same reaction conditions of 300 °C with a short residence time of 10 minutes once the final reaction temperature had been reached. Heating rates for the smaller 25 ml reactor were approximately 7.5 °C/min and 9 °C/min for the larger 300 ml reactor.

5.2.1. Preliminary HTL processing in 25 ml batch reactor

For each experimental run (**Table 5.1**) a number of product fractions were produced, including; gaseous, various liquids and solids. For these initial experiments the gases were vented to atmosphere and no analysis was undertaken of the gaseous products. In all cases a solid residue was produced alongside a liquid fraction which in some runs also included a visibly separate thick oil fraction.

Table 5.1 shows the results from the hydrothermal liquefaction of micro- and macroalgae at a reaction temperature of 300 °C for a residence time of 10 minutes under different reaction atmospheres along with processing parameters.

Table 5.1. Products Obtained from Liquefaction Experimental Runs all treated at 300 °C, residence time of 10 minutes

Run Number	Algae Species	Reaction Atmosphere	Product Fractions		
			Aqueous	Solid	Visible Oil/Tar
1	<i>Arthrospira platensis</i>	Nitrogen	✓	✓	✓
2	<i>Himanthalia elongata</i>	Nitrogen	✓	✓	-
3	<i>Nannochloropsis sp</i>	Nitrogen	✓	✓	✓
4	<i>Ulva lactuca</i>	Nitrogen	✓	✓	-
5	<i>Arthrospira platensis</i>	Hydrogen	✓	✓	✓
6	<i>Himanthalia elongata</i>	Hydrogen	✓	✓	-
7	<i>Nannochloropsis sp</i>	Hydrogen	✓	✓	✓
8	<i>Ulva lactuca</i>	Hydrogen	✓	✓	-

All separated bio-crude samples underwent elemental analysis for carbon, hydrogen, nitrogen and sulphur content with oxygen calculated by difference. The results from the elemental analysis are presented in **Table 5.2** alongside the respective bio-crude yields and calculated higher heating values using the Dulong formula [164].

Table 5.2. Yields (wt.% daf basis) of the HTL products at 300 °C and 10 min residence time with elemental composition (wt.% daf basis) and HHV (MJ/kg) of the bio-crude

Run Number	Algae Species	Bio-crude Yield	C	H	N	S	O	H/C	O/C	HHV	Energy Recovery (%)
Nitrogen atmosphere											
1	<i>Arthrospira platensis</i>	30.1	70.9	7.2	8.8	0.6	12.6	1.22	0.13	32.2	41.7%
2	<i>Himanthalia elongata</i>	16.6	72.3	7.5	4.6	0.6	15.0	1.24	0.16	32.6	48.4%
3	<i>Nannochloropsis sp</i>	47.4	66.9	9.5	4.6	0.4	18.6	1.69	0.21	33.0	89.7%
4	<i>Ulva lactuca</i>	18.2	70.6	8.2	5.8	0.4	15.0	1.38	0.16	33.0	51.0%
Hydrogen atmosphere											
5	<i>Arthrospira platensis</i>	31.3	71.8	7.6	6.5	0.5	13.6	1.27	0.14	32.9	44.3%
6	<i>Himanthalia elongata</i>	17.5	73.5	7.4	4.4	0.5	14.2	1.20	0.15	33.0	51.6%
7	<i>Nannochloropsis sp</i>	48.6	68.6	10.1	3.8	0.4	17.2	1.75	0.19	34.7	96.7%
8	<i>Ulva lactuca</i>	18.5	71.7	8.4	5.9	0.4	13.6	1.40	0.14	34.0	53.2%

Yields for the microalgae and cyanobacteria (*Spirulina*) were a lot higher compared to the macroalgae, 30-49 wt.% vs 16-19 wt.% respectively. The high protein low lipid cyanobacteria *Arthrospira platensis*

showed a yield of 30 wt.%, the microalgae *Nannochloropsis sp.* achieved a higher yield of 47 wt.%, both of these values far exceed the lipid content of the raw feedstock. The bio-crude yield achieved for all algae samples is well above their crude lipid content. Despite *Arthrospira platensis*' low lipid content (6 wt.%) it was still able to achieve a high biocrude yield not that far from that of *Nannochloropsis sp.* (28 wt.% lipids) this is partly due to the significant difference in ash content due to their growth environment of freshwater versus marine. The yields were markedly lower for the two macroalgae species, the brown macroalgae *Himanthalia elongata* exhibits the lowest yield of 16.6 wt.% whereas the green macroalgae *Ulva lactuca* achieved a slightly higher yield of 18.2 wt.%. Both macroalgae have very low lipid levels, high ash due to marine species and high carbohydrate content. The effect of applying a hydrogen reaction atmosphere shows only a small increase in bio-crude yield for both the macro and micro algae of between 0.3 and 1.2 %.

Overall, the elemental composition shows that the bio-crudes produced from all species were of high quality. The content of heteroatoms (N, O and S) is quite high in all bio-crudes produced, these should be as low as possible as they lead to undesirable emissions following combustion such as NO_x and SO_x, these heteroatoms additionally negatively impact the HHV (excluding N). The highest HHV was obtained from *Nannochloropsis sp.* with hydrogen reaction atmosphere at 34.7 MJ/kg with the other bio-crudes in the region of 32.2 – 34 MJ/kg. The nitrogen content of the bio-crudes ranges from 4.6 to 8.8 wt.%, these values are directly related to the nitrogen content of the original algal feedstock. The high protein *Arthrospira platensis* produced an oil with the highest nitrogen content of 8.8 wt.% whereas the microalgae *Nannochloropsis sp.* produced a bio-crude with 4.6 wt.% N. These values for N are far greater than for typical petroleum crude oil ~ 0.1-2 wt.% [125] and oils derived from the pyrolysis of lignocellulosic biomass of 0.5 to 1.6 wt.% [174, 175]. The high nitrogen content in the bio-crude produced from the liquefaction of high protein feedstock is a major drawback when processing whole-cell microalgae. Heteroatoms are a major challenge for the necessary upgrading of the bio-crude, it places a large demand on external hydrogen in order to remove the large amounts of both nitrogen and oxygen as ammonia and water respectively, through hydrogenolysis reactions hydrodenitrogenation (HDN) and hydrodeoxygenation (HDO) respectively.

There are a number of solutions to reduce heteroatom content in the bio-crude, but each has its challenges and associated increase in production costs. One is to cultivate only high lipid, low protein algae but these are slower to produce, more complex to obtain and therefore more expensive.

The changes seen in the elemental composition for the bio-crudes formed under a hydrogen atmosphere shows only very small changes/improvements in product composition. All samples saw small increases in carbon and hydrogen content coupled with small decreases in nitrogen content,

most notably for *Arthrospira platensis* where nitrogen decreased from 8.8 wt.% to 6.5 wt.%. As a consequence of the improved elemental composition the calculated HHV increased slightly for each species investigated.

When comparing the bio-crudes produced from liquefaction against the original algae feedstock it is clear that there has been a significant upgrade in fuel quality. **Figures 5.1a & b** show the Van Krevelen plots of the raw algal feedstock and the resultant HTL bio-crudes. Atomic O/C is plotted against atomic H/C in **Figure 5.1a** and atomic N/C is plotted against atomic H/C in **Figure 5.1b**, improvement of the fuel characteristics is clearly shown from the hydrothermally converted macro and microalgae. Hydrothermal liquefaction produces bio-crudes with reduced O/C ratios of 0.15 to 0.21 when compared to the values for the raw feedstock of 0.22 to 0.46 and 0.81 to 0.87 for micro and macroalgae respectively. This is due to the majority of the oxygen containing compounds such as those derived from the carbohydrate fraction more favourably partitioning to the aqueous phase, this is more noticeable for the macroalgae due to their very high carbohydrate contents.

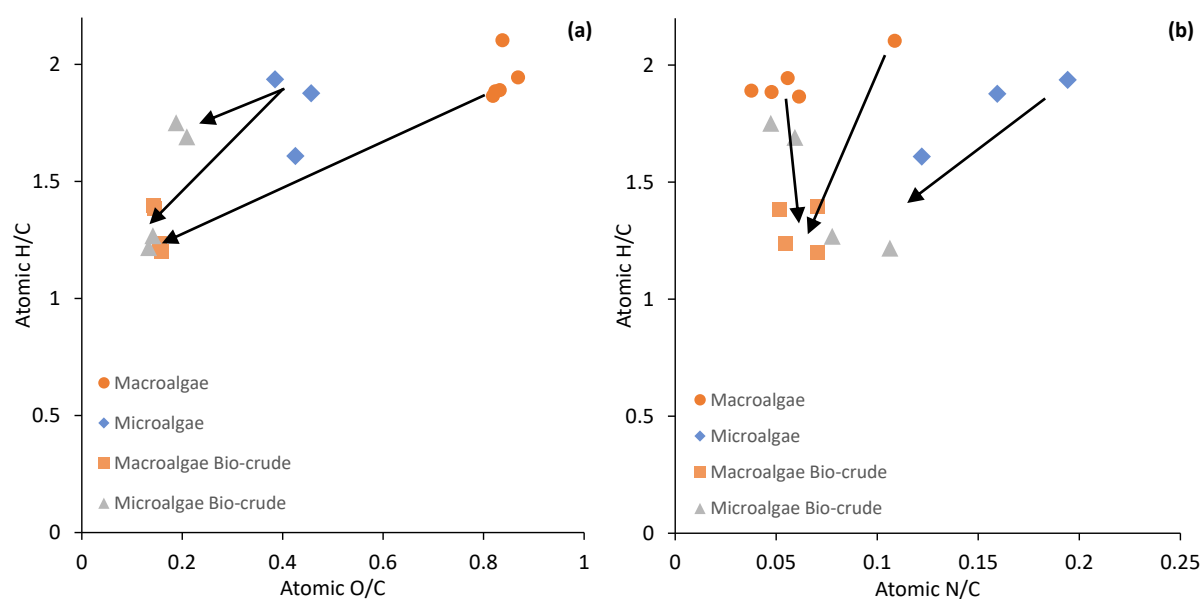


Figure 5.1. Van Krevelen diagrams for micro and macroalgae feedstock and HTL derived algal bio-crudes

5.2.1.1. GC-MS analysis of the small-scale HTL bio-crude

Figures 5.2 displays the GC-MS chromatograph for the bio-crude product from the hydrothermal treatment of *Arthrospira platensis* as a representative of microalgal species. It is anticipated that these GC-MS spectra do not give a full account of all the compounds present within the bio-crude samples, as many of the compounds will have very high molecular weights and be hard to volatise and therefore not elute from the GC column and be detected [59, 65].

The chromatogram of *Arthrospira p.* displayed a slightly more complicated chromatograph than GC-MS results for other microalgal samples. This same trend is reflected in the GC-MS bio-crude oil produced during the hydrothermal liquefaction treatment of each species. The chromatogram from *Arthrospira p.* shows a greater number and spread of major compounds, particularly those of low molecular weight, retention time <30 minutes. Including Phenol (13.4 min.), 4-methyl phenol (15.7 min.), Indole and methyl indole at (21.7 and ~23.4 min.) and hexadecane (25 min.). All microalgae share the major components. that of two carboxylic acids, tetradecanoic acid (30.6 min.) (C:14) and hexadecanoic acid (C:16) (34.5 min.). Tetradecanoic and hexadecanoic acid originate from the hydrolysis of lipids [59], therefore its overwhelming presence microalgal samples due to their higher lipid content compared to macroalgae.

There were also a number of long chain hydrocarbons detected, hexadecane (25 min.), resulting from the decarboxylation of fatty acids. 3,7,11,15-tetramethyl-2-hexadecene (28.2 min.) was also detected from both species, thought to derive from chlorophyll [180].

Nitrogen containing compounds were also detected, the major nitrogen containing compounds being indole and indole derivatives having retention times of ~21.7, ~23.4 and ~25.5 minutes originating from the hydrolysis of proteins, hence their greater abundance in the oil obtained from *Arthrospira p.*[93]. Other compounds including; phenol (13.4 min.) and 4-methyl phenol (15.7 min.) are also thought to be derived from the side-chains of proteins.

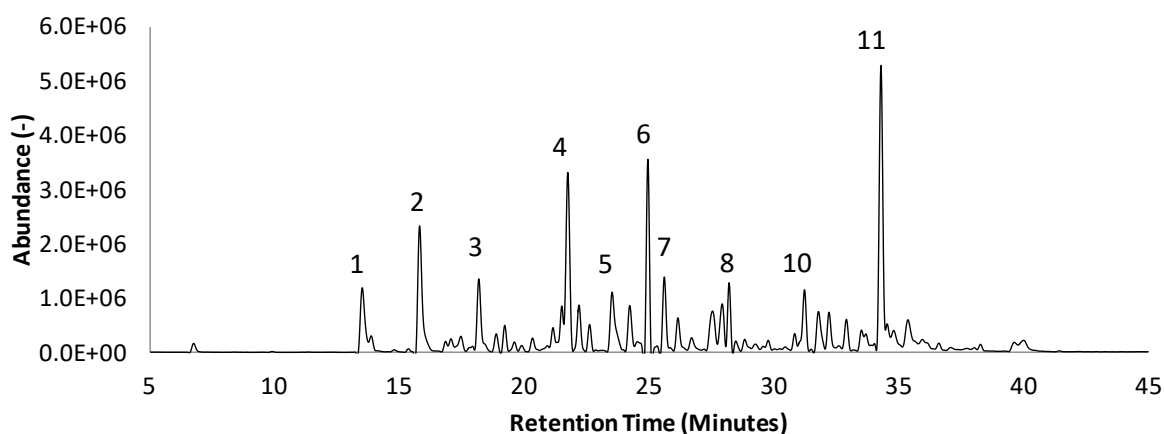


Figure 5.2. Run 5 GC/MS profile at 300 °C for the liquefaction treatment of *Arthrospira platensis* with hydrogen atmosphere

Following on from the first part of this initial study it was proposed that the liquefaction of one species of microalgae should be concentrated on, based on the results from the initial feedstock characterisation discussed previously (**Chapter 4**) and the initial liquefaction runs discussed in this chapter. The chosen species *Nannochloropsis sp* was stated to have moderate levels of lipids (28 wt.%), the major pre-cursor to forming bio-crude.

5.2.2. HTL processing of microalgae in 300 ml batch reactor

5.2.2.1. Effect of HTL temperature

Larger scale batch hydrothermal liquefaction runs were conducted using a Parr 300 ml autoclave, *Nannochloropsis sp.* was used in this study to investigate the effect of reaction temperature on bio-crude yield and elemental composition. For this set of experiments a constant residence time of 10 minutes was used, this is defined as the hold time once the desired reaction temperature had been reached. **Table 5.3** presents the yield and elemental data for these experimental runs, 4 experiments were undertaken in triplicate spanning a temperature range from 200 °C to 350 °C. The yields achieved increase significantly from 8.5 wt.% at 200 °C to a maximum of 51.6 wt.% at 300 °C then decreasing again to 41.5 wt.% at the maximum temperature investigated of 350 °C. From the initial reactor testing in the methodology (**Section 3.3.1**) temperatures above 350 °C were not investigated due to the reactor design and maximum operating conditions, the reactions carried out at 350 °C were considered to be potentially unreliable due to the proximity to the saturation curve, potentially resulting in partial gasification conditions. Future liquefaction experiments for bio-crude generation will be conducted at 300 °C as this is the point at which there is maximum bio-crude yield combined with acceptable operating conditions for the 300 ml batch reactor.

The elemental analysis of the bio-crudes produced at different liquefaction temperatures is presented in **Table 5.3**. It shows that overall the elemental composition of the bio-crude produced over a wide range of temperatures does not vary that greatly consequently the calculated higher heating values are in the region of 30 – 32 MJ/kg.

Table 5.3. Effect of final reaction temperature on elemental composition, HHV, atomic ratios and energy recovery

Temperature (°C)	Bio-crude yield (wt.%)	C	H	N	S	O	HHV (MJ/kg)	H/C	O/C	N/C	Energy Recovery (%)
200	8.5	60.1	10.3	2.6	0.3	26.7	30.4	2.04	0.33	0.037	14.8
250	21.9	61.4	10.1	3.3	0.3	24.8	31.0	1.97	0.30	0.046	38.9
300	51.6	63.2	9.8	4.5	0.4	22.1	31.6	1.84	0.26	0.061	93.5
350	41.5	64.1	9.7	4.0	0.4	21.8	31.9	1.81	0.25	0.053	75.8

Figure 5.3 presents the graphical representation of bio-crude yields achieved at different temperatures during the HTL processing of the microalgae *Nannochloropsis sp.*.

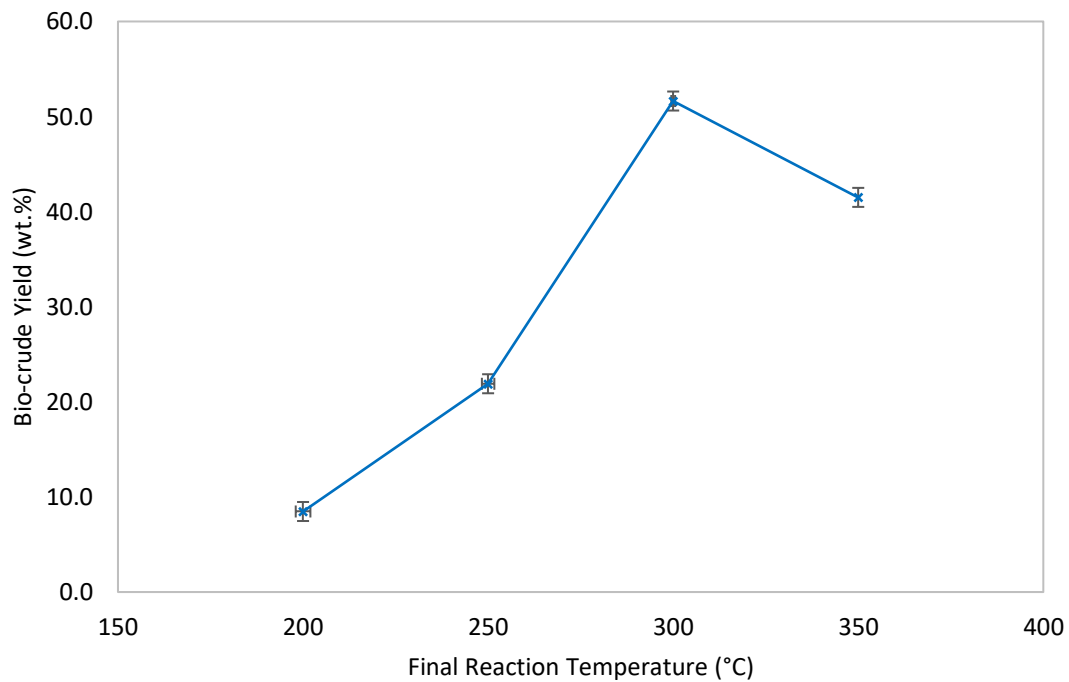


Figure 5.3. Bio-crude yields with varying HTL final reaction temperature.

When compared to petroleum crude oil having typical elemental distribution of carbon 83-87%, hydrogen 10-14%, nitrogen 0.1-2%, sulphur 0.05-6% and oxygen 0.05-1.5% [125] with a HHV of 41-48 MJ/kg [181].

The results show that the most noticeable differences over the investigated temperature range occur with respect to the nitrogen and oxygen contents. When considering the nitrogen content, it can be seen to increase from a minimum of 2.6 wt.% at 200 °C to a maximum of 4.5 wt.% at 300 °C then decreases again to 4.0 wt.% at the highest operating temperature of 350 °C. The increase in nitrogen content is due to the higher reaction temperatures resulting in a greater proportion of the protein fraction breaking down then leading to the repolymerisation of these smaller molecules which shift and contribute to the bio-crude fraction.

The oxygen content in the bio-crude steadily decreases with temperature from a maximum of 26.7 wt.% at 200 °C to a minimum of 21.8 wt.% at a temperature of 350 °C. This finding agrees with the findings from the majority of other studies investigating microalgae HTL over a subcritical temperature range. Due to the high nitrogen, oxygen and sulphur content the biocrude without further upgrading work is not suitable for direct use in transportation fuel applications.

From **Table 5.3** it can be seen that following HTL treatment the ratios of oxygen to carbon decreased from 0.5 to a range of 0.33 - 0.26, similarly the nitrogen to carbon ratio was decreased from 0.14 to a range of 0.037-0.054, finally the carbon to hydrogen ratio increased slightly from 1.67 to 1.8-2.0. Increasing the content of carbon and hydrogen in the bio-crude is vital to increasing the fuels HHV and therefore utility as a transportation fuel

5.2.3. Model Compound Liquefaction

Conducting thermochemical conversion experiments with whole cell microalgae provides essential information required for such things as optimising reaction conditions, pre-treatment requirements, informing equipment design and process economics. All of these factors are essential for process development and optimisation. In order to fully understand the conversion process, an understanding of the reaction fundamentals is paramount. The complexity of microalgae biomass has many tiers, with its huge compositional variation across species, added to this an extra layer of complexity related to the specific species growth conditions means that a biorefineries feedstock can vary markedly and potentially in a very short space of time.

For better understanding of the bio-crude formation pathways during the microalgae HTL processing, a set of liquefaction experiments with a number of model compounds was undertaken. **Table 5.4** presents the HTL runs with model components at set process parameters.

Table 5.4. Outline of model compound liquefaction runs

Run #	Model Compound	Gas	Solvent	Final Temp (°C)	Residence Time (Minutes)
1	<i>Starch</i>	Nitrogen	Deionised water	300	10
2	<i>Cellulose</i>	Nitrogen	Deionised water	300	10
3	<i>Soya Protein</i>	Nitrogen	Deionised water	300	10
4	<i>Stearic Acid</i>	Nitrogen	Deionised water	300	10
5	<i>L-Leucine</i>	Nitrogen	Deionised water	300	10
6	<i>Glucose</i>	Nitrogen	Deionised water	300	10
7	<i>L-Glutamine</i>	Nitrogen	Deionised water	300	10
8	<i>Oleic Acid</i>	Nitrogen	Deionised water	300	10

The model compounds were treated to the same reaction conditions as the whole microalgal cells discussed previously, each experimental run was taken to a final reaction temperature of 300 °C held for 10 minutes using deionised water as the solvent and under an inert nitrogen atmosphere initially pressurised to 50 barg.

These experiments have also been undertaken in order to gain more understanding into the fate of nitrogen during HTL treatment of whole algal cells. It is anticipated in the future that the likely algal feedstock used for HTL will not be the most desirable 'high lipid' algae but will instead be algae grown on municipal wastewater which will have much greater proportions of carbohydrates and proteins. High levels of nitrogen in the produced bio-crudes is a major problem/challenge within the field of liquefaction of algae, if the fate of nitrogen can be better understood and corrected then the bio-crudes produced from liquefaction could in theory be upgraded in existing fossil derived crude oil infrastructure as blends or upgraded independently.

Figures 5.4 to 5.6 show the reactor contents produced from the liquefaction of all the model compounds detailed in **Table 5.4**.

Just based on visual inspection it can be seen that oily substances have been produced. **Figure 5.4** shows the products from the liquefaction treatment of the lipid fraction model compounds. These are oleic and stearic acid, these are both C:18 chain fatty acids. In **Figure 5.4(a)** an immiscible oil can be clearly seen floating on top of a very clear aqueous phase, the clarity of the aqueous phase is also common to the stearic acid sample. In contrast the liquefaction of stearic acid has produced a thick tarry substance. The raw oleic acid model compound is a colourless oily liquid whereas stearic acid is introduced into the reactor as a white solid.

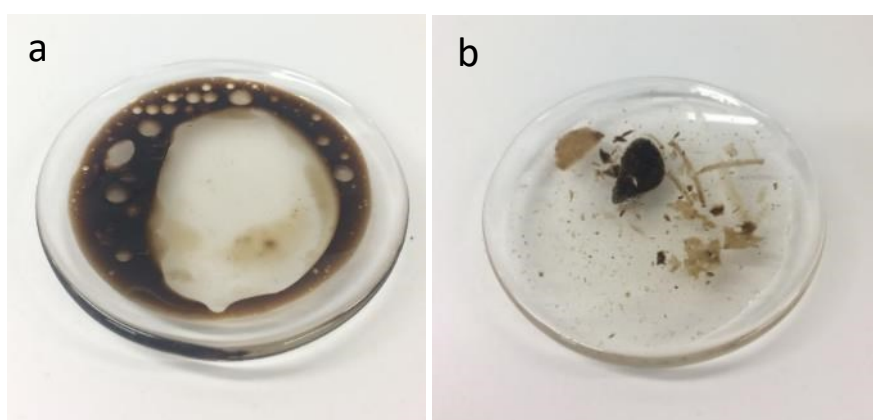


Figure 5.4. Fatty Acids **(a)** Oleic acid and **(b)** Stearic Acid

The soy protein and amino acids in **Figure 5.5** are seen to produce a much darker coloured aqueous fraction when compared to that produced from the liquefaction of fatty acids previously. The

liquefaction of soybean protein isolate (**Figure 5.5(a)**) produced a large, agglomerated globule of a tarry substance alongside a dark aqueous phase and a small amount of solid residue.

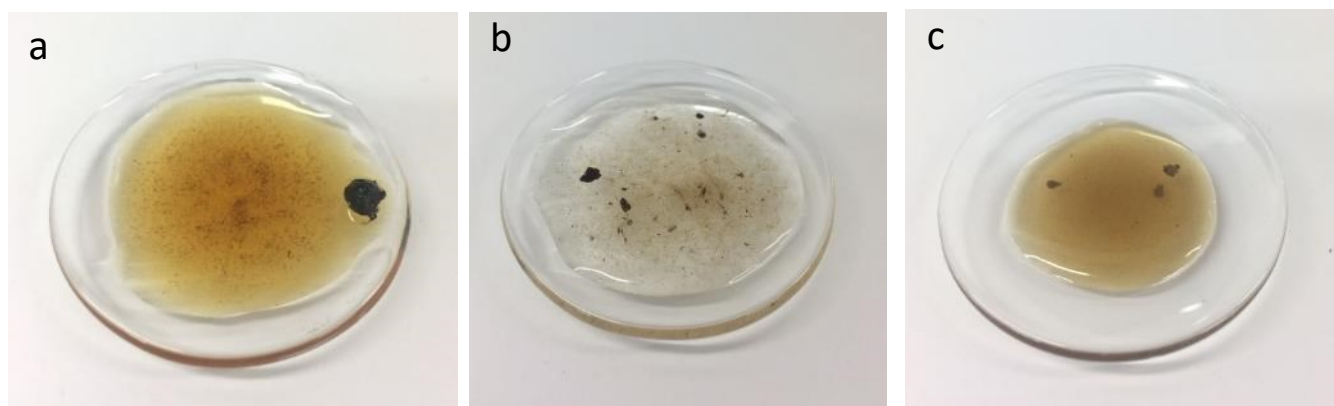


Figure 5.5. Protein Fractions, **(a)** Soybean protein isolate and amino acids **(b)** L-Leucine and **(c)** L-Glutamine

It is clear from **Figure 5.6** that the carbohydrates model compounds produce the greatest amount of char-like solid particles which are very dark in colour.

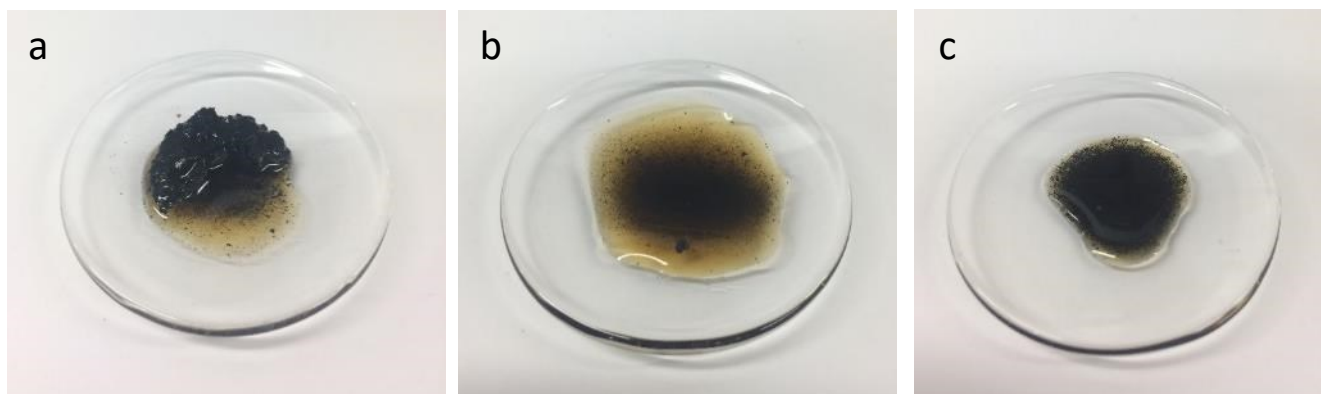


Figure 5.6. Carbohydrate Fractions, **(a)** Glucose, **(b)** starch from corn and **(c)** cellulose

In all cases the products from the HTL treatments of the model compounds needs to be separated into the main product fractions, namely, gas, solid residue, aqueous phase and bio-crude (DCM soluble). This is done following the methodology outlined in **Section 3.5.1**.

5.2.3.1. Yields of model compounds

The yields of all the product fractions for the nine model compounds studied alongside three microalgae species are summarised in **Figure 5.7**. Gas yields were calculated by difference from the yields produced for bio-crude, aqueous phase and solid residue (char). For all the model compounds, except for the lipid analogues, the largest phase where the bulk of the reaction products are distributed to is the aqueous phase, accounting for between 60 to 81 wt.%. Solid residue is markedly higher for the carbohydrate compounds in the region of 17 to 22 wt.% when compared to the values for the other model compounds 5 to 10 wt.%. Bio-crude yield is highest for the lipid analogues at 79 to 80 wt.%, with the remainder going to the aqueous fraction which is considerably lower than the other model compounds at between 8 to 9 wt.% finally, a 5 to 6 wt.% equal split going to both the solid and gaseous fractions. When considering the protein fraction, soy protein achieves a much greater bio-crude yield of 17.2 wt.% when compared to the pure amino acids l-glutamine and l-leucine, 4.5 wt.% and 8.0 wt.% respectively.

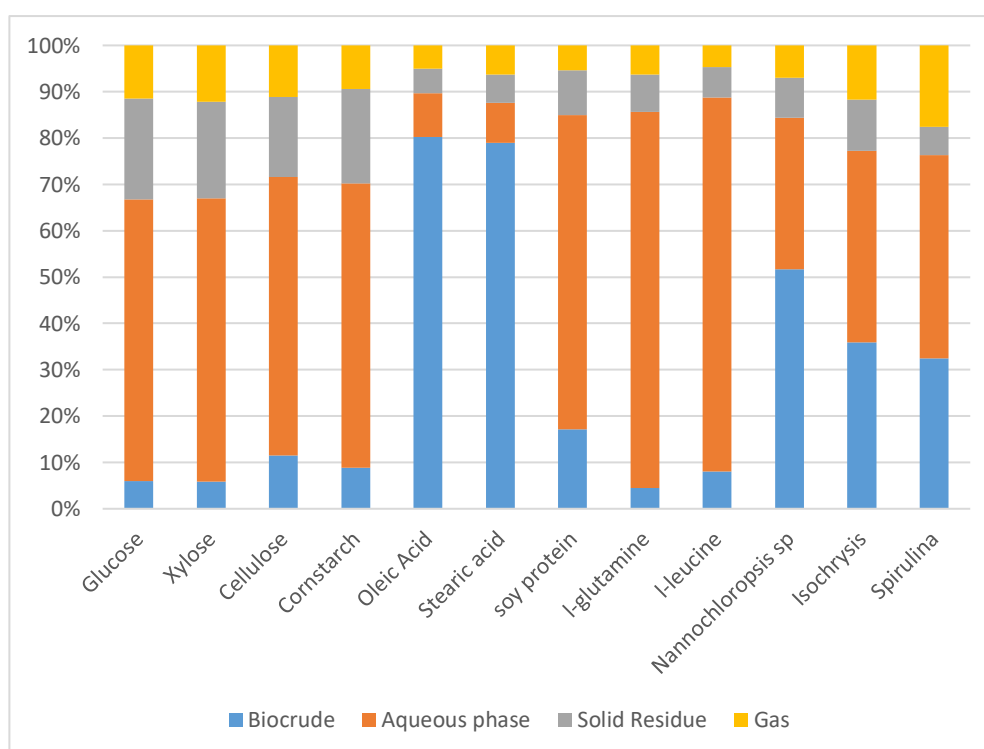


Figure 5.7. Product yields from the HTL treatment of algae and model compounds

5.2.3.2. Elemental analysis of the bio-crude

The number of model compounds were further narrowed down in order to focus on their analysis, one from each macromolecular group was chosen, glucose, oleic acid and soy protein. The elemental composition of the resultant bio-crudes is presented in **Table 5.5** alongside the elemental composition from a fast pyrolysis oil prepared from softwood for comparison.

With respect to the glucose derived bio-crude it is clear there has been a significant upgrade in terms of energy density. The proportion of hydrogen in the glucose bio-crude has remained static, this has led to a drop in the H/C value with respect to the original sample due to the carbon content increasing significantly to 64 wt.%, compared to 39.7 wt.%, higher H/C values are desirable for fuels due to hydrogens higher burning velocity and cleaner combustion. Nitrogen content has raised slightly but remains at trace levels likely due to contamination from the reactor. The oxygen content has been significantly reduced to 28.7 wt.% down from 53.5 wt.% in the original sample, resulting in a lowering of the O/C ratio to 0.33 from an original value of 1.01 and as a result of the beneficial compositional changes the heating value has increase to 26.3 MJ/Kg.

Table 5.5. Elemental Composition and Bio-Crude properties

Feedstock Property	HTL bio-crudes derived from different feedstocks				Fast Pyrolysis Oil
	<i>Nannochloropsis sp.</i>	Glucose	Oleic Acid	Soy Protein	
C (wt % db)	63.2	64.4	74.9	67.6	42.6
H (wt % db)	9.8	6.7	12.9	9.9	7.8
N (wt % db)	4.5	0.1	0	7.4	0.2
S (wt % db)	0.4	0	0	0.9	0
O* (wt % db)	22.1	28.7	12.2	14.2	49.5
O/C molar ratio	0.26	0.33	0.12	0.16	0.87
H/C molar ratio	1.84	1.24	2.06	1.75	2.19
HHV (MJ/kg) (db)	31.6	26.3	41.8	34.7	22.7
Energy Recovery (%)	85.8	11.5	80.1	28.7	n/a

*Oxygen calculated by difference

The elemental composition for the chosen lipid analogue oleic acid has remained unchanged, which supports the conclusion that long chain fatty acids are very stable in high pressure sub-critical water applications as reported in the literature [182].

The bio-crude produced from the hydrothermal treatment of soy protein isolate has resulted in a major upgrade, heteroatom content has been changed for the better, nitrogen content has been

reduced by almost 50% resulting in a final nitrogen content of 7.4 wt.%. Oxygen content has also been significantly reduced to 14.2 wt.% down from 27.1 wt.%. Both carbon and hydrogen content has increased from 44.7 wt.% and 7.3 wt.% to 67.6 wt.% and 9.9 wt.% respectively. The bio-crude molecular ratios show (Figure 5.8) that there has been a small drop in final H/C of 1.75 vs 1.94 but more crucially an O/C reduction of 65% has been achieved from an initial value of 0.46 to 0.16 resulting in a major increase in the overall fuel quality and calculated HHV to 34.7 MJ/Kg. Sulphur content has increased dramatically to 0.9 wt.%, up 67% with respect to the original sample value of 0.54 wt.%, the produced bio-crude would still fall into the desirable category of sweet crude having sulphur contents <1 wt.% [105].

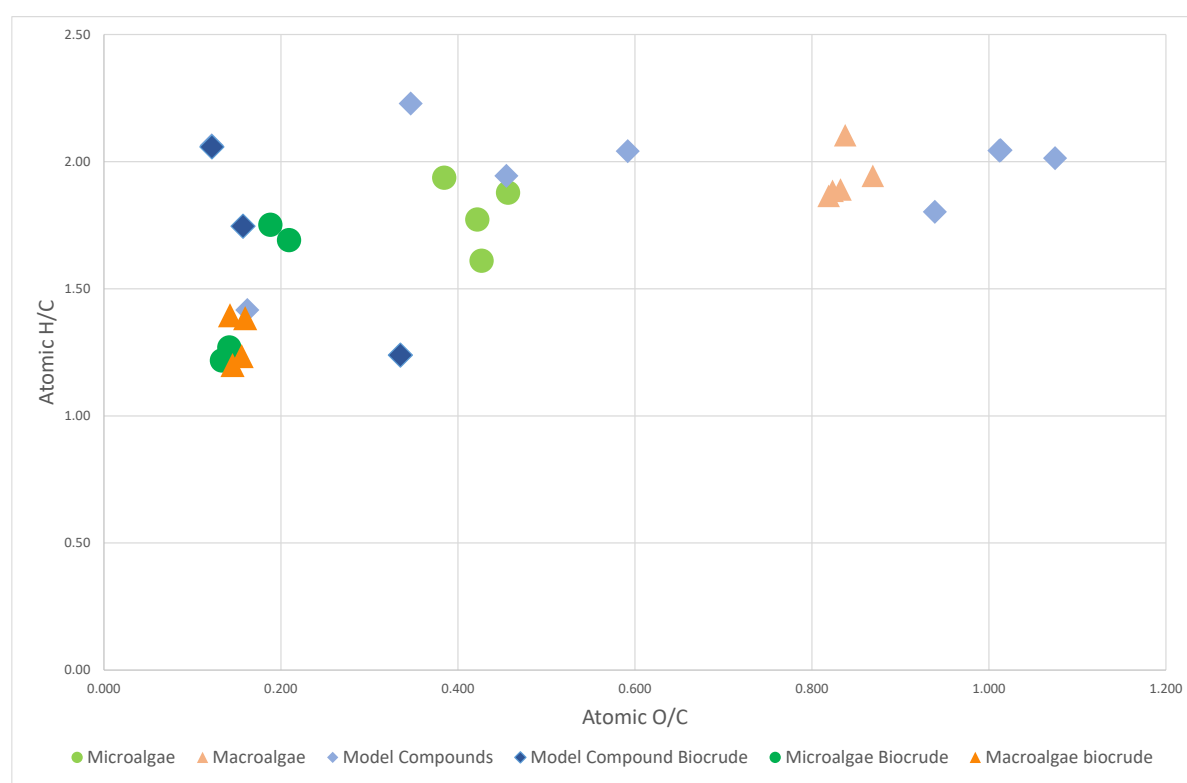


Figure 5.8. Van Krevelen plot H/C vs O/C for algae and model compound feedstock and HTL bio-crudes.

Table 5.5 presents the elemental composition of the HTL bio-crudes produced from the treatment of the selected model compounds along with *Nannochloropsis sp.* bio-crude and fast pyrolysis oil for comparison.

When examining the elemental composition of the *Nannochloropsis sp.* bio-crude it can be seen that each of the macromolecules imparts its own particular tendency to produce bio-crudes higher in certain elements and has a direct association to its individual biochemical composition. Proteins give the whole cell microalgae derived bio-crude its nitrogen and sulphur content, carbohydrates content

contributes a higher oxygen content and depending on the reaction conditions, triglycerides are likely to be extracted from the algal cell and converted to lipids and other aliphatic reaction products, the degree to which depends on their molecular size, reaction severity and duration. The biochemical composition of *Nannochloropsis sp.* used in this study is 52 wt.% (db) protein, 28 wt.% lipid, 12 wt.% carbohydrate and 5.9 wt.% ash. The resultant bio-crude elemental composition is very similar to that of soy protein bio-crude, attributed to the fact that the raw microalgae is 52 wt.% protein, whilst the carbon and hydrogen contents are very similar the algae derived bio-crude possesses a significantly lower nitrogen and sulphur content of 4.5 wt.% and 0.4 wt.% respectively when compared to the pure protein derived bio-crude. Comparatively, the oxygen content of 22.1 wt.% is raised due to contribution from the carbohydrate fraction. Overall, the quality of the bio-crude from an elemental perspective is very similar to the soy protein derived bio-crude, as confirmed by similar values for H/C and a slightly lower HHV due to increased oxygen content.

In contrast results from the analysis of the fast pyrolysis oil shows respectively lower carbon content of 53.8 wt.% and very high oxygen content of 38.1 wt.%. Compared to microalgae, the softwood pyrolysis feedstock contains a high cellulose content, cellulose degradation during pyrolysis produces a majority of monosaccharide and levoglucosan compounds resulting in high bio-oil oxygen content [183]. As a result the calculated HHV is 22.7 MJ/kg, water content for the fast pyrolysis oil is also markedly increased at 26.2 wt.% compared to typical values for microalgal HTL bio-crudes of between 1 to 6 wt.% [93].

The energy recovery was determined using the calculated higher heating values, it excludes the energy used in processing the feedstock using the following equation:

$$Energy\ recovery\ (\%) = \frac{HHV_{bio-crude} \times Y_{bio-crude}}{HHV_{feedstock}} \quad (Eq. 5.1)$$

Where $HHV_{bio-crude}$ is the higher heating value of the bio-crude, $HHV_{feedstock}$ is the higher heating value of the feedstock and $Y_{bio-crude}$ is the yield of the biocrude.

The values achieved for the energy recovery for the model compound bio-crudes varies greatly from a low of 11.5% for glucose to a high value of 80.1% for oleic acid, the soy protein achieved an energy recovery of 28.7% whereas the microalgae *Nannochloropsis sp.* achieved a value of 85.8%. The large range in these figures can be attributed to the large differences seen in bio-crude yield and to a slightly lesser extent the heating value of the resultant bio-crude. For example, the liquefaction of glucose

produced a relatively large amount of char, a high yield of aqueous fraction and a low yield of bio-crude, resulting in low energy recovery into the bio-crude fraction. During liquefaction of carbohydrates conditions above 200 °C promote the formation of oxygen substituted 5 ringed compounds such as furfurals and its derivatives, 1,2,4-benzenetriol and indanone occurs, these compounds have low HHVs.

5.2.3.3. GC-MS characterisation of bio-crudes derived from model compounds

The chromatographs for the GC-MS analysis of the bio-crudes formed from the liquefaction of (a) *Nannochloropsis sp.*, (b) soy protein, (c) oleic acid, (d) glucose and for comparison (e) fast pyrolysis oil from softwood are shown in **Figure 5.9**.

The peak identification for GC chromatograms was carried out by assessment of the best matches for the individual fragmentation patterns using NIST library.

The peaks listed in the individual tables found in **Appendix B Tables B1-B5** and labelled on the chromatograms in **Figure 5.9** are based only on compounds for whom the individual peak area in the total ion chromatogram is over 1.0%. It is important to note that the peak areas quoted only represent a comparative or semi-quantitative content of each component in the produced bio-crude. Typically for each sample - excluding the sample from HTL treatment of oleic acid bio-crude - the GC-MS chromatograms show more than 60 detected peaks in the total ion chromatogram, in all cases the compounds identified with a peak area greater than 1.0% accounted for 80-90% of the total peak area.

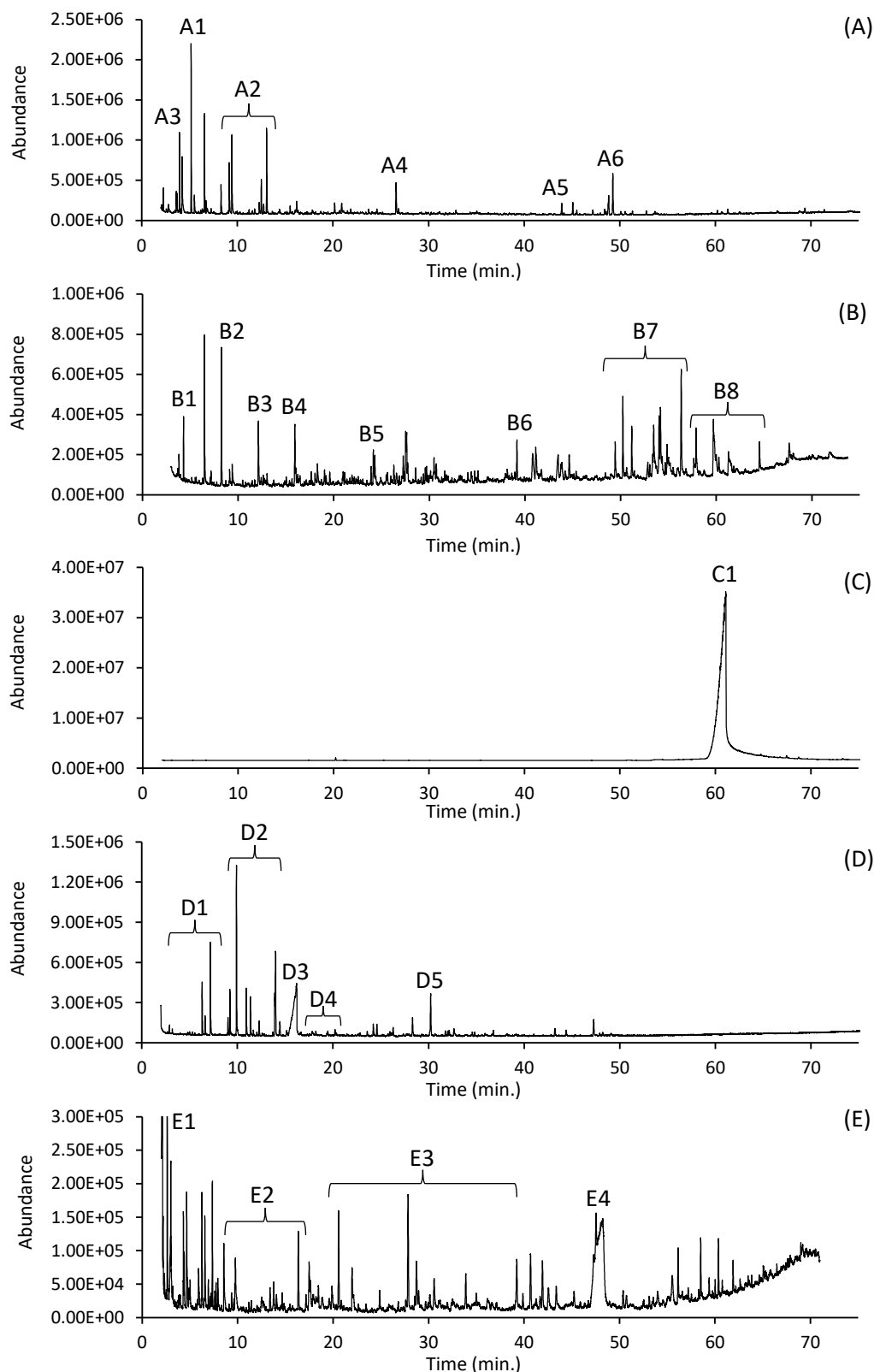


Figure 5.9. GC-MS chromatograms for the bio-crudes formed from the HTL treatment of *Nannochloropsis sp.* (A), the model compounds: soy protein (B), oleic acid (C) and glucose (D) alongside a softwood fast pyrolysis oil (E) for comparison.

(Detailed retention times and assignments for identified compounds are given in Tables B1-5– Appendix B)

As previously stated, the bio-crude was also likely to contain additional components such as very heavy, high molecular weight compounds unlikely to elute from the separation column to be detected. At the same time highly-volatile lighter components were likely lost during evaporation of the extraction solvent and any remaining in the sample are likely to be undetected because of the use of a solvent delay of 2.5 minutes in the GC program.

The GC-MS analysis of the biocrude from *Nannochloropsis sp.* (**Figure 5.9(A)**) indicates that the most abundant compounds are short chain ketones such as 4-methyl-3-penten-2-one (A1) and its derivatives, nitrogen heterocycles such as N-alkylated pyrrolidines (A2), N-alkylated piperidines (A3), and indole (A4) derivatives likely products from the protein fraction of the microalgae. Long chain aliphatic compounds were also present such as nonadecane (A5) and 3,7,11,15-tetramethyl-2-hexadecene (A6). Contrary to many studies long chain fatty acids were not present even in low concentrations minimum 0.2% peak area, this is potentially due to the long heat up time required to reach the final reaction temperature, allowing for their complete conversion via combination with other reaction intermediates into smaller molecular weight species such as the short chain ketones.

HTL of the commercial soy protein isolate **Figure 5.9(B)** resulted in a vast array of nitrogen containing compounds, most common were cyclic compounds such as toluene (B1), styrene (B2), phenol (B3) and cresols (B4), nitrogen containing heterocyclics such as indoles (B5), pyrimidines (B6), long chain arachidamine compounds (B7) and pyrrolidine derivatives (B8).

Oleic acid was shown to be very stable in hydrothermal conditions with a short residence time of 10 minutes used in this study, as can be seen in the chromatogram **Figure 5.9(C)** there is only one major peak for oleic acid itself (C1).

The GC/MS chromatogram for the HTL treatment of glucose **Figure 5.9(D)** shows that the most abundant compounds are short chain aliphatic ketones (D1) such as 2-butanone and as well as diketones (D2) such as 2,5-hexanedione and 3,6-heptanedione, levulinic acid (D3), furanyl compounds (D4) n-Caproic acid vinyl ester (D5).

For comparison the GC/MS spectrum for a pyrolysis oil is presented in **Figure 5.9(E)**, the most abundant compound present is acetic acid, this is due to fragments formed from the depolymerisation of cellulose and hemicellulose undergoing ring scission to produce acetic acid through diacylation of the fragments. Acetic acid (E1) can also be formed as a by-product from the lignin fraction through depolymerisation and cracking reactions [184]. It is also apparent that it contains virtually no nitrogen containing compounds with only 0.2 wt.% N found from the elemental analysis, it is however highly oxygenated, the most common oxygenated compounds include organic acids (E1), alcohols (E2), phenol and its derivatives (E3) levoglucosan (E4) and other dehydrated carbohydrates.

5.2.4. NMR spectroscopy of model compounds and algal derived HTL bio-crudes

The majority of studies attempt to characterise the bio-crudes produced from the HTL of microalgae, this is typically through the use of a number of common instrumental analytical techniques, most notably Gas Chromatography in order to identify and quantify the individual compounds within the sample.

It is anticipated that these GC-MS spectra do not give a full account of all the compounds present within the bio-crude samples, as many of the compounds may have high molecular weights such as long chain fatty acids and carbohydrate oligomers and therefore can be hard to volatise and will consequently not elute from the GC column and be detected [65] [59]. The GC-MS methodology (**Section 3.2.6**) used in this analysis had a final column temperature of 280 °C, insights from the small scale TGA distillation of the bio-crude show that approximately 60% of the *Nannochloropsis sp.* bio-crude sample remained unvolatized, supporting the hypothesis that the GC/MS analysis of bio-crude samples presents a narrowed view of their composition. Valdez et al [185] also postulated that approximately 65% of the bio-crude belongs to higher molecular weight compounds which are not able to be analysed using a capillary GC column. Therefore, these techniques only characterise a portion of the bio-crude and do not provide a more meaningful holistic summary of bio-crude composition.

Nuclear Magnetic Resonance (NMR) techniques have been previously used by researchers in order to more fully understand the whole bio-crude/bio-oil composition from various feedstocks and conversion technologies. These NMR studies are normally in a supportive capacity to other techniques in that they use ^1H and ^{13}C NMR to obtain only approximate ratios for the chemical environments of the proton and carbon atoms. From the literature review an in-depth NMR analysis of HTL derived bio-crudes produced from microalgal and selected model compounds for both the percentages of carbons associated with chemical functional groups and the degree of substitution of carbons in these functional groups was not available.

This information is valuable for determining which feedstocks, HTL conditions and how each individual biochemical group present in the feedstock produce bio-crudes with certain desired characteristics such as functionality, aromaticity, degree of branching and saturation, essential for consideration in downstream processing. The following sections reports the use of ^1H and ^{13}C NMR including the use of 2D techniques (HSQC and HMBC) additionally supported by the application of advanced edited NMR technique PENDANT (Polarisation Enhancement Nurtured During Attached Nucleus Testing). PENDANT has a distinct advantage when compared to other techniques for ^{13}C spectral editing, such

as DEPT (Distortionless Enhancement by Polarisation Transfer) in that it is also capable of detecting quaternary carbon atoms (CH_0) in addition to the signals of CH_1 , CH_2 and CH_3 groups.

5.2.4.1. ^{13}C Spectra

The ^{13}C spectra for the investigated bio-crudes are shown in **Figure 5.11**, the values for the integrated regions are shown in **Table 5.6** with information on the carbon content of the bio-crudes, through the integration of the spectra over certain chemical shift ranges information can be gained on the nature of chemical functional groups and their relative amount.

Table 5.6. The integrated regions specified for functional groups from the ^{13}C NMR spectra of all the bio-crudes shown in Figure 5.10.

The strong resonance at 39.52 ppm represents the DMSO (CH_3) solvent peak along with a strong resonance at 54.84 ppm (Dichloromethane (DCM), residual extraction solvent) were excluded from the peak integration analysis.

Chemical Shift (ppm)	Carbon Assignments	Algal Oil	Oleic Acid	Glucose	Soy Protein	Pyrolysis Oil
0-28	Short chain aliphatics	14.1%	27.9%	18.0%	30.1%	12.0%
28-55	Long chain and branched aliphatics	70.4%	56.1%	53.6%	51.4%	36.1%
0-55	Total aliphatics	84.5%	84.0%	71.6%	81.5%	48.1%
55-95	Alcohols, ethers carbohydrate sugars	1.6%	0.8%	7.8%	0.7%	30.3%
95-165	Aromatics, olefins, phenolics	11.8%	12.2%	16.2%	16.1%	19.7%
165-180	Esters, carboxylic acids	1.1%	2.9%	1.3%	2.0%	1.7%
180-215	Ketones, aldehydes	1.1%	0.1%	3.1%	0%	0.1%

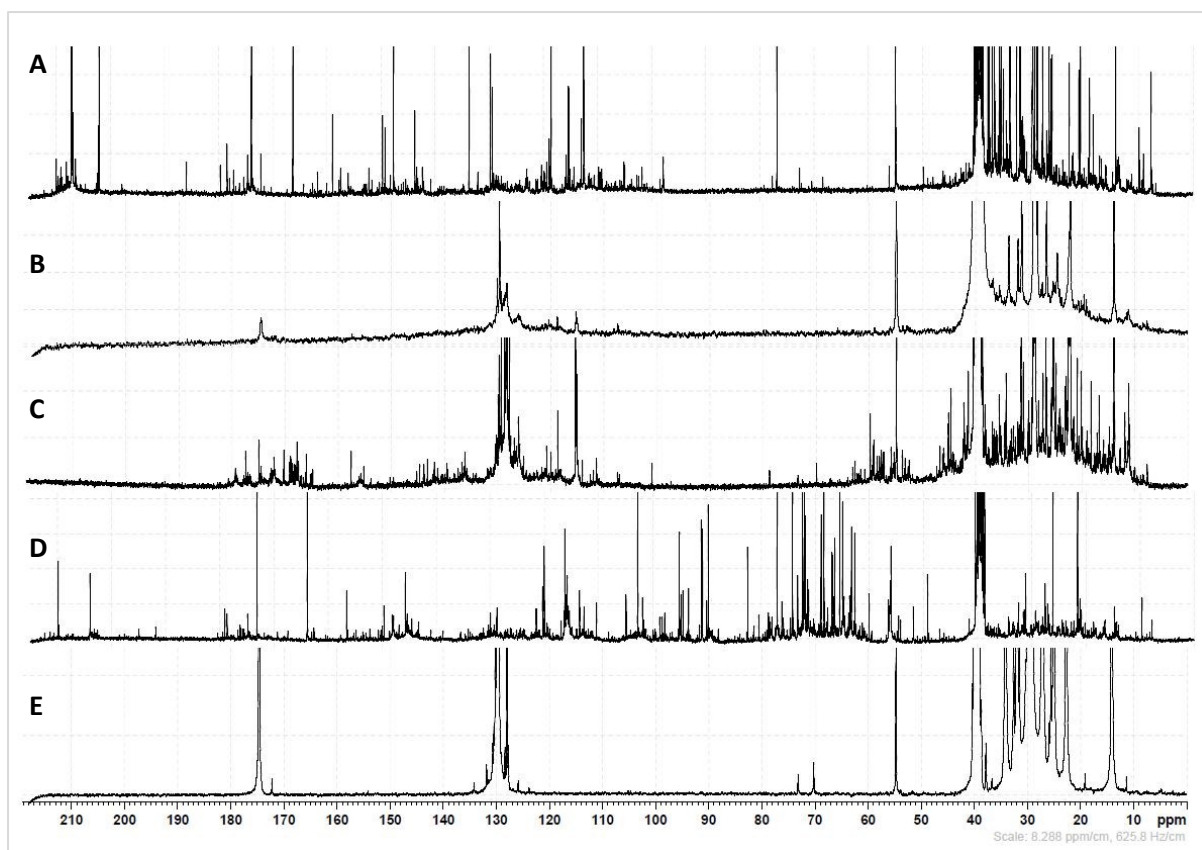


Figure 5.10. ^{13}C NMR spectra of bio-crudes from (A) Glucose, (B) Microalgae - *Nannochloropsis sp.*, (C) Soy Protein, (D) Pyrolysis Oil, (E) Oleic acid.

Table 5.6 separates the carbon content into 5 main fields, those of: 0-55 ppm for aliphatics, 55-95 ppm for alcohols and ethers, 95-165 ppm for aromatics, olefins and phenolics, 165-180 ppm for carboxylic acids and esters and finally 180-215 ppm for aldehydes and ketones. It has been reported that primary, secondary and tertiary carbons could not be subdivided within the shift range of 0-55 ppm due to significant overlapping of primary carbons with secondary and tertiary carbons in the region 24-34 ppm [23] unless a method such as DEPT or PENDANT is used. The aliphatic region can though be further divided into two more generalised sections that of short (0-28 ppm) and long (28-55 ppm) chain length aliphatics.

From the data in **Table 5.6** and the quantitative ^{13}C spectra presented in **Figure 5.10**, the alkyl region (0-55 ppm) possesses the highest percentage of carbons resonating in all bio-crude samples analysed, with up to 84% of carbons for oleic acid associated with this region. In contrast pyrolysis oil had the lowest percentage (48.1%) of carbons associated with the aliphatic region which agrees well with a previous study from Mullen et al [186] focused on the ^{13}C analysis of fast pyrolysis oils with similar wood like feedstocks of guayule, guayule bagasse and chicken litter. It is reported that a higher percentage of carbons resonating in the alkyl (0-55ppm) range results in a higher bio-crude HHV, this

is demonstrated by comparing typical pyrolysis oil HHVs of $\sim <20$ MJ/kg [104] to typical HTL microalgae HHVs of 33-36 MJ/kg.

The percentage of carbon resonating in the most upfield region of 0-28 ppm varies greatly in all the samples analysed, 16% of algal bio-crude carbons were found in this region whereas the values for all the model compounds were higher than this in the region of 18-30.1%. As the HTL treatment of oleic acid and soy protein produce bio-crude with 27.9% and 30.1% respectively within the short chain aliphatic region (0-28 ppm) and noting the biological composition of *Nannochloropsis sp.*, together protein and lipids account for 80 wt.% of the algal mass therefore the amount of short chain aliphatics may be expected to be higher than the measured value. A possible explanation for these results is firstly how the short chain aliphatic compounds are formed and secondly how they interact with other reaction products. It is generally accepted that there are two overarching reaction mechanisms taking place with respect to the hydrothermal treatment of microalgae, hydrolysis and repolymerisation. The macromolecules are first hydrolysed to much smaller fragmented compounds, these intermediate compounds then undergo repolymerisation to form larger molecules. As the raw algae contains all the major macromolecular compounds (lipids, carbohydrates and proteins) this may result in the repolymerisation/condensation into other molecules containing carbons that don't resonate within the short chain aliphatic region (0-28 ppm). This contrasts with the model compounds as these are not mixtures but a single or similar family of compounds.

The percentage of carbons resonating in the long chain and branched aliphatic region (28-55 ppm) is very similar across all of the model compounds (51.4-56.1%). Although there is significant difference in the long to short chain aliphatic carbon ratios. The highest ratio is Algae Oil>Glucose>Oleic acid>Soy protein, with values of 3.43:1, 2.98:1, 2.01:1 and 1.71:1 respectively. This further supports the earlier suggestion that the formed intermediate degradation products interact with the degradation products from the other major macromolecular compounds to produce longer chain aliphatics or compounds with different functionalities.

The ^{13}C region of 55-95 ppm is associated with carbons situated next to an O atom in alcohols, ethers and carbohydrates. The algae bio-crude and model compounds oleic acid and soy protein show very little carbon resonance within this region (1.6, 0.8 and 0.7% respectively). In this region resonating carbons are associated with carbohydrates and their respective hydroxylated degradation products, demonstrating that carbohydrates do not easily survive HTL conditions. This is in stark contrast with the ^{13}C spectra for fast pyrolysis oil of which 30.3% of resonating carbons are present in this region. The integration (**Table 5.6**) of the ^{13}C spectra for glucose gives a resonating carbon percentage of 7.8%, a possible explanation for this high value compared to the algal bio-crude despite the 12 wt.%

carbohydrate content of *Nannochloropsis sp.* is that the intermediates formed from the liquefaction of glucose that are shown to resonate within this region are readily reacted with the other algal macromolecular reaction products/intermediates present when processing complex feedstocks.

The next ^{13}C region of 95-165 ppm is associated with aromatic and olefin carbon content, this chemical shift range also includes phenolic compounds as well as carbon atoms within heteroaromatics. The percentage of carbons resonating within this region is reasonably uniform amongst all samples (12.2-19.7%). The compound with the lowest percentage of resonating carbons within this shift range is oleic acid bio-crude, this resonance is mainly due to the allylic carbons either side of the carbon-carbon double bond (omega 9), with two peaks resonating at ~ 130 ppm. Notable is the almost absence of other peaks in this shift range due to the aforementioned stability of fatty acids in high pressure subcritical water. Some of the very low intensity resonating carbons within this chemical shift region are possibly due to the carbon resonance of other double bonds in low concentration long chain alkene reaction products.

In contrast to oleic acid the carbon resonance within this region (95-165 ppm) from the HTL treatment of soy protein (16.1% of total resonating carbons) are associated with more aromatic, phenolic and heterocyclic compounds. **Figure 5.10(C)** shows the high number of unique resonances found within this shift region. These reaction products occur through firstly the hydrolysis of the protein to the individual amino acids, further decomposition via decarboxylation results in various amino compounds. The amino acids and amino acid derivatised compounds can then also repolymerise into aromatic ring type compounds such as pyrazine and pyrimidine and their derivatives which is where the majority of the signals in this region originate.

The ^{13}C spectrum for glucose (**Figure 5.10(A)**) shows that within the region of 95-165 ppm there are a considerable number of peaks with relatively high intensities. 16.2% of glucose's resonating carbons lie within this region which is a very similar percentage to soy protein (16.1%). In general, the first step occurring during HTL treatment of carbohydrates at a low temperature range of up to 100 °C is the hydrolysis of the carbohydrates to produce reduced and non-reduced sugars, as the temperature increases above 100 °C to approximately 200 °C cyclic oxygenates are produced from these reduced sugars. Above 200 °C the formation of oxygen substituted 5 ringed compounds such as furfurals and its derivatives, 1,2,4-benzenetriol and indanone occurs.

Acid and ester carbonyl compounds are found in the next downfield region (165-180 ppm), as expected the percentage of resonating carbons for oleic acid was found to be the highest (2.9%) with one distinct peak visible at 175 ppm for the carboxyl group carbon of the oleic acid molecule. The next compound with the highest proportion of resonating carbons in this range is the soy protein derived

bio-crude (2.0%). The carboxyl group of the amino acids from the hydrolysis of protein will contribute greatly to the carbons found resonating in this region. The amino acids can also undergo deamination resulting in short chain carboxylic acids such as lactic acid, propionic acid and glutamic acid among others which will also resonate in this region. Of the model compound bio-crudes, it is glucose that has the lowest percentage of resonating carbons within this region, resonating carbons for glucose bio-crude is most likely from the carbons bonded to oxygen atoms in heterocyclic rings such as those found in furans, furfurals and the carboxyl groups of short chain carboxylic acids. It is important to note that even though the values for the proportion of resonating carbons (1-3%) in the more downfield regions of the spectras (165-180 ppm) and (180-215 ppm), this still signifies that a large proportion of the molecules within each sample are likely to have these types of functional groups. This is illustrated from the oleic acid bio-crude sample, as previously mentioned the composition has not changed dramatically during thermal treatment and the resonating carbons within the sample are 2.9% for an almost pure long-chain carboxylic acid.

It can be seen from the spectras in **Figure 5.10** that it is only the glucose bio-crude from the selected model compounds that gives any discernible carbon resonances (3.1%) in the 180-215 ppm shift region associated with ketones and aldehydes. From the values for the lipid and protein model compounds (0.1 & 0% respectively) it is clear that these bio-constituents of the microalgal feedstock do not contribute to the resonance seen in this shift range, it is therefore likely that the carbohydrates within the raw algae are the main sources of resonating carbons seen in this most downfield shift range. The main carbohydrate HTL derived compounds responsible for the resonating carbons in this region are likely short chain aldehydes such as glycolaldehyde, pyruvaldehyde and glyceraldehyde.

5.2.4.2. ^{13}C PENDANT NMR spectroscopy

Looking in more detail towards the model compounds themselves the pulse program PENDANT was applied; PENDANT has a distinct advantage when compared to other techniques for ^{13}C spectral editing in that it is also capable of detecting quaternary carbon atoms. PENDANT spectra have both negative and positive peaks, with CH_0 and CH_2 appearing as negative signals and CH_1 and CH_3 giving positive signals.

Within the first region of 0-55 ppm there are two primary strong resonance signals, one at 39.52 ppm which represents the DMSO (CH_3) solvent peak along with a strong resonance at 54.87 ppm (Dichloromethane (DCM), residual extraction solvent for some of the samples).

5.2.4.2a -Soy protein bio-crude PENDANT

Analysis of the PENDANT spectra (**Figure 5.11**) shows that the bio-crude obtained from the HTL treatment of soy protein (**Figure 5.11(C)**) shows a significant variety in the number of chemical environments present within the sample. For the first major chemical shift region of 0-55ppm there appears to be three discernible sections associated with long and short chain aliphatics. From the spectra they are; 0 – 20 ppm where there are only positive signals resulting from resonating carbons in methyl CH_3 groups with terminal methyl groups being in the most upfield region (11-17 ppm). The second region possesses overlapping positive and negative signals occurring between 17- 25 ppm. The positive signals within this range are most likely to be due to substituted methyl groups on aromatic rings (typically at ~ 22 ppm) such as cresol. This region would also be where positive signals would be observed for branching methyl groups on aliphatic chains. The negative signals within this range are likely due to methylene (CH_2) groups in short chain aliphatics. The third section beyond 25 ppm approaching 55 ppm contains resonating carbons that produce exclusively negative signals, indicating either quaternary CH_0 or secondary CH_2 carbon groups, the carbons resonating within this region are typically associated with long chain and multi-branched aliphatics.

The HTL treatment of proteins results in the hydrolysis of the protein to the individual amino acids, further decomposition via decarboxylation results in various amino compounds. These amino acids and amino compounds are carbon chains with branched amino groups, carboxyl groups and carboxamide side chains. The majority of these signals in this region are therefore believed to be due to CH_2 groups within these carbon backbones of such reaction products as open chain molecules like amino acids. Methylene (CH_2) carbons that are more than two bonds from a terminal methyl group in an alkane chain tend to have a negative carbon resonance of >29 ppm up to a maximum of approximately 32 ppm. CH_2 groups adjacent to branch points tend to occur at more downfield regions of 37-40 ppm. The PENDANT spectra are particularly useful here as from the results it is believed that there is a very low degree of methyl group branching due to the absence of the characteristic CH_1 (positive) signals seen in the more downfield region of 30-40 ppm not present in this sample.

Alongside the amino acids and their decomposition products there are a number of other reported high abundance reaction products, namely saturated heterocycle compounds like piperazine, piperidine, and pyrrolidine derivatives. The CH_2 carbon groups bonded next to the amine group within these saturated heterocyclic compounds typically resonate between 40-48 ppm producing negative signals which are present in the spectra. The CH_2 carbons two or more bonds away from the amine group within molecules such as in piperidine have chemical shift ranges similar to those of long open aliphatic chains between 20-30 ppm.

The second chemical shift region of ^{13}C of 55-95 ppm represent carbons situated next to an oxygen atom in alcohols, ethers and carbohydrates, it is also the region where carbon atoms adjacent to nitrogen atoms resonate. From the ^{13}C NMR spectra integration in **Table 5.6**, the HTL treated soy protein isolate shows very little carbon resonance (0.7%) within this shift region. More information for this region can be obtained from the PENDANT spectra (**Figure 5.11(C)**), most of the signals within this region are positive, denoting resonance from CH_1 groups, present within the most upfield region of 50- 63 ppm. Broadly speaking it is typically carbons bonded to an amine group in structures such as amino acids together with compounds such as branched short chain alcohols with an amino group substitution. There are further positive low intensity signals resonating more downfield which are associated CH_1 carbons bonded to more electronegative species such as to a hydroxy group.

There are also a small cluster of low intensity negative peaks within this spectral region, these are most likely associated with CH_2 groups resonating at 61.5, 62.0 and 63.1 ppm. Review of the 2D HSQC spectra collected for the same sample shows these carbon resonances correlate to ^1H at 3.54, 3.46 and 3.38 ppm respectively, therefore most likely to come from structures such as hydroxyl groups in primary alcohols. There is one stronger negative signal further downfield at 69.9 ppm which is correlated to ^1H at 3.5 ppm from HSQC and HMBC spectras. This signal is likely due to an alcohol, notably as the carbon is more downfield where the resonating methylene carbon is adjacent to a carbon bonded to an electronegative atom or it could be due to resonance from a quaternary carbon in a tertiary alcohol.

The third major chemical shift range of 95-165 ppm contains 16.1% of total resonating carbons (**Table 5.6**) from the soy protein bio-crude product, the carbons within this spectral region are associated with more aromatic, phenolic and heterocyclic compounds. Based on the results from PENDANT spectra as seen in **Figure 5.11(C)** the overriding majority of the signals within this region are positive, as this is the aromatic and alkene chemical shift region these will be almost exclusively primary CH_1 carbons within aromatic ring structures. The majority of carbons resonating lie within a narrow shift region of 127-131 ppm correlating to the ^{13}C shifts observed for benzene ring at 128.5 ppm. There are a small number of low intensity negative signals within this region relating to CH_0 groups, the small number of these peaks indicates minimal variety in the type of functional group substitutions within the aromatic structures. The subsequent strongest signals are positive signals in the region of 115 – 115.3 ppm these are primary CH_1 groups within alkenes (either side of the double bond) or within aromatic rings, support of the assignments was obtained from the 2D ^1H and ^{13}C HSQC NMR spectrum for the sample (**Figure 5.15**). This shows the couplings between a carbon and a methine CH_1 proton that is directly bonded to it at $\delta^1\text{H}$ 6.7 ppm indicating that it is likely a CH_1 carbon in the ortho position within a phenolic ring.

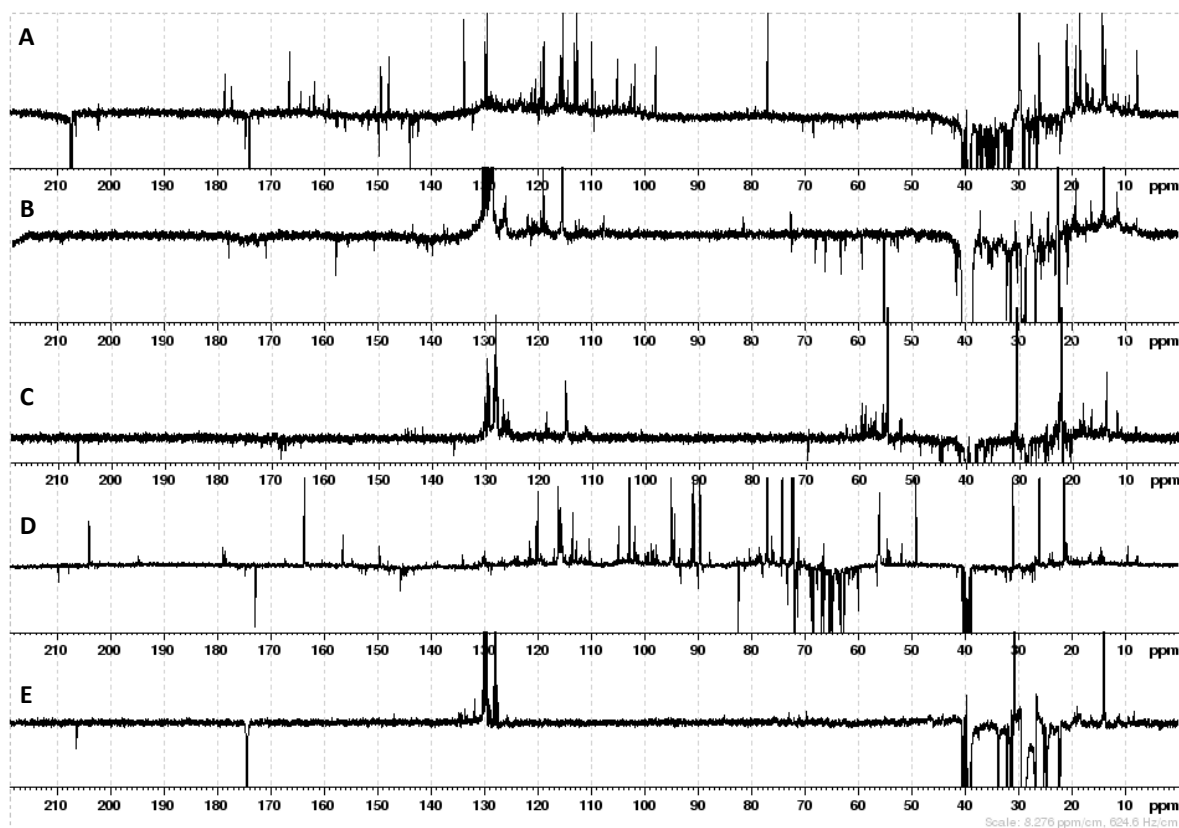


Figure 5.11. PENDANT ^{13}C NMR spectra of the HTL bio-crudes from the model microalgae and model compound treatment with a fast pyrolysis oil for comparison, (A) Glucose, (B) *Nannochloropsis sp*, (C) Soy Protein, (D) Pyrolysis oil and (E) Oleic acid.

Indole has been identified via GC/MS as one of the major reaction products from the HTL treatment of proteins and protein fractions, indole is an aromatic heterocyclic compound with a bicyclic structure. The two quaternary CH_0 carbons at the intersection of the two ring species can be tentatively identified from the ^{13}C PENDANT spectra (**Figure 5.11(C)**) as minor negative signals at 127 ppm and 136 ppm for the carbon bonded to the nitrogen within the fused pyrrole ring. Indole also has a number of CH_1 carbons accounting for the positive signals also observed at 102.6, 111.8, 120.3, 121.3, 122.3, 125.2 ppm.

There are a number of additional minor distinctive negative signals at approximately 157.5, 155.2, 153.8, 152.4 and 150.2 ppm due to quaternary carbon resonances found in such compounds as phenol and its derivatives. These products result from the degradation of individual amino acids and their subsequent repolymerisation by Fischer-Tropsch type reactions to produce aromatics with substituted highly electronegative species such as oxygen in monocyclic/heterocyclic ring structures alongside more complex substituted bicyclic molecules.

Other potential minor products with similar quaternary carbon resonances in this band could potentially include the products from the degradation of larger compounds within the soy protein

feedstock such as soy isoflavones like glucosides such as glycitin to products such as chromenone structures where a benzene ring is fused to a pyrone ring.

Acid and ester carbonyl compounds are found in the next downfield region (165-180 ppm), soy protein possesses the second most resonating carbons within this region (2.0%) (**Table 5.6**). The PENDANT spectra **Figure 5.11(C)** confirms all signals are attributable to quaternary CH_0 within this region. The carboxyl group of the amino acids from the hydrolysis of the protein will contribute greatly to the carbons found resonating in this region. The amino acids can also undergo deamination resulting in short chain carboxylic acids such as lactic acid, propionic acid and glutamic acid among others which will also resonate in this region. Soy protein was shown to produce no discernible signals in the region of 180-215 ppm where resonances associated with aldehydes and ketones are expected to be seen.

5.2.4.2b. Glucose bio-crude PENDANT

The first major chemical shift region of 0-55 ppm containing 18% of the resonating carbons are within this region for the glucose bio-crude sample. The PENDANT spectra for glucose oil (**Figure 5.11(A)**) shows a number of strong resonances within this region with two visibly distinct sections, those of; 0-25 ppm containing almost exclusively positive signals associated with terminal methyl groups (CH_3) and secondly the more downfield region of 25-40 ppm which comprises of primarily negative signals associated with secondary carbons (CH_2) present in open chain aliphatics. With signals further towards the most downfield area of this region for secondary carbons adjacent to a carbon bonded to an electronegative species such as in a carbonyl or hydroxy group. Beyond the DMSO solvent peak at 39.52 ppm the PENDANT spectra is devoid of further discernible carbon resonances.

The second major region associated with alcohols, ethers and carbohydrates within the chemical shift range of 55-95 ppm are very similar to the ^{13}C spectra (**Figure 5.10**) for the other algal model compounds, in that the glucose oil shows very few signals within this region. There are a small number of negative signals between the chemical shifts of 60-70 ppm, expected to be due to CH_2 resonance from carbons bonded to a hydroxy group as part of an open chain structure.

There is one large positive signal at 76.9 ppm correlated to ^1H at 4.6 ppm from the HSQC spectra meaning that this is a primary carbon CH_1 resonance potentially from a secondary alcohol. The small number of low intensity signals within this region from the treatment of a pure carbohydrate feedstock signifies that the carbohydrate structures and their hydroxylated degradation products are completely transformed to compounds with different functionality or that these carbohydrate type reaction products are displaced out of the bio-crude fraction.

Table 5.6 shows that 16.2 % of the resonating carbons for this sample are found within the next major chemical shift range of 95-165 ppm, associated with olefinic, aromatic and heterocyclic compounds. The PENDANT spectra **Figure 5.11(A)** reveals that the downfield region of ~100 to 120 ppm comprises almost exclusively of positive CH₁ signals like those found in benzene rings with attached electronegative functional groups. Such as phenols and its derivatives alongside oxygen substituted 5 ringed compounds such as furfurals and its derivatives, 1,2,4-benzenetriol and indenone.

Glucose oil shows 1.3% (**Table 5.6**) of its resonating carbon within the next downfield region of 165-180 ppm where carbons associated with acid and ester carbonyl compounds are found. From the PENDANT spectra **Figure 5.11(A)** it can be seen that glucose is the only model compound sample that produces positive CH₁ signals within this region. There are three major positive signals seen in this region, the first two are shifted to the most downfield section, those at 177.2 and 178.4 ppm, these carbon resonances are likely to be due to the carbon resonance of formyl group substitution on heterocyclic furan rings and their derivatives (e.g. HMF). The final positive CH₁ signal seen at 166.4 ppm is tentatively proposed to be the carbon resonance for the primary carbon in formic acid, this reaction product has been reported as being a major product during the subcritical liquefaction of glucose. Formic acid is the only acid that would produce a positive signal in this region, all other carboxyl carbons present in this region will produce negative quaternary carbon resonances. These are seen as a number of negative resonances within this region, with two major resonances at 173.9 and 174.6 ppm, associated with quaternary carbons from carboxyl groups present in the short chain carboxylic acids, known to be typical reaction products.

Glucose oil shows the only discernible amount (3.1%) (**Table 5.6**) of carbon resonances with the region associated aldehyde and ketone carbons (180-215ppm) when compared to the other algal model compounds. The region contains only negative quaternary carbon (CH₀) signals signifying the absence of aldehyde compounds and the sole presence of ketones.

5.2.4.2c. Oleic acid bio-crude PENDANT

It is first pertinent to mention that when comparing the ¹³C spectra of HTL treated oleic acid to a raw sample of the same compound little difference can be distinguished. These findings further support the conclusion that long chain fatty acids are very stable in high pressure sub-critical water applications as reported in the literature [182]. Even so the oleic acid didn't remain completely unchanged as the ¹³C spectra **Figure 5.11(E)** shows some additional low intensity peaks, particularly at ~172 ppm potentially associated with the resonating carbon bonded to oxygen in esters. Small resonances around 130 ppm associated with olefins, two resonances at 70 & 73 ppm potentially attributable to ethers and finally a small number of low intensity resonances in the aliphatic region

attributable to the formation of long and short chain alkanes. This finding demonstrates that the reaction conditions investigated results in a minimal degree of conversion to long chain hydrocarbons via decarboxylation

The first major chemical shift region of 0-55 ppm accounts for a total of 84% of the resonating carbons for this sample, split between 27.9% for short chain aliphatics (0-28 ppm) and 56.1% for long chain and branched aliphatics (28-55 ppm). There is a large positive peak for the terminal methyl CH₃ group seen at 13.9 ppm. The next peak is a large negative resonance at 22.2 ppm corresponding to the secondary CH₂ carbon bonded next to the terminal methyl group. The resonance at 24.6 ppm corresponds with the secondary carbon 2 bonds away from the carboxy carbon. The next peak at 26.7 ppm corresponds to the two allylic carbons bonded to the two methine carbons. The negative peaks between the chemical shift values of 28.6 and 29.3 ppm are for the methylene group (CH₂) 4 bonds either side of the methine carbons. The negative peak at 31.4ppm is due to the methylene carbon two bonds away from the terminal methyl group. The next carbon resonance is a negative signal at 33.7 ppm due to the CH₂ carbon one bond away from the carboxyl carbon.

There are also a number of weaker CH₂ carbon resonances within this region, these will be due to the reaction/degradation products of oleic acid, i.e. reduced length long-chain alkene molecules.

The HTL treatment of oleic acid produced no resonance within the second major chemical shift region of 55 – 95 ppm associated with alcohols, ethers and carbohydrate type compounds.

The third major ¹³C region of 95-165 ppm represents the aromatic and olefin content Some of the very low intensity positive signals resonating carbons (CH₁) within this chemical shift region are possibly due to the carbon resonance of other methine carbons in low concentration long chain alkene reaction products.

Acid and ester carbonyl compounds are found in the next downfield region (165-180 ppm), as expected the percentage of resonating carbons for oleic acid was found to be the highest (2.9%) (**Table 5.6**) with one distinct negative quaternary CH₀ peak visible at 174.4 ppm for the carboxyl group carbon of the oleic acid molecule.

5.2.4.2d. Fast pyrolysis oil PENDANT

When comparing the NMR spectra obtained from the algal oil and model compounds to that of pyrolysis oil there are a large number of differences seen in the spectra.

The integration values found in **Table 5.6** show that the alkyl region (0-55 ppm) for the model compounds and algal oil samples had a range of 71-84% of resonating carbons associated with this

region. In contrast, pyrolysis oil has only 48.1% of resonating carbons associated with the aliphatic region. This agrees well with similar previous studies on the ^{13}C analysis of fast pyrolysis oils with similar wood-like feedstocks of guayule, guayule bagasse and chicken litter [186].

It is reported that the higher the percentage of carbons resonating in the alkyl (0-55ppm) range results in a higher HHV of the bio-crude, this is demonstrated by comparing typical pyrolysis oil HHVs of ~ 20 MJ/kg to typical HTL microalgae HHVs of 33-36 MJ/kg.

The PENDANT spectra (**Figure 5.11(D)**) for the pyrolysis oil shows that the majority of signals in the 0-55ppm region are positive signals, this signifies the presence of CH_1 or CH_3 carbons. CH_1 in this upfield region are due to branch points such as in a tertiary alkyl, they could also be a CH_3 carbon (benzylic hydrogen) in a substituted benzene ring like toluene.

The greatest relative difference in NMR spectra results for pyrolysis oil is within the region of 55-95ppm. Negahdar et al [104] describes two regions within this chemical shift range of between the regions of 54-70 as the methoxy/hydroxy region, this will be mainly due to carbons bonded to oxygen in ethers or alcohols and a to a lesser extent a small number of carbon bonded to nitrogen resonances. Secondly the more down field region between 70-103 ppm as the carbohydrate region corresponding to carbons adjacent to oxygen in carbohydrates type molecules resonate.

The HTL oils show very little resonance within this region (<1.6 %) excluding glucose bio-crude whereas uniquely for the pyrolysis oil, carbohydrate type structures containing oxygen are incorporated within the oil product, giving rise to the much higher oxygen content, observable also from the elemental analysis results. Approximately 30% of the total carbon content in the pyrolysis oil were found to be within this region. From the PENDANT spectra **Figure 5.11(D)** it can be seen that there are some distinct features, the overwhelming majority of signals from 55 to 72 ppm are negative, therefore associated with CH_2 or CH_0 carbons, the more downfield portion of this region between 72 and 95 ppm contains predominantly positive signals therefore associated with either CH_1 or CH_3 carbons.

Similarly, to glucose bio-crude, pyrolysis oil also produces positive signals in the ester and carboxylic acids range ($\delta^{13}\text{C}$ 165-180 ppm) region in contrast to all other samples. These are likely to be due to the carbon resonance of formyl group substitution on heterocyclic furan rings and their derivatives such as HMF.

In contrast to all of the HTL derived bio-crudes the PENDANT NMR spectra reveals that pyrolysis oil is the only sample to give positive carbon resonance beyond 180 ppm, this is due to the carbonyl (CH_1) carbon present in aldehydes. With the more upfield positive aldehyde signals at ~ 180 ppm attributed to furfural and its derivatives.

5.2.4.3. 2D HSQC NMR spectroscopy

Two-dimensional ^1H - ^{13}C HSQC (Heteronuclear Single Quantum Coherence) spectra were collected with a focus on supporting the identification of the varieties of structures and functional groups within the bio-crude samples. The HSQC spectrum contains a peak for each unique proton attached to a carbon atom. In 2D ^1H - ^{13}C HSQC spectra, intersected peaks indicate correlations derived from the strong (125-160 Hz) one bond J_{HC} coupling, due to this coupling HSQC is very valuable in that it can uncover overlapping signals present in the individual 1D spectra. **Figures 5.12 to 5.14** present the 2D ^1H - ^{13}C HSQC NMR spectra of the bio-crudes produced from the HTL treatment of *Nannochloropsis sp.* and selected model compounds.

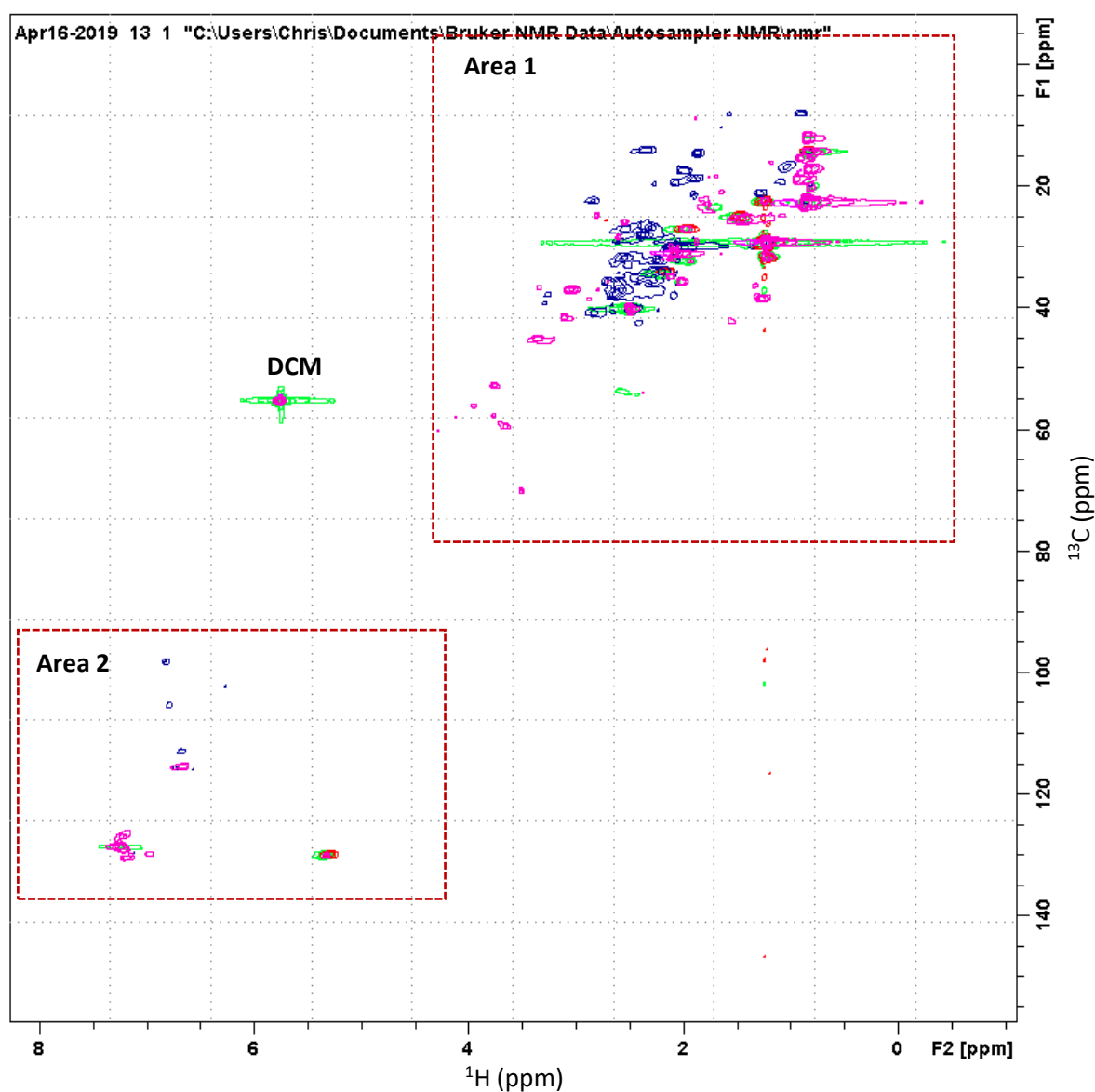


Figure 5.12. 2D HSQC NMR spectra for the HTL bio-crudes produced from *Nannochloropsis sp.* (green), Glucose (blue), Soy protein (pink) and oleic acid (red).

Area 1: More detailed view – Figure 5.14.; Area 2: More detailed view – Figure 5.15.

Figure 5.13 presents the 2D HSQC spectrum of the DCM soluble bio-crudes produced from the HTL treatment of *Nannochloropsis sp.* and the three selected model compounds; glucose, soy protein and oleic acid. The total spectra can be grouped into two distinct regions, firstly the aliphatic region (Area 1) (**Figure 5.14**) corresponding at ($\delta^1\text{H}$ 0.8-5.5 ppm and $\delta^{13}\text{C}$ 8-80 ppm) and secondly the aromatic region (Area 2) (**Figure 5.15**) at ($\delta^1\text{H}$ 4.5-10.0 ppm and $\delta^{13}\text{C}$ 95-140 ppm) [101]. From the total 2D HSQC spectra (**Figure 5.13**) it can be seen that the spectra is devoid of signals in the range of $\delta^{13}\text{C}$ 70-90 ppm and $\delta^1\text{H}$ 4.5-10.0 ppm, this is the region where carbon atoms associated with carbohydrates occur, this shows that any carbohydrates present in the algae feedstock are converted to other compounds during hydrothermal liquefaction or displaced into the other reaction fractions [105][88].

5.2.4.3a. Aliphatic region

The aliphatic region can again be subdivided into further two regions, the aliphatic **C-O** region ($\delta^1\text{H}$ 2.75-6.0 ppm and $\delta^{13}\text{C}$ 50-90 ppm) and the aliphatic **C-C** region ($\delta^1\text{H}$ 0.5-3.0 ppm and $\delta^{13}\text{C}$ 5-50 ppm) shown in **Figure 5.13**.

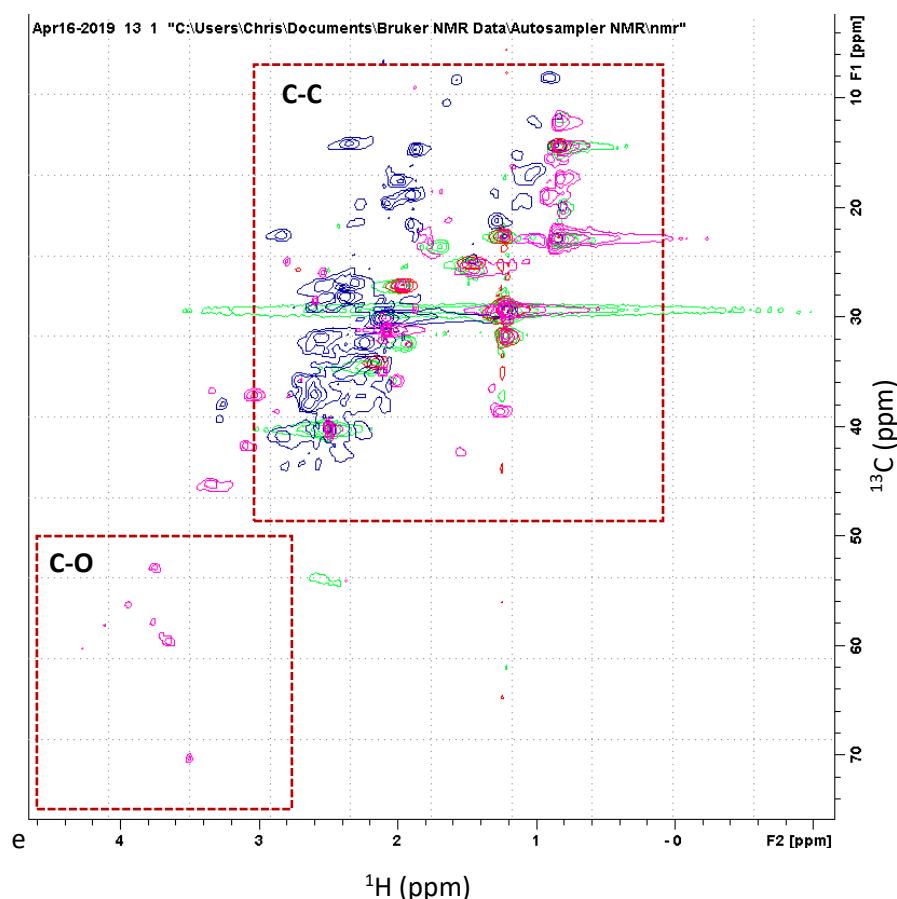


Figure 5.13. Highlighted Area 1 (Aliphatic region) from Figure 5.13, for the HTL bio-crudes produced from *Nannochloropsis sp.* (green), Glucose (blue), Soy protein (pink) and oleic acid (red).

For all samples analysed it is only the soy protein bio-crude that gives resonances in the **C-O** aliphatic region beyond (downfield) $\delta^1\text{H} > 3.2$ ppm, those resonating at this proton shift with carbon signals between 50-60 ppm are indicative of carbons bonded to an amine group or short chain primary alcohol groups. Another major unique feature in the soy protein spectra is the strong peak at $\delta^1\text{H}$ 3.5 & $\delta^{13}\text{C}$ 70 ppm indicative of a hydroxyl group in a primary alcohol.

It is clear that all samples produce signals in the **C-C** aliphatic region but in contrast to the other bio-crude samples, glucose bio-crude produces relatively more downfield proton resonance > 1.2 ppm within the ^{13}C region of $\delta^{13}\text{C} \sim 8-30$ ppm which is indicative of hydrogen in terminal methyl groups next to carbon atoms bonded to electronegative species such as in ketones and aldehydes.

5.2.4.3a. Aromatic region

Figure 5.14 shows the cropped 2D HSQC spectra related to the area associated with aromatic resonating proton and carbon signals. The glucose sample shows a large number of resonances in the broad region of $\delta^1\text{H}$ 6.3-7.4 and $\delta^{13}\text{C}$ 95-120 ppm these resonances are associated with phenolic, alkene and furanyl compounds.

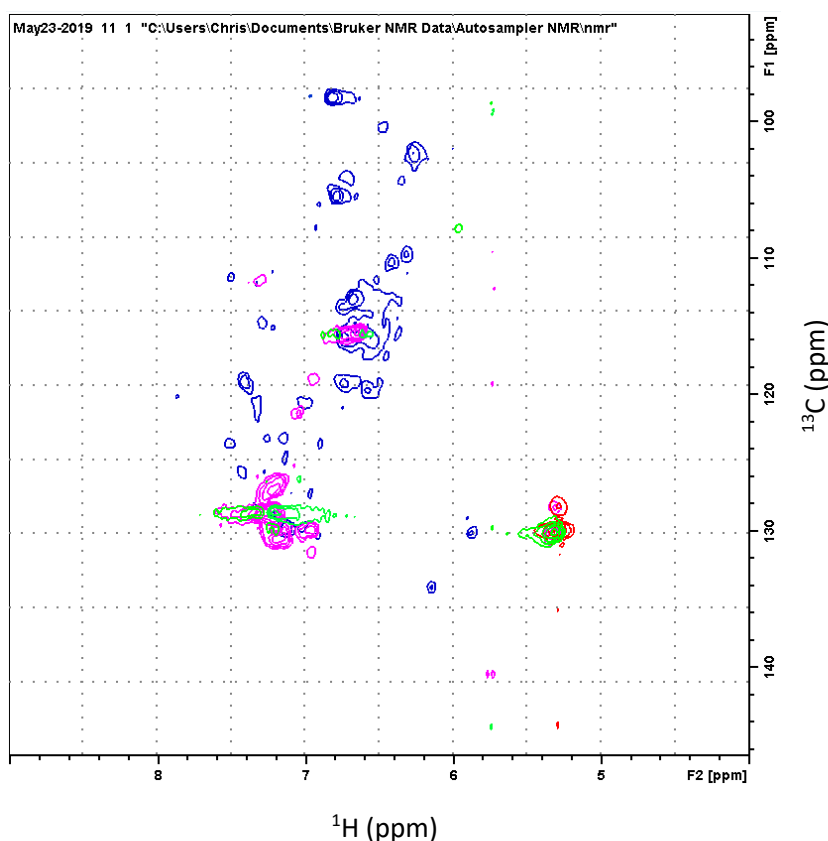


Figure 5.14. Highlighted Area 2 (Aromatic region) from Figure 5.13, for the HTL bio-crudes produced from *Nannochloropsis sp.* (green), Glucose (blue), Soy protein (pink) and oleic acid (red).

Also, within this region lies a key peak for soy protein and *Nannochloropsis sp.* bio-crude associated with $\delta^1\text{H}$ 6.7 ppm and $\delta^{13}\text{C}$ 115 ppm, expected to be attributable to pyrrole and its derivatives.

The only signal in this region for oleic acid is also present for the algae bio-crude and soy protein sample, this is the distinct peaks at approximately ($\delta^1\text{H}$ 5.3 ppm and $\delta^{13}\text{C}$ 130 ppm), attributed to cis carbon-carbon double bonds in extended alkyl chains. The majority of which for the oleic acid bio-crude sample associated with the double bond (cis-9) present in the unconverted feedstock. For the algal sample this resonance is associated with various unsaturated fatty acid compounds and potentially also accounting for the long chain alkene 3,7,11,15-tetramethyl-2-hexadecene (phytane) present as a product from chlorophyll decomposition.

For both the bio-crudes from *Nannochloropsis sp.* and soy protein there are significant cross peak resonance at $\sim\delta^1\text{H}$ 7.3 ppm and $\delta^{13}\text{C}$ 129 ppm attributed to benzene rings.

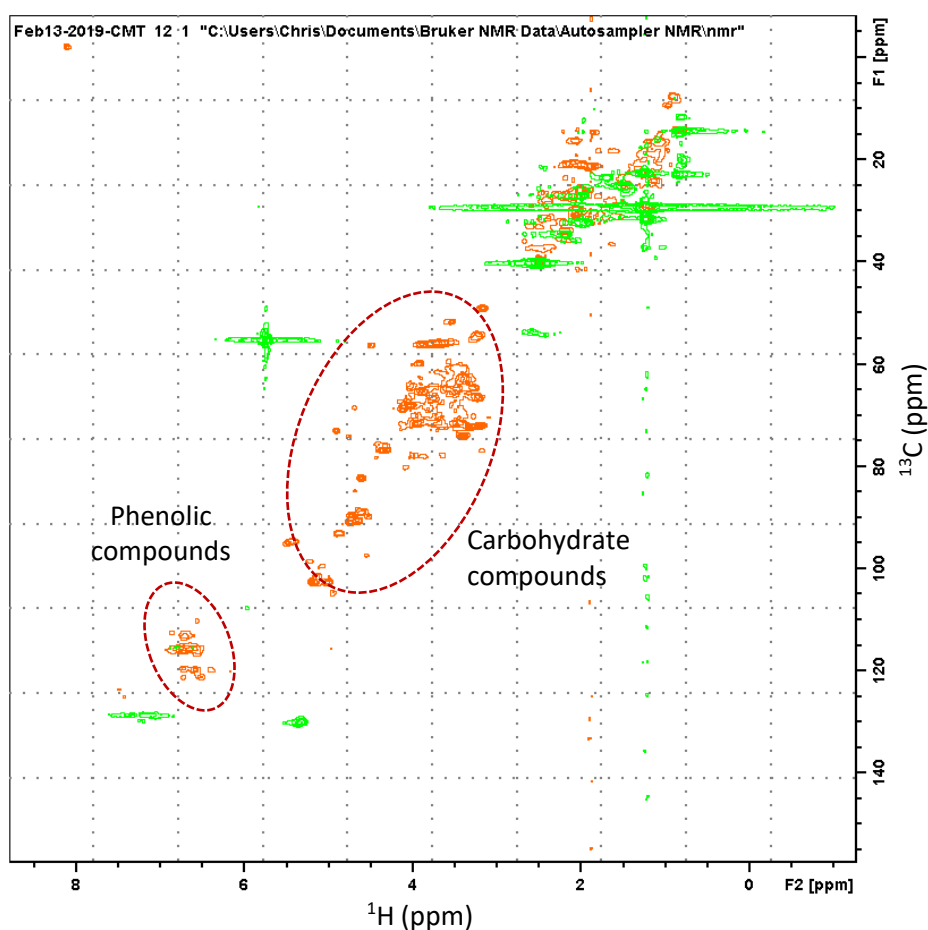


Figure 5.15. Full 2D HSQC NMR spectra comparison of *Nannochloropsis sp.* biocrude (green) and fast pyrolysis oil (orange).

Also apparent within the aromatic region the HSQC spectras show that similarly to the results from the glucose and oleic acid bio-crudes the pyrolysis oil contains no visible non-phenolic aromatics. The

vast majority of the resonance within this region is from phenolic type compounds with aromatic C-H bonds in the orthro position in phenol resonating at $\sim\delta^1\text{H}$ 6.6 & $\delta^{13}\text{C}$ 112 ppm, meta position at $\sim\delta^1\text{H}$ 6.6 & $\delta^{13}\text{C}$ 120 ppm and the para position at $\delta^1\text{H}$ 7 & $\delta^{13}\text{C}$ 130 ppm presented in **Figure 5.15** combined with resonances for catchetols.

Levogluconan is one of the main compounds present in soft wood pyrolysis oils and accounts for a major portion of the resonance seen in the carbohydrate region of the 2D HSQC spectra (**Figure 5.15**). **Figure 5.16** shows the cropped HSQC spectra with labelled assignments of each carbon environment present in levogluconan.

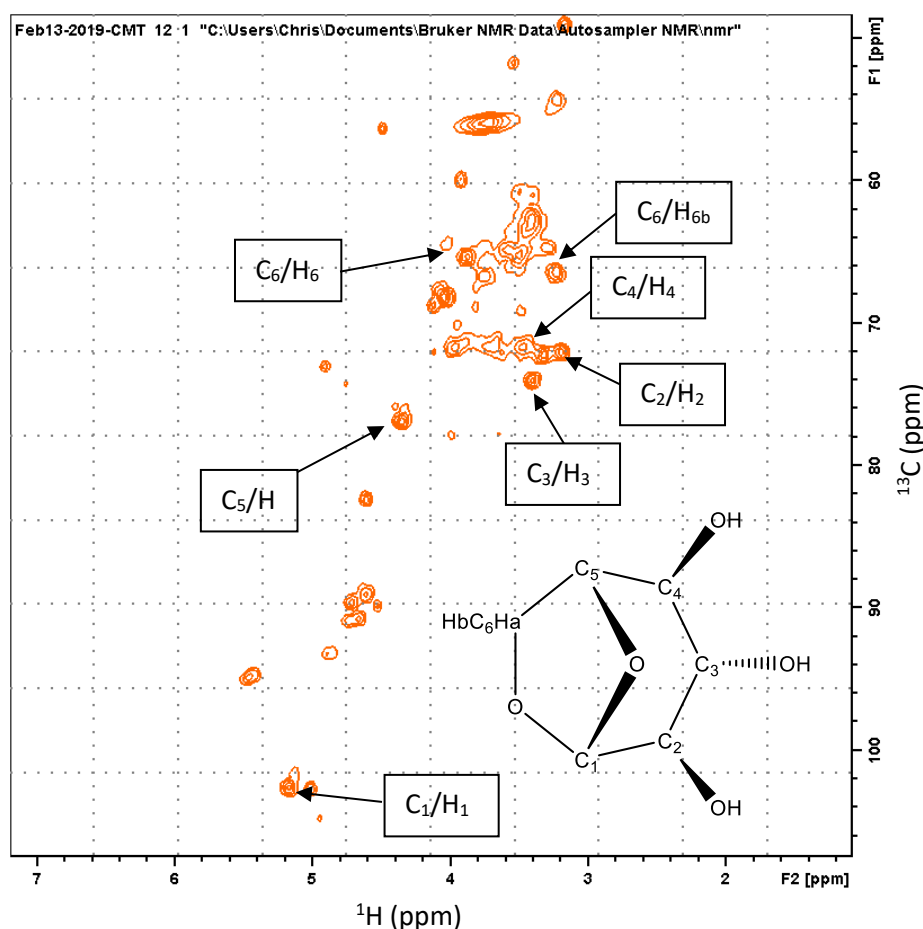


Figure 5.16. HSQC NMR spectra of soft wood fast pyrolysis oil with assignments of each carbon in levogluconan.

5.3. Conclusions

The small-scale liquefaction of two microalgal and two macroalgal species was conducted, average bio-crude yields were shown to be far higher for the microalgal species 30.1 - 48.6 wt.% versus 16.6-18.5 wt.% respectively. The produced bio-crudes were found to have high nitrogen and oxygen contents of 3.8-8.8 wt.% and 12.6-18.6 wt.%, respectively for all species. Higher heating values were found to increase significantly from the base feedstock showing increased energy density of the bio-crude products. The effect of reaction temperature was investigated on a larger scale basis by way of liquefaction of the microalgae *Nannochloropsis sp.*, maximum bio-crude yields (51.6 wt.%) were found at a processing temperature of 300 °C. Bio-crude yields above the lipid content of the algae were found, supporting existing findings presented in the literature – that the HTL of algae can process whole algal cells whilst also improving the energy recovery from the feedstock. GC-MS analysis of the bio-crude revealed similar and, in some cases, exact matches to compounds found during the analytical pyrolysis of the raw feedstock, demonstrating the benefit of Py-GC-MS as a quick screening tool. The bio-crude produced from the microalgae *Nannochloropsis sp.* possessed high levels of heteroatom content, 4.5 and 22.1 wt.% for nitrogen and oxygen, respectively. Heteroatom concentrations are many times higher than typical fossil crude oils, and further reduction is required for utilisation as fuels in transport applications.

As a result of the high yields achieved and the molecular nature of the bio-crudes produced, HTL bio-crudes from microalgae show great potential for upgrading for further improvement of the characteristics and quality of the fuel.

The effect of algal biochemical composition on final bio-crude composition was investigated through the liquefaction of selected model compounds chosen to represent the key macromolecular constituents of algae. The protein fraction was represented by a soy protein isolate and two amino acids l-leucine and l-glutamine, carbohydrate content was represented by glucose, xylose, and corn starch, and finally, the lipid content was represented using oleic and stearic acid.

The results show that long-chain fatty acids are very stable under the liquefaction reaction conditions applied. Bio-crude yields from the liquefaction of the model compounds demonstrated the hierarchy of contribution to the algal bio-crude yield. The order of model compound bio-crude yields achieved is 79-80.3 wt.%, 4.5-17.2 wt.% and 5.9-11.6 wt.% for lipids, proteins and carbohydrates, respectively.

Advanced Nuclear Magnetic Resonance techniques were applied to analyse the produced bio-crudes from *Nannochloropsis sp.* and the three model compounds. The literature relevant to HTL of biomass the application of NMR spectroscopy is limited to basic one dimensional and conventional pulse

programs for ^1H and ^{13}C experiments. A novel combination of advanced techniques on top of the mentioned NMR techniques are two-dimensional techniques of Heteronuclear Single Quantum Coherence (HSQC), Heteronuclear Multiple Bond Correlation (HMBC) and the spectral edited ^{13}C pulse sequence known as PENDANT (Polarization Enhancement During Attached Nucleus Testing). Utilization of these advanced techniques allowed for the characterization of the whole bio-crude sample, not just the fraction that is able to elute from a GC column. Findings show that algal bio-crudes and those produced from the liquefaction of model compounds are very complex in nature. Key similarities were observed between the model compound bio-crudes and the algal bio-crudes.

Chapter 6 Catalytic upgrading

6.1. Introduction

The previous chapter outlined the production of HTL bio-crudes. Algal derived bio-crudes were found to be very complex in nature, in general it is composed of a small amount of water and ash with the remainder organic compounds. The organic components consist mainly of linear and branched hydrocarbons, heterocyclic compounds, phenolic derivatives and other oxygenates, fatty acids and esters. Particular attention is needed in the reduction of heteroatom content prior to the oils use as a transportation fuel. Following the literature review in **Chapter 2 Section 2.7** the application of catalytic supercritical water upgrading was selected for investigation with the aim of establishing its ability for heteroatom removal and improvement of fuel characteristics.

6.2 Materials and Methods

The following section outlines the materials used in this study, methodology for the upgrading experiments is outlined in **Section 3.4.3**, product separation methodology is the same as that for HTL bio-crude recovery also found in **Section 3.5.1**.

6.2.1 Catalysts

The catalysts used in this study include Pt/C, Ru/C, Pd/C, NiMo/Al₂O₃ and HZSM-5. Pt/C, Pd/C and Ru/C all had metal loadings of 5 wt.% purchased from Sigma Aldrich, they were used as received and the measured surface area of each catalyst is 1484 m²/g, 1496 m²/g and 1472 m²/g respectively, surface area was measured using BET, the methodology can be found in **Section 3.4.2.1**. Ammonium ZSM-5 zeolite with a surface area of 400 m²/g and a 30:1 mole ratio of SiO₂:Al₂O₃ was purchased from Alfa Aesar (45880). NiMo/Al₂O₃ was purchased from Alfa Aesar, prior to use it was sulphided, the methodology of which is discussed in **Section 3.4.1**.

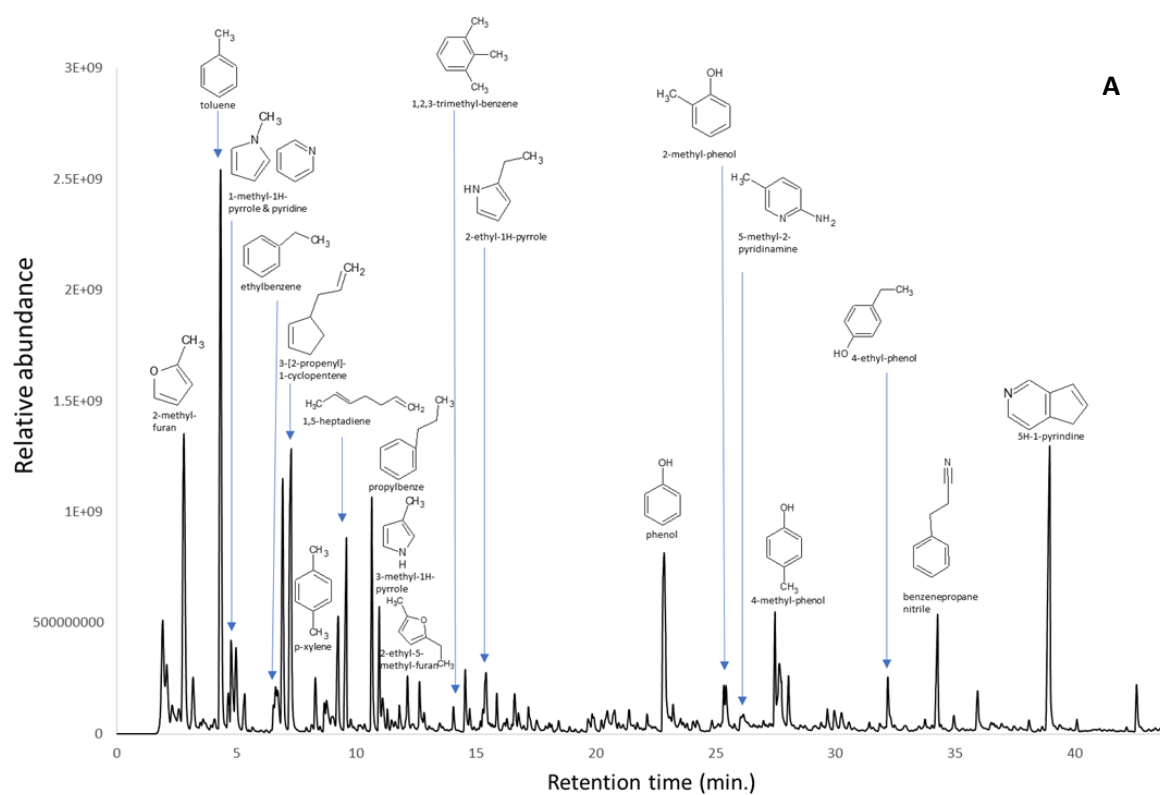
6.2.2 HTL bio-crude feed

The HTL bio-crude used in these upgrading experiments was obtained from the HTL treatment of the microalgae *Nannochloropsis sp.* (Reed Mariculture Nanno 3600), HTL experiments were conducted at 300 °C with a residence time of 10 minutes in a 300 ml autoclave (Parr Instrument Company, Illinois) with a microalgae loading of 18 wt.%. Full methodology on HTL experiments and product handling can be found in **Section 3.3**. Elemental composition of the bio-crude upgrading feedstock is presented in **Table 6.2**.

6.3. Results and discussion

Results presented in this research chapter are focused on the potential reaction networks from the analytical pyrolysis screening of model compounds and the chosen *Nannochloropsis sp.* with and without commercially available catalysts. Upgrading studies of microalgal HTL derived bio-crude was investigated using 50 ml batch reactor with catalysts followed by in-depth characterisation using standard GC-MS methods and application of novel one and two-dimensional NMR techniques.

6.3.1 Catalyst screening results



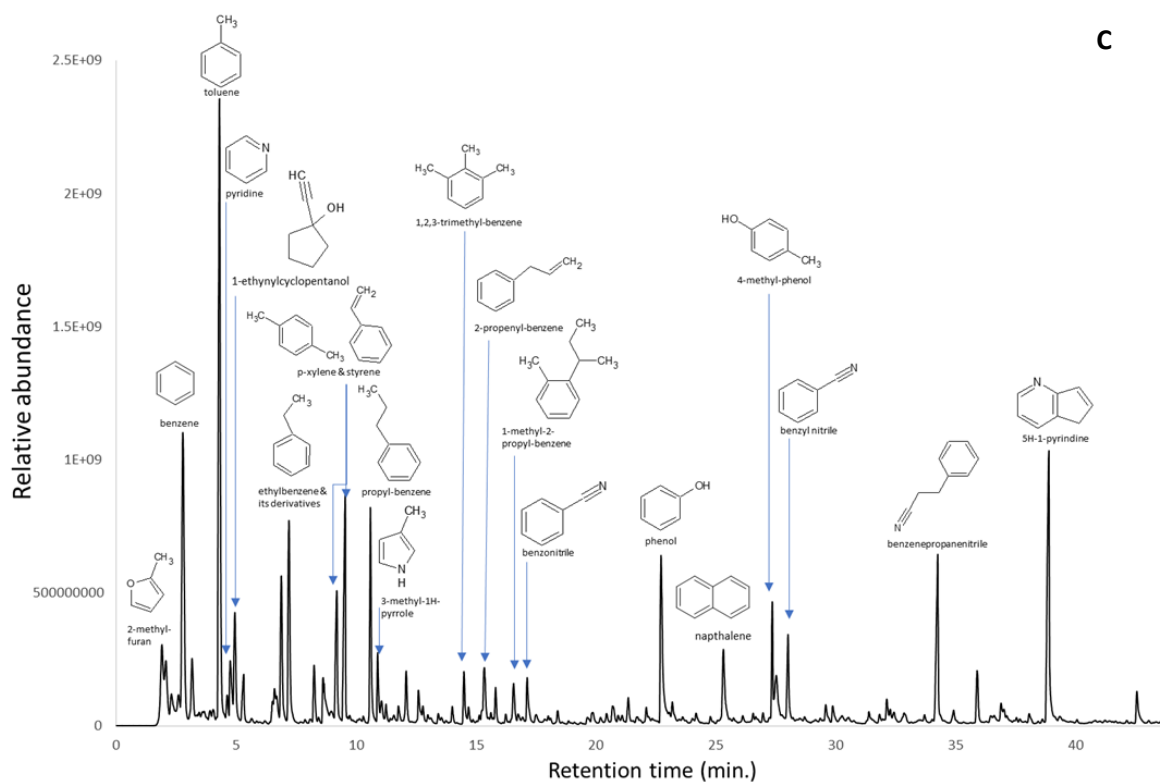
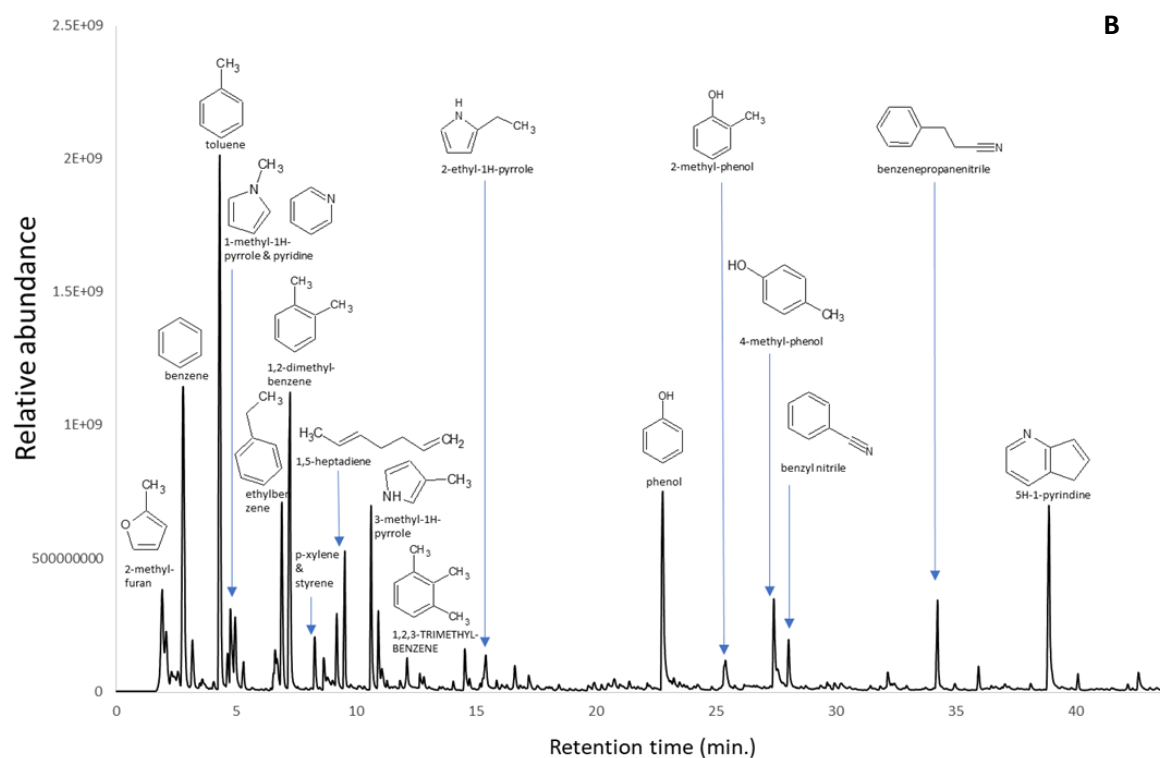


Figure 6.1. GC-MC pyrolysis chromatograms of *Nannochloropsis* sp. pyrolysed with Pd/C (A), Pt/C (B) and Ru/C (C).

Results from the catalytic pyrolysis of *Nannochloropsis sp.* presented in **Figure 6.1** show that the precious metal catalysts (Pd/C, Pt/C and Ru/C) predominantly act as aromatisation agents with minuscule differences in results between each catalyst type. Therefore further catalytic pyrolysis experiments were carried out with the Py-GC-MS system. Three selected model compounds (glucose, soy protein and oleic acid) were selected for screening of precious metal and zeolite catalysts to understand possible intermediates and end-products from the upgrading studies of HTL-derived bio-crudes

The most abundant compounds present in the pyrogram for glucose pyrolysed with Ru/C (**Figure 6.2**) were tetrahydrocyclopental[1,3]dioxin-4-one (2.1 min.) at 14.14 wt.%; 2-methyl-furan (2.3 min.) at 7.33 wt.%; (1-ethyl-2-methylpropyl)methylamine (2.5 min.) at 6.67 wt.%; 2,5-dimethyl-furan (3.1 min.) at 3.37 wt.%; methyl.alpha.-d-glucosepyranoside (3.6 min.) at 4.32 wt.%; 2(5H)-furanone (8.2 min.) at 4.83 wt.% and 3-furaldehyde (9.4 min.) at 3.86 wt.%.

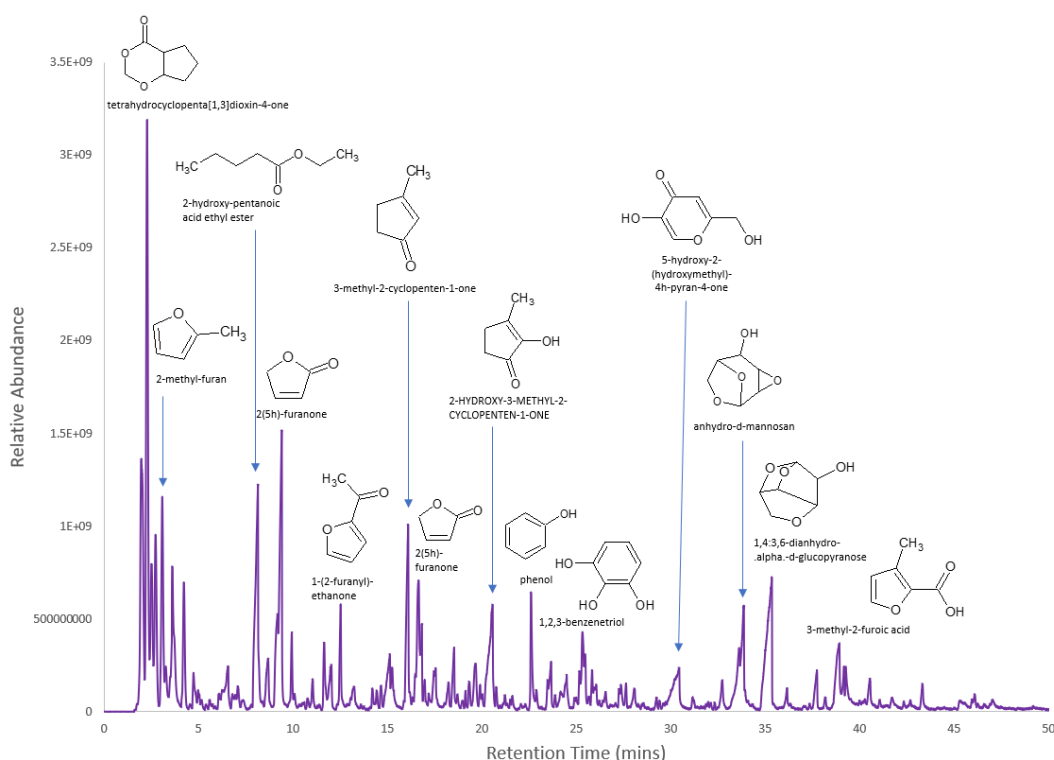


Figure 6.2. Pyrogram of glucose pyrolysed with Ru/C catalysts at 500 °C.

Precious metal catalysts were seen to promote the formation of anhydrous sugars such as 1,4:3,6-dianhydro- α -D-glucopyranose (35.4 min.) and anhydro-D-mannosan at the expense of glucopyranose. The generation of phenol (22.6 min.) and 1,2,3-benzenetriol (25.3 min.) is accounted for due

to aromatisation properties previously observed in precious metal catalysts during catalytic Py-GC-MS. It is also noticeable that a wide range of cyclopentane derivatives such as 2-methyl-furan (2.3 min.) and 2,5 diemthyl-furan (3.1 min.). These cyclopentane and furan derivatives are abundant among all analytical pyrolysis products.

The GC-MS chromatogram from the catalytic Py-GC-MS of soy protein is given in **Figure 6.3**.

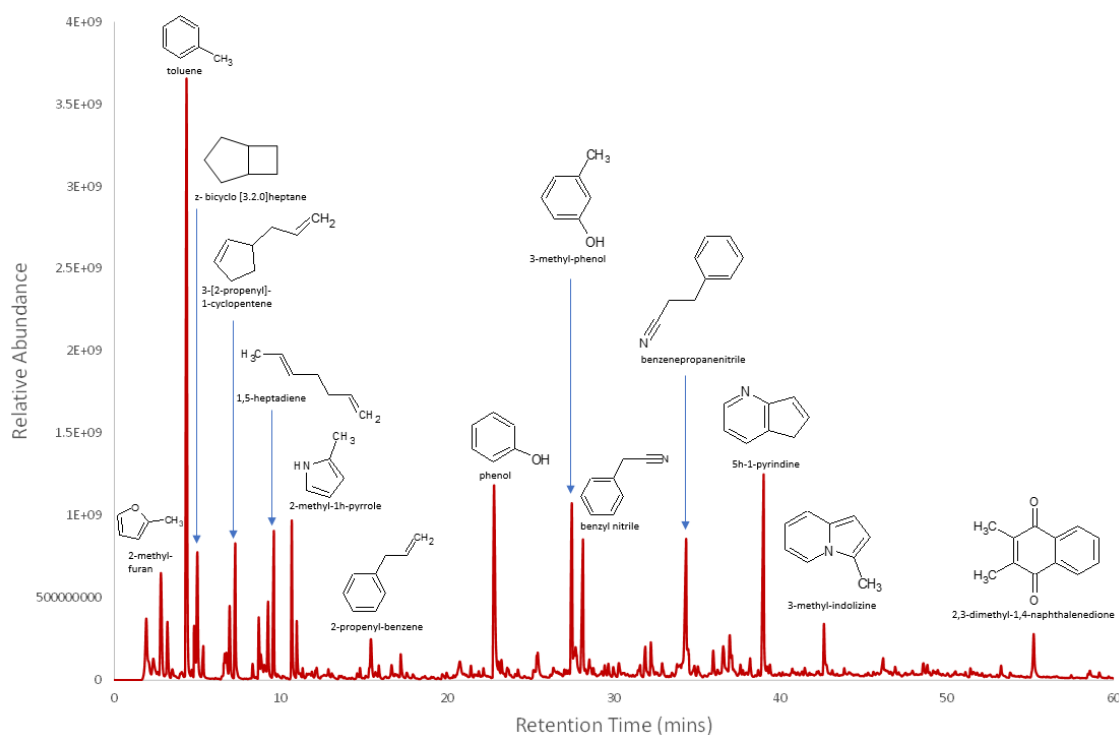


Figure 6.3. Pyrogram of soy protein pyrolysed with Ru/C catalysts at 500 °C.

The most abundant compounds from thermal degradation of soy protein with Ru/C catalytic are: 2-pentene (1.9 min.) at 3.28 wt.%; 2-methyl-furan (2.3 min.) at 5.96 wt.%; 2-pyridine carboxylic acid (2.8 min.) at 4.09 wt.%; toluene (4.3 min.) at 11.39 wt.%; 2-bicyclo[3.2.0]heptane (5.3 min.) at 11.39 wt.%; 1,5-heptadiene (9.6 min.) at 3.10 wt.%; phenol (22.8 min.) at 5.32 wt.% and 5-H-1-pyridine (38.9 min.) at 3.17 wt.%.

Toluene was found to be the most abundant pyrolysis product (under the precious metals and zeolite catalysts). Its intermediates (prior to the removal of hydroxyl groups and alkylation reactions under pyrolytic conditions) are phenol (22.8 min.) and 3-methyl-phenol (27.5 min.), and those were found with a relatively high abundance. The presence of catalysts also promoted the formation of benzene nitrile (28.4 min.) and benzenepropanenitrile (34.3 min.), which can follow condensation reactions with pyrroles and form, for example, 5-H-1-pyridine (38.9 min.).

2-pentene (1.9 min.) and 2-methyl-furan (2.3 min.) have also been observed among low molecular weight components when applying catalysts.

Oleic acid was also subjected to catalytic pyrolysis, and the GC-MS chromatogram with key thermal degradation products is presented in **Figure 6.4**.

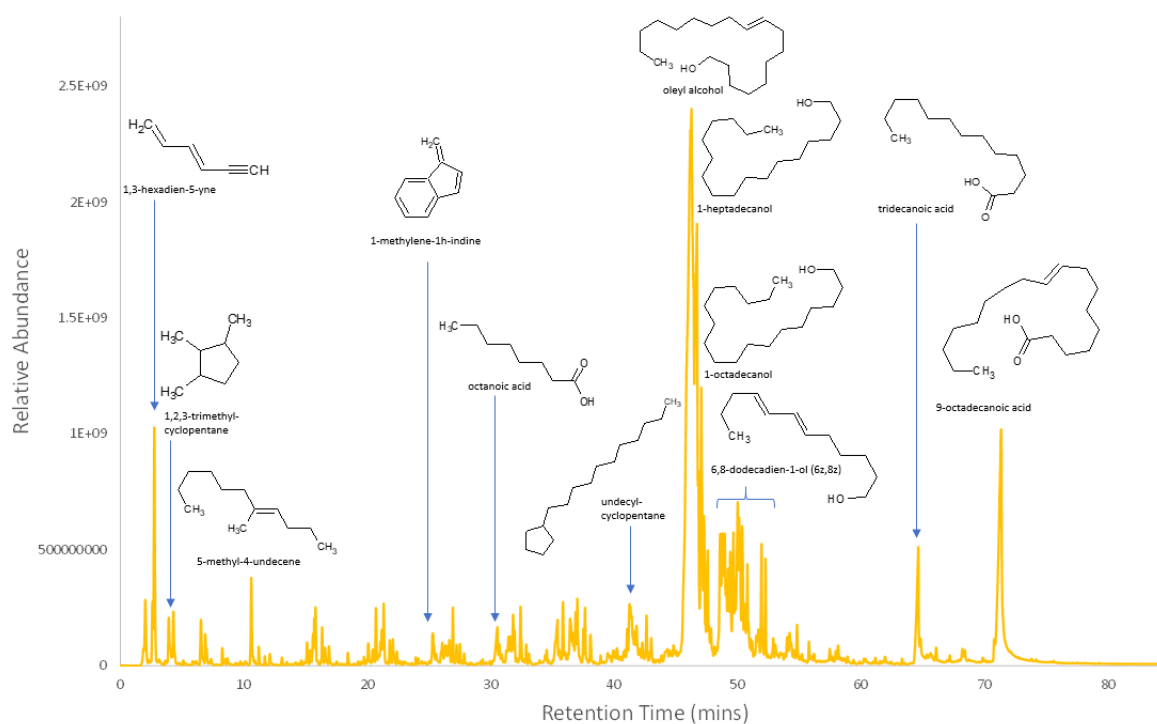


Figure 6.4. Pyrogram of oleic acid pyrolysed with Ru/C catalysts at 500 °C.

Highest yielding compounds included 1,3-hexadien-5-yne (2.7 min.) at 3.35 wt.%; oleyl alcohol (46.3 min.) at 23.16 wt.%; 1-heptadecanol (46.7 min.) at 8.15 wt.%; 1-octadecanol (47.1 min.) at 2.84 wt.%; cis-9-tetradecen-1-ol (47.8 min.) at 2.70 wt.%; 6,8-dodecadien-1-ol-(6z,8z) at 2.12 wt.%; tridecanoic acid (64.6 min.) at 2.24 wt.% and 9-octadecanoic acid/oleic acid (71.4 min.) at 6.68 wt.%.

The zeolite and precious metal catalysts promoted cracking and removing oxygen groups, particularly carbonyl groups, to form alcohols when enabling catalytic thermal degradation of long-chain fatty acids. The most abundant compound in the Py-GC-MS chromatogram above is oleyl alcohol (46.3 min.) which is the product of the removal of the carbonyl group from oleic acid. Long-chain fatty acids are known for their thermal stability. Therefore, the presence of partially cracked and deoxygenated products of oleic acid such as 1-heptadecanol (46.7 min.); 1-octadecanol (47.1 min.) and some unreacted oleic acid was expected. Some short-chain carboxylic acids, such as octanoic acid (30.5 min.), are present due to increased cracking. It was also observed that shorter chain alcohols and carboxylic

acids are more abundant following Pt/C or Ru/C and zeolite catalytic Py-GC-MS than compounds found following non-catalytic Py-GC-MS. These short-chain compounds, e.g. 1,3-hexadien-5-yne (2.7 min.) are likely to undergo cyclisation to form cyclic and benzene-like structures that may later re-polymerise to form compounds such as 1-methyne-1H-indine (25.3 min.).

6.3.2 SCW upgrading product yields

Table 6.1 presents the mass yields of the upgraded oil, gaseous and coke products after catalytic hydrotreating, also included is the mass losses during the experiment which can be attributed to some organic compounds transferring to the aqueous phase alongside experimental losses such as the loss of volatile compounds during the evaporation of the extraction solvent, residual products remaining in the reaction vessel and losses due to multiple sample transfers during the preparation of samples. The mass loss is calculated as 100% minus the yield of the products (upgraded oil, gas and coke in wt.%).

Table 6.1. Product yields for the upgrading experiments of bio-crude oils from the HTL treatment of *Nannochloropsis sp.*

Catalyst type	Upgraded oil (d.b)	Coke	Gas	Lost
No catalyst	51.1	18.1	10.7	20.1
Pt/C	55.9	22.4	11.7	10.1
Pd/C	54.7	20.1	11.7	13.5
Ru/C	57.5	19.1	16.4	7.0
HZSM-5	32.9	33.2	14.2	19.7
NiMo/Al ₂ O ₃	39.7	17.5	11.0	31.8

Table 6.1 shows the product yields and the effect of different catalysts on the product formation from the catalytic upgrading of algal HTL bio-crude in SCW at 450 °C for 4 h. The initial hydrogen pressure was 10 MPa resulting in a final water density of ~0.17 g/ml at supercritical conditions.

It is apparent that between 7.0 wt.% and 31.8 wt.% of the bio-crude loaded into the reactor was lost during the process for reasons mentioned previously.

It is apparent that the noble metal catalysts promoted the increased production of upgraded bio-oil relative to the yield achieved from the non-catalytically treated experiments. Experiments with the zeolite HZSM-5 and NiMo/Al₂O₃ catalysts resulted in yields below that achieved from non-catalytically

treated experiments. The total upgraded oil yields were in the range of 32.9 wt.% for HZSM-5 to a high of 57.5 wt.% for Ru/C, the noble metal catalysts fit into a tighter range of 54.7 wt.% to 57.5 wt.%. The NiMo/Al₂O₃ catalyst achieved a low yield of 39.7 wt.%, these results agree well with those found in the literature [132, 137]. The low upgraded oil yield achieved from the catalytic treatment with HZSM-5 is possibly due to their propensity to drive cracking reactions [141] and form high levels of coke. The cracking reactions will form light volatiles and gases with the former being potentially lost during the solvent removal process.

Lower yields (52.3 wt.% [143] and 53.1 wt.% [132]) of upgraded oil with HZSM-5 have also been observed by others relative to uncatalyzed and catalysed with other catalysts during the SCW upgrading of algal HTL bio-crude, these studies have all performed upgrading experiments at a lower temperature of 400 °C, the higher temperature of this study has resulted in a further reduction of upgraded oil yield due to increased production of gas, coke and light volatiles which are potentially lost during solvent removal.

Williams et al [187] has shown that increasing reaction temperature (400 to 550 °C treatment of pyrolysis bio-oil in a fixed bed reactor) for HZSM-5 catalysts has been shown to decrease oil yield >50%, increase gas yields >50% and catalyst coking. Higher temperatures resulted in an increased rate of cracking reactions but a reduction in oxygen content -> 55%. Duan et al [188] also found that increasing reaction temperature during SCW upgrading of algal HTL bio-crude led to dramatic increases in gas yield with increased temperature resulting in the bio-crude carbon to gas conversion factors ranging from 0.04 at 430 °C to 0.43 at 530 °C.

The majority of the catalysed gas yields are quite consistent in a range of between 11.0 to 11.7 wt.%. The uncatalyzed reaction resulted in a gas yield of 10.7 wt.%, comparable to that achieved from Pt/C, Pd/C and NiMo/Al₂O₃ catalysed reactions. Showing that for these particular catalysts gas formation is predominantly a thermal rather than a catalytic process as they display no catalytic activity towards cracking reactions that form gaseous and light volatile compound.

A notable difference is observed with respect to the zeolite HZSM-5 and Ru/C catalysts, producing appreciably higher gas yields of 14.2 wt.% and 16.4 wt.% respectively This is suggestive of some slight catalytic activity towards cracking compared to the other catalysts investigated in this study. Bai et al [132] also noted higher gas yields from the Ru/C catalysed reactions during SCW upgrading. Ru/C has been shown to be very effective in the hydrothermal gasification of biomass in supercritical water to form a fuel rich synthetic gas containing CH₄, H₂ and carbon oxides [189-191].

A study from Matsumara et al [192] showed that the gasification with a Ru/C catalyst (7 wt.% ruthenium on carbon) of a 10wt.% slurry of dairy cattle manure solids at 350 °C for 4 h resulted in over

85% conversion of carbon in the feed to gas products. It has also been found that the rate of gasification during the supercritical water gasification of lignin is increased with increasing water density with the application of a Ru/TiO₂ catalyst. Above 0.33 g/cm³ water density the yield of gas products was approximately 100%, when water density was decreased to 0.1-0.2 g/cm³ the yields were also reduced to ~65% and ~70% respectively [193]. The formation of high amounts of light ends such as C1-C4 hydrocarbon gases is undesirable as they are less valuable than liquid products [194].

Coke yields were typically in the range of 17.5 wt.% to 22.4 wt.% with the exception of the HZSM-5 catalysed reaction which had very high coke yields of 33.2 wt.%. All catalysts except NiMo/Al₂O₃ increased the formation of coke when compared to the uncatalysed reaction which is consistent with previous studies [132, 143]. The mechanism for coke formation is principally formed at high temperatures, high temperatures also favour the polymerisation and polycondensation reactions between aromatic species. The formation of these species is in the inner part of the zeolites, the compounds then expand which results in the blockage of the pores present in the zeolite catalysts [195].

The carbon deposition (coking) and rapid catalyst deactivation for zeolite catalysts is far more conspicuous when compared to noble metal catalysts, lifetimes of approximately 100 h have been achieved with Pd/C catalyst for the HDO of fast pyrolysis bio-oil in a continuous flow arrangement at an upgrading temperature of 340 °C [196]. Similarly, a lifetime of approximately 200 h was shown for the upgrading of pine wood bio-oil at 450 °C with a Co-MoS₂/Al₂O₃ catalyst [197]. Conversely for the HZSM-5 treatment of bio-oil, significant catalyst deactivation occurred after 90 minutes of operation due to carbon deposition [198].

6.3.3 Characterisation of upgraded bio-crude

6.3.3.1 Elemental analysis

Table 6.2 compares the elemental compositions and HHV alongside H/C, O/C and N/C molar ratios of the *Nannochloropsis sp.* feedstock, HTL bio-crude and upgraded oils resulting from the upgrading of the bio-crude with 5 different catalysts.

Table 6.2. Elemental composition (wt.% daf) of the algae feedstock, HTL bio-crude and upgraded oils produced with different catalysts.

Sample	Moisture (wt.%)	Ash (wt.%)	C	H	N	S	O	HHV (MJ/kg)	H/C	O/C	N/C
Bio-crude	2.1	0.12	63.2	9.8	4.5	0.39	19.9	31.6	1.84	0.26	0.06
No cat	0.3	0.0061	79.7	10.5	3.8	0.21	5.4	41.2	1.58	0.05	0.04
Pd/C	0.3	0.0056	83.2	11.3	2.6	0.07	2.5	44.0	1.62	0.02	0.03
Pt/C	0.3	0.0053	81.5	10.9	2.4	0.07	4.8	42.5	1.59	0.04	0.03
HZSM-5	0.3	0.0055	85.2	8.8	1.9	0.08	3.7	40.8	1.23	0.03	0.02
NiMo/Al ₂ O ₃	0.3	0.0058	81.7	11.3	2.6	0.08	4.0	43.2	1.65	0.04	0.03
Ru/C	0.3	0.0052	84.3	11.4	2.6	0.07	1.3	44.8	1.62	0.01	0.03

With respect to the raw bio-crude the carbon and hydrogen content of the upgraded oils was always higher with one exception for the hydrogen content of the HZSM-5 treated oil. Whereas the heteroatom content was reduced in all instances from a bio-crude value of 19.9 wt.% and 4.5 wt.% to 1.3-5.4 wt.% and 1.9-3.8 wt.% for oxygen and nitrogen respectively. With respect to nitrogen removal the best performing catalyst was the zeolite HZSM-5, with a reduction in nitrogen content to 1.9 wt.%. The degree of oxygen removal was most successful through the use of the Ru/C catalyst, resulting in a final value of 1.3 wt.%. In relation to the bio-crude the reduction in oxygen content was overall more successful, achieving a reduction of >73% in all cases. Even though all catalyst tested showed catalytic activity for denitrogenation the degree of nitrogen reduction was not as successful. Resulting in a reduction of 16% for the uncatalyzed sample and a higher range of 42-57% reduction for the catalysed treatments. The overall reduction in heteroatom content should be sufficient in order for the upgraded bio-oils to enter traditional refinery infrastructure for co-processing with fossil fuels [111].

The combination of increased carbon and hydrogen content with reduced heteroatom content led to significantly increased energy densities for all upgraded oil samples. The higher heating values (HHV)

were increased to values of between 41.2-44.8 MJ/kg from a raw bio-crude value of 31.6 MJ/kg. The highest values achieved from the upgraded oils are comparable to fossil derived diesel fuels at 45 MJ/kg [199]. Sulphur content was decreased to levels below 0.1 wt.% (<1000 ppm), although standards (EN 590) set for sulphur content for diesel fuels specify sulphur content below 10 ppm indicating further reduction is required.

Interpretation of the elemental analysis using atomic ratios is also shown in **Table 6.2** and presented graphically as Van Krevelen diagrams found in **Figure 6.5**. H/C ratios are slightly reduced for the majority of the upgraded oils falling within a range of 1.58-1.65 with an outlying value for the H-ZSM5 treated oil of 1.23. More notable are the reductions achieved for the O/C ratio which drop from 0.26 to a range of 0.01-0.04, likewise the N/C ratios are also reduced from 0.06 to a range of 0.02-0.03 for the catalysed upgrading experiments. From the Van Krevelen diagrams found in **Figure 6.5** it can be seen that the quality of the upgraded oils are improving as they approach the atomic ratio figures typical for fossil fuels, graphical regions for diesel and biodiesel given by Guo et al [130] are also highlighted on the diagrams.

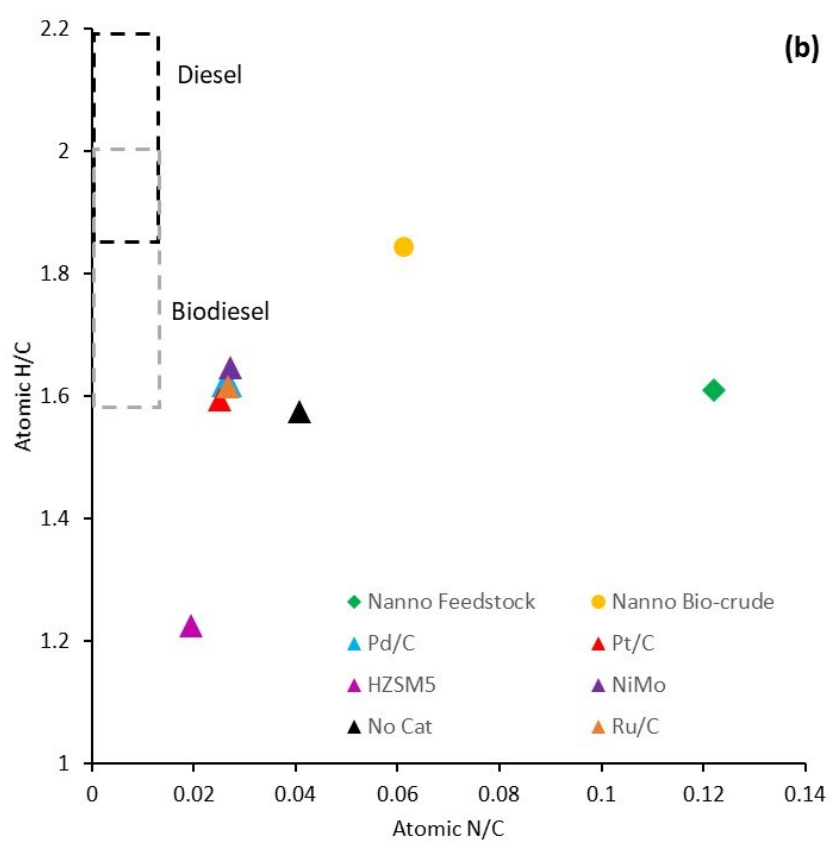
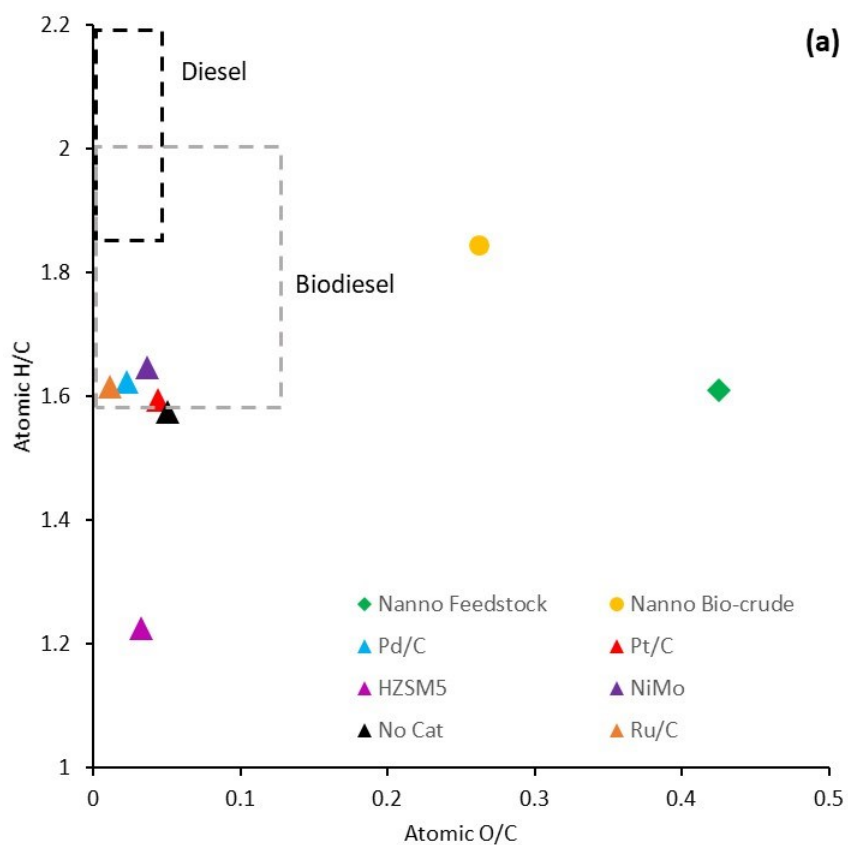


Figure 6.5. Van Krevelen diagrams of raw algal feedstock, HTL bio-crude and upgraded oil products.
(a) H/C vs O/C (b) H/C vs N/C

6.3.3.2. GC-MS characterisation of upgraded liquids

The molecular composition of the upgraded oils was analysed using GC-MS following the methodology set out in **Section 3.2.6**. **Figure 6.6** shows the GC-MS chromatograms from the raw bio-crude and three of the upgraded oil products. **Table C.1 Appendix C** also summarises the identified compounds in the upgraded oils treated with different catalysts.

Upgrading of the raw bio-crude in supercritical water conditions at a temperature of 450 °C for 4 hours significantly affects the composition of the bio-crude. From the chromatograms presented in **Figure 6.6** it is clear that for the noble metal catalysts the peaks present more well defined and regularised structure in comparison to the raw bio-crude sample. With the aim of drawing some global conclusions, the compounds identified from the GC-MS analysis have been summarised in **Table 6.3** based on their general structures. All compounds have been sorted into groups present in both the raw bio-crude and the upgraded oils shown in **Figure 6.6** with those included in the table accounting for >80% of the total peak area. This exercise shows that the GC amenable raw bio-crude sample has an approximate split of 60:30:10 to saturated hydrocarbons, unsaturated hydrocarbons and aromatics respectively. The supercritical water upgrading with heterogeneous catalysts affects these group ratios significantly, the unsaturated content for all upgraded oils falls below 12% with the noble metals achieving a lower range of 0.1 to 3.8% of peak area. The noble metals also produced a large proportion of aromatic compounds accounting for between 48.5 and 56.5% of peak area, up from a value of 8.9 for the raw bio-crude. The effect of the NiMo/Al₂O₃ catalyst was shown to be less severe with respect to the degree of conversion from one group type to another, the saturated hydrocarbon peak area was reduced slightly, unsaturated hydrocarbons were reduced greatly combined with a significant increase in aromatic content.

Table 6.3. Composition of the bio-crude and catalytically upgraded oils (% of total peak area from GC-MS)

Bio-oils	Saturated hydrocarbons (alkanes)	Unsaturated hydrocarbons (alkenes)	Aromatics
Bio-crude	60.5	28.4	8.9
Pd/C upgraded	39.9	0.1	56.5
Pt/C upgraded	42.4	3.8	48.5
Ru/C upgraded	44.5	2.1	49.8
NiMo/Al ₂ O ₃ upgraded	58.0	11.4	19.6
HZSM-5 upgraded	6.9	0.1	89.6

The raw bio-crude was found to mainly contain short chain ketones such as 4-methyl-3-penten-2-one and its derivatives, nitrogen heterocycles such as N-alkylated pyrrolidines, N-alkylated piperidines, alcohols, long chain aliphatic compounds were also present such as branched decanes, nonadecane, 3,7,11,15-tetramethyl-2-hexadecene and aromatics. Saturated hydrocarbon content was shown to decrease for all upgraded oils, however long chain alkane content in the upgraded oils was found to be much higher than that of the bio-crude, for the Pt/C catalyst the most abundant compound was pentadecane, also the second most abundant compound for Pd/C upgraded oil after toluene. Overall alkanes ranging from C6 to C40 were found in the noble metal upgraded oils conversely the bio-crude possessed a low number of alkanes in a range of C14 to C19 in low concentration. The presence and abundance of the shorter <C14 alkanes (17.1% (Pd/C) and 16.8 % (Pt/C) peak area) suggests these lighter alkanes are formed from the cracking of longer chain alkanes during upgrading. The original alkene content in the raw bio-crude (28.4% peak area) has been dramatically reduced for all upgraded oils, 3,7,11,15- tetramethylhexadec-2-ene, (2-phytene) (~9.3% peak area) was reduced to below detection levels, however large amounts of 2,6,10,14-tetramethyl-hexadecane (phytane) appeared in the upgraded oils.

The nitrogen heterocyclic compounds such as the derivatives of pyrroles, piperidines, pyrrolidines and pyridines were not seen in the upgraded oils due to being below detection limits for the noble metal catalysts or in meaningful amounts for the other catalysts, suggestive of denitrogenating activity.

At the temperature investigated in this study (450 °C) supercritical water upgrading shows that for the noble metal catalysts the main reaction products are alkyl substituted benzenes, polycyclic compounds such as naphthanes and its derivatives, alkyl substituted indenenes and a small amount of phenanthrenes. High temperatures have been shown to promote the formation of aromatic compounds, Duan et al [188] have shown that supercritical water upgrading at temperatures of 480 °C and 530 °C produced 88-90% and 88-97% peak area respectively for aromatic compounds.

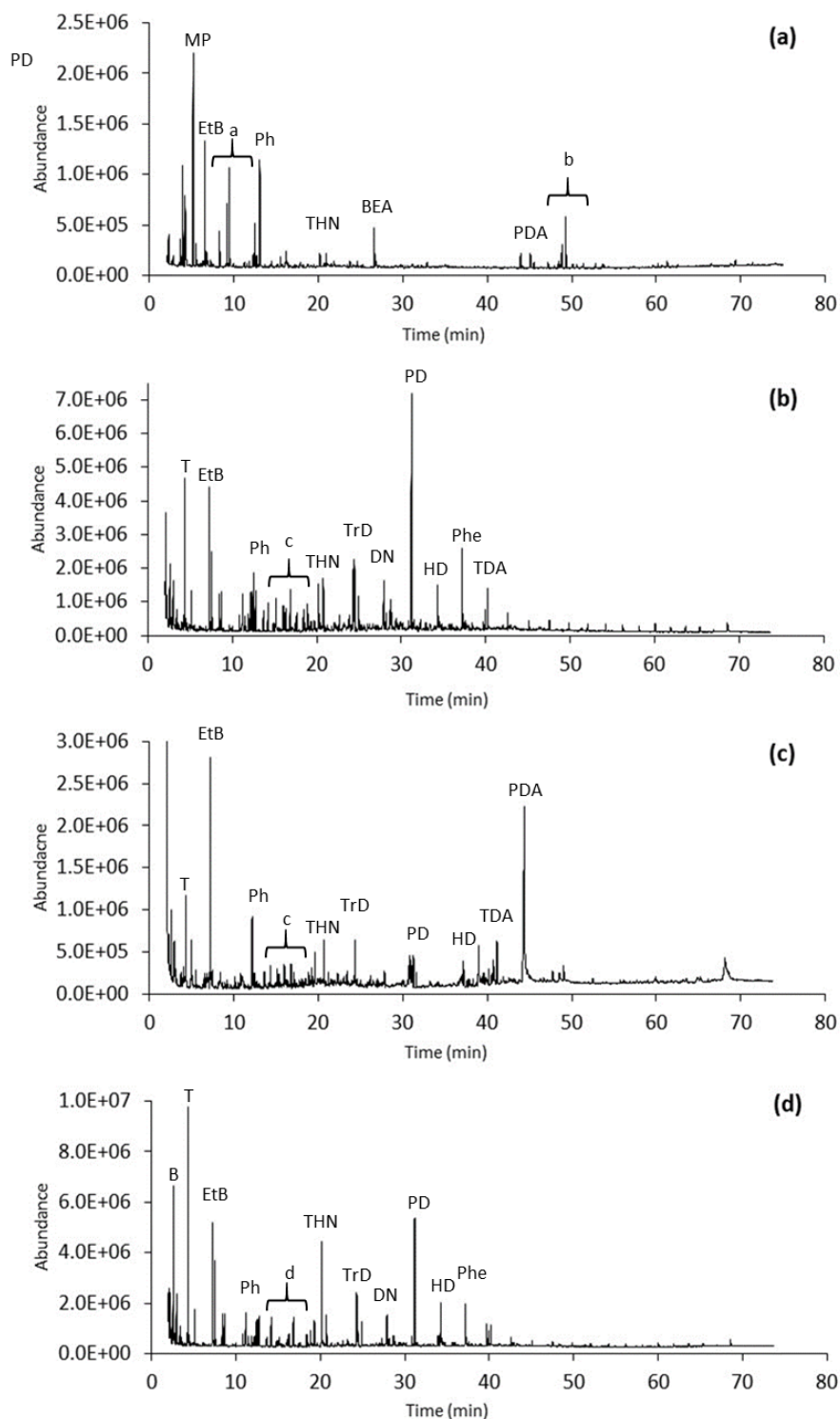


Figure 6.6. Total ion chromatogram from bio-crude (a) and selected upgraded bio-oils from the supercritical water upgrading with Pt/C catalyst (b), NiMo/Al₂O₃ (c) and Pd/C catalyst (d).

B – benzene; *T* – toluene; *MP* – 1-methyl-piperidine; *EtB* – ethylbenzene; *Ph* – phenol, *THN* – 1,2,3,4-tetrahydro-naphthalene; *BEA* – benzeneethanamine; *DN* – 1,2-dimethyl-naphthalene; *PD* – pentadecane; *HD* – hexadecane; *TDA* – Tetradecanoic acid; *Phe* – phenanthrene; *PDA* – pentadecanoic acid; (a): 3,3,4-trimethyl-Decane; 1-ethyl-3-methyl-Benzene; (b): 3,7,11-trimethyl-1-Dodecanol; 3,7,11,15-Tetramethylhexadec-2-ene; (c): Indane + phenol derivatives; (d): indane + 1-pentyl-piperidine

6.3.3.4. NMR Spectroscopy

6.3.3.4a ^{13}C PENDANT pulse program

Figure 6.7 presents the stacked PENDANT ^{13}C NMR spectra for the raw HTL bio-crude from *Nannochloropsis sp.* with three upgraded oils from the catalytic SCW upgrading in high pressure hydrogen.

Comparing the raw bio-crude PENDANT NMR spectrum **Figure 6.7(d)** to the spectrum for the upgraded oils, there is an almost complete removal of signals within the 45-110 ppm range. These were predominantly negative signals and up to the chemical shift range of 95 ppm were likely due to methylene (CH_2) groups resonances from carbons bonded to oxygen atoms present in ethers, alcohols and carbohydrates and their hydroxylated reaction products.

There is also a significant increase in the number of positive methyl (CH_3) signals in the short chain aliphatic region of 0-22ppm, these are from terminal methyl groups. There is a sudden shift to exclusively negative signals from 22ppm onwards, these are associated with methylene carbons (CH_2) from longer chain alkanes. The majority of the carbon resonances are found within the aromatic and olefinic region of 95-165ppm, all the upgraded oils show increased variety and intensity of the carbon resonances found within this region. There are a slightly increased number of positive carbon resonances (CH_1) in the region of 110-125 ppm associated with the C2 and C6 position carbon resonance in phenol for example. The carbon shift between 128-131ppm is associated with benzylic carbons, the spectra show a high density of positive (CH_1) carbon resonances within this narrow region. This signifies a greater variety and overall proportion of aromatic compounds present in the upgraded oils.

One key change to the spectra for the upgraded oils is in the presence of an array of negative signals at 132 to 144ppm that are not present in the raw bio-crude sample. These are likely due to quaternary carbon (CH_0) resonances from a carbon in a benzene ring bonded to an alkyl group. Further downfield from this region there are a number of small negative signals at ~ 155 ppm, again due to quaternary carbon atoms within aromatic rings but bonded to an electronegative species such as the hydroxy group in phenol and its derivatives.

No signals beyond 180 ppm were detected meaning no aldehyde or ketone compounds are present in detectable amounts.

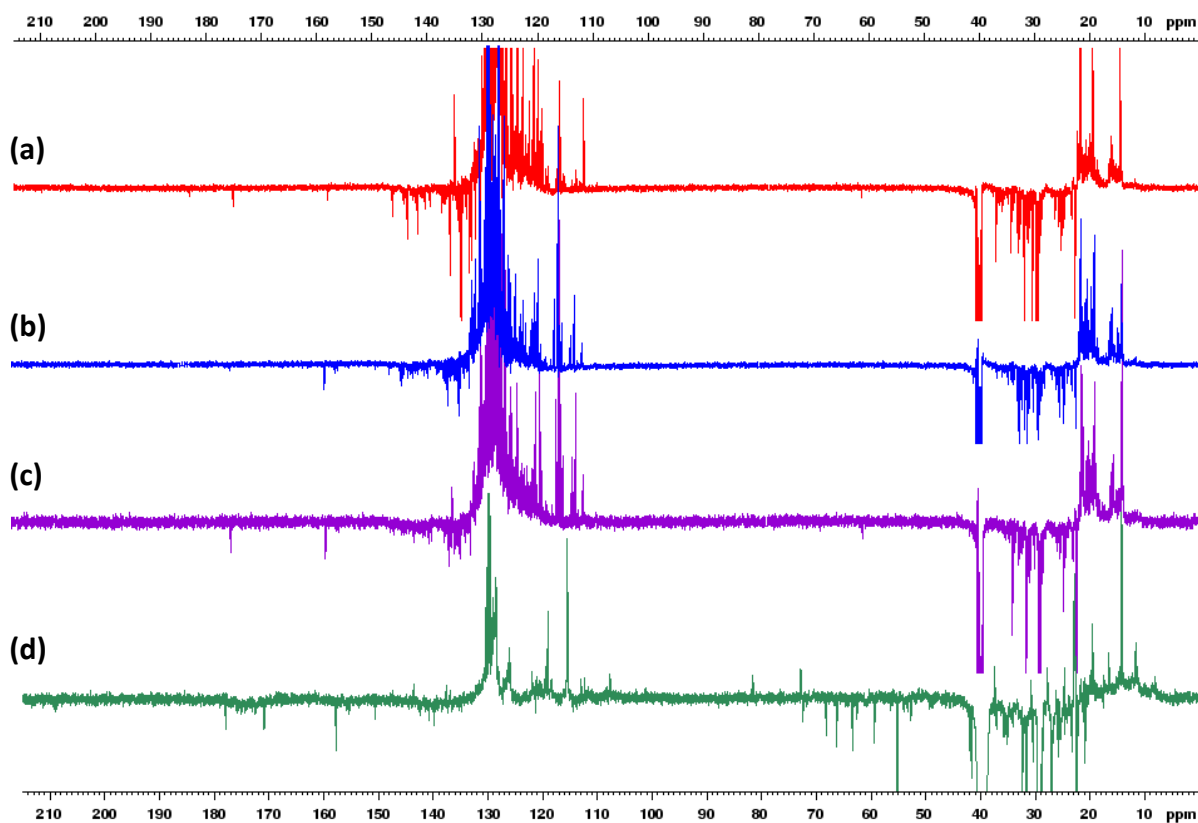


Figure 6.7. PENDANT ^{13}C NMR spectra of the HTL bio-crude (d) with the SCW treated oils by HZSM5 (a), Pd/C (b) and Pt/C (c).

6.3.3.4b 2D HSQC NMR spectroscopy

Two-dimensional ^1H - ^{13}C HSQC (Heteronuclear Single Quantum Coherence) spectra were collected for the upgraded oils in order to characterise the molecular structural composition and gain insight into the effect of catalytic upgrading in SCW conditions.

Figure 6.8 presents the superposition of the total HSQC spectra for the HTL bio-crude (300 °C, 10 minute retention time), and upgraded oils from the application of Pt/C, Pd/C and HZSM5 catalysts. The spectra has two areas of concentrated cross peaks, firstly within the aliphatic region of $\delta^1\text{H}$ 0.7-4.4 ppm and $\delta^{13}\text{C}$ 10-40 ppm. Secondly the aromatic region of $\delta^1\text{H}$ 5-10ppm and $\delta^{13}\text{C}$ 100-140 ppm. The algal bio-crude's (**Figure 6.8(green)**) spectra shows that the both of these areas have undergone significant change in both the proton and carbon environments during the SCW upgrading of algal HTL bio-crude.

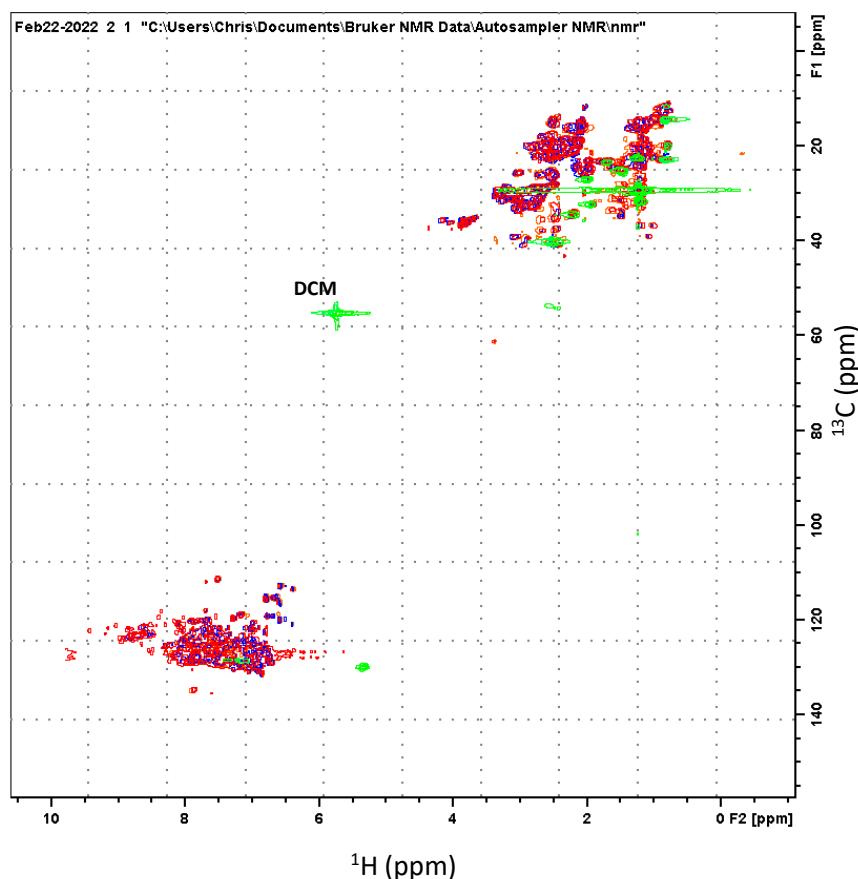


Figure 6.8. Superposition of the total 2D HSQC NMR spectra for the HTL bio-crude (green) and SCW upgraded oils with the catalysts Pd/C (blue), Pt/C (orange) and HZSM5 (red).

The aliphatic region shown in **Figure 6.9(A)** reveals that the upgraded oils exhibit a significant addition of cross peak resonances and shift in proton resonance values to an additional and more down field position. The more downfield proton resonances of $\delta^{1\text{H}}$ 2-3.5ppm within the same carbon shift region as the majority of the bio-crudes cross peaks ($\delta^{13\text{C}}$ 10-35 ppm) suggests the increased amount of aromatic compounds producing proton resonance therefore an increased number of benzylic carbons.

There is also a greater abundance of more upfield proton resonance with similar carbon resonance to the benzylic carbons mentioned above, these are associated with methyl groups (CH_3) as part of branched alkyl chains or terminal methyl groups.

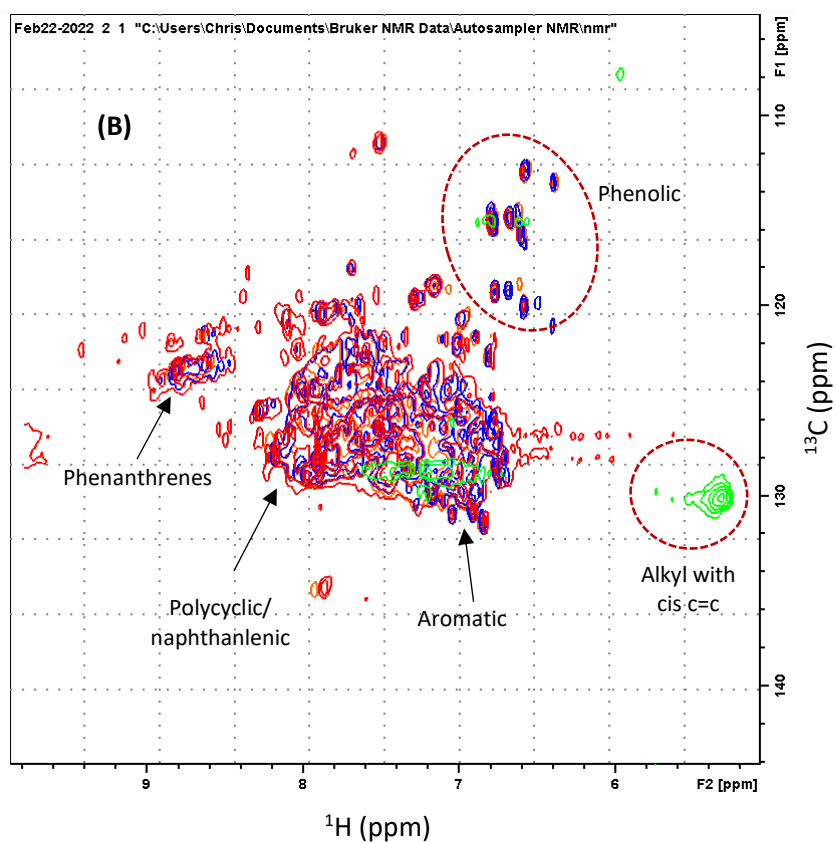
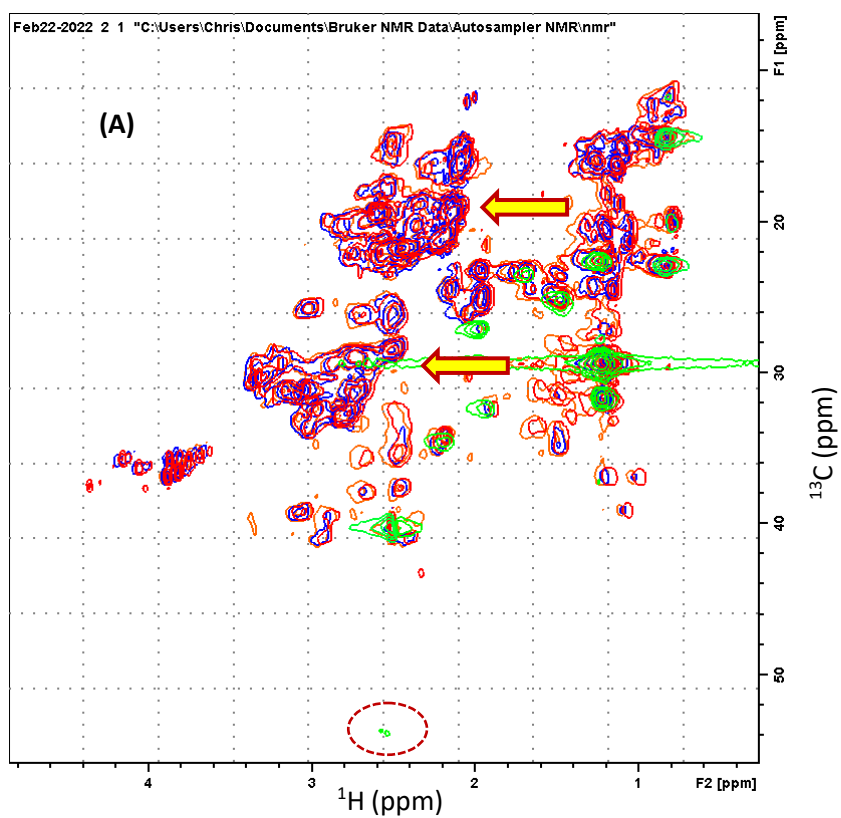


Figure 6.9. Superposition of the 2D HSQC NMR spectra for the HTL bio-crude (green) and SCW upgraded oils with the catalysts Pd/C (blue), Pt/C (orange) and HZSM5 (red).

The aliphatic (A) region is shown on the top and aromatic region (B) is shown on the bottom

The aromatic region for the HTL bio-crude (**Figure 6.9(B)**) shows that the major cross peak resonances occur for alkyls with cis carbon double bonds ($\delta^1\text{H}$ 5.3 & $\delta^{13}\text{C}$ 130ppm), benzene derivatives ($\delta^1\text{H}$ 7.2 & $\delta^{13}\text{C}$ 129ppm) and some phenolic content at ($\delta^1\text{H}$ 6.7 & $\delta^{13}\text{C}$ 115ppm). Following SCW upgrading the number of cross peaks within the aromatic region is greatly increased. The alkene content seen in the bio-crude sample is dramatically reduced

Confirmation of the presence of phenanthrenes with cross peak resonance in the small cluster in the region of $\sim\delta^1\text{H}$ 8.7 & $\delta^{13}\text{C}$ 123ppm.

6.4. Conclusions

The bio-crude produced from HTL requires upgrading prior to use as a transportation fuel in order to reduce heteroatom content and improve its physical characteristics. The screening of catalysts was undertaken using Py-GC-MS and upgrading of HTL bio-crude via supercritical water upgrading at 450 °C for 4 hours under a high-pressure hydrogen atmosphere.

Collecting together all analytical thermal degradation studies (Py-GC-MS) with and without catalysts with representatives of algal “building blocks” (model components – carbohydrates, lipids and proteins) allowed to propose specific reaction networks taking into degradation during HTL followed by subsequent catalytic upgrading towards more defined compounds. Three proposed reaction networks for each main macromolecular constituent of microalgae are presented in **Appendix C Figures C.1-C.3**.

The application of catalysts resulted in only small increases in upgraded oil yield when compared to the uncatalysed experiment. Experiments with HZSM-5 and NiMo/Al₂O₃ resulted in lower upgraded oil yields. HZSM-5 and Ru/C were shown to promote the formation of gaseous products. In all cases improvements were seen in atomic ratios and HHV; overall H/C ratios were adversely reduced by a small amount. The application of catalysts achieved a reduction in nitrogen content of the upgraded oils to levels of 1.9-2.6 wt.% compared to the uncatalysed experiment and the raw bio-crude values of 3.8 and 4.5 wt.%, respectively, resulting in atomic N/C ratios of 0.02-0.04 for the catalytically upgraded oils. Oxygen content was dramatically reduced, the performance of the uncatalysed experiment generated an upgraded oil with 5.4 wt.% oxygen (down from 19.9 wt.%), the inclusion of catalysts led to a further reduction to values ranging between 1.3-4.8 wt.%. Analysis of the upgraded oil revealed the content was predominantly composed of C6-C16 alkanes and substituted aromatic compounds. Compositional analysis from feedstock characterisation, algal and model compounds HTL bio-crudes and upgraded oils were leveraged to propose a reaction network following the conversion of algal chemical species through to bio-crude and finally upgraded oils.

Chapter 7 - Techno-economic assessment

7.1. Introduction

The focus of this chapter is in the application of microalgae in the energy sector, through their thermochemical conversion to produce bio-liquids that can be direct feed in fuels for current transportation platforms. Microalgae also have a much wider application in non-energy sectors such as nutraceuticals, animal feeds, chemicals and pigments among others as outlined in **Section 2.3**. Supplying more valuable products produced from microalgae to these other markets will play an essential part in making algae derived biofuels economically viable.

As outlined in **Chapter 2** microalgae have received a lot of attention as an alternative and next generation bio-fuel feedstock, utilisation of this feedstock is thought to be able to overcome some of the disadvantages associated with lignocellulosic biomass. Even with extensive studies and work within this area in recent years it is still projected that adoption of algal based biofuels is still out of reach. This is due to many factors which ultimately culminate in high production costs and therefore the unattractiveness of the fuel from an economical perspective. Whilst these challenges remain, algal biomass as a feedstock towards liquid fuel production still warrants investigation due to several important factors: algae can be grown on land not suitable for terrestrial crops i.e. marginal or contaminated land, they have potential to accumulate large amounts of important macromolecules such as lipids, proteins and carbohydrates, dependant on species and cultivation conditions which can be selected/tuned for the desired feedstock composition. They can be grown in saline or wastewater for remediation purposes without pesticides or herbicides and algae are the fastest growing group of plants in the world and have a 7-31 times higher per acre yield of oil compared to palm oil [49].

Initially the favoured production route of algal derived biofuels was through the transesterification of extracted algal lipids, this process has distinct disadvantages, long algal growth periods and nutrient restriction required in order to maximise lipid content, use of organic solvents, residues and needing a dry feedstock. This study will focus on the thermochemical treatment of microalgae to produce renewable biofuels. The conversion pathway chosen is via hydrothermal liquefaction. Other thermochemical treatment routes have been discussed in **Chapter 2**.

As mentioned previously, HTL is ideally suited and more economically advantageous to process feedstocks with very high moisture contents such as algae and waste sludges with moisture contents typically greater than 50 wt.%. There are many advantages to HTL over other conversion technologies such as; production of bio-crudes with high heating values, high bio-crude yields, no need for

feedstock drying and potential for recycling the nutrient rich aqueous phase among others. The main disadvantage in the HTL of microalgae comes from the very high operating pressures and temperatures, necessitating the need for high pressure equipment resulting in increased capital investment and operational costs when compared to other biomass thermochemical conversion routes.

7.2. HTL Model Development

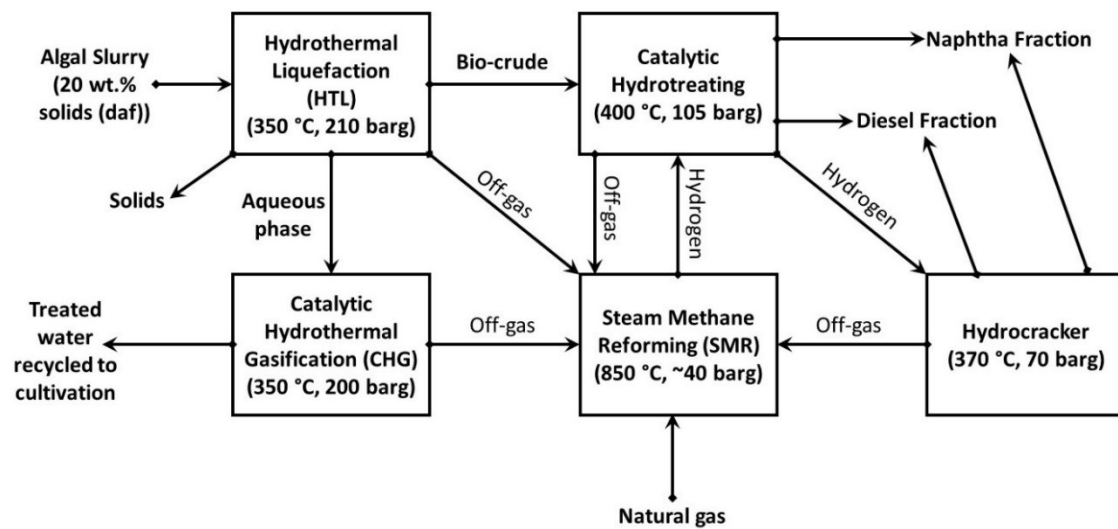


Figure 7.1. Block diagram for the overall microalgae HTL conversion process to transportation fuels.

Figure 7.1 shows the proposed microalgae biorefinery, the base case plant is designed to process a water algae slurry containing 2000 kg/h dry ash free algal biomass and operating for 330 days/year (7920 hours). The block diagram shows a number of systems, firstly the core hydrothermal liquefaction, following this there is hydrotreating of the bio-crude and fractionation to produce upgraded fuels. Auxiliary processes are also included, these are aqueous fraction treatment through catalytic hydrothermal gasification, hydrogen generation through steam methane reforming and hydrocracking of heavy fractions. The internal generation of hydrogen and overall heat integration has the potential to reduce operating costs significantly. The mass balances from the Aspen models for the HTL and hydrotreating processes are presented in **Appendix D Tables D3** and **D4**.

7.2.1. Hydrothermal liquefaction

Table 7.1. presents the assumptions used in the aspen model in order to produce mass and energy balances for the process that will provide the inputs necessary for economic assessment.

Table 7.1. Aspen model assumptions

Operating Parameters	Value
Plug flow reactor	
Temperature	350 °C
Pressure	210 barg
Feed Solids (ash free)	
Feed Solids (ash free)	20 wt.%
Algae ash content	13 wt.%
Product yields	
Bio-crude (dry)	51 wt.%
Aqueous	30 wt.%
Solids	2 wt.%
Gas	4 wt.%
Ash	13 wt.%
Bio-crude moisture content	2 wt.%

Figure 7.2 presents the Aspen plus process flow diagram for the HTL treatment of an algal slurry. The algal slurry (20 wt.% dry ash free solids) is pumped to an operating pressure of 210 barg and passed through a shell and tube heat exchanger which preheats the slurry to 239 °C using the hot liquid products from the reactor. Following this the slurry is further heated to 350 °C by a fired heater using hot oil as the heat transfer medium, this is in order to bring the reactor feed up to the reaction temperature of 350 °C. This arrangement is an initial scheme for heat integration to minimise fuel/power costs, it is anticipated that further improvements could easily be realised. This preheated slurry is then fed to the plug flow type reactor where the algal slurry is converted to mainly an organic bio-crude and separate aqueous phase with small amounts of solids and gases, mainly consisting of carbon dioxide and a small proportion of fuel gases accounting for ~7 wt.% of total gas mass. The mass fractions of the compounds used in the Aspen model to model the resultant bio-crude, aqueous fraction and gases are given in **Appendix D Table D1**.

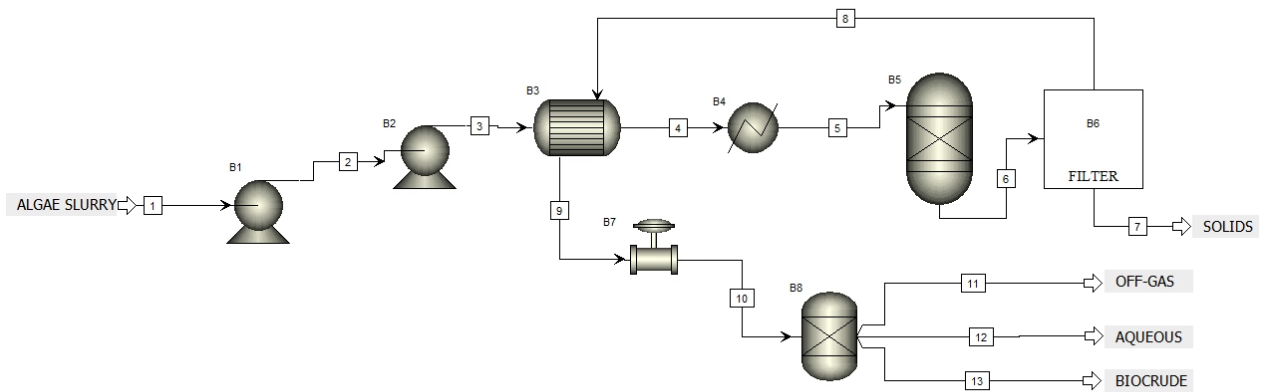


Figure 7.2. Aspen process flow diagram for the hydrothermal liquefaction process.

The reactor effluent then enters a hot filter where the solids are removed in order to reduce fouling potential downstream, the cleaned reactor effluent consisting of the two liquid phases and non-condensable gases are then cooled and separated in a three-phase separator to 96 °C and atmospheric pressure.

7.2.2. Catalytic hydrothermal gasification of aqueous phase

The aqueous phase which is mainly effluent water but also high in soluble organics, ammonia and metal salts is sent to the Catalytic Hydrothermal Gasifier (CHG) to create a fuel gas. CHG is a means to recover carbon and nitrogen from the process where all organics are converted to carbon dioxide and methane, the latter is to be used in the steam methane reforming process (SMR) discussed later.

The process flow diagram for the CHG set-up is very similar to the hydrothermal liquefaction process seen in **Figure 7.2**, the only major difference is the process fluid meets with a catalyst to form gaseous products. Firstly, the aqueous phase is pumped back up to ~200 barg and preheated in the same manner as the liquefaction process where heat is recovered from the reactor outlet stream. Final trim heat is supplied from a fired heater to bring the temperature to the desired 350 °C before entering the fixed bed reactor. The fixed bed reactor employs a ruthenium on carbon catalyst, this catalyst is very sensitive to sulphur contamination so prior to the feed entering the reactor the stream is subject to a sulphur scrubber which employs a Raney nickel guard bed to capture organic sulphur. The organic content of the aqueous phase is predominantly converted to CO₂ and CH₄, alongside the now cleaned effluent water that still contains useful algal growth nutrients which is sent back to the cultivation stage for utilisation. The produced off-gases are sent to the steam methane reformer process to generate hydrogen for the catalytic upgrading plant. Modelling of the gaseous products from the

aqueous phase treatment for the purposes of the economic model is based on the aqueous phase total flow leaving the 3 phase separator after the HTL reactor.

7.2.3. Bio-crude hydrotreating

Bio-crudes derived from microalgae are known to have high nitrogen and oxygen contents, for its utilisation as a transportation fuel it therefore needs to be improved. From 2015 the average total crude oil throughput of UK refineries has been ~1 million barrels per day with higher capacities achievable [200]. The move towards the decarbonisation of transportation via the increased market share from electric vehicles will free up capacity at UK refineries.

Table 7.2 presents the model assumptions used to create the Aspen plus model. The base case scenario considers on site upgrading where the hydrotreatment and hydrogen generation plant are located next to the liquefaction site. Potentially a more economical scenario is where the raw bio-crude would be transported to a centralised conventional crude oil refinery where the bio-crude feedstock would be blended with fossil crude oil. The impact of this off-site refining is likely significant as there are advantages in terms of economy of scale and no capital investment required for on-site refining.

Table 7.2. Hydrotreating Aspen plus model assumptions

Operating Parameters	Value
Plug flow reactor	
Temperature	400 °C
Pressure	105 barg
Feed Solids (ash free)	20 wt.%
Algae ash content	13 wt.%
Product yields	
Upgrade Oil	77 wt.%
Aqueous	16 wt.%
Gas	7 wt.%
Upgraded oil moisture content	0.16 wt.%
Hydrogen Consumption	0.043 wt/wt of the raw HTL bio-crude (wet)

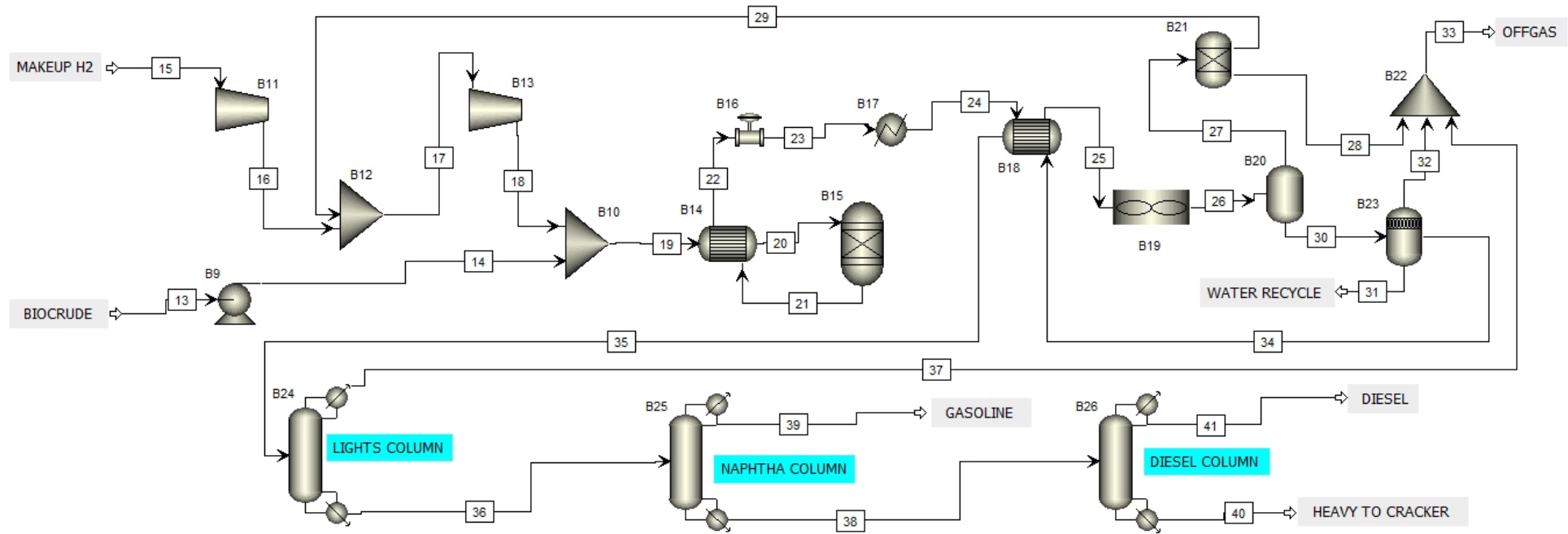


Figure 7.3. Aspen plus process flow diagram for the bio-crude hydrotreating block.

A simplified bio-crude hydrotreatment process flow diagram is presented in **Figure 7.3**, the separated bio-crude from the liquefaction reactor is sent to the hydrotreating section. Firstly, the bio-crude is pumped to 105 barg, then mixed with compressed hydrogen and passes through a preheating heat exchanger that recovers heat from the reactor product stream to increase the reactor inlet temperature to 400 °C with a fired heater to make-up any deficit. The preheated bio-crude then enters the hydrotreater where the oxygen content is reduced through hydrodeoxygenation to form carbon dioxide and water, nitrogen content is reduced to form ammonia and sulphur is removed in the form of hydrogen sulphide. The reactor is modelled as an RYield reactor using product yields given in **Appendix D Table D2**.

The upgraded bio-crude now contains a mixture of compounds that lie within the petrol, jet fuel and diesel boiling point ranges comprising of a mixture of aromatics, olefins, paraffins and naphthenes. The products from the reactor are then cooled in order to condense the hydrocarbon fraction and water. The upgraded hydrocarbon stream then undergoes fractionation using three RadFrac columns to produce a number of boiling point ranges such as light gas hydrocarbons $\leq C4$ (sent to SMR), naphtha (C4-C11), kerosene (C8-C16), diesel oil (C8-C28) and heavy oil bottoms range which is then sent to the hydrocracker to crack the long chain hydrocarbons into more desirable products.

7.2.4. Steam methane reforming

In order to utilise off gas streams within the process a common and widely used steam reforming plant is specified. Part of the off-gas streams from the liquefaction process and the hydrotreating process are used as fuel gas for the reforming unit. The remainder of the off-gases are mixed with superheated steam and make-up natural gas. The steam reformer produces syngas, in order to produce a syngas with a higher hydrogen content the syngas is directed to a water-gas shift reactor. Steam is raised from recouping heat from the reformer exhaust which results in the condensation of water vapour prior to the inlet of the water gas shift reactor. The gas is then further cooled in the same manner prior to entering the pressure swing absorption (PSA) columns which produces a highly purified hydrogen gas, the off-gas from the PSA is sent back to the reformer burner.

7.3. Techno-economic analysis

7.3.1. Introduction

A techno-economic analysis has been conducted in order to calculate the costs of a biorefinery plant to produce microalgae-based biofuels and other valuable secondary products where applicable. The methodology utilised in this study was a discounted cash flow rate of return (DCFROR) over the projected plant lifetime of 30 years to calculate the minimum fuel selling price (MFSP).

Table 7.3. Assumptions for the Nth plant model
Adapted from [93].

Assumption Description	Assumed value for model
Internal rate of return	10%
Plant financing debt/equity	60% / 40% of total capital investment (TCI)
Plant life	30 years
Income tax rate	35%
Interest rate for debt financing	8.0% p.a.
Term for debt financing	10 years
Working capital cost	15.0% of fixed capital investment (excluding land)
Depreciation (Straight-line) Period	10 Years
Construction period	3 years (8% 1 st year, 60% 2 nd year, 32% 3 rd year)
Plant salvage value	No value
Start-up time	6 months
Revenue and costs during start-up	Revenue = 50% of normal Variable costs = 75% of normal Fixed costs = 100% of normal
Operational	330 days per year (7920 hours per year)

To allow for the comparison against other studies nth plant assumptions were applied to all parts of the economic analysis. Nth plant assumes that all of the technology utilised within the system boundary is fully developed and all technologies are mature when the plant is operational. A list of all the assumptions made for the nth plant can be found in **Table 7.3**. Additionally, this definition means that this plant is not the first of its kind, this significantly reduces the risk associated with the project

and allows for lower debt financing terms of agreement and more predictable operational and capital cost estimates at the beginning of the project. By modelling the biorefinery using the nth plant assumptions it allows for the comparison between the modelled biorefinery herein and existing commercial bio-fuel operations. Any incentives, such as favourable tax allowances and other credits from any future government policies are not considered in this study which is completed to be independent of government subsidies.

7.3.2. Total capital investment (TCI)

Total capital investment is defined as the amount of capital needed to build and commission the production facility, it is split into two types of capital defined as Fixed Capital Investment (FCI) and Working Capital (WC). The fixed capital investment is usually the largest outlay and includes the cost of purchasing equipment and its installation and commissioning. Furthermore, fixed capital investment is comprised of direct and indirect costs. Direct costs are those for tangible assets such as the process equipment, warehousing, development of the plant site and additional piping. Indirect costs are those associated with the facilitation/implementation of the direct cost items. These are normally services, personnel costs associated with supervision, consumable items, insurance and contingencies, further detail of direct and indirect costs are presented in **Table 7.4**.

Table 7.4. Costs for Determining Total Capital Investment*Adapted from [201]*

Item	Description	Amount
Direct costs		
Purchased equipment cost	Individual equipment costs scaled from existing equipment	See Table 7.5 for scaling factors
Purchased equipment installation	Installation of process equipment on-site	See installation factor Table 7.6 for exact multiplier for each type of item.
Additional direct costs		
Buildings	On-site storage of equipment and supplies	4% of Total installed cost (TIC)
Site development	Fencing, curbing, parking lot, roads, drainage, general paving. This allows for minimum site development assuming a clear site with no unusual problems.	10% of TIC
Additional piping	To connect equipment to storage and utilities	4.5% of TIC
Total Direct Costs (TDC)		18.5% of TIC
Indirect costs		
Proratable expenses	This includes fringe benefits, burdens, and insurance of the construction contractor	10% of TDC
Field expenses	Consumables, small tool and equipment rental, field services, temporary construction facilities, and field construction supervision	10% of TDC
Home office construction	Engineering plus incidentals, purchasing, and construction	20% of TDC
Project contingency	Extra cash on hand for unforeseen issues during construction	10% of TDC
Other costs	Start-up, commissioning costs. Land, rights of way, permits, and fees. Piling, soil compaction, unusual foundations. Sales, use, and other taxes. Freight, insurance in transit, and import duties on equipment. Overtime pay during construction. Field insurance. Project team. Transportation equipment, bulk shipping containers, plant vehicles, etc	10% of TDC
Total Indirect Costs		60% of TDC

7.3.2.1. Direct capital costs

Equipment

The costs for the equipment will be calculated by scaling the base cost (BC) on the ratio of the production capacity of the pieces of equipment Equation 7.1. The equation also then updates the calculated scaled costs to the desired cost year accounting for the annualised inflation effects by applying the Chemical Engineering Plant Cost Index (CEPCI) [93].

$$\text{Scaled equipment Cost} = BC \times \left(\frac{\text{Actual equipment flowrate}}{\text{Original equipment flowrate}} \right)^{\text{Scale Factor}} \times \left(\frac{\text{CEPCI}_{\text{base year}}}{\text{CEPCI}_{\text{literature year}}} \right) \quad (\text{Eq. 7.1})$$

Location scaling must also be taken into account when the new plant is proposed to be built in a different country to where the original cost data is based using Equation 7.2.

$$\text{Cost in UK} = \text{Cost in Base Country} \times \left(\frac{\text{UK location Factor}}{\text{Base Country Location Factor}} \right) \quad (\text{Eq. 7.2})$$

Table 7.5. Scaling exponents for equipment costs based on [93].

Equipment type	Scaling Exponent
Agitators	0.5
Compressors (motor driven)	0.6
Heat exchangers	0.7
Inline mixers	0.5
Package quotes / skidded equipment	0.6
Pressure vessels	0.7
Pumps	0.8
Tanks (atmospheric)	0.7
Solids handling equipment	0.8

Installation cost

Once the purchased equipment cost has been determined the installation cost for each piece of equipment is then calculated by applying a multiplier to the purchased equipment cost, these multipliers account for the installation of the equipment into the building and the costs associated

with instrumentation and piping. The installation factors used in this study are provided in **Table 7.6** below [93].

Table 7.6. Installation factors

Item	Multiplier
Agitators (stainless steel)	1.5
Boiler	1.8
Compressors (motor driven)	1.6
Heat exchangers (shell and tube, stainless steel)	2.2
Heat exchangers (double pipe, stainless steel)	2.2
Inline mixers	1.0
Skidded equipment	1.8
Solids handling equipment (including filters)	1.7
Pressure vessels (stainless steel)	2.0
Pumps (stainless steel)	2.3
Tanks (field erected stainless steel)	1.5

Other direct costs

Following the calculation of the scaled equipment cost, adjustment to the desired cost year and multiplication by the installation cost factors the total installed cost (TIC) is found. There are a number of other direct costs to be added such as those costs for buildings, additional piping and general site development, these are estimated from the TIC. The total direct cost (TDC) is the sum of all the installed equipment costs plus the additional direct costs outlined in **Table 7.4**.

7.3.2.2. Indirect capital costs

As outlined in **Table 7.4** there are a number of additional indirect capital costs to consider, these indirect costs are associated with the intangible investment required. The indirect costs are calculated relative to the total direct costs. Indirect capital costs include those for project contingency, contractor's fees, construction expenses and engineering and supervision among others. The sum of all the direct and indirect costs is the fixed capital investment. Total capital investment is the fixed capital investment plus the working capital (WC), in this study WC is assumed to be 15% of FCI.

7.3.3. Operating costs

Operating costs include both fixed and variable costs. The fixed costs include employee salaries, independent of the percentage of the maximum production capacity achieved. Fixed operating costs also include plant maintenance and property insurance. Variable operating costs include the raw materials used in the process along with the provision of utilities.

7.3.3.1. Fixed operating costs

In order to estimate the costs associated with labour it is first necessary to make an estimate on the number of employees. Levels of staffing required for a similar sized plant (50% larger by slurry flow rate to the HTL reactor) were taken from Dutta et al [202]. Median values for salaries for employee positions presented in **Table 7.7** were gathered from reference [203].

Table 7.7. Biorefinery plant fixed operating costs

Adapted from [204]

Position	2020 Salary	Number Required	2020 Total Cost
Plant Manager	£55,000	1	£55,000
Plant Engineer	£32,070	2	£64,140
Maintenance Supervisor	£35,448	1	£35,448
Lab Manager	£40,000	1	£40,000
Shift Supervisor	£26,990	1	£26,990
Lab Technician	£21,425	2	£42,850
Maintenance Technician	£30,614	3	£91,842
Shift Process Operators	£22,601	15	£339,015
Warehouse Employees	£19,490	2	£38,980
Clerks & Secretaries	£22,331	1	£22,331
Subtotal			£756,596
Labour burden	90% of labour and supervision		£680,936
Maintenance capital	3% of TIC		£488,597
Insurance and taxes	0.7% of FCI		£216,155
Total Other Fixed Costs			£1,385,689

It is necessary to account for all costs required in order to enable an employee to carry out their work, this is known as labour burden and is the true cost of a company to have an employee. The cost of labour burden is assumed to be 90% of total the labour and supervision costs, labour burden includes such employee benefits that the company must or choose to offer to their employees, for example payroll taxes, employer pension contributions, health insurance etc. It also includes plant security,

communications, lighting, heating and employee safety. Finally, the maintenance cost is assumed to be 3% of the total installed cost of the equipment, the costs associated with plant insurance and local property tax is assumed to be 0.3% of the fixed capital investment.

7.3.3.2. Variable operating costs

The algae purchase price is assumed to be £400/tonne from an external supplier. The electricity cost of £0.15/kWh is based on UK government data for the year 2020 based on the prices paid by small non-domestic users (20-499 MWh). Make-up hydrogen is imported to the process at an assumed price of £2.35/kg. The cost associated with the purchase and renewal of the CHG catalyst (Ru/C) is calculated using **Equation 7.3** and **Equation 7.4** respectively.

$$\text{Initial catalyst purchase cost} = m_{cat} \left(C_{support} \times (1 - \omega) + C_{metal} \times \omega \times (1 + \delta) \right) \quad (\text{Eq. 7.3})$$

Where m_{cat} is the catalyst weight, $C_{support}$ is the carbon support cost, C_{metal} is the metal cost, ω is the catalyst loading and δ is the fabrication factor.

Table 7.8. Variable operating costs and supporting assumptions

Stream	Costs	Units	Reference
Algae feedstock	400	£/tonne	
Electricity	0.15	£/kWh	[205]
Make-up water	0.00023	£/kg	[93]
Hydrogen	2.35	£/kg	[206]
Upgrading catalyst (Renewal)	55,263	£/yr	calculated
Gasification catalyst (Renewal)	118,755	£/yr	calculated
Cooling water	0.19	£/tonne	[207]

The hydrotreating and hydrocracking catalyst lifetime are taken from Jones et al [93]. Renewal of the upgrading and gasification catalyst cost are calculated using **Equation 7.4**.

$$\text{Renewal Cost} = m_{cat} \left(C_{support} \times (1 - \omega) + C_{metal} \times \omega \times (1 + \delta) \times (1 - \rho) \right) \quad (\text{Eq. 7.4})$$

Where ρ is the metal recovery percentage.

The estimated cost for the gasification catalyst of £1076/kg is based on the assumptions detailed below in **Table 7.9**.

Table 7.9. Catalytic hydrothermal gasification ruthenium catalyst manufacture and renewal cost assumptions taken from [93]

Catalyst Component	Value
Carbon support cost	\$20/lb [93]
Ruthenium metal price	\$4000/lb [208]
Fabrication costs	50% of the total materials cost
Ruthenium loading	7.8 wt.% [93]
Ruthenium recovery	95% by burning off the support

7.3.4. Discounted cash flow

Discounted cash flow analysis is a standard method used in industry for the financial assessment of new projects. It is used to estimate the economic viability/return on the initial investment of a business based on its expected future cash flows.

In order to calculate the MFSP, the net present value (NPV) must be evaluated in order to see if the project will produce the target rate of return that is set out at the start of the process. A positive value achieved for NPV signifies that the cost of the investment at the base year is worthwhile as it is projected to generate positive discounted cash flows above the initial cost. Equation 7.5 below is used to calculate NPV [209].

$$NPV = \sum_{n=1}^{n=t} \frac{CF_n}{(1+i)^n}$$

(Eq. 7.5)

Where CF_n is the cash flow in year n , t is the project life in years and i is the discount (interest) rate.

As previously stated the DCFROR will be conducted in order to calculate the MFSP, **Table 7.3** presents the assumptions made for the n th plant model, the MFSP is defined as the selling price of the produced fuel that results in a NPV for the project equal to zero over the plant lifetime whilst including a 10% internal rate of return for investors. The discount rate (IRR) is set at 10%, for a plant lifetime of 30 years, the initial capital investment is based on 40% equity with the remainder debt financed at an assumed rate of 8% for a term of 10 years. Equation 7.6 [210] is used to calculate the annual payment

required to repay the total loan principal plus interest over the set time period at a fixed annual interest rate.

$$Y = \frac{Cr(1+r)^n}{(1+r)^n - 1}$$

(Eq. 7.6)

Where Y is the constant annual payment, C is the loan amount, n is the loan term (years) and r is the fixed annual interest rate.

At the end of the m th year where $m = 1 \rightarrow n$ the outstanding balance is found with Equation 7.7 [210] below.

$$C(1+r)^m - \frac{Y}{r}(1+r)^m + \frac{Y}{r}$$

(Eq. 7.7)

The construction time is assumed to be 3 years in total with the spread of capital expense of 8% in year 1, 60% in year 2 and the remaining 32% in year 3. Plant start-up time is assumed to be 6 months following the completion of the construction period, during this period the fixed costs are 100% therefore unchanged from times of normal operation, the variable costs incurred have been assumed to be 75% of normal whilst achieving a reduced revenue of 50% of normal. Depreciation, was calculated using the straight line method over a period of 10 years based on the TIC with no residual sale value (scrap) at the end of the plant lifetime.

7.3.5. Sensitivity analysis

There are a large number of process parameters that may vary during operation of the biorefinery plant. A sensitivity analysis was performed in order to identify the impact of any changes in the process parameters and to assess their impact on the MFSP. The sensitivity analysis will give clarity to which process parameters have the greatest impact on the process economics. The results from which are useful in guiding future research and developments into areas that will have the most impact on the process. In order to perform the analyses the main variables of interest were all varied by sensible amounts from base values. Varying only one parameter at a time helps in understanding their individual influence on process economics.

7.4. Process economics results and discussion

7.4.1. Economic assessment

The investigation of a microalgae fed hydrothermal liquefaction process to convert raw biomass to a transportation fuel is detailed. Data gathered from this study alongside those in literature were used to develop the process model of which the methodology is discussed previously. Mass and energy balances from the Aspen plus models act as inputs to the TEA.

The proposed base case plant is modelled around a microalgae slurry feed of 10,000 kg/h, with an on-stream time of 7920 h per year and a plant life of 30 years producing upgraded biofuels. Biomass entering the process was assumed to cost £400/tonne on a dry ash free basis, fed to the liquefaction reactor as a slurry at 20 wt.% solids.

For the base case scenario the total capital costs (TCI) are £35.51 million, **Figure 7.4** shows the distribution of the installed equipment capital costs. These main processing sections account for almost 46% of the total capital investment, the HTL unit has the highest investments costs of £5.5 million followed by the CHG water treatment, hydrogen plant, hydrotreating and finally ancillary plant items associated with costs of £3.83 million, £2.46 million, £3.93 million and £559k respectively. When compared to other biomass thermochemical conversion technologies such as pyrolysis the capital costs for HTL are higher due to the higher operating pressures requiring the use of more robust/higher specification and therefore more expensive process equipment.

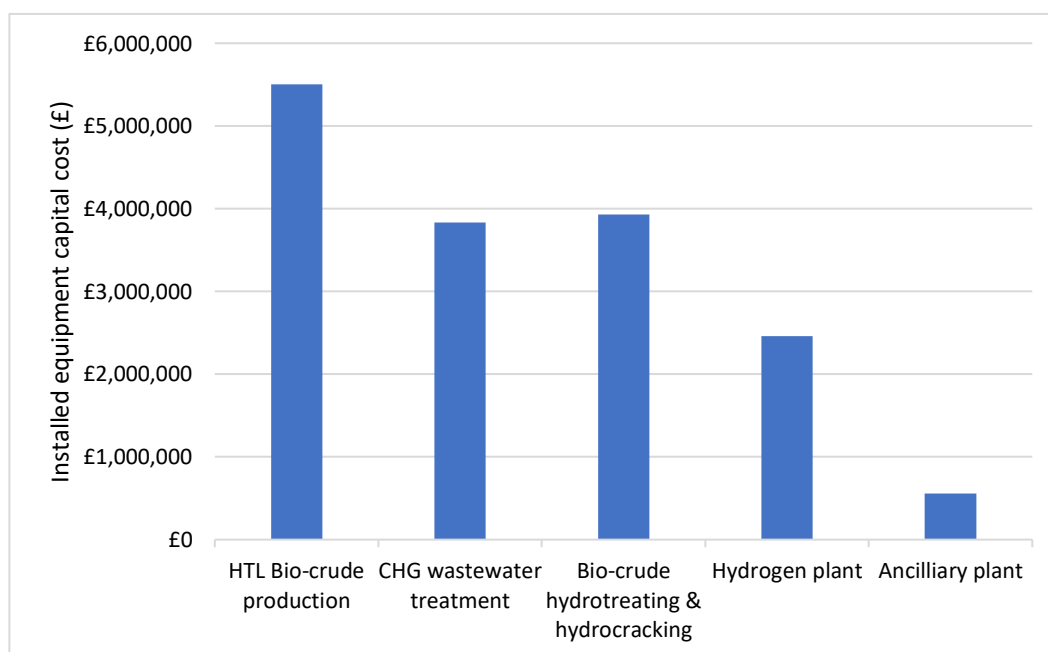


Figure 7.4. Installed plant equipment cost from the major processing zones.

The annual operating costs for the whole biorefinery are estimated to be ~£8.67 million/yr, this includes both fixed and variable costs. The diesel product yield is 6.24 million litres/year with a naphtha co-product of 1.16 million litres/year. The breakdown of operating costs is presented in **Figure 7.5**, the main contributor to the operating costs is the biomass feedstock price (£6.34 million) accounting for 73% of the operating costs, labour accounted for the second largest expense of £1.4 million/yr. Total production cost is estimated to be £9.34 million in the first year due to initial purchase of the required catalysts then ~£8.6 million/year thereafter, which equates to an average diesel fuel production cost of ~£1.38.

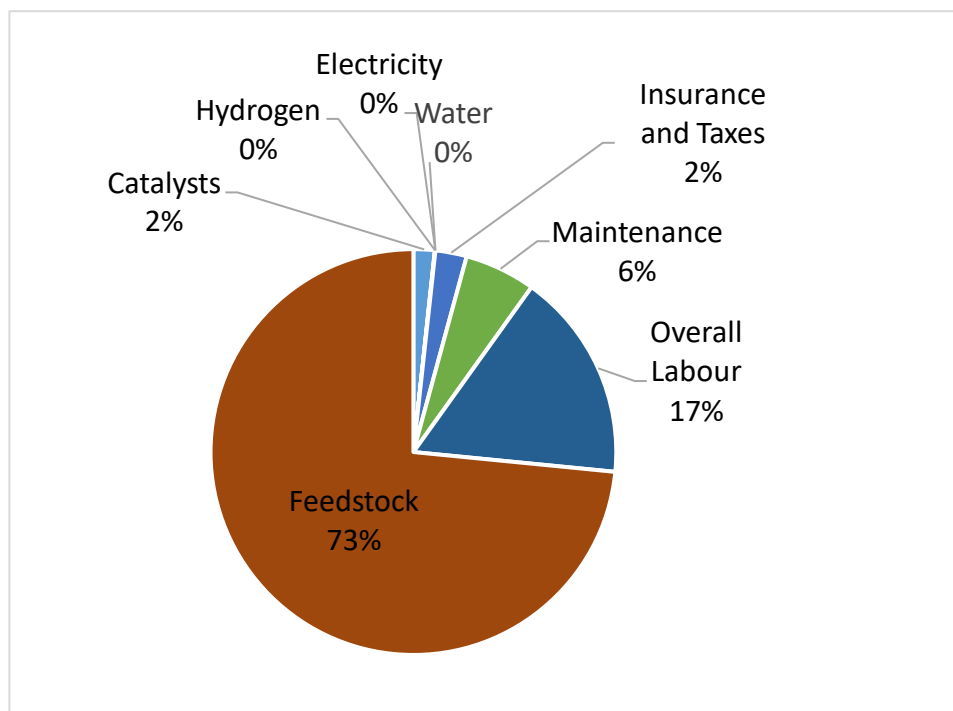


Figure 7.5. Breakdown of total operating costs (OPEX).

The diesel minimum fuel selling price (MFSP) was found to be £2.64/litre, when compared to the UK 5 year average (2017-2022) diesel price of £1.24/litre [211] it is a ~113% premium. When compared to current 2022 prices of approximately £1.74/litre it is less of a premium (52%). Approximately 50% of the cost of fossil diesel at the pumps is due to taxes, from March 2022 the fuel duty on diesel is 52.95 p/litre with 20% VAT then added on to the total, the remainder of the cost is associated with wholesale costs for the fossil fuel and the biodiesel portion (currently up to 7%, B7 diesel), the forecourt margin and transportation costs. Therefore, the cost for the fossil fuel is within the region of 75-80 p/litre, demonstrating that in order for the algae derived biofuel to be competitive there is a need for a combination of reduced production costs and lower duty and taxes applied.

A breakdown of the contribution costs to the MFSP is presented in **Table 7.10**. It shows that the algae feedstock is accountable for £1.15 per litre of diesel fuel produced.

Table 7.10. MFSP cost breakdown

Factor	£/l diesel	£/year	% of MFSP
Algae Feedstock Cost	1.15	£6,336,000	44%
Catalysts	0.02	£88,152	1%
Naphtha Credit	-0.06	-£313,632	-2%
Fixed Costs	0.39	£2,142,285	15%
Capital Depreciation	0.10	£542,886	4%
Av Income Tax	0.41	£2,235,246	15%
Average Return on Investment	0.64	£3,510,349	24%
	2.64	£14,556,285	

7.4.2 Sensitivity analysis

The sensitivity analysis was performed using sensible variations in key parameters such as those associated with technical, financial and market variables. **Table 7.11** presents the parameters investigated and their associated values.

Table 7.11. Variables represented in the sensitivity analysis

Scenario	Units	Lower	Base Case	Upper
Capital Expenditure (FCI)	£	$\frac{-30\%}{£21,615,530}$	£30,879,328	$\frac{+30\%}{£40,143,126}$
Discount Rate	(%)	$\frac{-100\%}{0}$	10	$\frac{+100\%}{20}$
Feedstock Cost	£	$\frac{-50\%}{200}$	400	$\frac{+50\%}{600}$
Slurry Concentration	wt.%	$\frac{-50\%}{10}$	20	$\frac{+50\%}{30}$
Bio-crude Yield	wt.%	$\frac{-20\%}{40.8}$	51	$\frac{+20\%}{61.2}$
Naphtha Value	£/tonne	$\frac{-20\%}{400}$	500	$\frac{+50\%}{750}$
Gasification Catalyst Life	years	$\frac{-50\%}{0.5}$	1	$\frac{+100\%}{2}$
Gasification Catalyst Price	£/kg	$\frac{-50\%}{538}$	1076	$\frac{+50\%}{1614}$

As shown in **Figure 7.6** there are a number of key factors that have a great influence on the MFSP these include: feedstock costs, discount rate, CAPEX, slurry feed concentration and bio-crude yield. The most significant factor is found to be the discount rate, in the base case scenario this is set at 10% which is widely acknowledged as the industry stand, below which investors are unlikely to participate in the project. An increase of discount rate to 20 % leads to an increase of 45% of £1.18/l to a final MFSP of £3.82/l.

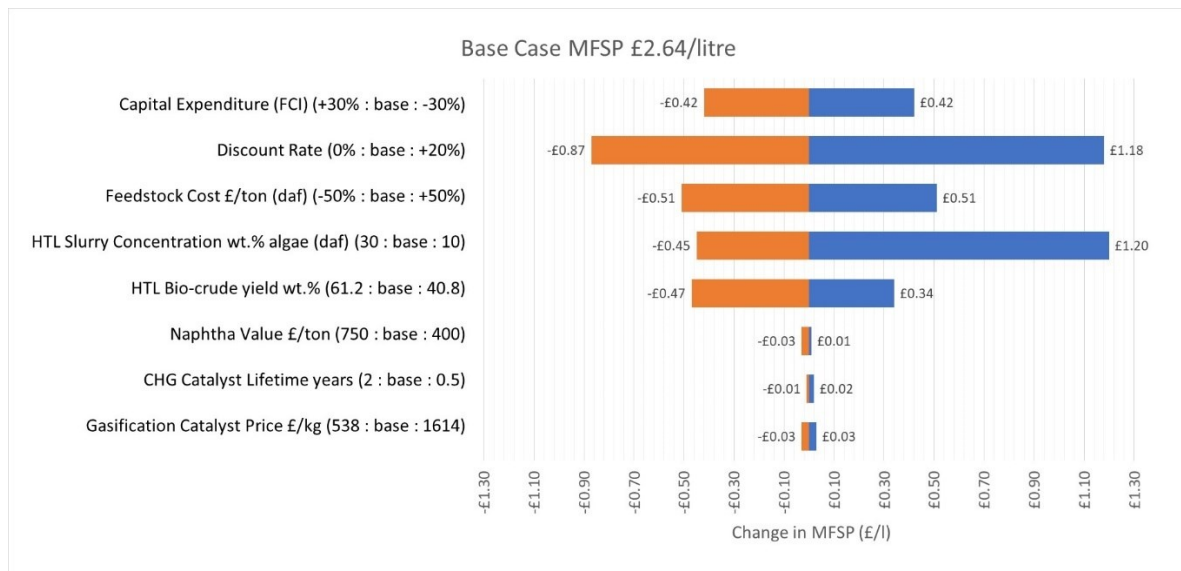


Figure 7.6. Tornado plot showing the effects of selected sensitivities with respect to the £/l of the MFSP.

The feedstock cost is also a significant factor, a reduction in feedstock cost by -50% to £200/tonne results in a reduction in MFSP of £0.51, whilst increasing the cost of feedstock by 50% leads to an increase of MFSP of £0.51, this represents a change of 19%.

The bio-crude yield is another key variable, the sensitivity analysis showed that altering the yield by $\pm 20\%$ results in a reduction of £0.47/l to the MFSP with respect to increasing the bio-crude yield to 61.8 wt.%. Reducing the yield by 20% to a value of 40.8 wt.% results in a slightly reduced effect, raising the MFSP to a lesser extent by £0.34/l, this is due to both decreases in diesel yield and an increase in the aqueous fraction yield. The higher aqueous yield therefore results in an increased throughput for the CHG process resulting in lower energy and hydrogen import due to more hydrogen production in the SMR.

Fixed capital investment is another key variable, a $\pm 30\%$ variation total investment leads to a change in MFSP of $\pm £0.42/l$, this represents a change of $\pm 16\%$.

The remaining variables include; the cost and lifetime of the CHG catalyst and the value of the by-product naphtha. These all have a very low individual influence on MFSP their impact can be seen in **Table 7.10**.

Effect of the plant size

Plant scale has a significant effect on the MFSP. The base case of 10,000 kg/hr slurry feed is considered a small scale process, the effect of increasing plant capacity is shown in **Figure 7.7**. It can be seen that due to economies of scale the MFSP initially reduces swiftly due to the CAPEX being found to be one of the key cost drivers in MFSP.

From **Figure 7.7** it can be seen that the optimum size of the plant is around 250,000 kg/hr slurry feed, at this scale the MFSP sits at approximately £1.62/litre. Doubling the capacity again to 500,000 kg/hr results in only a small decrease of £0.07/litre whilst requiring increased CAPEX of 77.5 % (+£319.5 million) to £731.7 million. The ideal scale should lie in the range of 200,000 and 300,000 kg/hr slurry feed.

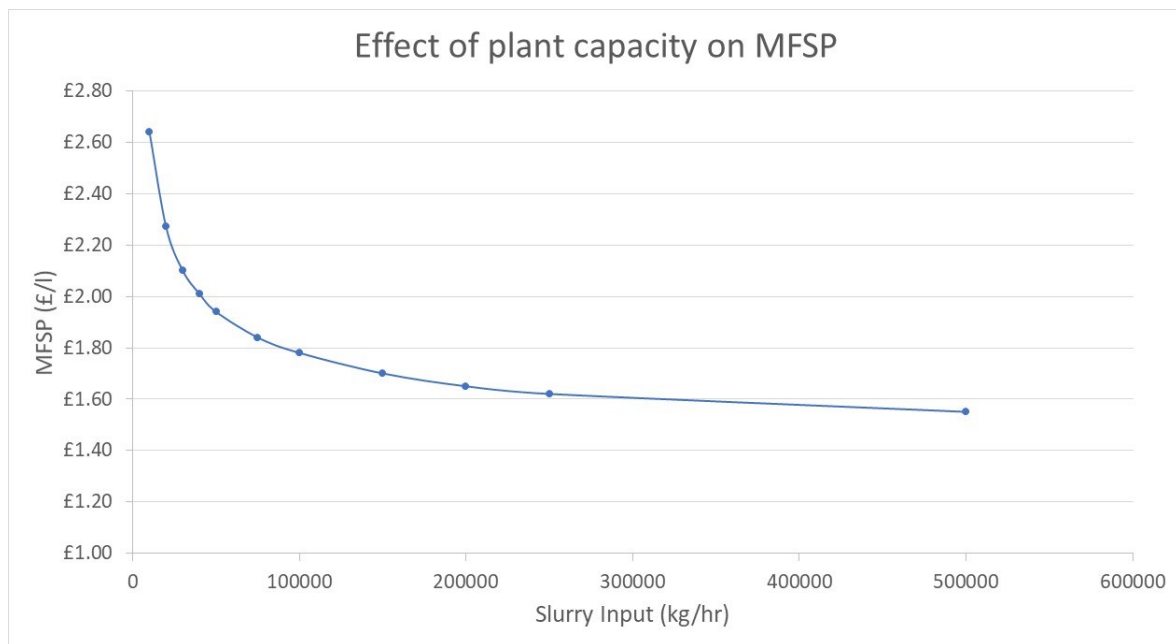


Figure 7.7. Effect of the plant capacity on the minimum fuel selling price (MFSP).

7.5. Conclusions

A techno-economic assessment of a microalgae fed hydrothermal liquefaction wet conversion technology was conducted. The study shows that microalgae based bio-fuels are technologically feasible but the price required for the fuel is uncompetitive with traditional fossil based fuels prices at the time of writing. Outputs show that at the scale proposed (2000 kg/hr daf microalgae) and producing only combustible liquid transportation fuels the process would lead to a net economic loss due to a calculated MFSP of £2.64/litre of bio-diesel. Costs must be lowered in order to make these fuels cost competitive. The oil produced from the HTL of microalgae has shown to be more suitable for road transportation applications due to its lower oxygen content when compared to pyrolysis oils. Heat integration in the process revealed that only low amounts of imported energy to the process are needed.

Sensitivity analysis on the factors affecting MFSP revealed that the feedstock cost, algal slurry concentration, bio-crude yield, CAPEX and project discount rate have the largest effect on the process economics. It is apparent that improvements in cultivation are required in order to further drive down the cost of the raw biomass, or for the algae to serve its primary role as a means of remediation (e.g. carbon sequestration and waste water treatment) with HTL conversion as a secondary process thereby reducing costs. Plant scale also has a large impact on MFSP, larger plants benefitting from economies of scale were found to substantially lower MFSP to values of ~£1.62/litre, suitability of the UK for production of enough algae to feed large-scale plants and the logistics of transporting algal feedstock to the processing site remain unclear.

Chapter 8 - Conclusions and recommendations

This PhD research project was achieved by planning and carrying out laboratory-scale work addressing hydrothermal liquefaction of algae with subsequent catalytic upgrading of generated bio-crudes for further assessment for their utilisation as biofuels or value-added chemicals. Research outputs from this PhD project were presented in four chapters (Chapter 4-7), with the global conclusions presented in **Section 8.1** below. **Section 8.2** addresses some limitations faced during the project and recommendations for future work.

8.1. Conclusions

The characterisation of the micro- and macroalgal feedstocks in **Chapter 4** sought to give an insight into their composition and subsequent suitability as feedstocks for thermochemical processing techniques. The characteristics investigated advanced the understanding of their propensity to form bio-crudes during hydrothermal liquefaction. Five macroalgae and three microalgae species were analysed. The microalgae demonstrated superior characteristics compared to macroalgae, such as higher volatile content, lower ash content and higher lipid content. Despite these advantages, microalgae were found to contain significantly higher nitrogen levels, which can lead to high levels in the resultant HTL bio-crudes, requiring a high degree of denitrogenation during upgrading processes. The characterisation of a number of model compounds was also undertaken. The application of analytical pyrolysis presented as an invaluable tool for the quick assessment of thermal degradation products from the building blocks of algae, requiring only micro amounts of feedstock. Results from analytical pyrolysis resulted in the development of a unique thermal decomposition network for the model compounds.

Chapter 5 presents the data on the hydrothermal liquefaction of algae and model compounds. Initially, at a small-scale with two microalgal and two macroalgal species, average bio-crude yields were shown to be far higher for the microalgal species 30.1 - 48.6 wt.% versus 16.6-18.5 wt.% respectively. The resultant bio-crudes were found to have high nitrogen and oxygen contents of 3.8-8.8 wt.% and 12.6-18.6 wt.%, respectively, for all species. Higher heating values were found to increase significantly from the base feedstock showing increased energy density of the bio-crude products. The effect of reaction temperature was investigated on a larger scale basis by way of liquefaction of the microalgae *Nannochloropsis sp.*, maximum bio-crude yields (51.6 wt.%) were found at a processing temperature of 300 °C. Bio-crude yields above the lipid content of the algae were found, supporting existing findings in the literature, that HTL of algae can process whole algal cells whilst improving the energy recovery

from the feedstock. GC-MS analysis of the bio-crude revealed similar and, in some cases, exact matches to compounds found during the analytical pyrolysis of the raw feedstock, demonstrating the benefit of Py-GC-MS as a quick screening tool. The bio-crude produced from the microalgae *Nannochloropsis sp.* possessed high levels of heteroatom content, 4.5 and 22.1 wt.% for nitrogen and oxygen, respectively. Heteroatom concentrations are many times higher than typical fossil crude oils, and further reduction is required for utilisation as fuels in transport applications.

As a result of the high yields achieved and the molecular nature of the bio-crudes produced, HTL bio-crudes from microalgae show great potential for upgrading for further improvement of the characteristics and quality of the fuel.

The effect of algal biochemical composition on final bio-crude composition was investigated through the liquefaction of selected model compounds chosen to represent the key macromolecular constituents of algae. The protein fraction was represented by a soy protein isolate and two amino acids l-leucine and l-glutamine, carbohydrate content was represented by glucose, xylose, and corn starch, and finally, the lipid content was represented using oleic and stearic acid.

The results show that long-chain fatty acids are very stable under the liquefaction reaction conditions applied. Bio-crude yields from the liquefaction of the model compounds demonstrated the hierarchy of contribution to the algal bio-crude yield. The order of model compound bio-crude yields achieved is 79-80.3 wt.%, 4.5-17.2 wt.% and 5.9-11.6 wt.% for lipids, proteins and carbohydrates, respectively.

Advanced Nuclear Magnetic Resonance techniques were applied to analyse the bio-crudes from **Chapter 5** and upgraded oils from **Chapter 6**. The literature relevant to HTL of biomass the application of NMR spectroscopy is limited to basic one dimensional and conventional pulse programs for ^1H and ^{13}C experiments. A novel combination of advanced techniques on top of the mentioned NMR techniques are two-dimensional techniques of Heteronuclear Single Quantum Coherence (HSQC), Heteronuclear Multiple Bond Correlation (HMBC) and the spectral edited ^{13}C pulse sequence known as PENDANT (Polarization Enhancement During Attached Nucleus Testing). Utilization of these advanced techniques allowed for the characterization of the whole bio-crude sample, not just the fraction that is able to elute from a GC column. Findings show that algal bio-crudes and those produced from the liquefaction of model compounds are very complex in nature. Key similarities were observed between the model compound bio-crudes and the algal bio-crudes.

The bio-crude produced from HTL requires upgrading prior to use as a transportation fuel in order to reduce heteroatom content and improve its physical characteristics. **Chapter 6** presents the screening of catalysts using Py-GC-MS and the undertaking of supercritical water upgrading at 450 °C for 4 hours under a high-pressure hydrogen atmosphere. The application of catalysts resulted in only small

increases in upgraded oil yield when compared to the uncatalysed experiment. Experiments with HZSM-5 and NiMo/Al₂O₃ resulted in lower upgraded oil yields. HZSM-5 and Ru/C were shown to promote the formation of gaseous products. In all cases improvements were seen in atomic ratios and HHV; overall H/C ratios were adversely reduced by a small amount. The application of catalysts achieved a reduction in nitrogen content of the upgraded oils to levels of 1.9-2.6 wt.% compared to the uncatalysed experiment and the raw bio-crude values of 3.8 and 4.5 wt.%, respectively, resulting in atomic N/C ratios of 0.02-0.04 for the catalytically upgraded oils. Oxygen content was dramatically reduced, the performance of the uncatalysed experiment generated an upgraded oil with 5.4 wt.% oxygen (down from 19.9 wt.%), the inclusion of catalysts led to a further reduction to values ranging between 1.3-4.8 wt.%. Analysis of the upgraded oil revealed the content was predominantly composed of C₆-C₁₆ alkanes and substituted aromatic compounds. Compositional analysis from feedstock characterisation, algal and model compounds HTL bio-crudes and upgraded oils were leveraged to propose a reaction network following the conversion of algal chemical species through to bio-crude and finally upgraded oils.

Finally, a techno-economic assessment presented in **Chapter 7** proposes the use of microalgae as the feed to a commercial-scale HTL processing plant. Undertaken in order to develop an understanding of commercial applications of microalgae in the biofuel sector from a UK perspective. The plant is designed for a throughput of 2,000 kg/h dry ash free algae, producing primarily diesel fraction and naphtha co-product liquid fuels. Whilst technically feasible, the economic results from the TEA propose an MFSP of £2.64/litre. Sensitivity analysis shows the process to be extremely sensitive to feedstock cost, capital expenditure, bio-crude yield and incoming algal slurry concentration.

8.2. Recommendations

Based both on the successful progress of the project and also some faced limitations, the following recommendations for future research can be withdrawn:

1. Application of in-depth gas analysis through gas chromatography methods should be introduced to quantify the gaseous reaction products from both HTL and upgrading experiments. The barrier ionisation detection (BID) technique was used in the core stage of this PhD project for the analysis of the GC separated HTL gases. Due to the COVID-19 shutdown of the labs, the equipment could not be brought back online. Alternatively, the application of a micro GC and FID (Flame Ionisation Detection) can be applied for the quantification of gas products.
2. Applied analytical pyrolysis of model components and algal feedstock was used to assess possible end-products from the HTL and upgrading experiments. To address the requirement

of high pressure and reactive gas (hydrogen) during the thermal liquefaction and upgrading, it is recommended to apply analytical pyrolysis in high-pressure mode with reactant gas.

3. Investigation of the effect of a potential pre-treatment method such as fractional distillation in order to reduce heteroatom content prior to catalytic upgrading.
4. Exploration of novel low-cost non-precious metal bimetallic catalysts for bio-crude upgrading.
5. Introduction of catalytic upgrading on a continuous basis via the use of a two-staged fixed bed reactor with two independent zones for application of different temperatures and catalysts. This would allow a better understanding of the bio-crude hydrotreatment stage before the catalytic hydrodeoxygenation. With potential TRL upscaling, this approach could yield results more comparable to commercial-scale operations.
6. The utilisation and recycling of the aqueous phase produced from HTL processing as the solvent/additive during the supercritical water upgrading of the raw bio-crude, potentially leading to higher conversion efficiencies and carbon recovery.
7. More in-depth techno-economic assessment including options around the recovery of valuable components of the microalgae prior to liquefaction and the impact of processing microalgae used for remediation purposes.

References

1. IPCC, *Climate Change 2021: The Physical Science Basis*. 2021.
2. Government, U., *Climate Change Act 2008*. 2008.
3. Government, U., *Climate Change Act 2008, 2050 amendment*. 2019.
4. Committee, C.C. *What is climate change?* 2022; Available from: <https://www.theccc.org.uk/what-is-climate-change/>.
5. Conti, J., et al., *International energy outlook 2016 with projections to 2040*. 2016, USDOE Energy Information Administration (EIA), Washington, DC (United States
6. Ziegler, M.S. and J.E. Trancik, *Re-examining rates of lithium-ion battery technology improvement and cost decline*. *Energy & Environmental Science*, 2021. **14**(4): p. 1635-1651.
7. Jin, B., et al., *Co-liquefaction of micro-and macroalgae in subcritical water*. *Bioresour Technol*, 2013. **149**: p. 103-110.
8. Anastasakis, K. and A.B. Ross, *Hydrothermal liquefaction of the brown macro-alga *Laminaria saccharina*: effect of reaction conditions on product distribution and composition*. *Bioresour Technol*, 2011. **102**(7): p. 4876-83.
9. Chisti, Y., *Biodiesel from microalgae*. *Biotechnol Adv*, 2007. **25**(3): p. 294-306.
10. Ación Fernández, F.G., et al., *Conversion of CO₂ into biomass by microalgae: how realistic a contribution may it be to significant CO₂ removal?* *Applied microbiology and biotechnology*, 2012. **96**(3): p. 577-586.
11. Brennan, L. and P. Owende, *Biofuels from microalgae—A review of technologies for production, processing, and extractions of biofuels and co-products*. *Renewable and Sustainable Energy Reviews*, 2010. **14**(2): p. 557-577.
12. Becker, E.W., *Microalgae: biotechnology and microbiology*. Vol. 10. 1994: Cambridge University Press.
13. Rodolfi, L., et al., *Microalgae for oil: strain selection, induction of lipid synthesis and outdoor mass cultivation in a low-cost photobioreactor*. *Biotechnol Bioeng*, 2009. **102**(1): p. 100-12.
14. Thomas, C., *Hydrothermal Liquefaction of Algal Feedstocks*, in *CE4011: MEng4 Research Project*. 2016, Aston University.
15. Thomas, C., *Hydrothermal Liquefaction of Algal Feedstocks* in *Qualifying Report*. 2018, Aston University.
16. Chen, C.Y., et al., *Cultivation, photobioreactor design and harvesting of microalgae for biodiesel production: a critical review*. *Bioresour Technol*, 2011. **102**(1): p. 71-81.

17. Borowitzka, M.A., *Commercial production of microalgae: ponds, tanks, tubes and fermenters*. Journal of biotechnology, 1999. **70**(1-3): p. 313-321.
18. Chisti, Y., *Biodiesel from microalgae beats bioethanol*. Trends Biotechnol, 2008. **26**(3): p. 126-31.
19. Halim, R., M.K. Danquah, and P.A. Webley, *Extraction of oil from microalgae for biodiesel production: A review*. Biotechnol Adv, 2012. **30**(3): p. 709-32.
20. McKendry, P., *Energy production from biomass (part 3): gasification technologies*. Bioresource technology, 2002. **83**(1): p. 55-63.
21. Guo, Y., et al., *A review of bio-oil production from hydrothermal liquefaction of algae*. Renewable and Sustainable Energy Reviews, 2015. **48**: p. 776-790.
22. Ciferri, O., *Spirulina, the edible microorganism*. Microbiological reviews, 1983. **47**(4): p. 551-578.
23. Fabregas, J. and C. Herrero, *Vitamin content of four marine microalgae. Potential use as source of vitamins in nutrition*. Journal of Industrial Microbiology and Biotechnology, 1990. **5**(4): p. 259-263.
24. Lubián, L.M., et al., *Nannochloropsis (Eustigmatophyceae) as source of commercially valuable pigments*. Journal of Applied Phycology, 2000. **12**(3): p. 249-255.
25. Guschina, I.A. and J.L. Harwood, *Lipids and lipid metabolism in eukaryotic algae*. Prog Lipid Res, 2006. **45**(2): p. 160-86.
26. Thompson Jr, G.A., *Lipids and membrane function in green algae*. Biochimica et Biophysica Acta (BBA)-Lipids and Lipid Metabolism, 1996. **1302**(1): p. 17-45.
27. Spolaore, P., et al., *Commercial applications of microalgae*. J Biosci Bioeng, 2006. **101**(2): p. 87-96.
28. Chen, C.-Y., et al., *Microalgae-based carbohydrates for biofuel production*. Biochemical Engineering Journal, 2013. **78**: p. 1-10.
29. Ho, S.H., et al., *Bioethanol production using carbohydrate-rich microalgae biomass as feedstock*. Bioresour Technol, 2013. **135**: p. 191-8.
30. Lorenz, R.T. and G.R. Cysewski, *Commercial potential for Haematococcus microalgae as a natural source of astaxanthin*. Trends in biotechnology, 2000. **18**(4): p. 160-167.
31. Olaizola, M., *Commercial development of microalgal biotechnology: from the test tube to the marketplace*. Biomolecular Engineering, 2003. **20**(4-6): p. 459-466.
32. Garcia-Gonzalez, M., et al., *Production of Dunaliella salina biomass rich in 9-cis-beta-carotene and lutein in a closed tubular photobioreactor*. J Biotechnol, 2005. **115**(1): p. 81-90.
33. Corteggiani Carpinelli, E., et al., *Chromosome scale genome assembly and transcriptome profiling of Nannochloropsis gaditana in nitrogen depletion*. Mol Plant, 2014. **7**(2): p. 323-35.

34. Kilian, O., et al., *High-efficiency homologous recombination in the oil-producing alga *Nannochloropsis* sp.* Proc Natl Acad Sci U S A, 2011. **108**(52): p. 21265-9.
35. Singh, R., T. Bhaskar, and B. Balagurumurthy, *Effect of solvent on the hydrothermal liquefaction of macro algae *Ulva fasciata*.* Process Safety and Environmental Protection, 2015. **93**: p. 154-160.
36. Toor, S.S., L. Rosendahl, and A. Rudolf, *Hydrothermal liquefaction of biomass: A review of subcritical water technologies.* Energy, 2011. **36**(5): p. 2328-2342.
37. Huber, G.W., S. Iborra, and A. Corma, *Synthesis of transportation fuels from biomass: chemistry, catalysts, and engineering.* Chemical reviews, 2006. **106**(9): p. 4044-4098.
38. Demirbaş, A., *Biomass resource facilities and biomass conversion processing for fuels and chemicals.* Energy conversion and Management, 2001. **42**(11): p. 1357-1378.
39. McKendry, P., *Energy production from biomass (part 2): conversion technologies.* Bioresource technology, 2002. **83**(1): p. 47-54.
40. Ross, A.B., et al., *Classification of macroalgae as fuel and its thermochemical behaviour.* Bioresour Technol, 2008. **99**(14): p. 6494-504.
41. Wu, K.-T., et al., *The characteristics of torrefied microalgae.* Applied Energy, 2012. **100**: p. 52-57.
42. Kadam, K.L., *Environmental implications of power generation via coal-microalgae cofiring.* Energy, 2002. **27**(10): p. 905-922.
43. Ward, A.J., D.M. Lewis, and F.B. Green, *Anaerobic digestion of algae biomass: A review.* Algal Research, 2014. **5**: p. 204-214.
44. González-Fernández, C., B. Molinuevo-Salces, and M.C. García-González, *Evaluation of anaerobic codigestion of microalgal biomass and swine manure via response surface methodology.* Applied Energy, 2011. **88**(10): p. 3448-3453.
45. Wang, S., et al., *Effect of inoculum to substrate ratios on methane production in mixed anaerobic digestion of pig manure and blue-green algae.* Transactions of the Chinese Society of Agricultural Engineering, 2009. **25**(5): p. 172-176.
46. Saxena, V., S. Tandon, and K. Singh, *Anaerobic digestion of green filamentous algae and waterhyacinth for methane production.* National Academy of Sciences, India, Science Letters, 1984. **7**(9): p. 283-284.
47. Ramamoorthy, S. and N. Sulochana, *Enhancement of biogas production using algae.* Current science, 1989. **58**(11): p. 646-647.
48. Yen, H.-W. and D.E. Brune, *Anaerobic co-digestion of algal sludge and waste paper to produce methane.* Bioresource technology, 2007. **98**(1): p. 130-134.
49. Demirbas, A. and M. Fatih Demirbas, *Importance of algae oil as a source of biodiesel.* Energy Conversion and Management, 2011. **52**(1): p. 163-170.

50. Fernandez-Serra, M. *A general phase diagram for a liquid-gas-solid system*. 2011; Available from: <https://mini.physics.sunysb.edu/~marivi/TEACHING-OLD/PHY313/doku.php?id=lectures:1>.
51. Fernandez, D.P., et al., *A database for the static dielectric constant of water and steam*. Journal of Physical and Chemical Reference Data, 1995. **24**(1): p. 33-70.
52. Wang, W., et al., *Hydrothermal liquefaction of microalgae over transition metal supported TiO₂ catalyst*. Bioresource technology, 2018. **250**: p. 474-480.
53. He, S., et al., *Hydrothermal liquefaction of low-lipid algae Nannochloropsis sp. and Sargassum sp.: Effect of feedstock composition and temperature*. Science of the Total Environment, 2020. **712**: p. 135677.
54. Zhang, J. and Y. Zhang, *Hydrothermal liquefaction of microalgae in an ethanol–water co-solvent to produce biocrude oil*. Energy & Fuels, 2014. **28**(8): p. 5178-5183.
55. Hossain, F.M., et al., *Experimental investigations of physical and chemical properties for microalgae HTL bio-crude using a large batch reactor*. Energies, 2017. **10**(4): p. 467.
56. Cheng, F., et al., *Hydrothermal liquefaction of high-and low-lipid algae: Mass and energy balances*. Bioresource technology, 2018. **258**: p. 158-167.
57. Vardon, D.R., et al., *Thermochemical conversion of raw and defatted algal biomass via hydrothermal liquefaction and slow pyrolysis*. Bioresource technology, 2012. **109**: p. 178-187.
58. Jena, U., K.C. Das, and J.R. Kastner, *Comparison of the effects of Na₂CO₃, Ca₃(PO₄)₂, and NiO catalysts on the thermochemical liquefaction of microalga Spirulina platensis*. Applied Energy, 2012. **98**: p. 368-375.
59. López Barreiro, D., et al., *Hydrothermal liquefaction of microalgae: Effect on the product yields of the addition of an organic solvent to separate the aqueous phase and the biocrude oil*. Algal Research, 2015. **12**: p. 206-212.
60. Duan, P. and P.E. Savage, *Hydrothermal liquefaction of a microalga with heterogeneous catalysts*. Industrial & Engineering Chemistry Research, 2011. **50**(1): p. 52-61.
61. Wang, H., et al., *Catalytic hydrothermal liquefaction of Spirulina over bifunctional catalyst to produce high-quality biofuel*. Fuel, 2020. **282**: p. 118807.
62. Han, Y., et al., *Use of co-solvents in hydrothermal liquefaction (HTL) of microalgae*. Energies, 2019. **13**(1): p. 124.
63. Biswas, B., et al., *Effects of temperature and solvent on hydrothermal liquefaction of Sargassum tenerrimum algae*. Bioresource technology, 2017. **242**: p. 344-350.
64. Zou, S., et al., *Bio-oil production from sub- and supercritical water liquefaction of microalgae Dunaliella tertiolecta and related properties*. Energy Environ. Sci., 2010. **3**(8): p. 1073-1078.
65. Brown, T.M., P. Duan, and P.E. Savage, *Hydrothermal Liquefaction and Gasification of Nannochloropsis sp.* Energy & Fuels, 2010. **24**(6): p. 3639-3646.

66. Jena, U., K.C. Das, and J.R. Kastner, *Effect of operating conditions of thermochemical liquefaction on biocrude production from Spirulina platensis*. *Bioresour Technol*, 2011. **102**(10): p. 6221-9.
67. Fuentes, M., et al., *Survey of influence of biomass mineral matter in thermochemical conversion of short rotation willow coppice*. *Journal of the Energy Institute*, 2008. **81**(4): p. 234-241.
68. Valdez, P.J., et al., *Hydrothermal liquefaction of Nannochloropsis sp.: Systematic study of process variables and analysis of the product fractions*. *Biomass and Bioenergy*, 2012. **46**: p. 317-331.
69. Garcia Alba, L., et al., *Hydrothermal Treatment (HTT) of Microalgae: Evaluation of the Process As Conversion Method in an Algae Biorefinery Concept*. *Energy & Fuels*, 2011. **26**(1): p. 642-657.
70. Akhtar, J. and N.A.S. Amin, *A review on process conditions for optimum bio-oil yield in hydrothermal liquefaction of biomass*. *Renewable and Sustainable Energy Reviews*, 2011. **15**(3): p. 1615-1624.
71. Peterson, A.A., et al., *Thermochemical biofuel production in hydrothermal media: A review of sub- and supercritical water technologies*. *Energy & Environmental Science*, 2008. **1**(1).
72. Biller, P. and A. Ross, *Potential yields and properties of oil from the hydrothermal liquefaction of microalgae with different biochemical content*. *Bioresource technology*, 2011. **102**(1): p. 215-225.
73. Li, H., et al., *Insight into the effect of hydrogenation on efficiency of hydrothermal liquefaction and physico-chemical properties of biocrude oil*. *Bioresour Technol*, 2014. **163**: p. 143-51.
74. Yin, S., et al., *Subcritical hydrothermal liquefaction of cattle manure to bio-oil: Effects of conversion parameters on bio-oil yield and characterization of bio-oil*. *Bioresour Technol*, 2010. **101**(10): p. 3657-64.
75. Barreiro, D.L., et al., *Hydrothermal Liquefaction of Microalgae in a Continuous Stirred-Tank Reactor*. *Energy & Fuels*, 2015. **29**(10): p. 6422-6432.
76. Elliott, D.C., et al., *Process development for hydrothermal liquefaction of algae feedstocks in a continuous-flow reactor*. *Algal Research*, 2013. **2**(4): p. 445-454.
77. Patel, B. and K. Hellgardt, *Hydrothermal upgrading of algae paste in a continuous flow reactor*. *Bioresource technology*, 2015. **191**: p. 460-468.
78. Jazrawi, C., et al., *Pilot plant testing of continuous hydrothermal liquefaction of microalgae*. *Algal Research*, 2013. **2**(3): p. 268-277.
79. Wagner, J.L., et al., *Design and operation of an inexpensive, laboratory-scale, continuous hydrothermal liquefaction reactor for the conversion of microalgae produced during wastewater treatment*. *Fuel Processing Technology*, 2017. **165**: p. 102-111.

80. Albrecht, K.O., et al., *Impact of heterotrophically stressed algae for biofuel production via hydrothermal liquefaction and catalytic hydrotreating in continuous-flow reactors*. *Algal research*, 2016. **14**: p. 17-27.
81. Biller, P., et al., *Hydroprocessing of bio-crude from continuous hydrothermal liquefaction of microalgae*. *Fuel*, 2015. **159**: p. 197-205.
82. Olivares, J., *National Alliance for Advanced Biofuels and Bioproducts Synopsis (NAABB) Final Report*. US DOE-EERE Biotechnologies Office, 2014.
83. Sintamarean, I.M., et al., *Two-stage alkaline hydrothermal liquefaction of wood to biocrude in a continuous bench-scale system*. *Biomass Conversion and Biorefinery*, 2017. **7**(4): p. 425-435.
84. Pedersen, T.H., et al., *Continuous hydrothermal co-liquefaction of aspen wood and glycerol with water phase recirculation*. *Applied Energy*, 2016. **162**: p. 1034-1041.
85. Baig, M.N., et al., *Evaluation and modelling of continuous flow sub-critical water hydrolysis of biomass derived components; lipids and carbohydrates*. *Chemical Engineering Research and Design*, 2013. **91**(12): p. 2663-2670.
86. Klemmer, M., et al., *Effect of aqueous phase recycling in continuous hydrothermal liquefaction*. *Industrial & Engineering Chemistry Research*, 2016. **55**(48): p. 12317-12325.
87. Biller, P., et al., *Effect of hydrothermal liquefaction aqueous phase recycling on bio-crude yields and composition*. *Bioresource technology*, 2016. **220**: p. 190-199.
88. Madsen, R.B., et al., *Analysis of organic gas phase compounds formed by hydrothermal liquefaction of Dried Distillers Grains with Solubles*. *Bioresource Technology*, 2015. **192**: p. 826-830.
89. Elliott, D.C., et al., *Hydrothermal processing of macroalgal feedstocks in continuous-flow reactors*. *ACS Sustainable Chemistry & Engineering*, 2014. **2**(2): p. 207-215.
90. Hammerschmidt, A., et al., *Catalytic conversion of waste biomass by hydrothermal treatment*. *Fuel*, 2011. **90**(2): p. 555-562.
91. Suesse, A.R., G.A. Norton, and J. van Leeuwen, *Pilot-scale continuous-flow hydrothermal liquefaction of filamentous fungi*. *Energy & Fuels*, 2016. **30**(9): p. 7379-7386.
92. Zhu, Y., et al., *Development of hydrothermal liquefaction and upgrading technologies for lipid-extracted algae conversion to liquid fuels*. *Algal Research*, 2013. **2**(4): p. 455-464.
93. Jones, S.B., et al., *Process design and economics for the conversion of algal biomass to hydrocarbons: whole algae hydrothermal liquefaction and upgrading*. 2014, Pacific Northwest National Lab.(PNNL), Richland, WA (United States).
94. Davis, R.E., et al., *Integrated evaluation of cost, emissions, and resource potential for algal biofuels at the national scale*. *Environmental science & technology*, 2014. **48**(10): p. 6035-6042.

95. Plaza, M., et al., *Innovative natural functional ingredients from microalgae*. Journal of agricultural and food chemistry, 2009. **57**(16): p. 7159-7170.
96. Guerin, M., M.E. Huntley, and M. Olaizola, *Haematococcus astaxanthin: applications for human health and nutrition*. Trends in Biotechnology, 2003. **21**(5): p. 210-216.
97. Mørup, A.J., et al., *Construction and commissioning of a continuous reactor for hydrothermal liquefaction*. Industrial & engineering chemistry research, 2015. **54**(22): p. 5935-5947.
98. Berglin, E.J., C.W. Enderlin, and A.J. Schmidt, *Review and assessment of commercial vendors/options for feeding and pumping biomass slurries for hydrothermal liquefaction*. 2012, Pacific Northwest National Lab.(PNNL), Richland, WA (United States).
99. Toor, S.S., et al., *Continuous production of bio-oil by catalytic liquefaction from wet distiller's grain with solubles (WDGS) from bio-ethanol production*. Biomass and Bioenergy, 2012. **36**: p. 327-332.
100. Benjumea, J., et al., *Depressurization System by Coiled Pipes Applied to a High Pressure Process: Experimental Results and Modeling*. The Open Chemical Engineering Journal, 2017. **11**(1).
101. Jensen, C.U., et al., *Fundamentals of Hydrofaction™: Renewable crude oil from woody biomass*. Biomass Conversion and Biorefinery, 2017. **7**(4): p. 495-509.
102. Energy, S. *Transforming Biomass Waste Into Low Carbon Intensity Fuels*. 2022 [cited 2022; Available from: <https://steeperenergy.com/>].
103. Nabi, M.N., et al., *Fuel characterisation, engine performance, combustion and exhaust emissions with a new renewable Licella biofuel*. Energy Conversion and management, 2015. **96**: p. 588-598.
104. Negahdar, L., et al., *Characterization and comparison of fast pyrolysis bio-oils from pinewood, rapeseed cake, and wheat straw using 13C NMR and comprehensive GCx GC*. ACS sustainable chemistry & engineering, 2016. **4**(9): p. 4974-4985.
105. Appenteng, M.K., et al., *Multi-element analysis of Ghanaian crude oils by instrumental neutron activation analysis*. Journal of Radioanalytical and Nuclear Chemistry, 2012. **292**(3): p. 1197-1206.
106. Liu, R., W. Fei, and C. Shen, *Influence of acetone addition on the physicochemical properties of bio-oils*. Journal of the Energy Institute, 2014. **87**(2): p. 127-133.
107. Lin, Y.-Y., W.-H. Chen, and H.-C. Liu, *Aging and emulsification analyses of hydrothermal liquefaction bio-oil derived from sewage sludge and swine leather residue*. Journal of Cleaner Production, 2020. **266**: p. 122050.
108. Chen, X., et al., *Hydrothermal liquefaction of Chlorella pyrenoidosa and effect of emulsification on upgrading the bio-oil*. Bioresour Technol, 2020. **316**: p. 123914.
109. Bhat, S., V.B. Borugadda, and A.K. Dalai, *Emulsification of bio-crude produced from agricultural waste via hydrothermal liquefaction process*. Fuel, 2021. **305**: p. 121602.

110. Eboibi, B.E.-O., et al., *Hydrothermal liquefaction of microalgae for biocrude production: Improving the biocrude properties with vacuum distillation*. Bioresource Technology, 2014. **174**: p. 212-221.
111. Taghipour, A., et al., *Fractional distillation of algae based hydrothermal liquefaction biocrude for co-processing: changes in the properties, storage stability, and miscibility with diesel*. Energy Conversion and Management, 2021. **236**: p. 114005.
112. Watson, J., et al., *Towards transportation fuel production from food waste: Potential of biocrude oil distillates for gasoline, diesel, and jet fuel*. Fuel, 2021. **301**: p. 121028.
113. Xie, L.-F., et al., *Hydrotreating the distillate fraction of algal biocrude with used engine oil over Pt/C for production of liquid fuel*. Catalysis Today, 2020. **355**: p. 65-74.
114. Frank, E.D., et al., *Life cycle comparison of hydrothermal liquefaction and lipid extraction pathways to renewable diesel from algae*. Mitigation and Adaptation Strategies for Global Change, 2013. **18**(1): p. 137-158.
115. Fushimi, C. and A. Umeda, *Comparison of Biodiesel Production by a Supercritical Methanol Method from Microalgae Oil Using Solvent Extraction and Hydrothermal Liquefaction Processes*. Energy & Fuels, 2016. **30**(10): p. 7916-7922.
116. Xu, Y., et al., *Effect of catalytic esterification on the friction and wear performance of bio-oil*. Wear, 2014. **311**(1): p. 93-100.
117. Xu, Y., et al., *Friction and wear behaviors of catalytic methylesterified bio-oil*. Tribology International, 2014. **71**: p. 168-174.
118. Yang, L., Y. Li, and P.E. Savage, *Near- and supercritical ethanol treatment of biocrude from hydrothermal liquefaction of microalgae*. Bioresource Technology, 2016. **211**: p. 779-782.
119. Xu, D., et al., *Biocrude Upgrading in Different Solvents after Microalgae Hydrothermal Liquefaction*. Industrial & Engineering Chemistry Research, 2021. **60**(21): p. 7966-7974.
120. Fahim, M.A., T.A. Alsahhaf, and A. Elkilani, *7. Hydroconversion*, in *Fundamentals of Petroleum Refining*. Elsevier. p. 153.
121. Mortensen, P.M., et al., *A review of catalytic upgrading of bio-oil to engine fuels*. Applied Catalysis A: General, 2011. **407**(1): p. 1-19.
122. Yue, L., et al., *Impacts of hydrogen to carbon ratio (H/C) on fundamental properties and supercritical cracking performance of hydrocarbon fuels*. Chemical Engineering Journal, 2016. **283**: p. 1216-1223.
123. Fahim, M.A., T.A. Alsahhaf, and A. Elkilani, *7.2.10.1 Naphtha and Gas Oil Hydrotreating Correlations*, in *Fundamentals of Petroleum Refining*. Elsevier. p. 172.
124. Fahim, M.A., T.A. Alsahhaf, and A. Elkilani, *7.2.3 Chemistry of Hydrotreating*, in *Fundamentals of Petroleum Refining*. Elsevier. p. 156.
125. Stauffer, E., J.A. Dolan, and R. Newman, *CHAPTER 7 - Flammable and Combustible Liquids*, in *Fire Debris Analysis*, E. Stauffer, J.A. Dolan, and R. Newman, Editors. 2008, Academic Press: Burlington. p. 199-233.

126. Grange, P., et al., *Hydrotreatment of pyrolysis oils from biomass: reactivity of the various categories of oxygenated compounds and preliminary techno-economical study*. Catalysis today, 1996. **29**(1-4): p. 297-301.
127. Yunquan, Y., et al., *Hydrodeoxygenation of phenolic model compounds over MoS₂ catalysts with different structures*. Chinese Journal of Chemical Engineering, 2008. **16**(5): p. 733-739.
128. Girgis, M.J. and B.C. Gates, *Reactivities, reaction networks, and kinetics in high-pressure catalytic hydroprocessing*. Industrial & Engineering Chemistry Research, 1991. **30**(9): p. 2021-2058.
129. Torri, C., et al., *Hydrothermal Treatment (HTT) of Microalgae: Detailed Molecular Characterization of HTT Oil in View of HTT Mechanism Elucidation*. Energy & Fuels, 2012. **26**(1): p. 658-671.
130. Guo, B., et al., *Hydrothermal liquefaction of Chlorella vulgaris and Nannochloropsis gaditana in a continuous stirred tank reactor and hydrotreating of biocrude by nickel catalysts*. Fuel Processing Technology, 2019. **191**: p. 168-180.
131. Patel, B., et al., *Catalytic Hydrotreatment of algal biocrude from fast Hydrothermal Liquefaction*. Renewable Energy, 2017. **101**: p. 1094-1101.
132. Bai, X., et al., *Hydrothermal catalytic processing of pretreated algal oil: A catalyst screening study*. Fuel, 2014. **120**: p. 141-149.
133. He, Z., et al., *Catalytic Upgrading of Water-Soluble Biocrude from Hydrothermal Liquefaction of Chlorella*. Energy & Fuels, 2018. **32**(2): p. 1893-1899.
134. Wang, Z., et al., *Upgrading of hydrothermal liquefaction biocrude from algae grown in municipal wastewater*. Fuel Processing Technology, 2016. **142**: p. 147-156.
135. Xu, D., et al., *Ni-Ru/CeO₂ Catalytic Hydrothermal Upgrading of Water-Insoluble Biocrude from Algae Hydrothermal Liquefaction*. Biomed Res Int, 2018. **2018**: p. 8376127.
136. Chen, L., et al., *Hydro-upgrading of algal bio-oil in tetralin for the production of high-quality liquid fuel: Process intensification*. Fuel Processing Technology, 2021. **224**: p. 107034.
137. López Barreiro, D., et al., *Heterogeneous catalytic upgrading of biocrude oil produced by hydrothermal liquefaction of microalgae: State of the art and own experiments*. Fuel Processing Technology, 2016. **148**: p. 117-127.
138. Kunwar, B., et al., *Nanoparticles of Pd supported on bacterial biomass for hydroprocessing crude bio-oil*. Fuel, 2017. **209**: p. 449-456.
139. Farneth, W.E. and R.J. Gorte, *Methods for Characterizing Zeolite Acidity*. Chemical Reviews, 1995. **95**(3): p. 615-635.
140. Junaid, A.S.M., et al., *Natural zeolites for oilsands bitumen cracking: Structure and acidity*. Microporous and Mesoporous Materials, 2011. **144**(1): p. 148-157.

141. Blay, V., et al., *Engineering Zeolites for Catalytic Cracking to Light Olefins*. ACS Catalysis, 2017. **7**(10): p. 6542-6566.
142. Li, Z. and P.E. Savage, *Feedstocks for fuels and chemicals from algae: Treatment of crude bio-oil over HZSM-5*. Algal Research, 2013. **2**(2): p. 154-163.
143. Duan, P., et al., *Catalytic upgrading of pretreated algal bio-oil over zeolite catalysts in supercritical water*. Biochemical Engineering Journal, 2016. **116**: p. 105-112.
144. Cui, Z., et al., *Integrated Extraction and Catalytic Upgrading of Biocrude Oil from Co-hydrothermal Liquefaction of Crude Glycerol and Algae*. Energy & Fuels, 2021. **35**(15): p. 12165-12174.
145. Xiu, S. and A. Shahbazi, *Bio-oil production and upgrading research: A review*. Renewable and Sustainable Energy Reviews, 2012. **16**(7): p. 4406-4414.
146. Saber, M., B. Nakhshiniev, and K. Yoshikawa, *A review of production and upgrading of algal bio-oil*. Renewable and Sustainable Energy Reviews, 2016. **58**: p. 918-930.
147. Duan, P., et al., *Catalytic upgrading of crude algal oil using platinum/gamma alumina in supercritical water*. Fuel, 2013. **109**: p. 225-233.
148. Duan, P. and P.E. Savage, *Upgrading of crude algal bio-oil in supercritical water*. Bioresource Technology, 2011. **102**(2): p. 1899-1906.
149. Xu, D. and P.E. Savage, *Supercritical water upgrading of water-insoluble and water-soluble biocrudes from hydrothermal liquefaction of Nannochloropsis microalgae*. The Journal of Supercritical Fluids, 2018. **133**: p. 683-689.
150. Pavlova, P.L., et al., *Supercritical Fluid Application in the Oil and Gas Industry: A Comprehensive Review*. Sustainability, 2022. **14**(2).
151. Cheng, Z.-M., et al., *Effects of Supercritical Water in Vacuum Residue Upgrading*. Energy & Fuels, 2009. **23**(6): p. 3178-3183.
152. Kokubo, S., et al., *Effective Demetalization and Suppression of Coke Formation Using Supercritical Water Technology for Heavy Oil Upgrading*. Journal of the Japan Petroleum Institute, 2008. **51**(5): p. 309-314.
153. Han, L.-n., R. Zhang, and J.-c. Bi, *Upgrading of coal-tar pitch in supercritical water*. Journal of Fuel Chemistry and Technology, 2008. **36**(1): p. 1-5.
154. Sato, T., et al., *Upgrading of asphalt with and without partial oxidation in supercritical water* ☆. Fuel, 2003. **82**(10): p. 1231-1239.
155. Paspek, S.C. and M.T. Klein, *SHALE OIL UPGRADING IN SUPERCRITICAL WATER SOLUTIONS*. Fuel Science and Technology International, 1990. **8**(6): p. 673-687.
156. Duan, P. and P.E. Savage, *Upgrading of crude algal bio-oil in supercritical water*. Bioresour Technol, 2011. **102**(2): p. 1899-906.
157. Hosseinpour, M., S.J. Ahmadi, and S. Fatemi, *Deuterium tracing study of unsaturated aliphatics hydrogenation by supercritical water in upgrading heavy oil. Part I: Non-catalytic cracking*. The Journal of Supercritical Fluids, 2016. **107**: p. 278-285.

158. Koseva, M.R., *Chapter 3 - Sources, Characterization, and Composition of Food Industry Wastes*, in *Food Industry Wastes*, M.R. Koseva and C. Webb, Editors. 2013, Academic Press: San Diego. p. 37-60.
159. He, C., et al., *Hydrothermal gasification of sewage sludge and model compounds for renewable hydrogen production: A review*. *Renewable and Sustainable Energy Reviews*, 2014. **39**: p. 1127-1142.
160. Laurent, E. and B. Delmon, *Influence of water in the deactivation of a sulfided NiMoY-Al₂O₃ catalyst during hydrodeoxygenation*. *Journal of Catalysis*, 1994. **146**(1): p. 281-291.
161. Gardner, D.W., et al., *Insights into the Hydrothermal Stability of ZSM-5 under Relevant Biomass Conversion Reaction Conditions*. *ACS Catalysis*, 2015. **5**(7): p. 4418-4422.
162. Hu, Y., et al., *Supercritical water gasification of biocrude oil from low-temperature liquefaction of algal lipid extraction residue*. *Fuel*, 2020. **276**: p. 118017.
163. Tushar, M.S.H.K., A. Dutta, and C. Xu, *Catalytic supercritical gasification of biocrude from hydrothermal liquefaction of cattle manure*. *Applied Catalysis B: Environmental*, 2016. **189**: p. 119-132.
164. Green, D.W. and R.H. Perry, *Perry's chemical engineers' handbook*. 2008: McGraw-Hill Education.
165. ASTM, *E1755-01(2020) Standard Test Method for Ash in Biomass*. 2020.
166. Ross, A.B., et al., *Investigation of the pyrolysis behaviour of brown algae before and after pre-treatment using PY-GC/MS and TGA*. *Journal of Analytical and Applied Pyrolysis*, 2009. **85**(1-2): p. 3-10.
167. Harman-Ware, A.E., et al., *Microalgae as a renewable fuel source: Fast pyrolysis of *Scenedesmus* sp.* *Renewable Energy*, 2013. **60**: p. 625-632.
168. Kebelmann, K., et al., *Intermediate pyrolysis and product identification by TGA and Py-GC/MS of green microalgae and their extracted protein and lipid components*. *Biomass and Bioenergy*, 2013. **49**: p. 38-48.
169. Doudin, K., A. Ahmad, and S. Al-Malaika, *Reactive processing of polymers: Structural characterisation of products by ¹H and ¹³C NMR spectroscopy for glycidyl methacrylate grafting onto EPR in the absence and presence of a reactive comonomer*. *Polymer degradation and stability*, 2009. **94**(10): p. 1599-1614.
170. Doudin, K., et al., *Effect of contact surfaces on the thermal and photooxidation of dehydrated castor oil*. *Polymer Degradation and Stability*, 2011. **96**(4): p. 438-454.
171. Zambare, A.S., et al., *Controlling the product selectivity in the conversion of methanol to the feedstock for phenol production*. *RSC advances*, 2019. **9**(41): p. 23864-23875.
172. Bartošová, A., L. Blinová, and K. Gerulová, *Characterisation of polysaccharides and lipids from selected green algae species by FTIR-ATR spectroscopy*. *Research Papers Faculty of Materials Science and Technology Slovak University of Technology*, 2015. **23**(36): p. 97-102.

173. Lopez Barreiro, D., et al., *Influence of strain-specific parameters on hydrothermal liquefaction of microalgae*. *Bioresour Technol*, 2013. **146**: p. 463-471.
174. Trinh, T.N., et al., *Comparison of Lignin, Macroalgae, Wood, and Straw Fast Pyrolysis*. *Energy & Fuels*, 2013. **27**(3): p. 1399-1409.
175. Greenhalf, C.E., et al., *Thermochemical characterisation of straws and high yielding perennial grasses*. *Industrial Crops and Products*, 2012. **36**(1): p. 449-459.
176. Siahbalaeei, R., G. Kavooosi, and M. Noroozi, *Protein nutritional quality, amino acid profile, anti-amylase and anti-glucosidase properties of microalgae: Inhibition and mechanisms of action through in vitro and in silico studies*. *Lwt*, 2021. **150**.
177. Araya, M., et al., *Determination of free and protein amino acid content in microalgae by HPLC-DAD with pre-column derivatization and pressure hydrolysis*. *Marine Chemistry*, 2021. **234**.
178. Bellou, S., et al., *Microalgal lipids biochemistry and biotechnological perspectives*. *Biotechnology advances*, 2014. **32**(8): p. 1476-1493.
179. Schulze, C., et al., *Carbohydrates in microalgae: Comparative determination by TLC, LC-MS without derivatization, and the photometric thymol-sulfuric acid method*. *Algal Research*, 2017. **25**: p. 372-380.
180. Changi, S., T.M. Brown, and P.E. Savage, *Reaction kinetics and pathways for phytol in high-temperature water*. *Chemical Engineering Journal*, 2012. **189**: p. 336-345.
181. Speight, J.G. and B. Ozum, *Petroleum refining processes*. 2001: CRC Press.
182. Shin, H.-Y., et al., *Thermal stability of fatty acids in subcritical water*. *Journal of Analytical and Applied Pyrolysis*, 2012. **98**: p. 250-253.
183. Azeez, A.M., et al., *Fast pyrolysis of African and European lignocellulosic biomasses using Py-GC/MS and fluidized bed reactor*. *Energy & Fuels*, 2010. **24**(3): p. 2078-2085.
184. Sarchami, T., N. Batta, and F. Berruti, *Production and separation of acetic acid from pyrolysis oil of lignocellulosic biomass: a review*. *Biofuels, Bioproducts and Biorefining*, 2021. **15**(6): p. 1912-1937.
185. Valdez, P.J., J.G. Dickinson, and P.E. Savage, *Characterization of Product Fractions from Hydrothermal Liquefaction of Nannochloropsis sp. and the Influence of Solvents*. *Energy & Fuels*, 2011. **25**(7): p. 3235-3243.
186. Mullen, C.A., G.D. Strahan, and A.A. Boateng, *Characterization of various fast-pyrolysis bio-oils by NMR spectroscopy*. *Energy & Fuels*, 2009. **23**(5): p. 2707-2718.
187. Williams, P.T. and P.A. Horne, *Characterisation of oils from the fluidised bed pyrolysis of biomass with zeolite catalyst upgrading*. *Biomass and Bioenergy*, 1994. **7**(1): p. 223-236.
188. Duan, P. and P.E. Savage, *Catalytic treatment of crude algal bio-oil in supercritical water: optimization studies*. *Energy & Environmental Science*, 2011. **4**(4): p. 1447-1456.

189. Elliott, D.C., *Catalytic hydrothermal gasification of biomass*. Biofuels, Bioproducts and Biorefining, 2008. **2**(3): p. 254-265.
190. Wambach, J., et al., *Characterization of a spent Ru/C catalyst after gasification of biomass in supercritical water*. Chimia (Aarau), 2012. **66**(9): p. 706-11.
191. Hunston, C., et al., *Investigating active phase loss from supported ruthenium catalysts during supercritical water gasification*. Catalysis science & technology, 2021. **11**(22): p. 7431-7444.
192. Matsumura, Y., et al., *Biomass gasification in near- and super-critical water: Status and prospects*. Biomass and Bioenergy, 2005. **29**(4): p. 269-292.
193. Osada, M., et al., *Water Density Effect on Lignin Gasification over Supported Noble Metal Catalysts in Supercritical Water*. Energy & Fuels, 2006. **20**(3): p. 930-935.
194. Panariti, N., et al., *Petroleum residue upgrading with dispersed catalysts: Part 2. Effect of operating conditions*. Applied Catalysis A: General, 2000. **204**(2): p. 215-222.
195. Guo, X., et al., *Analysis of coke precursor on catalyst and study on regeneration of catalyst in upgrading of bio-oil*. Biomass and Bioenergy, 2009. **33**(10): p. 1469-1473.
196. Elliott, D.C., et al., *Catalytic hydroprocessing of biomass fast pyrolysis bio-oil to produce hydrocarbon products*. Environmental Progress & Sustainable Energy: An Official Publication of the American Institute of Chemical Engineers, 2009. **28**(3): p. 441-449.
197. Bridgwater, A.V., *Production of high grade fuels and chemicals from catalytic pyrolysis of biomass*. Catalysis Today, 1996. **29**(1): p. 285-295.
198. Vitolo, S., et al., *Catalytic upgrading of pyrolytic oils over HZSM-5 zeolite: behaviour of the catalyst when used in repeated upgrading–regenerating cycles*. Fuel, 2001. **80**(1): p. 17-26.
199. Al-Degs, Y.S., M. Al-Ghouti, and G. Walker, *Determination of higher heating value of petro-diesels using mid-infrared spectroscopy and chemometry*. Journal of thermal analysis and calorimetry, 2012. **107**(2): p. 853-862.
200. Department for Business, E.I.S. *Digest of UK Energy Statistics (DUKES) 2021*. 2021 [cited 2022 08/03/2022]; Available from: <https://www.gov.uk/government/statistics/digest-of-uk-energy-statistics-dukes-2021>.
201. Knorr, D., J. Lukas, and P. Schoen, *Production of Advanced Biofuels via Liquefaction-Hydrothermal Liquefaction Reactor Design: April 5, 2013*. 2013, National Renewable Energy Lab.(NREL), Golden, CO (United States).
202. Dutta, A., et al., *Process design and economics for conversion of lignocellulosic biomass to ethanol: thermochemical pathway by indirect gasification and mixed alcohol synthesis*. 2011, National Renewable Energy Lab.(NREL), Golden, CO (United States).
203. talent.com. *Salary in United Kingdom*. 2022; Available from: <https://uk.talent.com/salary>.

204. Snowden-Swan, L.J., et al., *Conceptual Biorefinery Design and Research Targeted for 2022: Hydrothermal Liquefaction Processing of Wet Waste to Fuels*. 2017, Pacific Northwest National Lab.(PNNL), Richland, WA (United States).
205. Department for Business, E.I.S. *Gas and electricity prices in the non-domestic sector*. 2013 December 2021 08/03/2022]; Available from: <https://www.gov.uk/government/statistical-data-sets/gas-and-electricity-prices-in-the-non-domestic-sector>.
206. Stenberg, V., et al., *Techno-economic analysis of H2 production processes using fluidized bed heat exchangers with steam reforming – Part 1: Oxygen carrier aided combustion*. International Journal of Hydrogen Energy, 2020. **45**(11): p. 6059-6081.
207. Farooq, D., I. Thompson, and K.S. Ng, *Exploring the feasibility of producing sustainable aviation fuel in the UK using hydrothermal liquefaction technology: A comprehensive techno-economic and environmental assessment*. Cleaner Engineering and Technology, 2020. **1**.
208. dailymetalprice.com. *Metal Spot Price Charts*. 2022 [cited 2022 08/03/2022]; Available from: <https://www.dailymetalprice.com/metalpricecharts.php?c=ru&u=oz&d=0>.
209. Towler, G. and R. Sinnott, *Chemical engineering design: principles, practice and economics of plant and process design*. 2021: Butterworth-Heinemann.
210. McVeigh, J.C., *CHAPTER 7 - SOCIAL, LEGAL AND ECONOMIC ISSUES*, in *Sun Power (Second Edition)*, J.C. McVeigh, Editor. 1983, Pergamon: Oxford. p. 161-173.
211. Department for Business, E.I.S. *Weekly road fuel prices*. 2022 [cited 2022 08/03/2022]; Available from: <https://www.gov.uk/government/statistics/weekly-road-fuel-prices>.

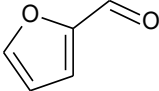
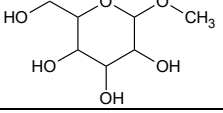
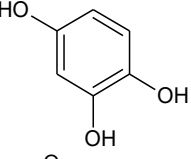
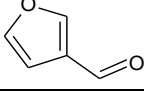
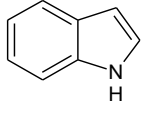
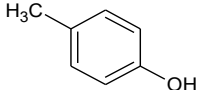
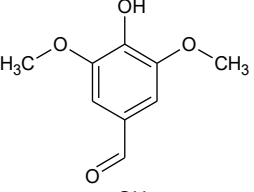
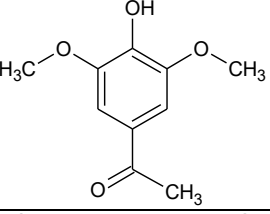
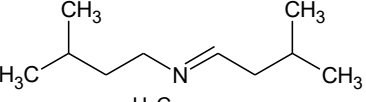
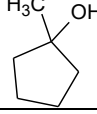
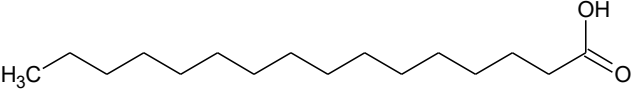
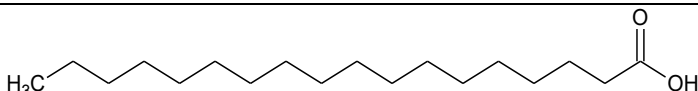
Appendices

Appendix A: Supporting data for Chapter 4

Table A.1. Biochemical composition of *Nannochloropsis sp.*
as specified by the supplier

<i>Nannochloropsis sp</i>		
Protein (dry wt)		58.6%
Lipid (dry wt)		14.5%
Carbohydrate (dry wt)		20.0%
Fatty Acid Profile (% of lipid content)		
12:0	Lauric acid	0.0
14:0	Myristic acid	2.2
16:0	Palmitic acid	21.5
16:1n7	Palmitoleic acid	3.3
16:2n4	Hexadecadienoic	0.2
18:0	Stearic Acid	0.4
18:1n9	Oleic Acid	18.0
18:2n6	LA	4.7
18:3n6	GLA	0.6
18:3n3	ALA	0.3
18:4n3	SDA	0.1
20:3n6	DGLA	0.3
20:4n6	ARA	3.6
20:5n3	EPA	30.3
22:5n3	DPA (n-3)	0.0
22:6n3	DHA	0.0

Table A.2. Peak areas and chemical structures of key markers from the Py-GC-MS analysis of model components

Model Component	Peak area (%)	Component Name	Structure
Xylose	22.8 %	furfural	
	16.4 %	methyl alpha-d-glucopyranoside	
Glucose	21.9 %	1,2,4-benzenetriol	
	14.5 %	3-furaldehyde	
Soy Protein	6.7 %	indole	
	5.4 %	p-cresol	
L-Glutamine	25.3 %	4-hydroxy-3,5-dimethoxy-benzaldehyde	
	11.3 %	1-(4-hydroxy-3,5-dimethoxyphenyl)-ethanone	
L-Leucine	57.9 %	3-methyl-N-(3-methylbutylidene)-1-butanamine	
	34 %	1-methyl-cyclopentanol	
Oleic Acid	15.9 %	n-hexadecanoic acid	
Stearic Acid	87.3 %	octadecanoic acid (stearic acid)	

Appendix B: Supporting data for Chapter 5

Table B.1. *Nannochloropsis* sp. Retention times and peak areas from the GC-MS analysis of bio-crude

Peak Number	Compound	Retention Time	Peak Area %
1	2-methyl-1-propanal	2.26	1.01
2	3-methyl-1-butanol	3.61	1.35
3	2-methyl-1-butanol	3.68	1.45
4	4-methyl-4-penten-2-one	3.95	5.46
5	1-methyl-piperidine	4.23	5.24
6	4-methyl-3-penten-2-one	5.17	12.4
7	1-(1,1-dimethylethyl)-2,3-dimethyl-aziridine	5.50	1.49
8	4-hydroxy-4-methyl-2-pentanone	6.56	8.07
9	1-ethyl-piperidine	6.74	1.25
10	1-butylpyrrolidine	8.30	2.74
11	1-(1,1-dimethylethyl)-2,3-dimethyl-aziridine	9.15	4.57
12	3,3,4-trimethyl-decane	9.42	7.84
13	Phenol	12.29	1.28
14	1-butylpyrrolidine	12.51	3.49
15	1-butylpyrrolidine	13.06	7.96
16	1-pentyl-piperidine	16.20	1.29
17	1,2,3,4-tetrahydro-naphthalene	20.18	1.15
18	2-piperidinone	20.92	1.55
19	N-(1-methylethylidene)-benzeneethanamine	26.60	4.12
20	Nonadecane	43.93	1.45
21	3,7,11-trimethyl-1-dodecanol	45.09	1.34
22	3,7,11,15-tertamethylhexadec-2-ene	48.85	3.37
23	3,7,11,15-tertamethylhexadec-2-ene	49.28	5.38

** = unidentified

Table B.2. Retention times and peak areas from the GC-MS analysis of **Glucose** model component bio-crude.

Peak Number	Compound	Retention Time	Peak Area %
1	2-cyclopenten-1-one	6.31	3.88
2	4-hydroxy-4-methyl-2-pentanone	6.62	1.25
3	2-butanone	7.17	6.22
4	2-methyl-2-cyclopenten-1-one	9.02	1.21
5	1-(2-furanyl)-ethanone	9.22	3.18
6	2,5-hexanedione	9.91	11.88
7	Dihydro-5-methyl-2(3H)-furanone	10.92	3.61
8	3-methyl-2-cyclopenten-1-one	11.36	2.97
9	Phenol	12.28	1.20
10	3,6-heptanedione	13.91	3.06
11	3-methyl-1,2-cyclopentanedione	14.00	7.76
12	2,3-dimethyl-2-cyclopenten-1-one	14.45	1.07
13	**	15.46	1.02
14	**	15.61	1.60
15	**	15.63	1.52
16	**	15.73	2.12
17	2-amino-1,5-dihydro-4H-imidazol-4-one	15.93	7.94
18	3-ethyl-2-cyclopenten-1-one	16.01	4.60
19	4-oxo-pentanoic acid	16.18	11.40
20	5-methyl-3-hexen-2-one	24.22	1.28
21	3,4-dimethylfuran	24.59	1.23
22	carvenone	28.32	1.99
23	n-caproic acid vinyl ester	30.22	4.37
24	**	47.27	1.74

** = unidentified

Table B.3. Retention times and peak areas from the GC-MS analysis of **Oleic acid** model component bio-crude.

Peak Number	Compound	Retention Time	Peak Area %
1	Oleic acid	59.70	2.61
2	Oleic acid	60.23	13.87
3	6-Octadecanoic acid	60.28	2.01
4	Oleic acid	60.52	13.87
5	Trans-9-octadecanoic acid pentyl ester	60.60	5.35
6	Cis-11-eicosenoic acid	60.63	2.73
7	Oleic acid	60.73	8.44
8	Oleic acid	60.80	6.96
9	Oleic acid	60.89	8.75
10	Oleic acid	60.96	8.87
11	Oleic acid	61.00	2.32

12	Cis-10-nonadecenoic acid	61.01	2.34
13	Oleyl alcohol trifluoroacetate	61.05	6.00
14	Oleic acid	61.09	7.83

** = unidentified

Table B.4. Retention times and peak areas from the GC-MS analysis of **Soy protein** model component bio-crude.

Peak Number	Compound	Retention Time	Peak Area %
1	Toluene	4.293	1.63
2	4-hydroxy-4-methyl-2-Pentanone	6.472	4.62
3	Styrene	8.253	4.81
4	Phenol	12.118	3.01
5	p-Cresol	15.928	2.95
6	Indole	24.140	1.60
7	Indole	24.295	1.30
8	**	27.268	1.35
9	**	27.521	2.96
10	**	27.625	2.13
11	**	27.734	1.13
12	Pyrimidine-2,4,6(1H,3H,5H)-trione, 1-(2-phenylethyl)-	39.159	1.77
13	**	40.795	3.29
14	**	41.117	2.51
15	2,5-Piperazinedione, 3,6-bis(2-methylpropyl)-	43.460	2.47
16	**	43.857	1.07
17	9H-Pyrido[3,4-b]indole, 1-methyl-	44.613	1.56
18	Tetradecanamide	49.435	2.07
19	N-methyl-arachidamide	50.236	3.76
20	N-ethyl-arachidamide	51.160	2.43
21	**	52.845	1.19
22	13-Docosenamide, (Z)-	53.451	2.80
23	**	54.023	2.92
24	Arachidamide, N-isobutyl-	54.160	4.41
25	**	54.863	1.24
26	Arachidamide, N-3-methylbutyl-	56.336	6.08
27	Pyrrolidine, 1-(1-oxooctadecyl)-	57.889	2.24
28	**	59.703	6.80
29	**	60.003	1.62
30	Arachidamide, N-3-methylbutyl-	60.272	1.13
31	**	64.523	1.58
32	**	67.618	1.23

** = unidentified

Table B.5. Retention times and peak areas from the GC-MS analysis of **Pyrolysis oil**

Peak Number	Compound	Retention Time	Peak Area %
1	Acetic acid	2.13	13.01
2	1-hydroxy-2-propanone	2.62	11.49
3	Propanoic acid	2.97	1.75
4	1,2-ethandiol	2.99	1.71
5	1-hydroxy-butanone	4.31	1.59
6	Succindialdehyde	4.65	2.04
7	Glyceraldehyde	5.90	1.00
8	Furfural	6.25	2.21
9	4-hydroxy-4-methyl-2-pentanone	6.56	1.70
10	2,2,4-trimethyl-1,3-dioxolane	7.35	2.21
11	1-acetate 1,2,3-propanetriol	8.55	1.56
12	2(5H)-furanone	9.76	1.05
13	3-methyl-1,2-cyclopentanedione	16.36	2.17
14	4-methyl-5H-furan-2-one	17.49	1.60
15	2-methoxy-phenol	20.58	2.66
16	Creosol	27.85	3.63
17	Catechol	28.73	1.46
18	2-methoxy-3-(2-peopernyl)-phenol	39.24	1.47
19	3-butoxy-2-methyl-1-butene	40.68	1.89
20	3-hydroxy-4-methoxy-benzaldehyde	41.93	1.56
21	Apocynin	47.55	2.41
22	**	47.74	1.83
23	**	47.88	1.41
24	**	48.04	1.72
25	1,6-anhydro-.beta.-D-glucopyranose	48.26	4.36
26	?	48.32	1.90
27	4-hydroxy-3-methoxy-benzenepropanol	56.15	1.33
28	Coniferyl aldehyde	58.51	1.27
29	**	60.37	1.23

** = unidentified

Appendix C: Supporting data for Chapter 6

Table C.1. Tentative identities and peak area % of the major peaks found in the total ion chromatogram for the bio-crude and selected upgraded oil.

Retention Time (min)	Compound	Bio-crude	Pd/C	Pt/C	NiMo
		Area %	Area %	Area %	Area %
2.048	n-Hexane	-	2.23	0.34	-
2.091	2-Butanone	-	-	1.61	2.76
2.27	methyl-Cyclopentane	-	2.40	0.90	-
2.562	3-methyl-2-Butanone	-	-	-	1.20
2.591	Benzene	-	5.59	-	-
2.606	2,4-Hexadiyne	-	-	2.08	-
3.609	3-methyl-1-Butanol	1.35	-	-	0.20
3.684	2-methyl-1-Butanol	1.45	-	-	-
3.946	4-methyl-4-Penten-2-one	5.46	-	-	-
2.979	Heptane	-	2.00	1.50	-
2.996	3-Pentanone	-	-	-	1.70
4.227	1-methyl-Piperidine	5.24	-	-	-
4.328	Toluene	-	9.54	4.13	2.46
4.922	Cyclopentanone	-	-	-	1.56
5.144	Octane	-	1.67	1.19	-
5.166	4-methyl-3-Penten-2-one	12.40	-	-	-
5.502	Aziridine, 1-(1,1-dimethylethyl)-2,3-dimethyl-, cis-	1.49	-	-	-
6.556	4-hydroxy-4-methyl-2-Pentanone	8.07	-	-	-
6.737	1-ethyl-Piperidine	1.25	-	-	-
7.228	Ethylbenzene	0.32	5.57	4.29	7.09
7.514	1,3-dimethyl-Benzene	-	4.45	2.86	-
8.295	1-Butylpyrrolidine	2.74	-	-	-
8.395	o-Xylene	-	1.45	1.10	0.61
8.645	Nonane	-	1.40	1.16	-
9.15	Aziridine, 1-(1,1-dimethylethyl)-2,3-dimethyl-	4.57	-	-	-
9.415	3,3,4-trimethyl-Decane	7.84	-	-	-
11.156	1-ethyl-3-methyl-Benzene	-	1.65	1.25	-
12.192	Phenol	1.28	0.46	1.36	2.75
12.458	1,2,3-trimethyl-Benzene	-	1.32	2.04	-
12.506	1-Butylpyrrolidine	3.49	-	-	-
12.724	Decane	-	1.32	1.16	0.18
13.059	1-Butylpyrrolidine	7.96	-	-	-
14.183	Indane	-	1.42	0.98	0.17
15.149	1-ethyl-3,5-dimethyl-Benzene	-	0.49	1.21	-
16.034	3-methyl-Phenol	-	-	1.66	0.77
16.196	1-pentyl-Piperidine	1.29	-	-	-
16.814	Undecane	-	1.31	1.25	0.60

18.83	2,3-dihydro-5-methyl-1H-Indene	-	0.86	1.06	-
19.299	1,2,3,4-tetrahydro-Naphthalene	1.15	1.55	0.54	0.98
19.566	4-ethyl-Phenol	-	0.13	0.28	1.31
20.176	Naphthalene	-	6.31	2.12	-
20.676	Tridecane	-	-	-	1.47
20.732	Undecane	-	1.69	2.33	-
20.917	2-Piperidinone	1.55	-	-	-
24.311	Naphthalene, 2-methyl-	-	3.16	2.68	-
24.421	Tridecane	-	1.98	2.36	1.32
24.921	Naphthalene, 2-methyl-	-	1.36	1.37	-
26.6	Benzeneethanamine, N-(1-methylethylidene)-	4.12	-	-	-
27.792	Naphthalene, 2-ethyl-	-	0.49	1.03	-
27.884	Hexadecane	-	1.60	1.78	0.46
28.669	Naphthalene, 1,2-dimethyl-	-	0.54	1.14	-
30.843	3-Hexadecene, (Z)-	-	-	-	1.25
31.173	Pentadecane	-	6.99	8.91	0.62
34.24	Hexadecane	-	2.26	1.55	-
37.163	Hexadecane	-	2.46	2.90	0.87
38.991	Tetradecanoic acid	-	-	-	2.64
39.704	Phenanthrene	-	1.48	0.34	-
40.198	Hexadecane, 2,6,10,14-tetramethyl-	-	1.29	1.56	0.61
42.572	Nonadecane	1.45	0.45	0.59	0.45
40.708	Acetic acid, 3,7,11,15-tetramethyl-hexadecyl ester	-	-	-	2.08
41.146	2-Pentadecanone, 6,10,14-trimethyl-	-	-	-	1.63
44.393	Pentadecanoic acid	-	-	-	16.70
45.09	1-Dodecanol, 3,7,11-trimethyl-	1.34	-	-	-
48.845	3,7,11,15-Tetramethylhexadec-2-ene	3.37	-	-	-
49.028	Octadecanoic acid	-	-	-	1.00
49.276	2-Hexadecene, 3,7,11,15-tetramethyl-, [R-[R*,R*-(E)]]-	5.38	-	-	-
68.141	Tetracontane-1,40-diol	-	-	-	3.71

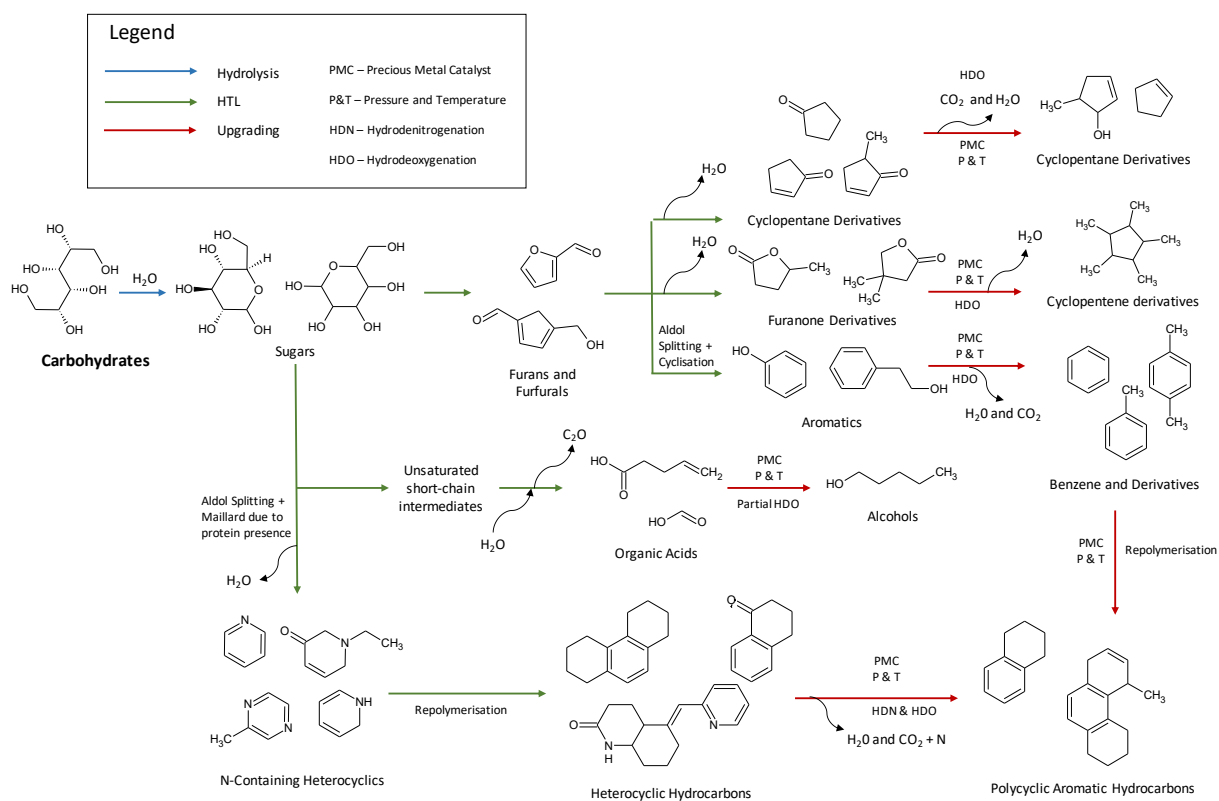


Figure C.1. Reaction network for carbohydrates undergoing thermal degradation (Py-GC-MS studies) without and with catalysts

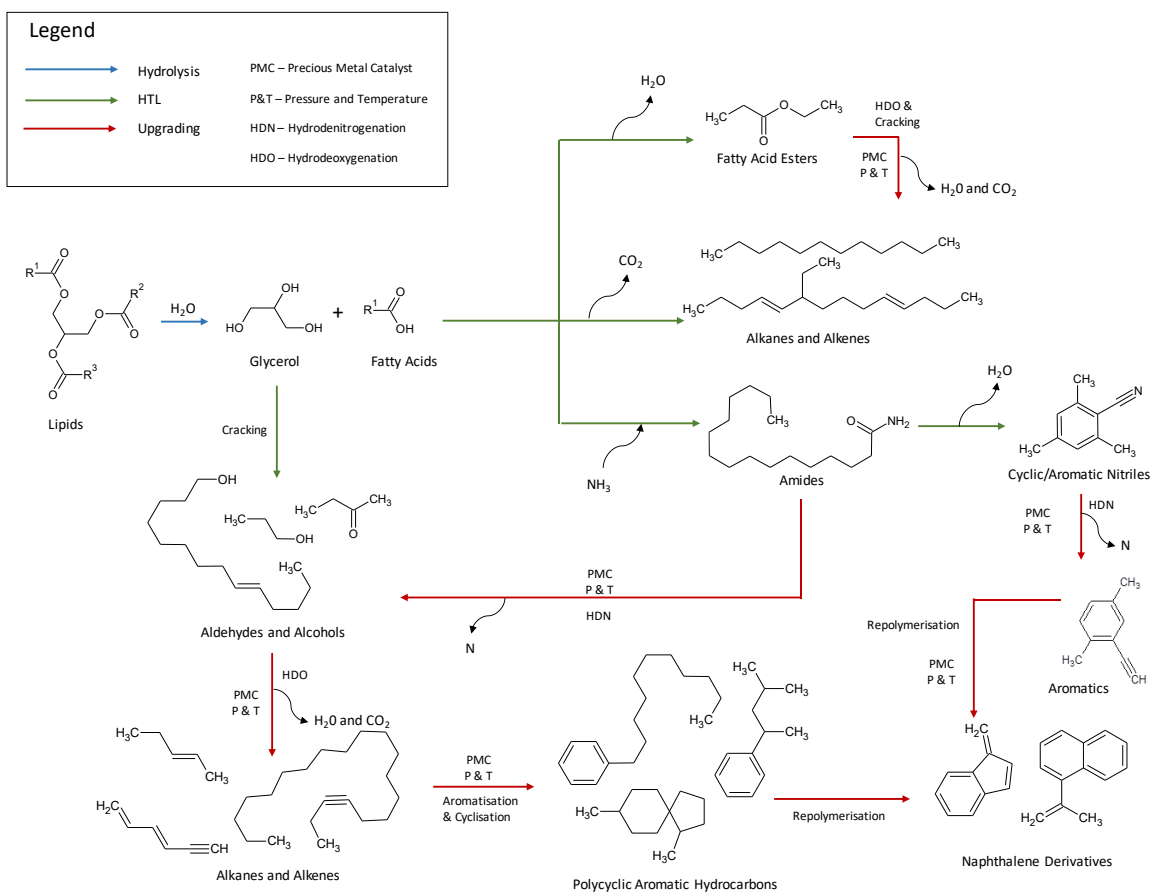


Figure C.2. Reaction network for lipids undergoing thermal degradation (Py-GC-MS studies) without and with catalysts

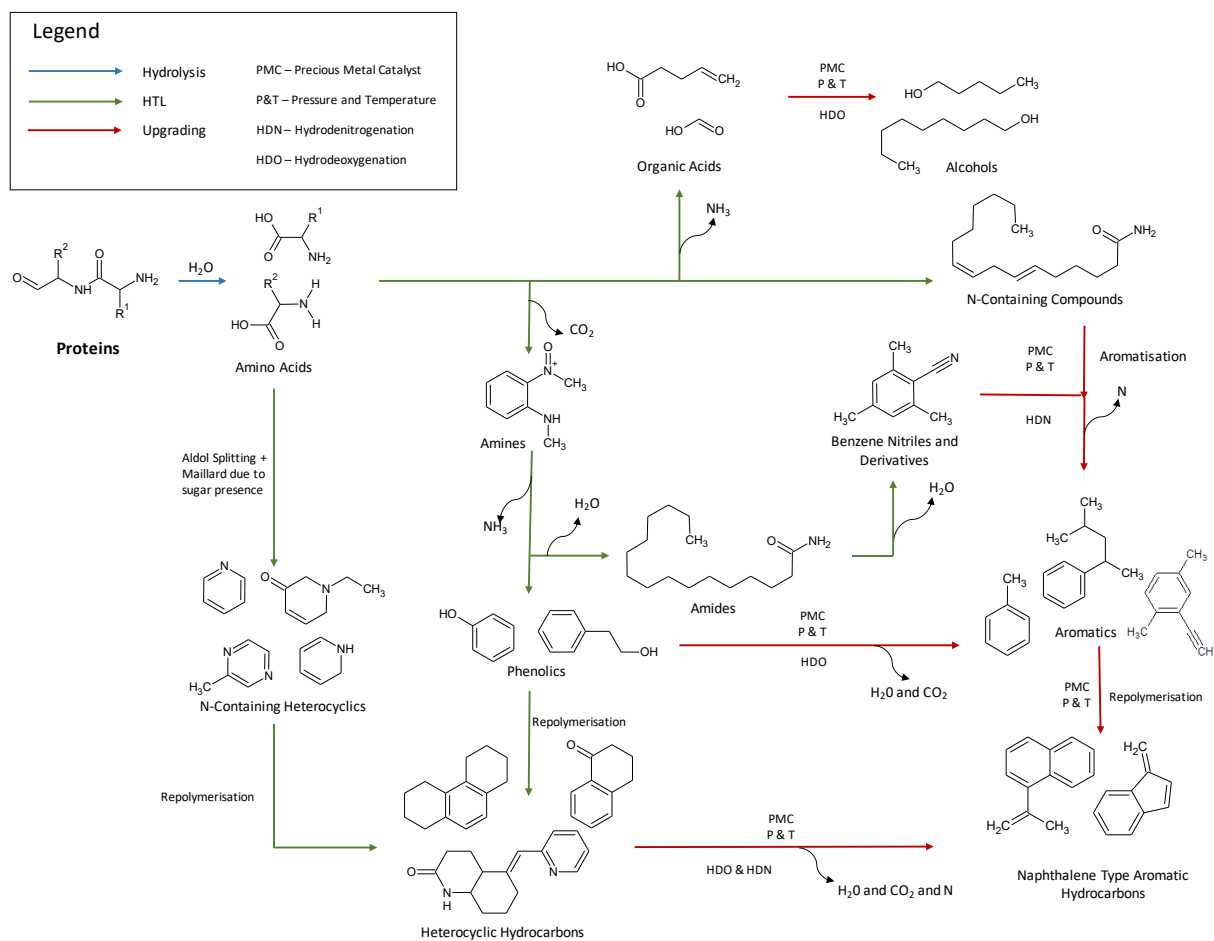


Figure C.3. Reaction network for proteins undergoing thermal degradation (Py-GC-MS studies) without and with catalysts

Appendix D: Supporting data for Chapter 7

Table D.1. HTL product composition inputs for the Aspen model

	Aspen Component ID	Yield (wt.%)
Bio-crude (dry)		51%
Composition		
1-ethyl-2-Pyrrolidinone	1-ETH-01	3.4635%
N-methylthiopyrrolidone	N-MET-01	0.5231%
Ethylbenzene	ETHYL-01	1.2988%
4-methyl-Phenol	P-CRE-01	2.5976%
4-ethyl-Phenol	P-ETH-01	2.5976%
Indole	INDOL-01	2.5976%
7-methylindole	7-MET-01	1.7318%
Myristic Amide	MYRIS-01	1.7318%
Palmitic acid Amide	PALMI-01	7.7929%
Octadecamide	OCTAD-01	3.4635%
9-Hexadecenoic acid	CIS-9-01	6.9270%
N-Hexadecanoic acid	N-HEX-01	5.1952%
Oleic acid	OLEIC-01	0.8659%
Naphthalene	NAPHT-01	2.5976%
Chloesterol	BETA--01	0.8659%
Diphenyl-phenylenediamine	N-N-D-01	4.1526%
N-Undecyl-phthalate	DI-N--01	2.5976%
Aqueous Phase		30%
Composition		
Methanol	METHA-01	4.3860%
Ethanol	ETHAN-01	0.8772%
Acetone	ACETO-01	0.8772%
Formic acid	FORMI-01	8.7719%
Acetic acid	ACETI-01	2.6316%
Glycerol	GLYCE-01	0.8772%
Carbon dioxide	CARBO-01	5.9649%
Ammonia	AMMON-01	2.7193%
3-Pyridinol	3-HYD-01	1.3158%
1-ethyl-2-Pyrrolidinone	1-ETH-01	0.5597%
N-methylthiopyrrolidone	N-MET-01	1.0193%
Gas		4%
Composition		
Carbon dioxide	CARBO-01	3.6717%
Methane	METHA-02	0.1993%
Ethane	ETHAN-02	0.1290%
Ash	ASH	13%
Filter Solids	FSOL	2%

Table D.2. Upgraded oil composition inputs for Aspen model

	Aspen Component ID	Yield (wt.%)
Bio-crude (dry)		77%
Composition		
Butane, 2-methyl-	2-MET-01	0.5929%
Pentane	N-PEN-01	0.5929%
Pentane, 2-methyl	2-MET-02	2.3870%
Hexane	N-HEX-02	1.1935%
Hexane, 2-methyl	2-M3T-03	2.3870%
Heptane	N-HEP-01	1.1935%
Cyclohexane, methyl	METHY-01	1.1935%
Piperidine	PIPER-01	0.5929%
Toluene	TOLUE-01	1.1935%
Heptane, 3-methyl	3-MET-01	1.1935%
Octane	N-OCT-01	1.1935%
Cyclohexane, ethyl	ETHYL-02	1.1935%
Ethylbenzene	ETHYL-01	2.3870%
o-Xylene	O-XYL-01	1.1935%
Nonane	N-NON-01	1.1935%
Cyclohexane propyl	N-PRO-01	2.3870%
Benzene, propyl	N-PRO-02	1.1935%
Nonane 4 methyl	4-NON-01	1.1935%
Decane	N-DEC-01	3.5728%
Benzene butyl	N-BUT-01	1.1935%
Undecane	N-UND-01	2.3870%
1 Phenyl-1-butene	BENZE-01	1.1935%
Dodecane	N-DOD-01	2.3870%
Naphthalene 1234 tetrahydro	1:2:3-01	1.1935%
Benxene hexyl	N-HEX-03	1.1935%
Naphthanlene 1234 tetrahydro 6 methyl	6-MET-01	1.1935%
Benzene heptyl	N-HEP-02	1.1935%
Benzene octyl	N-OCT-02	2.3870%
1,4-Cyclohexanedicarboxylic acid dimethyl ester	DIMET-01	1.1935%
Pentadecane	N-PEN-02	1.1935%
Hexadecane	N-HEX-04	9.5326%
Heptadecane	N-HEP-03	3.5728%
Octadecane	N-OCT-03	2.3870%
Nonadecane	N-NON-02	2.3870%
Eicosane	HEXAD-01	5.9598%
Heneicosane	N-HEN-O1	2.3870%
Tricosane	N-TRI-01	1.1935%
1,2-benzenedicarboxylic acid	DIISO-01	2.3870%
heptyl undecyl phthalate	HEPTY-01	2.3870%
Triacontane	N-TRI-02	0.0693%
Aqueous Phase	N/A	16%
Gas		7%
Composition		
Methane	METHA-01	3.1500%
C2+	Various	3.7800%
Ammonia	AMMON-01	0.0700%

Table D.3. Aspen model HTL mass balance

Line Number	1	2	3	4	5	6	7	8	9	10	11	12	13
From		B1	B2	B3	B4	B5	B6	B6	B3	B7	B8	B8	B8
To	B1	B2	B3	B4	B5	B6		B3	B7	B8			
Temperature (°C)	15	15	24	239	350	350	350	350	200	127	96	96	96
Pressure (barg)	0	6	210	210	210	210	210	210	210	2	0	0	0
Mass Vapor Fraction	0.00	0.00	0.00	0.00	0.00	0.29	0.00	0.30	0.00	0.35	1.00	0.24	0.00
Enthalpy Flow (MMBtu/hr)	-132.439	132.424	-131.925	-123.389	-117.234	-112.001	-3.81162	-108.189	-116.725	116.725	-0.70448	115.984	-2.01525
Average MW	21.5	21.5	21.5	21.5	21.5	21.5	39.2	21.2	21.2	21.2	40.1	19.0	156.5
Mole Flows (kmol/hr)	464.5	464.5	464.5	464.5	464.5	464.1	8.0	456.0	456.0	456.0	2.2	446.7	7.2
Mass Flows (kg/hr)													
Total Mass Flow	10000.0	10000.0	10000.0	10000.0	10000.0	10000.0	314.4	9685.6	9685.6	9685.6	87.7	8474.8	1123.1
H2O	7700.0	7700.0	7700.0	7700.0	7700.0	7700.0	0.0	7700.0	7700.0	7700.0	0.0	7679.0	21.0
AMMON-01	0.0	0.0	0.0	0.0	0.0	81.7	0.0	81.7	81.7	81.7	0.0	81.7	0.0
CARBO-01	0.0	0.0	0.0	0.0	0.0	202.0	0.0	202.0	202.0	202.0	80.8	121.2	0.0
METHA-02	0.0	0.0	0.0	0.0	0.0	4.2	0.0	4.2	4.2	4.2	4.2	0.0	0.0
ETHAN-02	0.0	0.0	0.0	0.0	0.0	2.7	0.0	2.7	2.7	2.7	2.7	0.0	0.0
METHA-01	0.0	0.0	0.0	0.0	0.0	131.8	0.0	131.8	131.8	131.8	0.0	131.8	0.0
ETHAN-01	0.0	0.0	0.0	0.0	0.0	26.4	0.0	26.4	26.4	26.4	0.0	26.4	0.0
ACETO-01	0.0	0.0	0.0	0.0	0.0	26.4	0.0	26.4	26.4	26.4	0.0	26.4	0.0
FORMI-01	0.0	0.0	0.0	0.0	0.0	263.5	0.0	263.5	263.5	263.5	0.0	263.5	0.0
ACETI-01	0.0	0.0	0.0	0.0	0.0	79.1	0.0	79.1	79.1	79.1	0.0	79.1	0.0
GLYCE-01	0.0	0.0	0.0	0.0	0.0	26.4	0.0	26.4	26.4	26.4	0.0	26.4	0.0
3-HYD-01	0.0	0.0	0.0	0.0	0.0	39.5	0.0	39.5	39.5	39.5	0.0	39.5	0.0
1-ETH-01	0.0	0.0	0.0	0.0	0.0	84.3	0.0	84.3	84.3	84.3	0.0	0.0	84.3
N-MET-01	0.0	0.0	0.0	0.0	0.0	32.3	0.0	32.3	32.3	32.3	0.0	0.0	32.3
ETHYL-01	0.0	0.0	0.0	0.0	0.0	27.2	0.0	27.2	27.2	27.2	0.0	0.0	27.2
P-CRE-01	0.0	0.0	0.0	0.0	0.0	54.4	0.0	54.4	54.4	54.4	0.0	0.0	54.4
P-ETH-01	0.0	0.0	0.0	0.0	0.0	54.4	0.0	54.4	54.4	54.4	0.0	0.0	54.4
INDOL-01	0.0	0.0	0.0	0.0	0.0	54.4	0.0	54.4	54.4	54.4	0.0	0.0	54.4
7-MET-01	0.0	0.0	0.0	0.0	0.0	36.3	0.0	36.3	36.3	36.3	0.0	0.0	36.3
MYRIS-01	0.0	0.0	0.0	0.0	0.0	36.3	0.0	36.3	36.3	36.3	0.0	0.0	36.3
PALMI-01	0.0	0.0	0.0	0.0	0.0	163.3	0.0	163.3	163.3	163.3	0.0	0.0	163.3
OCTAD-01	0.0	0.0	0.0	0.0	0.0	72.6	0.0	72.6	72.6	72.6	0.0	0.0	72.6
CIS-9-01	0.0	0.0	0.0	0.0	0.0	145.2	0.0	145.2	145.2	145.2	0.0	0.0	145.2
N-HEX-01	0.0	0.0	0.0	0.0	0.0	108.9	0.0	108.9	108.9	108.9	0.0	0.0	108.9
OLEIC-01	0.0	0.0	0.0	0.0	0.0	18.1	0.0	18.1	18.1	18.1	0.0	0.0	18.1
NAPHT-01	0.0	0.0	0.0	0.0	0.0	54.4	0.0	54.4	54.4	54.4	0.0	0.0	54.4
BETA--01	0.0	0.0	0.0	0.0	0.0	18.1	0.0	18.1	18.1	18.1	0.0	0.0	18.1
N-N-D-01	0.0	0.0	0.0	0.0	0.0	87.0	0.0	87.0	87.0	87.0	0.0	0.0	87.0
DI-N--01	0.0	0.0	0.0	0.0	0.0	54.4	0.0	54.4	54.4	54.4	0.0	0.0	54.4
ALGAE	2300.0	2300.0	2300.0	2300.0	2300.0	0.0	0.0	0.0	0.0	0.0	0.0	0.0	0.0
ASH	0.0	0.0	0.0	0.0	0.0	272.5	272.5	0.0	0.0	0.0	0.0	0.0	0.0
FSOL	0.0	0.0	0.0	0.0	0.0	41.9	41.9	0.0	0.0	0.0	0.0	0.0	0.0
Volume Flow (l/hr)	11346.59	11347.5	11378.17	14347.75	21109.35	28328.48	154.6825	28173.82	14187.32	1206956	66114.05	2722205	1692.489

Table D.5. Equipment costing

Equipment Title	Number Required	Quote Cost Per Unit	Year of Quote	Scaling Variable	Units	Scaling Exp	Installation Factor	New Variable Value	Units	Size Ratio	Total Scaled Purchase Cost Per Unit	Purchase Cost in Project Year	Installation Cost in Project Year	Cost After Location Factor	Cost After Currency Exchange	Reference
HTL Section																
Twin screw feeder and booster pump	1	\$1,094,100	2011	575 gal/min		0.8	2.3	10000 kg/hr	0.076		\$139,923	\$137,459	\$316,156	\$322,479	£232,185	Knorr 2013
Feed Heat Exchanger	1	\$31,860,000	2012	35540 ft^2		0.7	2.2	30 m^2	0.009		\$1,186,062	\$1,162,986	\$2,558,568	\$2,609,740	£1,879,013	Knorr 2013
Make-up Heater	1	\$998,850	2012	32.1 mmBTU/hr		0.7	2.2	1800 kW	0.191		\$313,875	\$307,768	\$677,089	\$690,631	£497,254	Knorr 2013
HTL Reactor	1	\$770,992	2014	33333 lb/hr		0.7	2	10000 kg/hr	0.661		\$577,260	\$557,799	\$1,115,598	\$1,137,910	£819,295	Snowden Swann 2017
Reactor Knock Out Drum	1	\$5,700,243	2011	304939 lb/hr		0.7	2	10000 kg/hr	0.072		\$906,313	\$902,275	\$1,804,550	\$1,840,641	£1,325,262	Knorr 2013
Solid filter	1	\$1,017,998	2011	2420 gal/min		0.6	1.7	10000 kg/hr	0.018		\$91,914	\$91,505	\$155,558	\$158,669	£114,242	Knorr 2013
Phase Separator	1	\$2,653,959	2011	2420 gal/min		0.7	2	9686 kg/hr	0.018		\$156,949	\$156,250	\$312,499	\$318,749	£229,500	Knorr 2013
Hot Oil System	1	\$1,200,500	2012	63.6 mmBTU/hr		0.6	1.8	2000 kW	0.107		\$314,573	\$308,453	\$555,215	\$566,320	£407,750	Knorr 2013
								Total			\$3,686,871	\$3,624,494	\$7,495,235	\$7,645,139	£5,504,500	
CHG Section																
Feed Pump	1	\$611,300	2011	201905 lb/hr		0.8	2.3	8475 kg/hr	0.093		\$91,056	\$89,453	\$205,741	\$209,856	£151,096	Jones 2014
Booster Pump	1	\$8,900	2011	201905 lb/hr		0.8	2.3	8475 kg/hr	0.093		\$1,326	\$1,302	\$2,995	\$3,055	£2,200	Jones 2014
Heat Exchanger	4	\$5,013,647	2011	7720 ft2		0.7	2.2	6.25 m^2	0.009		\$725,065	\$712,295	\$1,567,049	\$1,598,390	£1,150,841	Knorr 2013
Fired Heater	1	\$1,372,262	2011	115 mmBTU/hr		0.7	2.2	1500 kW	0.045		\$155,357	\$152,621	\$335,766	\$342,482	£246,587	Knorr 2013
Hydrocyclone	1	\$5,000,000	2009	968859 lb/hr		0.7	2	8475 kg/hr	0.019		\$315,220	\$275,937	\$551,873	\$562,910	£405,296	Jones 2014
CHG Reactor	4	\$2,041,875	2011	76235 lb/hr		0.7	2	2119 kg/hr	0.061		\$1,156,552	\$1,136,184	\$2,272,367	\$2,317,815	£1,668,827	Knorr 2013
Guard Bed 10% cost of CHG reactor	1						2				\$115,655	\$113,618	\$227,237	\$231,781	£166,883	Knorr 2013
Product Air fin cooler	1	\$204,100	2011	201905 lb/hr		0.7	1.5	8475 kg/hr	0.093		\$38,571	\$37,892	\$56,838	\$57,975	£41,742	Jones 2014
								Total			\$2,598,803	\$2,519,302	\$5,219,867	\$5,324,265	£3,833,471	
Bio-crude Upgrading and Separation																
Hydrotreater reactor, vessels, columns	1	\$27,000,000	2007	6524 bpd fd		0.7	1.5	1123.1 kg/hr	0.028		\$2,190,253	\$1,930,156	\$2,895,234	\$2,953,138	£2,126,259	Jones 2014
Hydrogen Compressor	1	\$1,385,600	2011	17.1 mmscfd H ₂		0.8	1.6	59 kg/hr	0.035		\$94,638	\$92,972	\$148,755	\$151,730	£109,246	Jones 2014
Pressure Swing Assorption H2 Recycle	1	\$1,750,000	2004	10 mmscfd H ₂		0.7	2.4	231.95 kg/hr	0.235		\$634,515	\$472,747	\$1,134,592	\$1,157,284	£833,244	Jones 2014
Hydrocracker Unit + Aux equip	1	\$25,000,000	2007	2200 bpd fd		0.7	1.5	113.87 kg/hr	0.008		\$884,338	\$779,321	\$1,168,981	\$1,192,361	£858,500	Jones 2014
								Total			\$3,803,744	\$3,275,195	\$5,347,561	\$5,454,513	£3,927,249	Jones 2014
Hydrogen Plant																
Steam Reformer system + Aux equip	1	\$32,765,625	2007	17 mmscfd H ₂		0.85	2	59 kg/hr	0.035		\$1,901,802	\$1,675,959	\$3,351,919	\$3,418,957	£2,461,649	Jones 2014
								Total			\$1,901,802	\$1,675,959	\$3,351,919	\$3,418,957	£2,461,649	
Power Generation																
Steam Turbine	1	\$1,493,000	2010	46666 lb/hr		0.85	1.08	2000 kg/hr	0.094		\$200,964	\$185,661	\$200,514	\$204,524	£147,257	Jones 2014
								Total			\$200,964	\$185,661	\$200,514	\$204,524	£147,257	
Cooling Water																
Cooling Tower System	1	\$2,000,000	2009	35631668 lb/hr		0.65	2.95	200000 kg/hr	0.012		\$115,126	\$100,779	\$297,297	\$303,243	£218,335	Jones 2014
Cooling water pump	1	\$445,700	2009	35631668 lb/hr		0.65	2.95	200000 kg/hr	0.012		\$25,656	\$22,459	\$66,253	\$67,578	£48,656	Jones 2015
Plant Air Compressor	1	\$32,376	2002	2000 mtpd		0.65	2.95	2000 kg/hr	0.001		\$363	\$241	\$711	\$725	£522	Jones 2016
Firewater pump	1	\$18,400	1997	2000 mtpd		0.65	2.95	2000 kg/hr	0.001		\$206	\$134	\$395	\$403	£290	Jones 2017
Instrument air dryer	1	\$8,349	2002	2000 mtpd		0.65	2.95	2000 kg/hr	0.001		\$94	\$62	\$183	\$187	£135	Jones 2018
Plant air reciever	1	\$7,003	2002	2000 mtpd		0.65	2.95	2000 kg/hr	0.001		\$79	\$52	\$154	\$157	£113	Jones 2019
Firewater storage tank	1	\$166,100	1997	2000 mtpd		0.65	2.95	100000 kg/hr	0.05		\$23,697	\$15,362	\$45,319	\$46,225	£33,282	Jones 2020
								Total			\$165,221	\$139,089	\$410,312	\$418,518	£301,333	
Plant Storage																
HTL Bio-crude intermediate storage 3 Da	1	\$470,000	2005	1056846 gallons		0.7	2.95	86023 litres	0.022		\$31,977	\$25,112	\$74,080	\$75,562	£54,404	Jones 2014
Naptha Storage 3 Day	1	\$320,384	2005	558000 gallons		0.7	2.95	10560 litres	0.005		\$7,851	\$6,165	\$18,188	\$18,551	£13,357	Jones 2014
Diesel Pool Storage 3 Day	1	\$320,384	2005	558000 gallons		0.7	2.95	56753 litres	0.027		\$25,476	\$20,007	\$59,020	\$60,201	£43,344	Jones 2014
								Total			\$65,304	\$51,284	\$151,288	\$154,314	£111,106	
TOTAL EQUIPMENT COST											\$12,422,710	\$11,470,984	\$22,176,696	\$22,620,230	£16,286,565	

Table D.6. Discounted Cash Flow Rate of Return (DCFROR)

Year	Fixed Capital Investment	Working capital	Total Capital Cost	Loan Interest Payment	Loan Principal	Loan Payment	Variable Operating Cost	Fixed Operating Cost	Total Production Cost	Forecast Diesel Fuel Sales	Forecast by-product Sales	Total Annual Sales	Depreciation	Annual Cash Income	Taxable Income	Tax Paid	Cash Flow	Cumulative Cash Flow	NPV	
-2	£2,470,346	£0	£2,470,346	£118,577	£1,482,208	£0	£0	£0	£0	£0	£0	£0	£0	£0	£0	£0	-£2,470,346	-£2,470,346	-£2,989,119	
-1	£18,527,597	£0	£18,527,597	£1,007,901	£12,598,766	£0	£0	£0	£0	£0	£0	£0	£0	£0	£0	£0	-£18,527,597	-£20,997,943	-£20,380,356	
0	£9,881,385	£4,631,899	£14,513,284	£1,704,539	£21,306,736	£0	£0	£0	£0	£0	£0	£0	£0	£0	£0	£0	-£14,513,284	-£35,511,227	-£14,513,284	
1	£0	£0	£0	£1,586,875	£19,835,943	£3,175,332	£7,201,157	£2,142,285	£9,343,442	£12,395,025	£235,224	£12,630,249	£1,628,657	£111,476	-£1,517,181	-£531,013	£642,489	-£34,868,738	£584,081	
2	£0	£0	£0	£1,459,799	£18,247,487	£3,175,332	£6,527,459	£2,142,285	£8,669,743	£16,480,462	£313,632	£16,794,094	£1,628,657	£4,949,019	£3,320,362	£1,162,127	£3,786,892	-£31,081,846	£3,129,663	
3	£0	£0	£0	£1,322,556	£16,531,954	£3,175,332	£6,472,195	£2,142,285	£8,614,480	£16,480,462	£313,632	£16,794,094	£1,628,657	£5,004,282	£3,375,626	£1,181,469	£3,822,813	-£27,259,033	£2,872,136	
4	£0	£0	£0	£1,174,334	£14,679,178	£3,175,332	£6,527,459	£2,142,285	£8,669,743	£16,480,462	£313,632	£16,794,094	£1,628,657	£4,949,019	£3,320,362	£1,162,127	£3,786,892	-£23,472,141	£2,586,498	
5	£0	£0	£0	£1,014,254	£12,678,180	£3,175,332	£6,477,911	£2,142,285	£8,620,195	£16,480,462	£313,632	£16,794,094	£1,628,657	£4,998,567	£3,369,911	£1,179,469	£3,819,098	-£19,653,043	£2,371,360	
6	£0	£0	£0	£841,368	£10,517,102	£3,175,332	£6,527,459	£2,142,285	£8,669,743	£16,480,462	£313,632	£16,794,094	£1,628,657	£4,949,019	£3,320,362	£1,162,127	£3,786,892	-£15,866,151	£2,137,602	
7	£0	£0	£0	£654,651	£8,183,139	£3,175,332	£6,472,195	£2,142,285	£8,614,480	£16,480,462	£313,632	£16,794,094	£1,628,657	£5,004,282	£3,375,626	£1,181,469	£3,822,813	-£12,043,337	£1,961,708	
8	£0	£0	£0	£452,997	£5,662,458	£3,175,332	£6,527,459	£2,142,285	£8,669,743	£16,480,462	£313,632	£16,794,094	£1,628,657	£4,949,019	£3,320,362	£1,162,127	£3,786,892	-£8,256,445	£1,766,613	
9	£0	£0	£0	£235,210	£2,940,122	£3,175,332	£6,472,195	£2,142,285	£8,614,480	£16,480,462	£313,632	£16,794,094	£1,628,657	£5,004,282	£3,375,626	£1,181,469	£3,822,813	-£4,433,632	£1,621,246	
10	£0	£0	£0	£0	£0	£3,175,332	£6,533,174	£2,142,285	£8,675,458	£16,480,462	£313,632	£16,794,094	£1,628,657	£4,943,304	£3,314,647	£1,160,127	£3,783,177	-£650,455	£1,458,579	
11	£0	£0	£0	£0	£0	£0	£6,472,195	£2,142,285	£8,614,480	£16,480,462	£313,632	£16,794,094	£0	£8,179,614	£8,179,614	£2,862,865	£5,316,749	£4,666,294	£1,863,488	
12	£0	£0	£0	£0	£0	£0	£6,527,459	£2,142,285	£8,669,743	£16,480,462	£313,632	£16,794,094	£0	£8,124,351	£8,124,351	£2,843,523	£5,280,828	£9,947,122	£1,682,635	
13	£0	£0	£0	£0	£0	£0	£6,472,195	£2,142,285	£8,614,480	£16,480,462	£313,632	£16,794,094	£0	£8,179,614	£8,179,614	£2,862,865	£5,316,749	£15,263,871	£1,540,073	
14	£0	£0	£0	£0	£0	£0	£6,527,459	£2,142,285	£8,669,743	£16,480,462	£313,632	£16,794,094	£0	£8,124,351	£8,124,351	£2,843,523	£5,280,828	£20,544,699	£1,390,607	
15	£0	£0	£0	£0	£0	£0	£6,477,911	£2,142,285	£8,620,195	£16,480,462	£313,632	£16,794,094	£0	£8,173,899	£8,173,899	£2,860,865	£5,313,034	£25,857,734	£1,271,898	
16	£0	£0	£0	£0	£0	£0	£6,527,459	£2,142,285	£8,669,743	£16,480,462	£313,632	£16,794,094	£0	£8,124,351	£8,124,351	£2,843,523	£5,280,828	£31,138,562	£1,149,262	
17	£0	£0	£0	£0	£0	£0	£6,472,195	£2,142,285	£8,614,480	£16,480,462	£313,632	£16,794,094	£0	£8,179,614	£8,179,614	£2,862,865	£5,316,749	£36,455,311	£1,051,890	
18	£0	£0	£0	£0	£0	£0	£6,527,459	£2,142,285	£8,669,743	£16,480,462	£313,632	£16,794,094	£0	£8,124,351	£8,124,351	£2,843,523	£5,280,828	£41,736,139	£949,803	
19	£0	£0	£0	£0	£0	£0	£6,472,195	£2,142,285	£8,614,480	£16,480,462	£313,632	£16,794,094	£0	£8,179,614	£8,179,614	£2,862,865	£5,316,749	£47,052,888	£869,331	
20	£0	£0	£0	£0	£0	£0	£6,533,174	£2,142,285	£8,675,458	£16,480,462	£313,632	£16,794,094	£0	£8,118,636	£8,118,636	£2,841,523	£5,277,113	£52,330,002	£784,409	
21	£0	£0	£0	£0	£0	£0	£6,472,195	£2,142,285	£8,614,480	£16,480,462	£313,632	£16,794,094	£0	£8,179,614	£8,179,614	£2,862,865	£5,316,749	£57,646,751	£718,455	
22	£0	£0	£0	£0	£0	£0	£6,527,459	£2,142,285	£8,669,743	£16,480,462	£313,632	£16,794,094	£0	£8,124,351	£8,124,351	£2,843,523	£5,280,828	£62,927,579	£648,728	
23	£0	£0	£0	£0	£0	£0	£6,472,195	£2,142,285	£8,614,480	£16,480,462	£313,632	£16,794,094	£0	£8,179,614	£8,179,614	£2,862,865	£5,316,749	£68,244,328	£593,765	
24	£0	£0	£0	£0	£0	£0	£6,527,459	£2,142,285	£8,669,743	£16,480,462	£313,632	£16,794,094	£0	£8,124,351	£8,124,351	£2,843,523	£5,280,828	£73,525,156	£536,139	
25	£0	£0	£0	£0	£0	£0	£6,477,911	£2,142,285	£8,620,195	£16,480,462	£313,632	£16,794,094	£0	£8,173,899	£8,173,899	£2,860,865	£5,313,034	£78,838,190	£490,372	
26	£0	£0	£0	£0	£0	£0	£6,527,459	£2,142,285	£8,669,743	£16,480,462	£313,632	£16,794,094	£0	£8,124,351	£8,124,351	£2,843,523	£5,280,828	£84,119,018	£443,090	
27	£0	£0	£0	£0	£0	£0	£6,472,195	£2,142,285	£8,614,480	£16,480,462	£313,632	£16,794,094	£0	£8,179,614	£8,179,614	£2,862,865	£5,316,749	£89,435,768	£405,549	
28	£0	£0	£0	£0	£0	£0	£6,527,459	£2,142,285	£8,669,743	£16,480,462	£313,632	£16,794,094	£0	£8,124,351	£8,124,351	£2,843,523	£5,280,828	£94,716,596	£366,190	
29	£0	£0	£0	£0	£0	£0	£6,472,195	£2,142,285	£8,614,480	£16,480,462	£313,632	£16,794,094	£0	£8,179,614	£8,179,614	£2,862,865	£5,316,749	£100,033,345	£335,165	
30	£0	£0	£0	£0	£0	£0	£6,533,174	£2,142,285	£8,675,458	£16,480,462	£313,632	£16,794,094	£0	£8,118,636	£8,118,636	£2,841,523	£5,277,113	£105,310,458	£302,424	
																			Total NPV	£0
															MFSP £/kg	3.11			MFSP £/l	2.64

© Christopher Michael Thomas, 2022